Investigating The Role Of Extracellular Vesicles And MicroRNA-155 In Cerebrovascular Function In Inflammation

Thesis

Investigating the role of extracellular vesicles and microRNA-155 in cerebrovascular function in inflammation

David Roig-Carles, BSc, MSc

A thesis submission to the Open University for the degree of Doctor of Philosophy

October 2020

Declaration

I declare that the work presented in this thesis is my own and contributions made by other researchers are acknowledged in relevant parts of the text. This work does not contain any material submitted for any award or other degree.

ABSTRACT

Blood-brain barrier (BBB) dysfunction is an early feature of several central nervous system (CNS) pathologies and is characterised by increased leukocyte migration to the CNS and increased paracellular permeability of brain endothelial cells (BECs). The mechanisms by which the BBB actively participates in the inflammatory events that contribute to the progression of many CNS diseases is still poorly understood. Extracellular vesicles (EVs) are a novel mechanism of cell-to-cell communication. Endothelial cell-derived EVs are upregulated in circulating blood in different pathologies (e.g. multiple sclerosis) and systemic inflammation. TNFα-stimulated BECs secrete a higher number of EVs, which carry a pro-inflammatory cargo. However, the role of cerebrovascular EVs modulating inflammation at the BBB is still unclear.

In this project, EVs secreted from BECs were characterised based on number, size and RNA cargo. Indeed, BECs secreted higher number of EVs in inflammation that carried pro-inflammatory modulators (e.g. miRNA-155). Uptake of EVs by NVU cells and their role in BEC function was investigated. Interestingly, EVs decreased transendothelial resistance and increased T cell adhesion to BECs via up-regulation of adhesion molecules.

TNFα/IFNγ–mediated BECs dysfunction is partially modulated by miRNA-155. However, the mechanism by which miRNA-155 modulates T cell adhesion remains to be elucidated. WNK1 was identified as possible target of miRNA-155 and shown to modulate T cell adhesion.

Finally, unexpected increased polydipsia in female aged miRNA-155 knock-out mice was investigated but this unexpected phenotype was attributed to a miRNA-155-independent pathway.

Results from this work constitute the first evidence that BEC-derived EVs modulate BBB function in inflammation, which is likely to be a mechanism of the cells to amplify pro-inflammatory cytokine signalling in the vasculature. Additionally, this work has demonstrated endothelial WNK1 as a modulator of T cell adhesion. Genotyping tissue from miRNA-155 KO mice will serve for future identification of novel modulators of water balance.

ACKNOWLEDGEMENTS AND DEDICATIONS

I would like to dedicate this thesis to both my parents (Amparo and Rafa) and my brother (Javier) for being a loving supporting family who has always believed in me. I would also

like to dedicate this work to my friends in Milton Keynes (James, Alexia, Alvaro, Adri, Rafat, Mauro and Lidia); without them this PhD journey would have been more difficult that it was. I also would like to dedicate this work to my "Biotec" friends, whose friendship and passion for Biotechnology inspired me to build a career in biomedical research.

I would specially like to acknowledge Nacho for giving me the opportunity of carrying a research lab-based project when I was a Master student and then further supporting me during my PhD. You have been an extraordinary role model during these years. Of course, a special mention for Dr. Cheryl Hawkes who has been a brilliant supervisor and has inspired me during these years.

I would like to acknowledge the support given by the Neurovascular unit group and all their members (Dr. David Male, Dr. Jane Loughin, Shereen, Edu, Ester, Nayab, Conor, Zerin, Mo, Radka, Perla, Rebecca, Laura, Sarai) as well as my fellow PhD students at the OU (Nadia, Sarah, Sonia, Tala, Gonçalo, Pelumi).

I would like to acknowledge the technical support given by the BRU team (Agata, Iwona, Gareth and Karen) as well as the lab support (George, Brett, Julia, Igor). I am very grateful to the members of Oxford University for the support given on the characterisation of EVs: Dr. Dan Anthony (Department of Pharmacology), Dr. Naveed Akbar (Radcliffe Department of Medicine) and both Dr. Eduard Willms and Dr. Imre Mager (Matthew Woods Group). Thanks to both Dr. Ruud Fontijn and Prof. Helga de Vries for helping with the TEER experiments. To Dr. Francesco Crea for supporting my research career the last year and a half while this thesis was being written.

Lastly, I would like to acknowledge Prof Basil Sharrack and The Open University for the funding given to support this PhD work.

Table of Content

List of Figures

List of Tables

List of Equations

Conference items and publications

Publications

Roig-Carles, D., Cerutti, C., Lopez-Ramirez, M.A., Wu, D., Male, DK., de Vries, H. E. and Romero, I. A., (2017). microRNAs in Brain Endothelium and Inflammation. The Blood Brain Barrier and Inflammation. R. Lyck and G. Enzmann. Cham, Springer International Publishing: 153-173.

Roig-Carles, D., Willms, E., Fontijn, R., Martinez-Pacheco, S., Mäger, I., de Vries, H. E., Hirst, M., Sharrack, B., Male, DK., Hawkes, CH. and Romero, I. A., (2020). Endothelial-derived extracellular vesicles induce cerebrovascular dysfunction in inflammation. Scientific Reports (Submitted October 2020).

Roig-Carles, D., Martinez-Pacheco, S., Sharrack, B., Male, DK., Hawkes, CH. and Romero, I. A., WNK1 contributes to shear-resistant leukocyte adhesion to human brain endothelium in vitro. (Manuscript in preparation).

International conference presentations

Roig-Carles, David "Brain endothelial derived extracellular vesicles modulate cerebrovascular function in inflammation: oral presentation at 21st *International Symposium on Signal Transduction at the Blood-Brain Barrier 19*th to 21st September 2018. Arad (Romania). (Oral Presentation)

Roig-Carles, David "Investigating the pro-inflammatory role of brain endothelial-derived extracellular vesicles at the blood-brain barrier: poster presentation at 12th *International Conference on Cerebral Vascular Biology* 28th November to 1st December 2017. Monash University, Australia. (Poster presentation)

National conference presentation

Oral presentations on The UK & Ireland Early Career Blood-Brain Barrier Symposiums 9th (Oxford University, 2018), 8th (University of Portsmouth, 2017) and 7th (Trinity College Dublin, 2016)

Roig-Carles David "Inflammation-induced cerebrovascular cross-talk by extracellular vesicles promotes blood-brain barrier dysfunction" oral presentation at UKEV 2018 Forum (Sheffield, UK).

ABBREVIATIONS

AD	Alzhheimer´s disease
ANXA2	Annexin A2
AP-1	Activator protein-1
APCs	Antigen presenting cells
AQP4	Aquaporin-4
arEC	Arterial endothelial cells
arSMCs	arteriolar smooth muscle cells
AVP	Arginine vasopressin hormone
BBB	Blood-Brain Barrier
BCSFB	Blood-Cerebrospinal Fluid Barrier
BECs	Brain endothelial cells
bFGF	basic fibroblast growth factor
BIC	B-cell Integration cluster
BM	Basal membrane
BRCP	Breast cancer resistance protein
BSA	Bovine serum albumin
capEC	Capillary endothelial cells
CCM	Cell culture conditioned media
CEACAM1	Carcinoembryonic antigen-related cell adhesion molecule 1
CFS	Cerebrospinal Fluid
CLDN-5	Claudin-5
CMFDA	5–chloromethylfluoresceindiacetate
CNS	Central Nervous System
Cytokine-sEVs	cytokine-treated hCMEC/D3 cell-derived small EVs
DDAVP	DDAVP
ddH2O	Double-distilled water
DGCR8	DiGeorge syndrome critical region 8
DMSO	Dimethyl sulfoxide
EAE	Experimental Autoimmune Encephalomyelitis
EBM-2	Endothelial basal membrane-2
EBV	Epstein-Barr Virus
EC	Endothelial cells
ECIS	Electric cell-impedance sensing
ECL	Enhanced chemiluminescence
ECM	Extracellular cell matrix
EGF	Epithelial growth factor
ELISA	Enzyme-linked immunosorbent assay
EM	Electron Microscopy
Eps	Extracellular particles
Evs	Extracellular vesicles
FBS	Foetal bovine serum
FOV	Field of vision
FPB1	Fibroblast-like type 1

FPB2	Fibroblast-like type 2
GA-1000	Gentamycin
GAPDH	Glyceraldehyde 3-phosphate dehydrogenase
GDFN	Glial-derived neurotrphic factors
GLUT-1	Glucose transporter 1
GPCRs	G protein-coupled receptors
hA	Human primary cortical astrocytes
HBMP	Human brain pericytes
HBSS	Hank's Balanced Salt Solution
hCMEC/D3	Human brain microvascular endothelial cell
HMC-1	Human mast cell line-1
HSPGs	Heparan sulfate proteoglycans
hTERT	human telomerase reverse transcrptase
HUVECs	Human vein umbilical cell line
ICAM1	Intercellular cell adhesion molecule 1
IFNγ	Interferon gamma
IGF	Insulin growth factor
ILV	Intraluminal vesicles
ISEV	International Society of Extracellular Vesicles
JAM	Junctional adhesion molecules
KO	Knock-out
KS-WNK1	Kidney-specific WNK1
Large-Evs	Large Extracellular Vesicles
LFA-1	Integrin αLβ2
lncRNAs	long non-coding RNAs
LPS	Lipopolysaccharide
MC/9	Mast cell line 9
MG	Microglia
MHC	Major histocompability complex
miRNAs	microRNAs
MMPs	Metalloproteinases
mRNA	messenger RNA
MS	Multiple Sclerosis
MVB	Multivesicular body
n	number of independent experiments
NAWM	Normal appearing white matter
ncRNAs	non-coding RNAs
NDS	Normal donkey serum
NF	Nuclear factor
NFAT5	Nuclear factor of activated T cells 5
NTA	Nanoparticle tracking analysis
NVU	Neurovascular Unit
OCLN	Occludin
OCT	Optimal cutting temperature
OG	Oligodendrocytes
OXC	Oxytocin

P/S	Penicillin and streptomycin
PBS	Phosphate saline buffer
PD	Parkinson´s disease
PDCs	Plasmacytoid dendritic cells
PDGF-B	Platelet-derived growth factor B
PEG	Poly ethylene glycol
PFA	*p*-formaldehyde
P-gp	P-glycoprotein
piRNAs	(PIWI)-interacting RNAs
PM	Plasma membrane
Pol II	Polymerase II
pre-miRNA	stem-loop precursor microRNA
pri-miRNA	primary microRNA transcrcipt
PSGL-1	P-selectin glycoprotein ligand-1
PTX3	Pentraxin 3
RPMI	Roswell Park Memorial Institute
RT	Room temperature
SEM	Standard error of the mean
sEVs	small Extracellular vesicles
siRNA	small inhibitory RNA
SMSs	Smooth muscle cells
SOCS1	Suppresor of cytokine signalling
TBS-T	Tris-buffered saline
TEM	Transmission electron microscopy
TfR	Transferrin receptor
TGFB	Transforming growth factor-β
TJP1	Tight junction protein 1
TLR7	Toll-like receptor 7
TNFα	Tumour necrosis factor alpha
TRBP	TAR RNA-binding protein
UTR	Unstranslated region
VCAM1	Vascular cell adhesion molecule 1
VE	Vascular endothelial
vEC	Venous endothelial cells
VEGF-B	Vascular growth factor-B
VEGFR-1	Vascular growth factor receptor-1
VEGFRB	Vascular endothelial growth factor receptor B
VLA-4	integrin α4β1
vSMCs	venular smooth muscle cells
WNK1	Lysine deficient protein kinase 1
WT	wild-type
YY1	Yin and yang 1
ZO	Zonula occludens

CHAPTER 1: Introduction

1.1. Clinical significance of brain barriers research

The central nervous system (CNS) is highly protected from changes in the systemic blood circulation due to the presence of the brain barriers. There are different types of brain barriers that differ in their location, cellular origin and function (Redzic, 2011). In addition to the blood-brain barrier (BBB), which is associated with the endothelium, there is the blood-cerebrospinal fluid (CSF) barrier (BCSFB), which is located on the choroid plexus epithelial cells (Table 1.1.) (Redzic, 2011). Lastly, the arachnoid barrier is a tight barrier located at the subarachnoid space (Weller *et al.*, 2018). The brain barriers contribute to the fine modulation of the CNS microenviroment. These barriers form different types of tight junctions between cells to create a physical barrier and prevent the passive diffusion of molecules into the CNS (Table 1.1). Furthermore, specific expression of membrane proteins (e.g. specific solute carriers) contribute to the metabolic function of the CNS barriers by selectively exchanging the nutrients needed by the CNS and removing the waste. Finally, the CNS barriers also express a series of protein transporters (e.g. ATP-binding cassette (ABC) transporters) to exclude the entrance of unwanted proteins into the CNS (Table 1.1.) (Abbott, Adjanie A K Patabendige, *et al.*, 2010),

Table 1.1. Physical and molecular characteristics between the blood-brain barrier and the blood-CSF barrier

	Blood-Brain Barrier	Blood-CSF Barrier	Reference
Location	Brain Microvessel	Choroid Plexus epithelial cells	(Abbott, Adjanie A.K. Patabendige, *et al.*, 2010)
Physical barrier			
TEER	1500 Ω cm2 (pial vessels)	150 Ω cm2 (bull frog fourth CP)	(Crone and Christensen, 1981; Saito and Wright, 1984)
Tight Junctions			
Ocluddin	Yes	Yes	(Redzic, 2011)
JAMs A, -B, -C	Yes	Yes	(Redzic, 2011)
Claudins	3, 5, 12	1,2, 3, 11	(Wolburg *et al.*, 2001; Redzic, 2011)
Adherens Junctions			
Cadherins	Cadherin-10/ VE-cadherin	Cadherin-10/ VE-cadherin	(Williams *et al.*, 2005; Redzic, 2011)
Catenins	α, β, χ, ρ120	α, β	(Lippoldt *et al.*, 2000; Meng and Takeichi, 2009)
Metabolic Barrier			
Glucose Transporters			
GLUT1	Yes	Yes	(Redzic, 2011)
Aminoacid transporter			
LAT1	Yes	Yes	(Redzic, 2011)
EAATs	Yes	No/Yes	(Beschorner *et al.*, 2009; Redzic, 2011)
Monocarboxylate transporters			
MCT	MTC1, MTC7, MTC8	MTC1, MTC8	(Leino, Gerhart and Drewes, 1999; Enerson and Drewes, 2006; Roberts *et al.*, 2008)
Synthesis of TTR	No	Yes	(Power *et al.*, 2000; Redzic, 2011)
ABC-transporters			
P-gp	Blood-facing side +++	CSF-facing side +	(Gazzin *et al.*, 2008; Redzic, 2011)
Mrp1	+	+++	(Gazzin *et al.*, 2008; Redzic, 2011)
Ion Transporters			
NKCC1	Blood-facing side	CSF-facing side	(Redzic, 2011)

Abbreviations: CSF, cerebrospinal fluid; TEER, transendothelial resistance; JAM, junctional adhesion molecules; GLU1, glucose transporter 1; LAT1, system-L amino acid transporter 1; EAAT1, excitatory amino acid transporters; MCT, proton-linked monocarboxylate transporters; TTR, transthyretin; ABC, ATP-binding cassette; P-gp, P-glycoproteins; Mrp1, multidrug resistance-related protein; NKCC1, Na+-K+-2Cl--cotransporter 1. Expression level (+ and +++).

Dysfunction of the brain barriers is associated with cerebrovascular diseases, which includes a range of pathologies that affect the blood vessels of the brain. The most common examples of disorders affecting the vasculature are ischemic and haemorrhagic strokes (Ferrer and Vidal, 2018). However, the pathogenesis of other types of neurological disorders is strongly affected by the vasculature, which includes diseases such as Multiple Sclerosis (MS) or Alzheimer´s disease (Minagar and Alexander, 2003; Kalaria, 2018). For this reason, investigating the function of the cerebral vasculature and the contribution of the brain barriers in disease is of utmost importance to further understand unmet clinical goals in these neurological disorders. In particular, this project focuses specifically on investigating the BBB in disease and the remainder of the sections in the Introduction will be focused on this barrier.

1.2. The Blood-Brain barrier as a component of the neurovascular unit

The cerebral vasculature is a complex and specialised structure, whose length if unfolded has been estimated to be around 600 to 700 km (Begley and Brightman, 2003). The vasculature tree is composed of arteries, arterioles, capillaries, venules and veins (Abbott *et al.*, 2018). The brain vasculature is initially formed by the penetration of arteries that originate in the Circle of Willis into the brain through the subarachnoid space. A progressive decrease of the vessel lumen of the penetrating arteries leads to the formation of arterioles (lumen diameter ranges from 10 to 100 µm). As penetrating arterioles branch into the brain parenchyma, their lumen diameter further decreases to form capillaries (lumen diameter ranges from 5 to 10 µm). Blood returns to the heart along post-capillary venules (up to 100 µm of lumen diameter) that feed into the veins that are situated on the surface of the brain (Figure 1.1) (Abbott *et al.*, 2018). As described

in the previous section, the cerebral endothelium presents barrier properties that varies along the vascular tree. The BBB was a classical term used to refer to an endothelial centred barrier. Nowadays, it is clear that the BBB is an active structure influenced by the action of vascular-associated cells such as pericytes and CNS cells including astrocytes, microglia or neurons (Keaney and Campbell, 2015). This new concept of interactive BBB is known as the neurovascular unit (NVU). In the next section, the historical research into the BBB will be discussed to understand the experiments that marked the beginning of brain research in the CNS.

1.3. Historical overview of the blood-brain barrier

The first evidence of brain barriers was published in the late 1800s. In 1885, Paul Ehrilch observed that aniline dyes injected into the peritoneum of rats failed to stain the brain, which was attributed to differences in dye affinity to specific tissues (Ehrlich, 1885; Ribatti *et al.*, 2006). His student, Edwin Goldmann extended these findings by injecting trypan blue (molecular weight, MW, 960 KDa) directly into the CSF or the peripheral bloodstream (Goldmann, 1909, 1913; Ribatti *et al.*, 2006). He observed that dye injected into the CSF only stained the CNS whereas peripheral administration of trypan blue excluded the whole brain except from the chorus plexus and the pineal gland suggesting the presence of a barrier between the brain and the periphery.

The presence of a physical barrier and the concept of "blood-brain barrier" was first hypothesised by Max Lewandowsky (1876-1918) after he demonstrated that intravenous injection of sodium ferrocyanide or cholic acids had no pharmaceutical effect in the CNS whereas cerebro-ventrical injection did (Lewandwsky, 1909; Ribatti *et al.*, 2006). Further data supporting the hypothesis of a physical barrier between the brain and

the blood was provided by Lina Stern (1878-1968), who observed that intravenous injection of anti-tetanus failed to protect the brain after the pathogen had already reached the CNS (Stern and Gautier, 1921; Ribatti *et al.*, 2006).

Advances in electron microscopy (EM) techniques enabled scientists to examine ultrastructural brain morphology (Ribatti *et al.*, 2006). Using this technique, Reese and Karnovsky showed for the first time that the endothelium in mouse cerebral capillaries constituted a physical barrier to peroxidase extravasation (Reese and Karnovsky, 1967). The authors described the presence of specific and highly expressed tight junctions in brain endothelial cells (BECs) when compared to other endothelia (e.g. blood vessels of the skeletal muscle). The presence of tight junctions between brain endothelium greatly limits the paracellular flux of solutes and leads to the formation of polarised cells with distinct luminal and abluminal membrane compartments (Obermeier, Verma and Ransohoff, 2016).

Later research developed the understanding of the influence of other CNS cell types on modulating BBB function (Janzer and Raff, 1987; Hayashi *et al.*, 1997; Pardridge, 1999). However, it was not until 2001 when the first Stroke Progress Review Group meeting of the National Institute of Neurological Disorders and Stroke of the National Institutes of Health took place, that the concept of the NVU was emphasised (Iadecola, 2017). Traditionally, scientists had considered CNS and vascular cells as distinct entities, but the view of the scientific community evolved into an interactive relationship between CNS-resident cells and vascular cells, which is known now as the NVU. One evidence of this change on perspective is the exponential increased on publication citing NVU from 2001 until today (Iadecola, 2017).

.

1.4. Composition of the neurovascular unit

The composition of the NVU varies significantly across the cerebrovascular network (Figure 1.1). Morphologically, pial arterioles are larger vessels whose endothelium is separated from several layers of smooth muscle cells (SMCs) by a prominent elastic basal lamina (Figure 1.1). Functionally, pial arterioles are surrounded by perivascular nerves, which play an important role in controlling vessel contraction and blood flow (Iadecola, 2017). Pial arterioles branch into smaller arterioles that penetrate the brain parenchyma. In comparison to pial arterioles, penetrating arterioles are composed by a thinner layer of SMCs. Penetrating arterioles are surrounded by the perivascular space which contains perivascular macrophages, pial cells, and mast cells among others, as well as nerve and collagen fibres (Figure 1.1.). Emerging data suggest that the perivascular space contributes to the immune surveillance of the CNS as well as a waste clearance (Abbott *et al.*, 2018). When arterioles penetrate deeper into the brain, the perivascular space is minimised. These intra-parenchyma arterioles are characterised by having a single or discontinuous layer of SMCs and they are surrounded by astrocyte end-feet. Finally, cerebral capillaries are characterised by the presence of pericytes, which replaces SMCs, covering approximately 30% of the endothelial cells surface. Capillaries show a 90% coverage by the astrocytic end-feet surrounding (Iadecola, 2017).

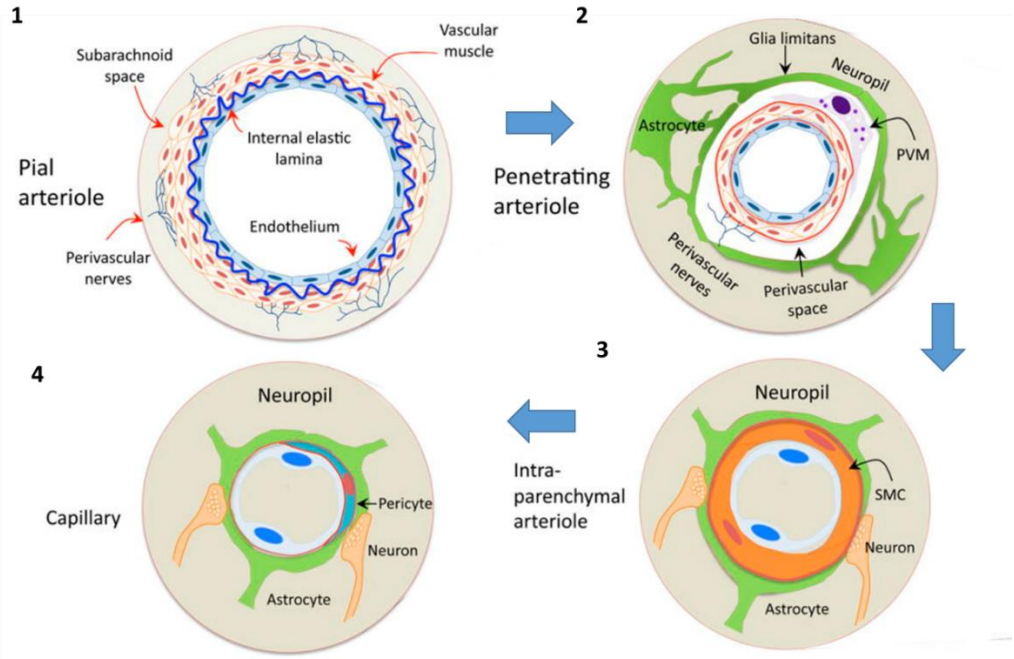

Figure 2.1. Schematic representation of the neurovascular unit at the different parts of the cerebrovascular network. The neurovascular unit changes across the vascular tree: 1) pial arteriole, 2) penetrating arterioles, 3) intra-parenchymal arteriole and 4) capillary. Abbreviations: PVM, perivascular macrophage; SMC, smooth muscle cell. Image adapted from (Iadecola, 2017)

Understanding the characteristics of the NVU cellular components as well as their inter-cellular interactions is a highly attractive topic in the field of vascular biology both in physiology and pathology. In this project, there will be a special focus on the NVU in brain microvessels, with specific focus given to the endothelium at the capillary level.

1.4.1. Astrocytes

Astrocytes are polarised glial cells, whose morphology varies depending of their location and association with other cell types (Reichenbach and Wolburg, 2013). Astrocytes are known to interact between blood vessels and neighbouring cells. Indeed, astrocyte-end feet is shown to surround the microvessel wall and express high levels of specialised proteins that are relevant for the induction of BBB properties (Abbott, Rönnbäck and Hansson, 2006).

Strong *in vitro* data have demonstrated that astrocytes are necessary to promote the BBB phenotype on BECs. Indeed, astrocytes can induce the formation of tight junctions in BECs, hence increasing their trans-endothelial resistance (TEER) (for a review see (Abbott, 2002)). Mechanistically, astrocytes are able to secrete specific soluble factors which include transforming growth factor-β (TGFβ), glial-derived neurotrophic factor (GDFN) or basic fibroblast growth factor (bFGF) among others (Abbott, Rönnbäck and Hansson, 2006). These factors have already been demonstrated to promote BBB tightness. For instance, supplementation of BEC culture media with GDFN resulted in a dose-dependent increase of the endothelial TEER (Igarashi *et al.*, 1999).

Astrocyte-end feet contain high levels of specific proteins such as Aquaporin 4 (AQP4), dystroclycan and dystrophin (Tait *et al.*, 2008; Keaney and Campbell, 2015). The complex dystroglycan-dystrophin interacts with agrin to facilitate anchoring of the astrocyte-end feet to the vascular basal membrane. Agrin is located in brain microvessels and its expression is increased in areas of BBB tightening (Abbott, Rönnbäck and Hansson, 2006; Obermeier, Verma and Ransohoff, 2016).

Astrocytes act as an interface between neurons and blood vessels by releasing signals to control blood flow in response to neuronal changes. Therefore, astrocytes can modulate the contraction and dilation of SMCs on larger arterioles and pericytes in capillaries. Indeed, it has been shown that astrocytes can detect the level of glutamate-dependent synaptic activity, then signal to adjacent cerebral vessels, causing vasodilation by a mechanism involving prostanoids (Zonta *et al.*, 2003; Abbott, Rönnbäck and Hansson, 2006).

1.4.2. Pericytes

Pericytes are specialised perivascular cells with mesodermal origin and are located within the capillary wall. Pericytes are embedded via integrins within a basal membrane (BM) shared with BEC. Furthermore, pericytes´ elongated processes cover the capillary walls (Winkler, Bell and Zlokovic, 2011). Interestingly, the CNS vasculature presents a higher pericyte coverage than peripheral organs. Indeed, pericytes are present in the microvessels at a 1:3 ratio with respect to BECs (Shepro and Morel, 1993). Endothelial cell to pericytes ratio is reported to be lower in other vascular beds such as that in liver (10:1) or skeletal muscle (100:1) (Zhang *et al.*, 2020). Occasionally, pericytes and BECs show also direct contact via the formation of peg-and-socket structures containing cell-to-cell junction and gap proteins, structures that are considered to contribute to the transfer of nutrients, metabolites, secondary messengers and ions between the two cell types (Bobbie *et al.*, 2010; Winkler, Bell and Zlokovic, 2011)

Pericyte recruitment to endothelium during development is a critical step for vessel formation and involves different signalling pathways such as platelet-derived growth factor B (PDGF-B) and TGF-β (Winkler, Bell and Zlokovic, 2011). Different studies have shown that homozygous deletion of *Pdgfb* gene or some genes involved in TGF-β signalling were embryonic lethal in mice and resulted in a loss of CNS pericytes (Levéen *et al.*, 1994; Gaengel *et al.*, 2009; Bell *et al.*, 2010). In adulthood, pericytes are also critical in regulating BBB integrity and this has been demonstrated using mouse models with deletions in the *pdgf-B* signalling. For instance, aged pericyte-deficient mice show reduced levels of important endothelial tight junctions such as occludin and claudin-5 (Bell *et al.*, 2010).

It is suggested that pericytes are also important for processing toxic cellular compounds. Indeed, deposition of blood-borne macromolecules (e.g. fibrin or plasmin)

is considered to be responsible for the BBB breakdown and CNS impairment shown in aged pericyte-deficient mice (Chen and Strickland, 1997; Paul, Strickland and Melchor, 2007; Winkler *et al.*, 2012).

Pericytes are contractile cells, which can modulate the blood flow and capillary diameter. Recent studies have shown that pericytes express receptors for vasoactive mediators such as endothelin-1, angiotensin II or vasopressin (Winkler, Bell and Zlokovic, 2011). This is in accordance with an organotypic slice study where stimulation with different neurotransmitters resulted in dilation and contraction of pericytes (Peppiatt *et al.*, 2006). However, validation of these results *in vivo* is controversial and need further investigation (Bell *et al.*, 2010; Fernández-Klett *et al.*, 2010).

Research into pericyte biology is still needed as there are other pericyte functions that are not well understood such as their involvement in T cell transmigration to the CNS (Zachariah and Cyster, 2010). Pericytes and BECs share a common BM and the secretion of extracellular matrix (ECM) proteins as well as metalloproteinases might play an important role in T cell transmigration.

1.4.3. Basal or basement membrane

The BM is an extracellular structure composed by a multitude of ECM proteins the main types being collagen type IV, nidogen, laminin and heparan sulfate proteoglycans (HSPGs). In the brain, the BM is mainly associated with blood vessels and both number and localisation of BMs is dependent on the associated vessel type (Figure 1.1) (Lecrux and Hamel, 2011). Larger arterioles present several layers of BM between SMCs whereas the BM of capillaries is thinner. Capillary BMs are classified into two different types of BMs: an endothelial BM and a parenchymal BM. BECs are the primary

source for ECM proteins for the endothelial BM, whereas astrocytes secrete most of the ECM proteins comprising the parenchymal BM (Table 1.2). These two membranes are observed to be physically separated by pericytes but appear as one BM in areas with no pericytes (Yao, 2019).

Table 1.2. List of the source of several laminin isoforms and their location in the endothelial and/or parenchymal BM.

	Astrocytes	***Endothelial Cells***	***Pericytes***
Endothelial BM	-	Laminin-411 and -511	Laminin α4 and α5
Parenchymal BM	Laminin-211	-	Laminin α4 and α5

Abbreviations: BM, basal membrane

In physiology, the BM serves as a supporting structure for the NVU cells and facilitates the assembly of the different components (Xu, Nirwane and Yao, 2019). Under pathological conditions, the BM is considered to act as a physical barrier to protect the CNS from the peripheral circulation. This function is supported by the experimental measurement of the migration of T cells into the CNS. Interestingly, the time for T cell migration across endothelium is shorter than the time needed to cross the BM (Bartholomäus *et al.*, 2009; Yao, 2019). Furthermore, the cells of the NVU express specific receptors that can be activated by the ECM proteins composing the BM. Genetic deletion of ECM receptors or ECM proteins in animal models have demonstrated how important these proteins are for BBB integrity (Chen *et al.*, 2013; Nirwane and Yao, 2019; Yao, 2019). Furthermore, changes in ECM proteins have been observed in both haemorrhagic and ischemic stroke (Yao, 2019).

1.4.4. Brain endothelial cells

BECs are the main cellular component of the cerebral blood vessels. For arteries and venules, dozens of BECs may attach to form the vessel lumen, whereas a single BEC is sufficient to cover the lumen for capillaries (Aird, 2007). BECs are organised continuously across the capillary whereas other peripheral endothelial cells might be fenestrated or form a discontinuous layer too. Indeed, BECs are typically morphologically different from endothelial cells of other peripheral organs (Table 1.3) (Potente and Mäkinen, 2017). For instance, transmission EM (TEM) experiments reported that BECs have a lower number of pinocytotic vesicles. Indeed, BECs have a low rate of transcytosis, which results in a reduced vesicle-mediated transport of molecules (Obermeier, Verma and Ransohoff, 2016). Furthermore, the number and volume of mitochondria is higher in BECs than other endothelial cells, which suggest BECs have an increased metabolic activity.

Table 1.3. Organ-specific characteristics of endothelial cells.

Type of EC	Location	Organisation	Enriched Molecular Markers	Reference
BBB ECs	CNS	Continuous	MFSD2A GLUT1, SLC7A5, others	(Ben-Zvi *et al.*, 2014; Obermeier, Verma and Ransohoff, 2016)
Myocardial capillaries	Heart	Continuous	CD36, LPL, PPARγ	(Potente and Mäkinen, 2017)
Liver sinusoidal ECs	Liver	Discontinuous	Stabilin 1, Stabilin 2, HGF, WNT2	(Aird, 2007)
Glomerular ECs	Kidney	Fenestrated	ND	(Aird, 2007; Potente and Mäkinen, 2017)

Abbreviations: EC, endothelial cells; Mol., molecular; BBB, Blood-brain barrier; CNS, central nervous system; MFSD2A, sodium-dependent lysophosphatidylcholine symporter 1; GLUT1, glucose transporter 1; ; SLC7A5, solute carrier family 7 member 5; PL, lipoprotein lipase; PPARγ, peroxisome proliferator-activated receptor-γ; ; HGF, hepatocyte growth factor; WNT2, WNT family member 2; ND, no determined.

One of the most characteristic functions of BEC monolayers is the formation of a physical barrier that prevents the passive diffusion of larger molecules into the CNS via the arrangement of specialised tight junctions (TJs) (Figure 1.2). The TJ complex contributes to limit the diffusion of polar solutes through the paracellular space as well as preventing larger macromolecules from penetrating into the brain. Tight junctional proteins are classified into claudins, occludin and junctional adhesion molecules (JAM) (Abbott, Adjanie A.K. Patabendige, *et al.*, 2010).

- **Claudins** are essential proteins for the formation of the tight junctions and there are at least 24 different claudins (Redzic, 2011). These proteins are composed by four membrane-spanning regions, two extracellular loops and two cytoplasmic domains, a short N-terminal sequence and a long C-terminal sequence. BECs highly express claudin-5 but also claudin-3 and claudin-12 (Redzic, 2011). Indeed, genetic ablation of claudin-5 resulted in brain damage causing early death in a murine model (Nitta *et al.*, 2003).
- **Occludin** is a protein responsible for sealing the tight junctions thereby leading to high TEER between the blood and the CNS parenchyma (Bamforth *et al.*, 1999; Li *et al.*, 2005). This protein is formed by two extracellular loops, four trans-membrane domains and three cytoplasmic domains; the cytoplasmic domains include one intracellular short turn, N-terminal domain and a 150 amino-acids long carboxyl (C-) -terminal domain (Redzic, 2011). This latest domain is associated with *zonula occludens* proteins (ZO-1, ZO-2 and ZO-3), a set of regulatory proteins that anchor occludin to the cytoskeleton (Li *et al.*, 2005).
- **JAMs** are members of the immunoglobulin-like family and include JAM-A, B and C in BECs (Redzic, 2011). These proteins have a membrane-spanning domain, an extracellular domain, an extracellular N-terminus and a cytoplasmic C-terminus.

JAMs form homophilic and heterophilic interactions with other JAMs at the intracellular junction of BECs to contribute to the structure of tight junctions (Bazzoni *et al.*, 2000; Redzic, 2011).

BECs also form **adherens junctions** to support a tight endothelial monolayer. This complex is formed by cadherins and associated proteins into which actin filaments are linked (Redzic, 2011). Vascular endothelial (VE) cadherin (cadherin-5) and cadherin-10 are the two main cadherins expressed in BECs. However, recent evidence suggests cadherin-10 is highly expressed in BECs with BBB properties whereas VE-cadherin expression is subtler. Indeed, VE-cadherin, but not cadherin-10, was highly expressed in microvessels with loose BBB properties isolated from glioblastoma (Williams *et al.*, 2005). Cadherins associate with a series of catenins, proteins that include β, α, χ and p120 at the BBB, which are believed to associate with actin filaments to support endothelial adherens junctions (Meng and Takeichi, 2009; Redzic, 2011).

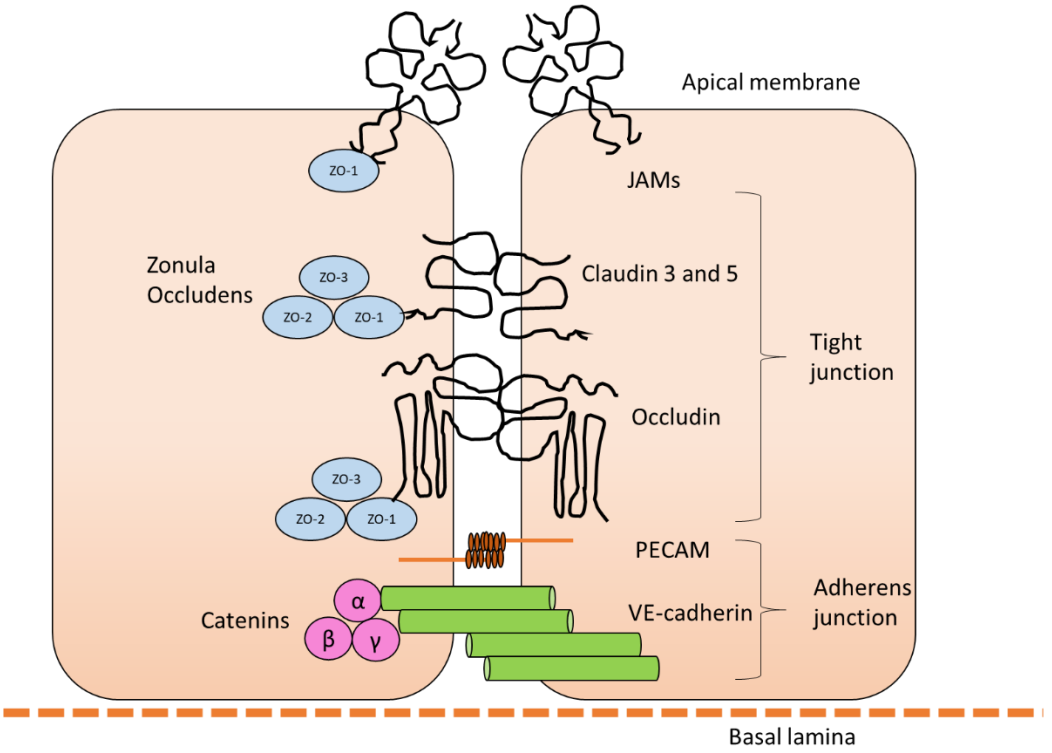

Figure 1.2. Structure of brain endothelial cell tight junctions. Tight junctional proteins include occludin and claudins (mostly 3 and 5). These proteins are linked to scaffolding proteins *zonula occludens* (ZO-1, ZO-2 and ZO-3), which are associated to the actin cytoskeleton. Junctional adhesion molecules (JAMs) are believed to contribute to leukocyte cell-adhesion. Adherens junctions are crucial for the formation of tight junctions. Drawn by David Roig via adaptation from Abbott, Adjanie A K Patabendige, *et al.*, 2010

Apart from the formation of tight junctions and adherens junctions to prevent the passive diffusion of solutes into the CNS, BECs also express specific transporters on the luminal side, some facilitating the passage of their substrates onto the brain parenchyma whereas other transporters function as neuroprotective and detoxifying barriers to blood-borne agents (Mahringer and Fricker, 2016). These latter proteins are known as ABC transporters and are composed by a large superfamily of membrane proteins of approximately 48 different types. BECs are known to predominately express *P*-glycoprotein (P-gp) but also multidrug resistance-related proteins MRPs and the breast cancer resistance protein (BCRP) (Redzic, 2011). Although these transporters play a

protective role in physiology, treatment of CNS disorders is limited due to the exclusion of many therapeutic molecules by ABC transporters (Mahringer and Fricker, 2016).

To accommodate the nutritional needs of the CNS, BECs express specific and high levels of membrane proteins such as specific solute carriers to transport ions, nutrient and macromolecules to the CNS (Redzic, 2011). Indeed, BECs highly express the ubiquitous glucose transporter 1 (GLUT-1) to efficiently provide glucose to the CNS cells. Indeed, a transcriptomic study on the rat BBB showed GLUT-1 as one of the most abundant transcripts in the brain microvessels (Enerson and Drewes, 2006).

Genetic and epigenetic modifications leading to changes in the function of the NVU as discussed above have been associated with a multitude of neurological disorders. In the next section, the implications of BBB dysfunction in CNS pathologies will be addressed.

1.5. The blood-brain barrier as a central feature in neurological disorders

Growing evidence suggest that the loss of BBB normal function is a key step in the development and progression of several CNS disorders (Daneman, 2012). This BBB dysfunction is predominantly characterised by the loss of BBB integrity (e.g. BBB breakdown or increased paracellular permeability) (Jiang *et al.*, 2018) or the increased of immune cell extravasation into the CNS (Lopes Pinheiro *et al.*, 2016). Other phenotypes might include effects on membrane transporter function or expression (e.g. GLUT-1 deficiency) or loss of pericytes**.** However, the causes and consequences of the disruption in the BBB are poorly understood, although knowledge of the contribution of the BBB to the pathogenesis of neurodegenerative disorders appears to differ widely (Table 1.4). Here, loss of BBB integrity and leukocyte transmigration will be described in more detail.

Table 1.4. List of characteristics involved in blood-brain barrier dysfunction in three different neurodegenerative disorders.

CNS pathologies	Alzheimer´s Disease	Parkinson´s Disease	Multiple Sclerosis
Genetic Mutations*	*APP, PSEN1, PSEN2, APOE, SOR1 etc*	*IRRK2, MDR1*	-
BBB breakdown			
Blood-derived molecules deposition	*Yes (Fibrin, thrombin, IgG)*	Yes (Fibrin, IgG, hemosiderin)	Yes (Fibrin in developing lesions)
RBC extravasation	*Yes*	Yes	ND
Reduced tight juntions proteins	*Yes*	Yes	Yes
Cell degeneration			
Loss of pericytes	Yes (confirmed by EM and IHC)	ND	No and role still poorly understood
Dysregulated EC transporters	Yes (GLUT1, LRP1)	Possibly LRP1	
Alteration BM	Yes	Yes	Yes
Inflammation			
Immune cell extravasation	Yes	Yes	Yes
Pro-inflammatory cytokines	Yes (IL-1, IL-6,TNFα)	Yes (IL-1, IL-6, TNFα, TGF-β)	Yes (IL-17,IL-22, IL-1, IL-12, TNFα, IFNy)
References	(Horwood and Davies, 1994; Deane *et al.*, 2004; Cullen, Kócsi and Stone, 2005; Zipser *et al.*, 2007; Cortes-Canteli *et al.*, 2010; Su, Bai and Zhang, 2016; Sweeney *et al.*, 2019)	(Sui *et al.*, 2014; Gray and Woulfe, 2015; Pienaar *et al.*, 2015; Alam *et al.*, 2016; Lee *et al.*, 2019; Sweeney *et al.*, 2019)	(Kirk *et al.*, 2003; Cramer *et al.*, 2015; Lopes Pinheiro *et al.*, 2016; Wang *et al.*, 2018; Rivera, Hinrichsen and Silva, 2019; Sweeney *et al.*, 2019)

*Detection of inherited genetic mutations with associated cerebrovascular pathology within the specific neurodegenerative disorder

Abbreviations: CNS, central nervous system; BBB, blood-brain barrier; RBC, red-blood cell; EC, endothelial cells; BM, basal membrane; APP, PSEN1, PSEN2, APOE, SOR IRRK2, MDR1; IgG, inmunoglobin G; EM, electron microscopy; IHC, immunohistochemistry; GLUT1, glucose transporter 1; IL-, interleukin; TNFα, tumour necrosis alpha; TGF-β, transforming growth factor beta; IFNy, interferon gamma; ND, not determined.

1.5.1. Loss of BBB integrity in CNS pathologies

As summarised in Table 1.4, the loss of integrity of the BBB is a common feature of neurodegenerative disorders, including Alzheimer's disease (Zlokovic, 2005), MS (Minagar and Alexander, 2003), Parkinson's disease (Cabezas *et al.*, 2014) but also acute neurological pathologies such as stroke or traumatic brain injury (Sweeney *et al.*, 2019). Indeed, BBB disruption is critical for assessing the outcome of both ischemic and haemorrhagic stroke (Jiang *et al.*, 2018). Increased permeability and disruption of TJs promote the extravasation of blood-borne molecules and cells to the brain (Jiang *et al.*, 2018). For instance, Knowland and colleagues observed decreased endothelial occludin and ZO-1 staining in a mouse model of stroke, and this deregulated expression correlated with parenchymal depositions of IgG (Knowland *et al.*, 2014).

This vascular "leakiness" observed in BBB dysfunction can be exacerbated by pro-inflammatory CNS modulators such a tumour necrosis factor alpha (TNFα) in MS, lipopolysaccharide (LPS) in systemic infection or β-amyloid in Alzheimer's disease, which can alter the formation or/and organization of TJ proteins, thereby increasing paracellular permeability (Varatharaj and Galea, 2017). Indeed, the organisation of occludin appears discontinuous in MS lesions when compared to normal appearing white matter (NAWM). Additionally, loss of BBB integrity exacerbates infiltration by leukocytes, which further damage the brain tissue (Anrather and Iadecola, 2016).

1.5.2. Leukocyte transmigration into the brain in CNS pathologies

As described above, inflammation induced either locally or via systemic cytokines and chemokines, is a principal component of many neurodegenerative conditions. For example, analysis of post-mortem MS tissue revealed CNS-immune infiltrates as well as BBB disruption as an early feature of MS (Alvarez, Cayrol and Prat, 2011). Although most studies in MS have researched BBB alterations after immune infiltration, growing evidence suggests that there is an earlier immune cell-independent disruption of the BBB. In fact, conversion of optic neuritis to MS has been predicted according to the state of the general BBB disruption in the CNS (Cramer *et al.*, 2015). In the following paragraph, the mechanism of migration of immune cells into the CNS and the importance of the BBB in this process will be discussed.

During neuroinflammation, peripheral immune cells are able to cross the BBB and enter into the brain parenchyma following a multistep process (Figure 1.3.) (Lopes Pinheiro *et al.*, 2016). For example, experimental autoimmune encephalomyelitis (EAE) in mice (a widely accepted model for demyelinating diseases) develops only after immune cells enter the CNS (Engelhardt and Ransohoff, 2012), whereas no clinical signs develop if immune cells are only detected in the perivascular or leptomeningeal spaces (Toft-Hansen *et al.*, 2006; Engelhardt and Ransohoff, 2012).

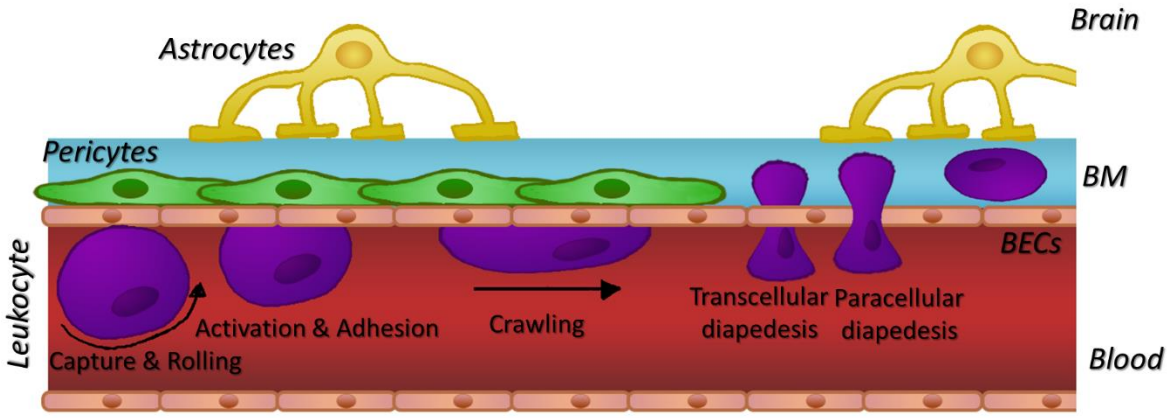

Figure 1.3 Cascade of steps for lymphocyte diapedesis to brain parenchyma. Transendothelial migration of lymphocytes is a multistep process that involves capture, rolling, activation, adhesion and crawling of the leukocyte. Then, leukocyte might migrate either across the brain endothelial cells (BECs), transcellular diapedesis, or between BECs, paracellular diapedesis. Once in the basal membrane (BM), leukocytes need to cross both the BM and astrocytes to enter to the brain. Figure drawn by David Roig-Carles.

Before blood-derived leukocytes migrate into the brain, it is hypothesised that a first wave of immune cells reach the CNS via the choroid plexus, although the molecular mechanisms are poorly understood (for a review see Lopes Pinheiro *et al.*, 2016). After overcoming the BCSFB, these immune cells can release pro-inflammatory mediators such as cytokines, which can diffuse into the brain parenchyma and activate the brain endothelium thereby facilitating the entry of blood-derived leukocyte into the CNS as a second wave of immune cell migration. These events promote the formation of inflammatory lesions typically observed in MS (Raine CS1, Cannella B, Duijvestijn AM, 1990; Reboldi *et al.*, 2009b).

Blood-derived leukocyte migration into the brain is a specialised and multistep process that involve the rolling, capture, activation, arrest, crawling and finally diapedesis across the brain endothelium (Engelhardt and Ransohoff, 2012) (Figure 1.4.). The process of leukocyte migration across brain endothelium is tightly controlled by the expression

and release of specific proteins from both endothelial cells and leukocytes (Muller, 2011) (Table 1.5).

Table 1.5. Proteins involved in the process of transmigration of leukocytes into the brain and their cell of origin.

	Capture & Rolling	Activation & Adhesion	Crawling	Transcellular Diapedesis	Paracellular Diapedesis
Endothelial cell	E-selectin P-selectin	ICAM-1 VCAM-1	ICAM-1 ICAM-2	ICAM-1 JAM-A Caveolin-1 PECAM CD99	VE-cadherin JAM-A ESAM PECAM1 CD99
Leukocyte	PSGL1 L-selectin	LFA-1 VLA-4	LFA-1 VLA-4 MAC-1	LFA-1 CD49 PECAM CD99	LFA-1 PECAM1 CD99

Abbreviations: ICAM-1, intercellular adhesion molecule 1; VCAM-1, vascular cell adhesion molecules 1; ICAM-2, intercellular adhesion molecule 2; JAM-A, junctional adhesion molecule A; PECAM, platelet endothelial cell adhesion molecule; VE-cadherin, vascular endothelial cadherin; ESAM; endothelial cell-selective adhesion molecule; PSGL1, P-selectin glycoprotein 1; LFA-1, lymphocyte function-associated antigen1; very late activation antigen 4; MAC-1, macrophage-1 antigen.

- **Capture & rolling**. When a neuro-antigen-specific T cell crosses one of the brain barriers and recognise its specific antigen on the antigen-presenting cells (APCs), it will initiate the inflammatory cascade responsible for the expression of inflammatory mediators that will support the rolling and capture of immune cells (Bartholomäus *et al.*, 2009). Mechanistically, up-regulation of endothelial molecules of the selectin family interact with leukocyte-expressing selectin-ligand proteins, such as P-selectin glycoprotein ligand-1 (PSGL-1) to facilitate T cell tethering and rolling (Battistini, 2003). Indeed, PSGL-1 expression is increased in CD4+ T cells in MS when compared to healthy donor's cells (Bahbouhi *et al.*, 2009). PSGL-1-mediated T cell interactions promote leukocyte tethering, slowing the movement of leukocyte along

the vascular wall and promoting them to roll onto the endothelium (Engelhardt and Ransohoff, 2012).

- **Activation.** Brain endothelia release chemokines that can bind to lymphocytes and activate them. In EAE, encephalitogenic T cell adhesion to brain meningeal microvessels is dependent on G protein-coupled receptor (GPCR) signalling. Therefore, chemokines or eicosanoids need to be up-regulated in order to enhance T cell adhesion to BEC. The concentration of chemokines CCL19 and CCL21 are increased in the cerebral endothelium of EAE mice, thus mediating firm Th1 adhesion to frozen section of brain microvessels *in situ* (Alt, Laschinger and Engelhardt, 2002). However, many other chemokines and their respective receptors have been proposed to mediate lymphocyte adhesion to brain microvessels (McCandless *et al.*, 2006; Shulman *et al.*, 2012).

- **Adhesion.** Chemokine activation is also important because it promotes clustering of leukocyte integrins as well as conformational changes in the integrin proteins that increase their affinity and avidity for ligands on brain endothelium (Engelhardt and Ransohoff, 2012). Integrin activation is a crucial step for lymphocyte arrest to CNS microvessels, which occurs at the post-capillary venule. Increased levels of integrin α4β1 (VLA-4) and αLβ2 (LFA-1) ligands, vascular cell adhesion molecule 1 (VCAM1) and intercellular cell adhesion molecule -1 (ICAM1) respectively, are found to be up-regulated in the endothelium of the BBB as well as in the BCSFB in EAE (Engelhardt and Ransohoff, 2012). LFA-1 positive cells are observed to locate and accumulate on ICAM1+ venules of MS and EAE tissue samples, whereas VLA-4+ cells not always are found to accumulate in MS lesions but they do in EAE samples

(Sobel, Mitchell and Fondren, 1990; Peterson *et al.*, 2002). Additionally, VCAM1 and ICAM1 role in modulating T cell adhesion to inflamed endothelium has been extensively proven *in vitro* using both static and flow-based assays (Steiner *et al.*, 2010).

- **Crawling.** Sophisticated *in vitro* time lapse imaging techniques in a system that include shear stress and primary mouse endothelial cell showed ICAM1/2-LFA-1 was the only interaction needed for T cells to polarize and crawl across the endothelium (Steiner *et al.*, 2010). T cells can crawl against the flow in order to find an optimal site for diapedesis. Crawling long distances is also a unique characteristic to CNS endothelium, since it has been shown that leukocytes crawl significantly lower distances on peripheral endothelium compared to CNS endothelium (Engelhardt and Ransohoff, 2012).

- **Diapedesis.** In the absence of ICAM1 and ICAM2, fewer T cells migrate across the endothelium (Steiner *et al.*, 2010). These results suggested that T cell diapedesis may be both dependent and independent of ICAM1/2-mediated crawling. In peripheral tissues, T cells prefer to migrate via a paracellular route, which involves crossing between endothelial junctions. Because the TJs of the BECs are tighter and more complex than those in the periphery, transcellular diapedesis is hypothesised to be the preferential route of lymphocyte entry into the brain because this does not require TJ opening and re-sealing (Engelhardt and Ransohoff, 2012). The route of T cell entry is dependent on ICAM1 levels. ICAM1-deficient endothelial cells lead to paracellular diapedesis whereas high levels of ICAM1 result in transcellular diapedesis across a pore formed in a single endothelial cell (Steiner *et al.*, 2010; Engelhardt and

Ransohoff, 2012). Recently evidence suggest that activated leukocyte cell adhesion molecule (ALCAM) also plays a role in leukocyte extravasation (Cayrol *et al.*, 2008). ALCAM can form homophile interactions between endothelial and leukocyte-expressing ALCAM (Marchetti and Engelhardt, 2020). Recently, Engelhardt´s group demonstrated ALCAM play a lesser role in T cell transmigration and shown antibody-inhibition of ALCAM reduced CD4+ Th1 but not Th17 under unstimulated condition. No effect was observed under inflammatory conditions. In contract, it was observed inhibition of ALCAM highly affected the different steps of monocyte extravasation (arrest, adhesion, crawling and diapedesis) *in vitro* (Lyck *et al.*, 2017). These processes are still poorly understood and more research is needed to elucidate which molecules decide the fate of the leukocytes.

- **Migration across the BM.** Finally, T cells migrate through the endothelial basal membrane. It has been shown that leukocytes prefer to cross in areas of basal membrane where there is laminin isoform α4 and little or none of laminin α5 (Wu *et al.*, 2009). Metalloproteinases (MMPs) are endopeptidases whose function is to degrade different proteins of the extracellular matrix (Cui, Hu and Khalil, 2017). MMPs are constitutively expressed or induced by pro-inflammatory cytokines and chemokines in leukocytes and CNS-resident cells. In EAE, it was shown that CD4+ T cell migrating to the brain parenchyma required of focal activation of MMP2 and MMP9 (Agrawal *et al.*, 2006). Mechanistically, MMP2 and MMP9 has been shown to cleave dystroglycan, an astrocyte-feet-specific receptor, to facilitate leukocyte infiltration through the parenchymal BM (Agrawal *et al.*, 2006). Chemokines are substrates of MMPs and help to activate and modify the extracellular environment to enhance T cell transmigration into the brain (Engelhardt and Ransohoff, 2012).

Furthermore, disruption of the BM has been linked to NVU dysfunction resulting in an increase of leukocyte extravasation to the brain parenchyma, which is a main hallmark of many neuroinflammatory pathologies (Obermeier, Verma and Ransohoff, 2016).

As described in the sections above, pro-inflammatory modulators can induce the activation of BECs that lead to different aspects of BBB dysfunction. Activated signalling pathways affect gene expression via canonical routes (e.g. transcription factors) or non-canonical routes, which may include epigenetic changes (Wei *et al.*, 2017). In the next section, the definition and role of non-coding RNAs (ncRNAs) in modulating BBB function in inflammation will be discussed.

1.6. Non-coding RNAs and cell function

Sequencing of the human genome revealed that although two thirds of the genome is transcribed, less than 2% encodes for regions of protein-coding genes (Djebali *et al.*, 2012). Part of that "extra DNA" plays an important role in the maintenance of DNA structures as well as modulating the expression of messenger RNA (mRNA) (e.g. promoters, transcription binding sites and enhancer regions) (Wang and Chang, 2011). However, the rest of non-coding DNA was traditionally considered "junk DNA". For the past two decades, many studies have showed evidence that a significant proportion of this "junk DNA" is transcribed into ncRNAs. Therefore, currently, it is estimated that around 80% of the genome is functional and that 62% is transcribed into ncRNAs. NcRNAs can be classified as housekeeping and regulatory ncRNAs. This last subtype can further be divided based on their size including long ncRNA (lncRNAs) (>200 nucleotides) or short ncRNA (<200 nucleotides) (Matera, Terns and Terns, 2007). Short ncRNAs include small

inhibitory RNAs (siRNAs), P-element Induced WImpy testis (PIWI)-interacting RNAs (piRNAs) and microRNAs (miRNAs) (for a review see (Wei *et al.*, 2017)).

MiRNAs have widely been described to regulate cell function both in physiology and pathology. In fact, many miRNAs are deregulated in disease, hence, understanding miRNAs is a promising approach for novel therapeutic target development. This project will focus in miRNAs and a more extensive description is given in the following sections.

1.7. Discovery and definition of miRNAs

MiRNAs are highly conserved, small ncRNA oligonucleotides of 20-25 nucleotides in length that influence gene expression by post-transcriptional regulation at the mRNA level (R W Carthew and Sontheimer, 2009). Although miRNAs constitute a novel field of research, the discovery of the first miRNA, *lin-4*, was achieved in 1993 by two independent groups studying the nematode *Caenorhabditis elegans* (*C. elegans*) (Lee, Feinbaum and Ambros, 1993; Wightman, Ha and Ruvkun, 1993). A few years later, another miRNA, *let-7*, was identified in *C. elegans* (Pasquinelli *et al.*, 2000; Reinhart *et al.*, 2000). However, the concept of miRNAs was not fully addressed until the early 2000s, when three independent research groups contributed to define miRNAs as a novel and abundant group of gene expression regulators (Lagos-Quintana *et al.*, 2001; Lau *et al.*, 2001; Lee and Ambros, 2001). From those early discoveries up to today, the field of miRNAs has grown exponentially.

According to the miRNA database (miRbase, www.mirbase.org) more than 2,500 miRNAs have been annotated in the human genome (release March 2018) (Kozomara, Birgaoanu and Griffiths-Jones, 2019). MiRNAs play a crucial role in regulating many physiological functions, which include cell cycle, cell development, differentiation and

apoptosis as well as contributing to the progression and regulation of diseases in various model organisms and in humans (Friedman and Jones, 2009).

1.8. MicroRNA biogenesis

In humans, miRNA genes are defined to be either intergenic (between two genes) and/or within genes, currently described as either intronic or exonic (Griffiths-Jones *et al.*, 2006). The majority of miRNAs follow a similar canonical biogenesis pathway, but there are exemptions in which the process differs at some point (non-canonical pathway) (Graves and Zeng, 2012).

In the canonical pathway, the host miRNA gene is transcribed by RNA polymerase II (Pol II) into the primary miRNA transcript (pri-miRNA) following transcriptional mechanisms, which are similar to the ones used for protein-coding mRNAs. Pri-miRNAs are large RNAs that contain at least one hairpin structure and are capped, spliced and polyadenylated (Han *et al.*, 2004) (Figure .4).

In the nucleus, the process to convert the structure of a pri-miRNA into a mature miRNA requires two endonuclease processing steps (Richard W. Carthew and Sontheimer, 2009) Firstly, the microprocessor complex, which includes the nuclear enzyme DROSHA (Rnase III type endonuclease) and a RNA-binding protein DGCR8 (DiGeorge syndrome critical region gene 8), recognizes and cleaves the pri-miRNA releasing the stem-loop precursor (pre-miRNA) from the flanking pri-miRNA sequences (Gregory *et al.*, 2004; Han *et al.*, 2004). The pre-miRNA is a 70 nucleotide structure that is actively transported to the cytoplasm by the nuclear export receptor exportin-5 (Yi *et al.*, 2003; Kim, 2004; Lund *et al.*, 2004).

In the cytoplasm, exportin-5 releases the cargo into the cytosol (Bohnsack, Czaplinski and Gorlich, 2004; Lund *et al.*, 2004). Subsequently, the pre-miRNA is cleaved to generate the double stranded mature miRNA. This process is carried out by the DICER protein (RNase III endonuclease enzyme) associated with TAR RNA-binding protein (TRBP) and releasing the terminal loop of the pre-miRNA (Bernstein *et al.*, 2001). The double stranded miRNA is loaded into the RISC. The RISC complex is formed by the union of DICER with the AGO proteins mediated by TRBP. The loading of the miRNA duplex into the AGO protein is process requiring high energy that alters AGO conformation. When AGO protein returns to its original form, one strand of the miRNA (passenger strand) duplex exits the complex leaving the mature single stranded miRNA (this mature microRNA can be either the -5p or -3p strand, also known as leading strand). This mature miRNA is now guided to its target mRNA through base pairing (Zealy *et al.*, 2017). Then, together with the RISC complex recruit proteins of the TNRC6 family in order to mediate the post-transcriptional regulation of the target gene (Jabri, 2005; Parker and Sheth, 2007).

Fully mature miRNAs can regulate gene expression and affect both physiological and pathological signalling pathways (Bartel, 2009). In the following section, the molecular functions of miRNAs will be discussed in detail.

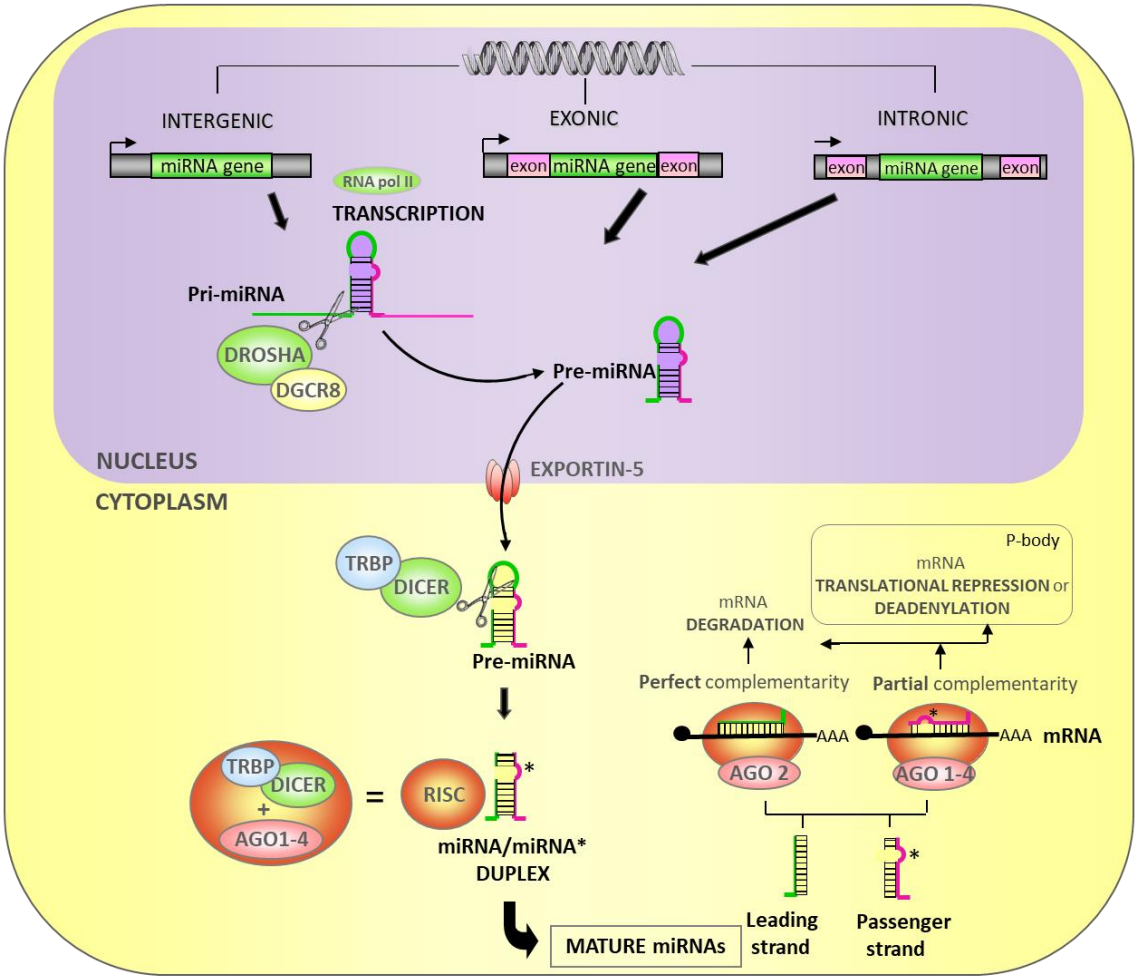

Figure 1.4.Overview of microRNA biogenesis. MicroRNA biogenesis starts in the nucleus (purple) with the transcription of either intergenic, intronic or exonic microRNA gene by the RNA pol II to generate pri-miRNAs or mirtrons. Subsequently, they are cleaved by DROSHA-DGCR8 complex and the spliceasome respectively in order to produce a 60-80 nucleotide pre-microRNA. This pre-microRNA is transported to the cytoplasm by association with exportin-5 protein. Then, the hairpin structure of the pre-microRNA is cleaved by the complex TRBP-DICER. The resulting mature microRNA (either the leading or passenger strand) is loaded into the RISC complex to regulate post-transcriptional gene expression by either inhibiting the translation or degrading the target mRNA. Figure adapted from Roig-Carles *et al.*, 2017

1.9. Molecular mechanisms underlying miRNA function

MiRNAs are powerful and complex regulators of gene expression at the post-transcriptional level (Berezikov, 2011). The interaction between mRNAs and miRNAs is very versatile and one single miRNA can potentially target hundreds of different mRNAs. Similarly, one mRNA can be regulated by many miRNAs. Indeed, it has been suggested that 60% of all protein-coding genes can be regulated by miRNAs in mammals (Friedman and Jones, 2009).

The microRNA-mRNA duplex is mediated by the binding of the miRNA´s seeding region to the complementary sequence at the 3' untranslated region (3'UTR) following Watson-Crick base pairing (Saugstad, 2010). The complementarity between the seed region and the sequence in the target mRNA influences the mechanism by which gene silencing occurs (Bartel, 2018). In humans, perfect matching is not required for microRNA/mRNA interactions. Mismatched base pairing leads to different methods of mRNA repression. The supporting proteins recruited by AGO complexes can induce deadenylation of the target mRNA to decrease the length of the poly(A) tail, which results in mRNA destabilization. Furthermore, miRNAs can also interfere with protein expression by inhibiting the initiation step for mRNA translation (Filipowicz, Bhattacharyya and Sonenberg, 2008).

The cellular environment as well as the subcellular location of the RISC-miRNA complex can influence the mechanism of action of miRNA-modulated mRNA expression. Recent evidence suggest that the RISC complex accumulates inside P-bodies, which are cytoplasmic foci enriched with mRNA-degradation´s machinery and depleted of ribosomes (O'Brien *et al.*, 2018) (Figure 1.9). In the nucleus, the RISC-miRNA

complex is enriched in the area where there is an active transcription of DNA whereas in the cytoplasm, the RISC-miRNA complex can diffuse across the cell, most likely associated to microtubules, and be located to different compartments where mRNA silencing is required (e.g. polysomes, endoplasmic reticulum) (O'Brien *et al.*, 2018)

In addition, mRNA turnover is highly variable within mammalian cells and can range from minutes to days, making it difficult to predict miRNA targets. MiRNA decay is specific of both cell conditions and the type of miRNA, which can be used by the cell in order to modulate the levels of gene expression (Bartel, 2018).

1.10. MiRNAs in inflammation and vascular function

As mentioned above, miRNAs play a crucial role both in the physiological and pathological function of any cellular type (Friedman *et al.*, 2009). In the context of inflammation, both pro- and anti-inflammatory stimulus have been reported to alter mRNA and protein levels (Garavelli, De Rosa and de Candia, 2018). These changes can be partially explained by alterations at the miRNA profile. Therefore, many publications have sought to identify, understand and characterise the role of miRNAs in modulating inflammation in different areas, which include immune cell differentiation, cancer progression or vascular function among others (Garavelli, De Rosa and de Candia, 2018).

1.10.1. MiRNA regulation of the immune cell response

MiRNA levels are highly variable in different T lymphocyte subpopulations and contribute to normal functioning of immune cells (Neilson *et al.*, 2007). The fate of T cells can be controlled by a single miRNA or a cluster of miRNAs based on the cellular context. For example, the levels of the miRNA-17-92 family are increased upon viral

infection weighting the balance of T cells toward a more pronounced pro-inflammatory type-1 phenotype, which results in increased interferon gamma production (IFNγ) (Ventura *et al.*, 2008).

1.10.2. MiRNAs in vascular function

Chronic inflammation is associated with many vascular pathologies in which the presence of a pro-inflammatory stimulus increase the permeability to soluble compounds and migration of leukocytes across the blood vessel, which ultimately contribute to the inflammatory response (Reijerkerk *et al.*, 2013). For example, miRNA-126 expression is down-regulated in atherosclerosis leading to increased levels of its direct target, VCAM1. Increased levels of VCAM1 are directly related with the number of leukocytes that adhere to the endothelium (Harris *et al.*, 2008). Down-regulation of miRNA-21 in VSMCs has been shown to be associated with decreased proliferation and increased apoptosis *in vitro* (Ruirui *et al.*, 2007). Therefore, miRNA-21 is proposed to be a regulator of the formation of the neointimal lesion, a process in which VSMCs migrate primary in the tunica intima leading to increased blood vessel thickness (Ruirui *et al.*, 2007). .

In the context of the BBB, miRNAs have recently emerged as potent modulators of the BBB phenotype, including paracellular permeability and extravasation of immune cells into the CNS, both in physiological and inflammatory conditions. MiRNAs have also shown to play a role in astrocytic function. Some of the best characterized miRNAs at the BBB include miRNA-155, miRNA-126 or miRNA-146a (Table 1.6).

Table 1.6. Summary of inflammation-regulated miRNAs involved in modulating BBB function.

miRNAs	Cell type	Expression in inflammation	Phenotype	mRNA targets	Reference
miRNA-155-5p	BECs	↑	↑paracellular permeability	CLDN1, SYND, ANXA2, DOCK1	(MA. Lopez-Ramirez *et al.*, 2014)
	BECs	↑	↑T cell adhesion	ND	(Cerutti *et al.*, 2016)
	Astrocytes	↑	↑ MMP3 expression	ND	(Korotkov *et al.*, 2018)
miRNA-126-3p ***miRNA-126-5p***	BECs	↓	↑T cell adhesion	VCAM1, E-selectin	(Cerutti *et al.*, 2017)
miRNA-146a-5p	BECs	↑	↓T cell adhesion	RhoA NFAT5	(Wu, *et al.*, 2015)
	Astrocytes	↑	↓MMP and TIMPs expression	ND	(Broekaart *et al.*, 2020)
miRNA-146b-5p	BECs	↑	ND	ND	(MA. Lopez-Ramirez *et al.*, 2016)

Abbreviations: BECs, brain endothelial cells; MMP, metalloproteinases; TIMP, tissue inhibitor of metalloproteinases; ND, not determined; CLDN1, claudin 1; SDCBP, syntentin-1; ANXA2, annexin A2; DOCK1, dedicator of cytokinesis 1; VCAM1, vascular cell-adhesion molecule 1; NFAT5, nuclear factor of activated T cells 5.

In general, a single miRNA can regulate inflammation differently depending on the cell type or tissue in which the miRNA is expressed. For instance, miRNA-155-5p is well-known for being a pleiotropic miRNA that regulates inflammation on three different biological functions, which include immunity, cancer biology and vascular function (Faraoni *et al.*, 2009). Specifically, miRNA-155-5p has been described to be a negative regulator of BBB function (Lopez-Ramirez *et al.*, 2014), up-regulated in neurological disorders and modulator of leukocyte adhesion . Therefore, the study of miRNA-155 is of utmost interest to understand novel mechanisms of cell function during inflammation at the BBB.

1.11. MicroRNA-155: a pleiotropic microRNA

MiRNA-155 is a well-characterised miRNA, which is originated from the non-coding gene B-cell Integration Cluster (BIC or also known as MIR155HG) (for a review see Elton, Selemon, Elton, & Parinandi, 2013). Human MIR155HG is located on chromosome 21q21 in humans and includes three exons that comprise a 13 Kb region (Tam, 2001). Pre-MiRNA-155 sequence is conserved among different species (Figure 1.5.A). Cleavage of pre-miRNA-155 produces two single-stranded miRNA-155 (miRNA-155-5p and miRNA-155-3p). Human and murine mature miRNA-155-5p differs only by one nucleotide (Figure 1.5.B). Experimentally, human miRNA-155 origin was validated in HL-60 leukaemia cells (Kasashima, Nakamura and Kozu, 2004) and confirmed by a different group.

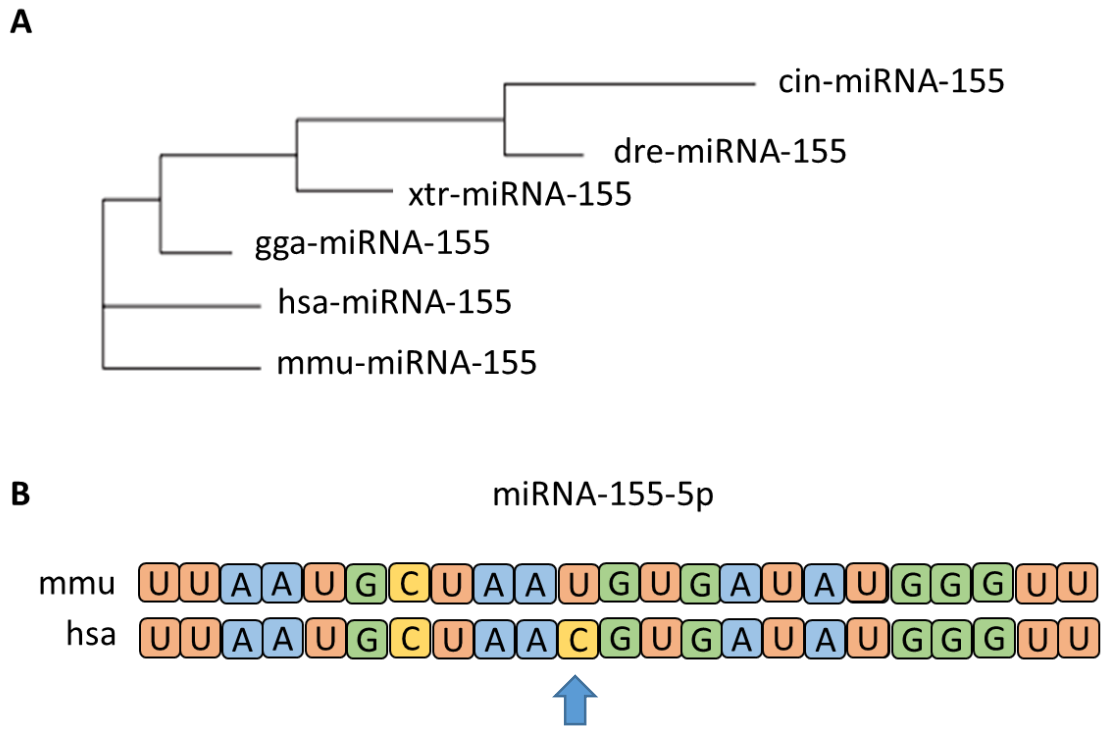

Figure 1.5. Species conservation of miRNA-155. (A) Phylogenetic tree on the sequence alignment of miRNA-155 loop sequence among 6 species that included *homo sapiens* (hsa), mus musculus (mmu), *gallus gallu* (gga), *xenopus tropicalis* (xtr), *dario rerio* (dre) and *ciona intestinalis* (cin). **(B)** Sequence alignment for mature miRNA-155-5p from human and mouse species. Adapted from Vigorito, Kohlhaas, Lu, & Leyland, 2013.

1.11.1. MicroRNA-155 in health and disease

Cleaved pre-miRNA products can differ in expression and function across cell types (Choo *et al.*, 2014). MiRNA-155-5p is expressed by many tissues and different cell types although relative expression is the highest in the thymus (Martin *et al.*, 2006). On the other hand, miRNA-155-3p expression is reported to be between 20 to 200 fold lower than microRNA-155-5p in a number of human tissues such as thymus or spleen (Elton *et al.*, 2013). Therefore, the biological relevance of miRNA-155-3p is currently uncertain (Elton, Sansom and Martin, 2010). Recent reports showed that stimulation with Toll-like receptor 7 (TLR7) agonist on human plasmacytoid dendritic cells (PDCs) increased levels of both miRNA-155-5p and -3p. Transcription kinetics studies demonstrated that miRNA-155-3p up-regulation occurred at an earlier stage than miRNA-155-5p,

suggesting a cooperative role among both variants (Zhou *et al.*, 2010). Therefore, more research is needed to understand how the two strands of miRNA-155 interact. However, for the rest of this work, the focus will be given to miRNA-155-5p, which will hereafter be referred to as miRNA-155 unless otherwise specified. As mentioned above, miRNA-155 has been related to a wide range of physiological and pathological conditions such as cancer, vascular pathologies, inflammatory and autoimmune diseases (e.g. rheumatoid arthritis) (Faraoni *et al.*, 2009). In the following section, focus will be given to miRNA-155 function in modulating inflammation.

1.11.2. MiRNA-155 in inflammation

Expression of miRNA-155 has been widely investigated in both *in vitro* and *in vivo* models of inflammation. Different studies relate inflammatory cytokines, such as TNFα or IFNγ, and inflammatory mediators (e.g. LPS) as modulators of miRNA-155 expression in monocytes, macrophages and various different endothelial cells (O'Connell *et al.*, 2007; Sun *et al.*, 2012). Under basal conditions, levels of miRNA-155 are relatively low but upon stimulation with TNFα, miRNA-155 levels are highly up-regulated and sustained over time in brain endothelial cells, macrophages and monocytes (Faraoni *et al.*, 2009; Lopez-Ramirez *et al.*, 2013). Furthermore, activation of pro-inflammatory pathways such as nuclear factor (NF)-κB and activator protein-1 (AP-1) promote miRNA-155 expression (Gatto *et al.*, 2008; Yin *et al.*, 2008). Thompson *et al.*, demonstrated the presence of a promoter at 178 nucleotides up-stream of MIR155HG transcription start site that is regulated by NF-kB p50/65 (Thompson, Vardinogiannis and Gilmore, 2013).

The first clinical evidence of miRNA-155 association with a neurological disorder such as MS was demonstrated in 2009 by miRNA profiling of active MS lesions (Junker *et al.*, 2009). The role of miRNA-155 in MS pathology is complex and diverse regarding the context of the BBB function, peripheral inflammation and CNS injury (**¡Error! No s e encuentra el origen de la referencia.**1.12.) (Wu and Chen, 2016). MiRNA-155 is crucial for DC to acquire a mature phenotype and helps producing inflammatory Th1 and Th17 cells. Th1 and Th17 cells (two distinct subsets of T cells) regulate the adaptive immune response (Chalovich and Eisenberg, 2005). In EAE, Th1-derived cytokines promote Th17 invasion into the CNS (Reboldi *et al.*, 2009a). Furthermore, miRNA-155 promotes production of cytokines such as IFNy and IL-6. Low levels of these cytokines in miRNA-155 KO mice leads to decreased levels of inflammation in the periphery and CNS, which results in a less severe phenotype in EAE (Wu and Chen, 2016). In addition to this, miRNA-155 has been found to supress anti-inflammatory proteins such as suppressor of cytokine signalling (SOCS1) in microglia (Wu and Chen, 2016). The suppression of SOCS1 leads to an increased production of inflammatory cytokines. Moreover, miRNA-155 targets SMAD2, CEBPbeta and CD206 thereby increasing phagocytic activity in microglia (Wu and Chen, 2016). MiRNA-155 has also been reported to be increased in CSF samples from patients with Alzheimer's disease (Alexandrov *et al.*, 2012) and regulate Japanese Encephalitis Virus-Induced Inflammatory (Thounaojam *et al.*, 2014).

Due to many observations such as those described above, miRNA-155 is classically defined as a pro-inflammatory miRNA. However, recent studies point to a dual role for microRNA-155 in inflammation. A negative feedback role was described for miRNA-155 in human vein umbilical cell line (HUVECs) (Wu *et al.*, 2014). After exposure to TNFα, expression of miRNA-155 was increased and led to decreased levels

of VCAM1, which reduced the pro-inflammatory status of the endothelial cells (Wu *et al.*, 2014).

1.11.3. MiRNA-155 in BBB function

As mentioned above, miRNA-155 has been recently proposed to be a negative regulator of BBB function and levels changed in inflammation (MA. Lopez-Ramirez *et al.*, 2014). *In vitro*, inflammatory cytokines were shown to induce a rapid increase of miRNA-155 in the human brain endothelial cell line hCMEC/D3. *Ex vivo*, miRNA-155 was demonstrated to be expressed at the NVU of MS patients as well as in EAE microvessels. In fact, it was reported that loss of miRNA-155 in EAE mice resulted in a reduced extravasation of systemic tracers into the CNS. Furthermore, it was shown that overexpression of miRNA-155 led to disorganisation of TJs and loss of focal adhesion plaques in hCEMC/D3 cells. Lopez-Ramirez identified that miRNA-155 was targeting molecules involved in focal adhesion components (DOCK1 and sysntenin-1) as well as in cell-cell complexes molecules (Annexin-2 and claudin-1).

In addition, miRNA-155 has also been shown to contribute to shear-resistant leukocyte adhesion to human brain endothelium *in vitro* (Cerutti *et al.*, 2016). In this study, overexpression of miRNA-155 led to an increase of monocyte and T cell line firm adhesion to human brain endothelium *in vitro*. Overexpression of miRNA-155 also led to an increase of BEC-adhesion molecules such as VCAM1 and ICAM1. These two molecules play a pivotal role in regulating leukocyte extravasation across the BBB. However, neither VCAM1 nor ICAM1 are direct targets of miRNA-155, therefore, the molecular pathway by which miRNA-155 stimulates the up-regulation of these two adhesion molecules is still unknown. A recent study has also identified a novel axis of

communication between the gut and the brain, where LPS released by the gut microbiome is transported via the systemic circulation to the brain and activated BECs through the NFκB pathway and expression of miRNA-155 (Alexandrov *et al.*, 2019).

In vivo miRNA-155 inhibition using antisense oligonucleotides was shown to promote recovery after experimental mouse stroke mediated by up-regulation of one of its target proteins, Rheb (Pena-Philippides *et al.*, 2016). In this study, *in vivo* loss of miRNA-155 led to improved preservation of tight junctions in cerebral microvessels following stroke as assessed by EM techniques and by ZO-1 staining.

Altogether, these studies indicated that inhibition of miRNA-155 may prove a suitable molecular target for supporting cerebral microvascular function in neuroinflammation. Furthermore, miRNAs can be transported and delivered from one cell to another via extracellular vesicles (EVs), which can then modulate the functions of the recipient cells (Howitt and Hill, 2016). In this next section, there will be a focus on understanding what EVs are, what role they play in inflammation and BBB and how their miRNA cargos are involved in this process.

1.12. Extracellular Vesicles: a novel mechanism of cell-to-cell communication

Cells can modify the cellular functions of neighbouring or distant cells by paracrine and endocrine pathways involving the secretion of soluble proteins, circulating RNAs and recently discovered EVs amongst other mechanisms (Ciardiello *et al.*, 2016; Nava and Llorens, 2016). This last pathway is especially interesting because of the ability of EVs to carry both proteins and RNA species in order to regulate the function of recipient cells both in physiological and pathological conditions (Bayraktar, Van

Roosbroeck and Calin, 2017). Therefore, the study of EVs as carriers of RNA species such as miRNAs and how these affect cell function has become a very attractive research topic in the last years.

EV is a generic term used to describe a type of cellular-secreted carrier, unable to replicate, that are formed by a lipid bilayer (Théry *et al.*, 2018). Secretion of EVs is believed to be a highly evolutionary-conserved process (Colombo, Raposo and Théry, 2014). In fact, both prokaryotic and eukaryote organisms are considered to secrete EVs into the extracellular environment. In mammals, EVs have been isolated from diverse body fluids, including blood (Crawford, 1971), urine, saliva, breastmilk, amniotic fluid, ascites, cerebrospinal fluid, bile and semen (Stegmayr and Ronquist, 1982).

1.13. Historical point of view of EV research

From a historical perspective, several independent studies reported evidence of EVs for the first time. For instance, Chargaff and West first reported the presence of "extracellular particles" derived from platelet cells in normal plasma (Chargaff and West, 1946). In 1967, these platelet-derived particles were named "platelet dust" by Wolf (Wolf, 1967). Furthermore, Anderson observed matrix vesicles during bone calcification (Anderson, 1969). In the following decade, independent research groups reported the presence of EVs in different contexts (Yáñez-Mó *et al.*, 2015). Different studies showed that EVs were released by rectal adenoma microvillus cells. EV were also isolated and detected in seminal plasma (Crawford, 1971). It was also reported the presence of virus-like particles in human cell culture supernatants, later termed proteasomes (Benz and Moses, 1974). In this decade, membrane fragments originating from tumours were identified in the extracellular space (Taylor, Homesley and Doellgast, 1980).

Until the 1980s, EVs were always described as membrane-enclosed vesicles generated by outward budding of the plasma membrane. In 1983, however, Harding *et al.* described a novel pathway of EV secretion when studying the differentiation of reticulocytes into erythrocytes (Harding, Heuser and Stahl, 1983). It was reported that reticulocytes released transferrin receptor (TfR) into the extracellular medium. Immunogold-labelled EM techniques were employed to follow the fate of endocytosed receptors across the cell. The authors found TfR to be enclosed within multivesicular endosomes and observed that the highest concentration of the staining was carried in small vesicles (~50nm) inside the multivesicular endosomes (Harding, Heuser and Stahl, 1983). These studies promoted the idea that EVs were a mechanism by which cells removed cytosolic content. Furthermore, the discovery of an endosomal biogenesis pathway allowed researchers to differentiate shedding EVs from endosomal EVs, or also referred as exosomes (Yáñez-Mó *et al.*, 2015).

Research into EVs was considered not very relevant until the late 1990's, when two publications highlighted the interesting role of EVs in the context of immunology (Raposo *et al.*, 1996; Zitvogel *et al.*, 1998). In 1996, Raposo *et al.*, demonstrated that exosomes derived from Epstein-Barr virus (EBV)-transformed B cells were enriched in major histocompatibility complex (MHC) class II molecules. The specific endosomal origin of these vesicles was also shown by EM, ruling out the criticisms that these vesicles could have been generated by outward budding of the plasma membrane. In addition to these findings, Zitvogel *et al.* reported the suppression of growth of established tumours *in vivo* after treatment with human dendritic cell-derived exosomes (Zitvogel *et al.*, 1998). Several studies investigated the role of traditional plasma membrane-derived vesicles, also referred as microvesicles, derived from immune cells (platelets, monocytes and neutrophils) to regulate blood coagulation (Sims *et al.*, 1989; Satta *et al.*, 1994). There

were also reports of vehicles for the transfer of inflammatory mediators (Mesri and Altieri, 1998; Gasser and Schifferli, 2004), regulation of lipid metabolism (Sims *et al.*, 1989) as well as on regulating the endothelial or immune cell survival (Baj-Krzyworzeka *et al.*, 2002). However, none of these studies using microvesicles reported the presence of MHC complexes.

In 2007, Valadi revolutionised the field of EVs when they demonstrated that exosomes carry both mRNA and miRNAs (Valadi *et al.*, 2007). The authors isolated exosomes from a mouse mast cell line (MC/9) and identified the presence of mouse-specific mRNAs. Subsequently, exposure of human mast cells (HMC-1) to mouse exosomes led to the production of mouse-specific proteins, indicating the transfer of mouse mRNA and its ability to be translated by the human recipient cells (Valadi *et al.*, 2007). Moreover, presence of nucleic acids in microvesicles and their role in regulating gene expression in recipient cells was also demonstrated in tumour- and stem cell-derived EVs (Baj-Krzyworzeka *et al.*, 2006; Ratajczak *et al.*, 2006). Thanks to these studies, exosomes and other EVs have emerged as carriers of genetic information with the potential to regulate the gene expression in targeted cells.

1.14. Classification of extracellular vesicles

EV are classified according to both size and biogenesis which includes exosomes, microvesicles (also referred to as ectosome or shedding microvesicles) or apoptotic bodies (Kalra, Drummen and Mathivanan, 2016) (Figure 1.6). Exosomes are generated as a result of the inward budding of the endosomal membrane, with a size range between 30 to 150 nm. Microvesicles are generated from outward budding of the plasma membrane and have a broader size range, ranging from 100 nm up to 1 µm. Apoptotic

bodies are also secreted following outward budding of the plasma membrane as a mechanism of cell debris removal during the later stages of apoptosis. Apoptotic bodies include vesicles from 40 up to 5000 nm (van der Pol *et al.*, 2012). Interestingly, research in apoptotic bodies is normally independent of both exosome and microvesicle research. In fact, many publications define EVs as the mixture of both exosomes and microvesicles. This heterogeneous population of EVs is a consequence of the lack of specific markers and optimised methods of isolation to distinguish exosomes from microvesicles. In contrast, the experimental conditions as well as the wide size distribution of apoptotic bodies result in a higher confidence for researchers to claim a reasonable purity of this type of vesicles (Kalra, Drummen and Mathivanan, 2016).

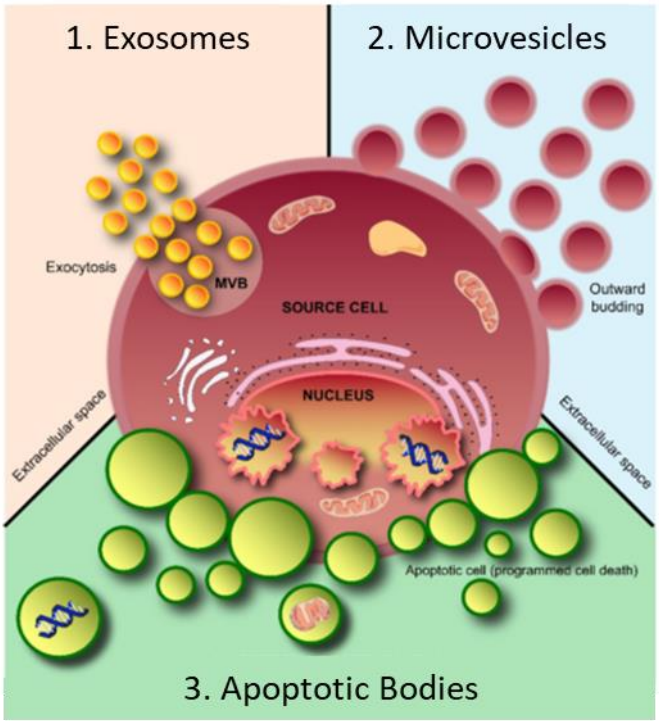

Figure 1.6. Schematic representation of extracellular vesicle subtypes. Cells can secrete mainly three types of vesicles. Exosomes (30-150nm) are originated by exocytosis, microvesicles (100-1000nm) are the result of outward budding of the plasma membrane and apoptotic bodies (50-5000nm) are secreted in the later stages of a cell dying through apoptosis to facilitate the removal of cell debris. Figure adapted from Kalra, Drummen and Mathivanan, 2016

Although the classification of EV is clear, the nomenclature of the different EVs have been highly heterogenous. For this reason, in 2018 the International Society of Extracellular Vesicle (ISEV) released a report containing the criteria regarding EV research (MISEV2018, Théry *et al.*, 2018). The authors recommended that researchers employ classical EV nomenclature (exosomes, microvesicles or apoptotic bodies) only if they could demonstrate specific cellular origin by, for example, showing stable expression of specific markers of subcellular origin. Théry *et al.*, proposed an alternative nomenclature that is based on the different characteristics of the EV population (Table 1.7). If the minimum information to describe the nature of the EV population is not reached, it is recommended that authors refer to the sample preparation as extracellular particles (EPs) (Théry *et al.*, 2018).

Table 1.7. List of different nomenclatures for extracellular vesicles.

Property for classification	Examples		
Size	Small EVs <200 nm	Large EVs >200nm	
Density	Low	Middle	High
Biochemical composition	CD63+/CD81+- EVs	Annexin A5-stained EVs	etc
Cell or condition of origin	Podocyte EVs	Hypoxic EVs	Large oncosomes
Not a EV	Extracellular Particles		

Abbreviations: EVs, extracellular vesicles. Information taken from (Théry *et al.*, 2018)

1.15. Biogenesis of the different subpopulations of EVs

In this section, the processes involved in the generation of exosomes and microvesicles, the two types of EVs under investigation in the present study, will be described.

Exosomes are vesicles originated in a complex and regulated process, (Figure 1.7). Briefly, the secreting cell generates an early endosome, which is transported through the cytoplasm. Subsequently, there is a maturation from early endosomes to late endosomes. Then, changes in the endosomal microenvironment lead to alterations of the endosomal membrane resulting in the creation of intraluminal vesicles (ILV) within the endosome or, now referred to as multivesicular bodies (MVB). The reorganisation of the endosomal membrane into tetraspanins-enriched microdomains, involving both CD9 and CD63, initiates the process of ILV formation (Pols and Klumperman, 2009). The ILVs contained within the MVB carry part of the cytosol containing proteins and nucleic acids, which are believed to be selectively sorted into the ILVs. The MVB have now two different fates. It has been demonstrated that MVB normally fuse with lysosomes to mediate the degradation of their cargo. The MVBs trafficking and fusion to the plasma membrane is a coordinated and highly regulated mechanism. Both tetraspanins and small RAB GRPases have been described to regulate MVBs fusion to the plasma membrane (Savina, Vidal and Colombo, 2002; Simons and Raposo, 2009; Ostrowski *et al.*, 2010). However, different *in vitro* studies revealed the different role and expression of some RAB proteins, suggesting the existence of alternate pathways for MVB fusion to the plasma membrane. When MVBs fuse with the plasma membrane of the cell and they release the cargo into the extracellular millennia and with it the ILV or now renamed exosomes (Zhang *et al.*, 2016).

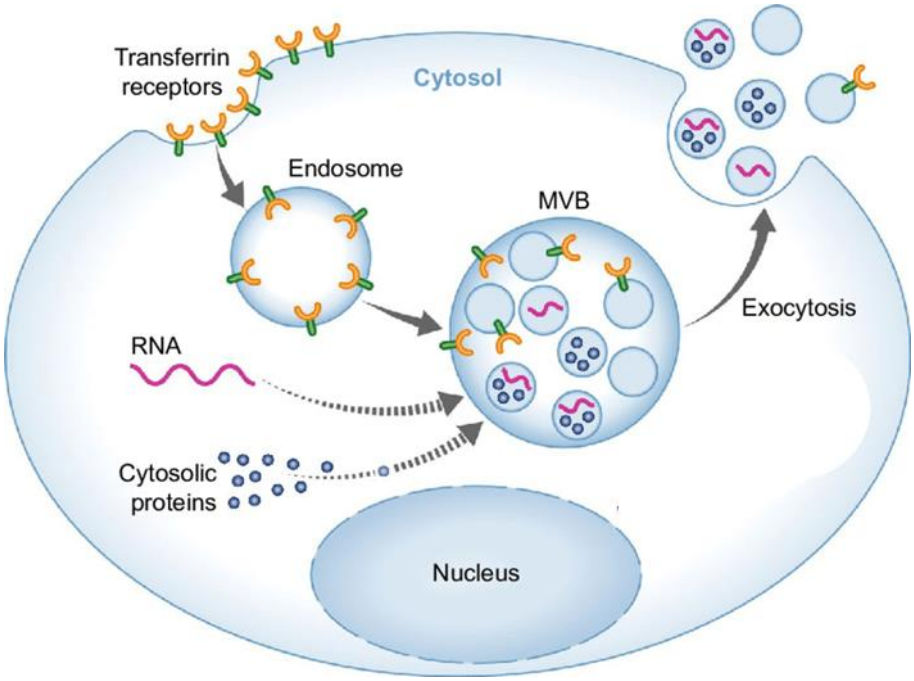

Figure 1.7. Schematic representation of exosome biogenesis. Multivesicular bodies (MVB) are created from inward budding of the palsma membrane. Intraluminal vesicles within the MVB carried cytosolic proteins and RNAs. MVBs secrete their content to the extracellular space via exocytosis. Figure adapted from (Schorey *et al.*, 2015)

On the other hand, microvesicles follow a different pathway. Direct outward budding of the plasma membrane is required for the formation of microvesicles and is controlled by mechanisms different to those involved in the exosome´s biogenesis (Cocucci, Racchetti and Meldolesi, 2009). The process of microvesicle production includes the rearrangement of the cytoskeleton and membrane constituents as well as the recruitment of membrane abscission-related proteins (Kalra, Drummen and Mathivanan, 2016). Cytosolic proteins and genetic material (e.g. mRNA and miRNAs) are loaded into the lumen of the future vesicle as a consequence of the gradual disassembly of the cytoskeleton. Budding and pinching off can occur by different mechanisms. On one hand, a high activity of translocases can produce a high enough plasma membrane curvature capable of turning the plasma membrane onto itself (Devaux *et al.*, 2008). However, it is considered that the excision of the plasma membrane is generally mediated by proteins

that promote cytoskeleton contraction, which involves the activation of actin-myosin-dependent contraction and pinching off the microvesicles (Filipowicz, Bhattacharyya and Sonenberg, 2008).

Despite the investigation and elucidation of these mechanisms controlling microvesicle biogenesis, the reality is that this process is more dynamic and complex and can be altered depending on the cell type and conditions by which is activated (Kalra, Drummen and Mathivanan, 2016).

1.16. Handling and isolation of extracellular vesicles

EVs can be detected in a wide range of biofluids as well as in cell culture conditioned media (CCM). Therefore, handling the source of EVs prior to their isolation is of utmost importance to ensure reproducibility and the highest EV purity. Thus, the MISEV2018 proposed certain recommendations regarding preparation and collection of EVs (Théry *et al.*, 2018).

CCM was described as the most common source for the isolation of EVs (Théry *et al.*, 2018). It is important that cell culture conditions (passage, seeding density, cell type) are identified for the EV-producing cells and that cultured cells are screened routinely for contamination (e.g. mycoplasma) because this can affect EV release. In addition, authors are recommended to report the volume of CCM, number of dead cells as well as cell culture surface area. Furthermore, researchers should describe the type of serum, if at all, that is present in the CCM. Most cells are unable to survive in serum-free media and serum is known to contain EVs, therefore, it is important to deplete serum from EVs prior to their use for the isolation of EVs (Beninson and Fleshner, 2015). For this purpose, serum can be manually depleted using ultracentrifugation at 120,000 x g for at least 18 h, which was shown to efficiently eliminate the serum-associated EVs (van

Balkom *et al.*, 2013). Alternatively, commercially available EV-depleted serum can be purchased.

Once the source of EVs has properly been handled and collected, EVs can be isolated and purified. The isolation of EVs is a controversial topic because there is still no protocol that has reached worldwide use. This results in a lack of reproducibility of results across the different labs working on EVs. A survey carried out by ISEV interrogated the methods for isolating EVs across different research groups around the world (Gardiner, Vizio, *et al.*, 2016). Ultracentrifugation resulted to be the preferred method, although a high number of researchers also preferred to use a combination of methods (Gardiner, Vizio, *et al.*, 2016). Given that the selection of a protocol will influence the heterogeneity of the isolated EVs, it is important to take into account the different limitations and advantages that the available isolation methods offer.

1.16.1. Ultracentrifugation

The first method was developed due to the need to purify exosomes secreted from reticulocytes into cultured medium (Johnstone *et al.*, 1987), then adapted to isolate these vesicles from immune cells (Raposo *et al.*, 1996; Zitvogel *et al.*, 1998) (Figure 1.14). This protocol employs, first, a series of differential centrifugation steps with increasing speeds in order to remove bigger vesicles. Then, the remaining supernatant is centrifuged at higher speed (100,000 x g) allowing the sedimentation of smaller vesicles, both exosomes and small microvesicles. These differential centrifugation steps ruled out the possibility of artificially creating smaller vesicles from larger ones by applying high speed centrifugation straight to the raw sample. This method has been widely modified, by changing both speed and sedimentation times (Tauro *et al.*, 2012), in order to improve yields or influence the type of isolated EVs. Many studies have demonstrated the

functional activity of EVs isolated by ultracentrifugation (Witwer *et al.*, 2013). However, this protocol shows a low vesicle recovery as well as long experimental time. In addition, ultracentrifugation can isolate a wider size distribution of EV population as well as protein aggregates especially if the protocol is not optimized properly (Van Deun *et al.*, 2014).

1.16.2. Precipitation-based methods

The lack of a universal isolation method as well as the technical problems associated with the traditional protocols were found to be an opportunity for many companies to develop quick and user-friendly kits for EV isolation (Witwer *et al.*, 2013). ExoQuick (System Bioscience), Total Exosome Isolation (Invitrogen), miRCURY Exosome Isolation (Exiqon but now merged with Qiagen) are some examples of available products in the market (Winter *et al.*, 2009).

Most of these commercial kits are based on a volume-excluding polymer, such as poly ethylene glycol (PEG), dextrans or polyvinyls. PEG is a non-toxic and non-denaturing water-soluble synthetic polymer that has been previously used as a method of plant virus isolation and protein complexes (Rider, Hurwitz and Meckes, 2016). Briefly, the biofluid (cell culture medium, urine, plasma, saliva etc.) is mixed with a specific volume of the precipitation buffer containing PEG. The mixture is incubated from 1 h and can be extended overnight at 4ºC. The incubation is followed by a low-speed centrifugation to pellet the EV's and remove the PEG. The precipitation is the result of the retraction of solvent by the polymer resulting in a concentration of biological materials until its solubility is reached and precipitation occurs (Umezu *et al.*, 2012).

These methods have become popular due to their minimal experimental requirements and easy to perform. Furthermore, a high concentration of isolated vesicles has been reported, however, they might precipitate soluble and aggregate proteins

together with the vesicles. The presence of bulked protein results in a decreased purity of the isolated EV population (Rider, Hurwitz and Meckes, 2016).

1.16.3. Size exclusion methods

Separation of EV based on the size and filtration through physical barriers may be achieved through the use of filters or chromatography. Usually, large particles can be removed through filtration across 0.8µm pore. If small vesicles are desired a filtration with 0.22 µm pore size will isolate both small MV and exosomes. However, protein contaminants are typical difficult to avoid, therefore, chromatography column presents an improved alternative for EV isolation. Column chromatography allows for sequential elution of EV size fractions from a single column (Witwer *et al.*, 2013). The most popular type of column chromoatography is qEV, which has been designed by IZON (Oxford, UK).

The qEV column isolates EVs in a process that typically takes less than 15 min, resulting in highly purified vesicles. Proteins and other contaminating molecules smaller than 75 nm enter the pores of the resin and are delayed in their passage through the column, eluting mainly in later fractions. However, EVs smaller than 75 nm in diameter also enter the resin and are delayed in their passage (Vogel *et al.*, 2016).

1.16.4. Other methods of isolation

EVs can be also isolated according to their density coefficient. Different methods used sucrose gradients to differ between high and low density EVs. After EVs have been separated in the gradient, they are usually washed and concentrated (e.g. ultracentrifugation). Iodixanol based density-gradient are an alternative to sucrose gradient and are reported to have a more accurate separate based on their buoyant density. On the other hand, some research group take advantage of common EV markers such as

CD63 or CD9 to isolate and enrich EVs that are carrying these markers using immunoaffinity assay. Furthermore, ultrafiltration has also been demonstrated to successfully isolated EVs from their source biofluid.

In conclusion, the selection of the isolation method is important and should be optimized empirically. Combination of different methods have been showed to improve the isolation EVs. Furthermore, technical details relevant to the isolation of EVs are very important to be recorded and reported in order to ensure reproducibility of experiments.

1.17. EVs in in inflammation and cerebrovascular function

The discovery of a role for EVs in intercellular communication has resulted in an exponential growth of EV research in the last decade. In fact, many publications have described the role of EVs as mediators of physiological conditions with an important role in the pathogenesis of many conditions (Kalra, Drummen and Mathivanan, 2016). EVs have been described as regulators of a wide range of diseases such as cancer (Ciardiello *et al.*, 2016), neurodegenerative conditions (Janas *et al.*, 2016), cardiovascular diseases (Osteikoetxea *et al.*, 2016) or inflammation (Momma, 2015). In this section, there will be a special focus on how EVs module inflammation and cerebrovascular function.

1.17.1. EVs in inflammation

In the context of inflammatory diseases, higher numbers of platelet-derived EVs were observed in patients with Crohns´ disease compared to healthy controls (Ardoin, Shanahan and Pisetsky, 2007). Similarly, endothelial, leukocyte and platelet EVs were shown to be increased in patients with progressive MS (Sáenz-Cuesta, Osorio-Querejeta and Otaegui, 2014).

EVs can stimulate the inflammatory response by carrying membrane-bound TNFα that interact with the acceptor cells (Olleros *et al.*, 2012). Furthermore, EVs have been shown to promote the production of pro-inflammatory cytokines such as TNFα, IL-6 and IL-8 (Withrow *et al.*, 2016). Additionally, EVs can trigger toll-like receptor 4, hence, promoting the inflammatory cascade (Abdollahi-Roodsaz *et al.*, 2007). Interestingly, EVs can also decreased the inflammatory response (for a review in the benefits of mesenchymal cell-derived EVs visit (Keshtkar, Azarpira and Ghahremani, 2018)).

1.17.2. EVs in cerebrovascular function

The first evidence of secretion of EVs by brain endothelia was reported in 2012 (Virgintino *et al.*, 2012). The authors observed an association of vesicles to the filopodia generated at the tip of endothelial cells from microvessels during brain development. The authors proposed that these vesicles might carry signalling molecules and, therefore may play a role in intercellular communication during vessel development (Virgintino *et al.*, 2012; András and Toborek, 2015). A year after, Haqqani *et al.*, published a method of EV isolation for the immortalized human brain microvascular endothelial cell line hCMEC/D3 (Haqqani *et al.*, 2013). The same study conducted a proteomic profile of hCMEC/D3-derived EVs and found that 58 proteins out of 65 described EV markers were expressed.

In the context of inflammation, brain endothelial-derived EVs regulate and mediate many pro-inflammatory processes (Figure 1.10) (András and Toborek, 2015; De Rivero Vaccari *et al.*, 2016). Indeed, inflammatory mediators such as cytokines (TNFα, IFN, IL1B) and LPS can activate BECs and, therefore significantly increase the release of EVs (Alexy *et al.*, 2014). Furthermore, EVs released after activation of BECs have been found to regulate both communication with another components of the NVU

(Yamamoto *et al.*, 2015) as well as vascular integrity of the endothelial monolayer (András and Toborek, 2015). Another study showed that EVs isolated from activated BEC transfer miRNAs to pericytes leading to an increase in vascular endothelial growth factor-B (VEGF-B) (Yamamoto *et al.*, 2015). VEGF-B is a ligand of VEGFR-1, which is a receptor expressed in both endothelial cells and pericytes. The up-regulation of VEGFR-1 has been linked to pericyte ablation and increased leaky endothelium (Cao *et al.*, 2010). Furthermore, EVs derived from activated BECs can modulate leukocyte and monocyte migration across the endothelium. In fact, a recent study suggested the transfer of claudin-5 from BECs to leukocytes through EVs (Paul *et al.*, 2016). Claudin-5 is incorporated in the leukocyte membrane helping the leukocyte to cross the endothelium between two BECs. Briefly, claudin-5 expressed in the leukocyte plasma membrane bridges with the endogenous endothelial claudin-5 leading to decreased tight junction integrity which promotes leukocyte extravasation (Paul *et al.*, 2016). A proteomic study of EV isolated from TNFα-activated hCMEC/D3 cells revealed that inflamed EVs carry pro-inflammatory proteins such as ICAM1 or VCAM1 (Dozio and Sanchez, 2017) (Figure 1.8). However, whether EVs derived from activated BECs can modulate neighbouring BECs is still largely unknown.

In addition to the role of endothelial-derived EVs, BBB function is also modulated by the action of inflamed-derived EV released by other cellular types (Sáenz-Cuesta, Osorio-Querejeta and Otaegui, 2014). For instance, activated T cells release EVs that can upregulate the levels of ICAM-1 in endothelial cells (Barry *et al.*, 1998). Astrocytes and neurons have been found to release EV containing both bGFG and VEGF (Proia *et al.*, 2008). However, the role of these EV on endothelium has not been described yet.

The role of plasma-derived EVs have been investigated in the context of neuroinflammation (Sáenz-Cuesta, Osorio-Querejeta and Otaegui, 2014). EV derived

from plasma of patients with MS were cultured with naïve hCMEC/D3 cells resulting in a decrease of electric cell-substrate impedance sensing as well as subcellular altered localization of ZO-1 and VE-Cadherin. The authors suggest that plasma-derived EV can affect BBB function and contribute to the progression of MS. In another study, EVs were purified from serum of LPS-challenged mice. Injection of these EVs into naïve mice induced neuroinflammation and leaky BBB (Li *et al.*, 2018). However, it is still not clear whether a type of EVs or combination of many types (e.g. platelet-, endothelial- or leukocyte-derived EVs) were responsible of the phenotypes observed in those articles. Furthermore, whether BEC-derived EVs modulate BBB function remains unknown as well as the different molecular players (miRNAs, mRNA or proteins) involve in this process.

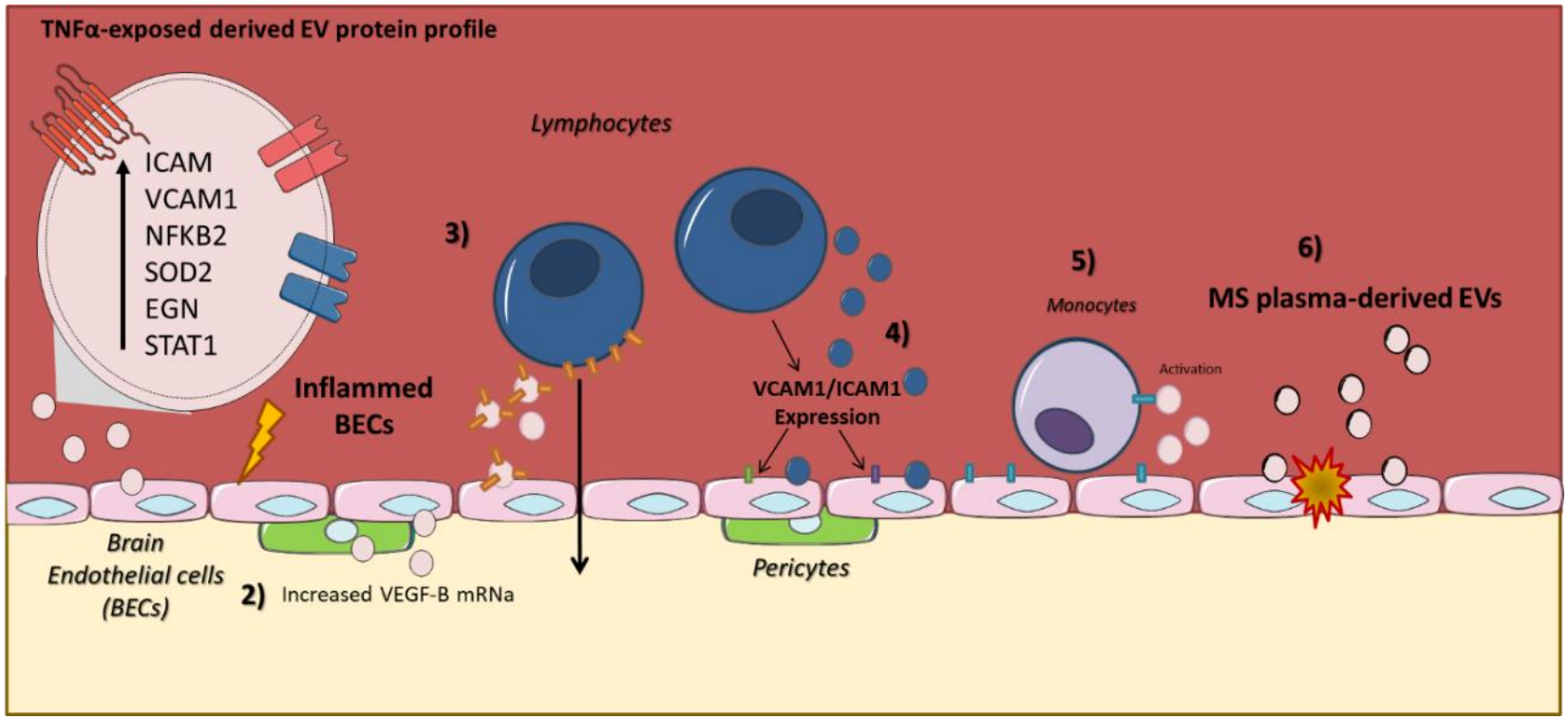

Figure 1.8 Summary of role of EVs in blood-brain barrier in inflammation. (1) Human brain endothelial cells (BECs) exposed to TNFα released EVs that carry pro-inflammatory proteins. Furthermore, **(2)** inflammation-induced brain endothelial-derived EV modulate pericyte expression of VEGF-B. Activation of brain endothelium promotes release of endothelial-derived EVs, which can modulate cell migration by **(5)** activating monocytes and **(3)** transferring claudin-5 to lymphocytes. Claudin-5 from lymphocytes facilitate the paracellular migration of the T cells by bridging with endothelial claudin-5. **(4)** Activated circulating lymphocytes release EVs and inflammatory mediators leading to activation of brain endothelium and up-regulation of adhesion molecules such as VCAM-1, ICAM-1 and E-selectin. Furthermore, **(5)** Systemic inflammation or neuroinflammatory diseases such as multiple sclerosis (MS) increase the release of endothelial-derived EVs, which can disrupt the brain endothelium. **(2)**. Cell-derived EV: pink (endothelial cell), blue (lymphocyte). Figure drawn by David Roig-Carles.

1.18. Aims and objectives

For this PhD work, we set out to investigate how miRNAs and EVs modulate the role of BBB in inflammation, in an attempt to elucidate the link between endothelial miRNAs and EVs in BBB function. To address this overall goal, the following aims were carried out:

1) Compare three common methods for the isolation of EVs based on number and size of isolated EVs as well as their protein purity (Chapter 3).
2) Characterise the physical and molecular properties of brain endothelium-derived EVs in inflammation (Chapter 3)
3) Investigate the uptake, effect and molecular changes of brain endothelium-derived EVs in BBB function in inflammation. (Chapter 4)
4) Study the mechanism of action by which miRNA-155 induced leukocyte adhesion to brain endothelium. (Chapter 5)

Finally, an unexpected phenotype on miRNA-155 KO mice was observed in the animal facility. Hence, I spend part of my first two years, characterising this phenotype and investigating the molecular cause driving this effect. (Chapter 6)

CHAPTER 2: Material and Methods

2.1. Materials

Tissue culture consumables including flasks, plates, cryo-tubes, sterile serological pipettes and tips were obtained from Greiner Bio-One (Stonehouse, Gloucestershire, UK). General-use consumables, including Eppendorfs® tubes, RT-qPCR tubes and phosphate saline buffer (PBS) were purchased from Fisher Scientific/Thermofisher (Paisley, Renfrewshire, UK). All other consumables were purchased from Merck Millipore (Watford, Hertfordshire, UK), unless stated otherwise.

2.2. Tissue Cell Cultures

The immortalised hCMEC/D3 was previously obtained from a primary cell culture at passage 0 by co-expression of human telomerase reverse transcriptase (hTERT) and SV40 large T antigen using a high efficient DNA-flap lentiviral vector system (Weksler *et al.*, 2005).

hCMEC/D3 cells were grown in Endothelial Basal Medium-2 (EBM-2) and supplemented with the following supplements: 0.025 % (v/v) VEGF, insulin growth factor (IGF) and epithelial growth factor (EGF), 0.1 % (v/v) bFGF, gentamycin (GA-1000) and ascorbic acid, 0.04 % (v/v) hydrocortisone and 2.5 % (v/v) foetal bovine serum (FBS), hereafter referred to as EBM-2 complete media (Lonza, Wilford, Nottinghamshire, UK). Prior to seeding the cells, tissue culture surfaces were coated with 1/20 (v/v) collagen type I from calf skin (0.1 % (w/v) solution in 0.1 M acetic acid) (Merk

Millipore, Watford, Hertfordshire, UK) in Hank's Balanced Salt Solution (HBSS) for 1 h at room temperature (RT). For all experiments, hCMEC/D3 cells (passage from 25 to 35) were grown on collagen-coated plates to sub-confluence unless otherwise specified. hCMEC/D3 medium was replaced every two days until cells were sub-confluent (approximately 90 % of confluent cells).

The T cell line Jurkat from acute T cells was a kind gift from Dr. V Male (Imperial College London, UK). Jurkat T cells were grown in suspension in Roswell Park Memorial Institute (RPMI) 1640 with GLUTAMAX I (Gibco® Invitrogen, Paisley, Renfrewshire, UK) culture medium containing 10 % (v/v) FBS and 1 % (v/v) penicillin and streptomycin (P/S). Cells were maintained at a concentration of 0.3 to $0.5x10^6$ cells/ml and fresh media was added every two days. At the end of every week, cells were spun down at 190 x g for 5 min, then pelleted cells were manually counted and cells were diluted in fresh medium at the concentration stated above.

Human brain pericytes (HBMP) were a gift from Dr. Bread (Oxford University, UK) and were grown in Pericyte Medium (Science cell, Carlsbad, CA, USA) supplemented with 1 % (v/v) of pre-made and commercially available cocktail of pericyte growth factors´ solution, 2 % (v/v) FBS and 1 % (v/v) P/S. HBMP were grown in tissue culture flasks/dishes that were pre-coated with poly-L-lysine solution for 1h at RT.

Human primary cortical astrocytes (hA) (Science cell, Carlsbad, CA, USA) were grown in Astrocyte medium (Science cell, Carlsbad, CA, USA) supplemented with 1 % (v/v) astrocyte growth factor´s solution, 2 % (v/v) FBS and 1 % (v/v) P/S. hAs were grown in tissue culture flasks/dished that have been pre-coated with 1/20 (v/v) calf-skin collagen diluted in HBSS for 1 h at RT.

Adherent cells were passaged at sub-confluence and were washed twice with HBSS without calcium and magnesium and de-attached using 0.25 % (w/v) porcine trypsin-EDTA (trypsin) for 3 min at 37 ^{o}C. Trypsin was inactivated by adding 10 % (v/v) of FBS, cells were spun at 300 x g for 5 min and pelleted cells were resuspended and sub-cultured in a new tissue culture flask at a dilution of 1:5 unless specified otherwise.

All spared cell passages were cryo-conserved by mixing 10^6 cells/ml with 10 % (v/v) dimethyl sulfoxide (DMSO) in complete cell culture medium (Merk Millipore, Watford, Hertfordshire, UK). Then, cells were kept for 24h in a cell-freezing chamber at -80 ^{o}C prior to transfer to liquid nitrogen for long-term storage.

All cell lines were maintained in a 95 % (v/v) humidified air and 5 % (v/v) CO_2 incubator at 37 °C. Cells were routinely screened for the presence of mycoplasma using MycoAlert Mycoplasma kit (Lonza, Wilford, Nottinghamshire, UK).

2.3. Isolation of brain endothelial cell-derived extracellular vesicles

hCMEC/D3 cells were seeded in 175 cm^2 collagen-coated tissue culture flasks. After 48 h, cells were washed with HBSS three times and EBM-2 complete medium was replaced with 15 ml of EBM-2 complete medium supplemented with 2.5 % (v/v) EV-depleted FBS (Gibco®Invitrogen, Paisley, UK) instead of normal FBS, hereafter referred to as EV medium. Cells were treated with TNFα and IFNγ (R&D Systems, Abingdon, Oxfordshire, United Kingdom) at concentrations ranging from 1 to 100 ng/ml (see figure legends for specific doses) or EV medium only. CCM was collected 24 h after medium was exchanged, when cells had reached 95–100 % confluency (15×10^6 cells per 175 cm^2 tissue culture flask). CCM was centrifuged at 300 x g for 10 min to remove remaining live/dead cells and at 2000 x g for 20 min to remove cell debris and large vesicles such

as apoptotic bodies. Large EVs (L-EVs) were isolated by centrifugation at 10,000 x g for 30 min and subsequently washed by resuspending the pellet in 30 ml of PBS. Resuspended L-EVs were filtered through a 0.8 µm filter unit (Merk Millipore, Watford, UK) and centrifuged at 10,000 × g for 30 min. Pelleted L-EVs were resuspended in either PBS, EV medium lacking IGF, EGF, VEGF and FBS or lysis buffer. L-EVs were aliquoted and stored at -80 ºC for up to two months to minimise vesicle/RNA degradation (Wu, Deng and Klinke, 2015). Supernatant from the first separation of L-EVs was used to recover the fraction of sEVs described in the following sections (Figure 2.1).

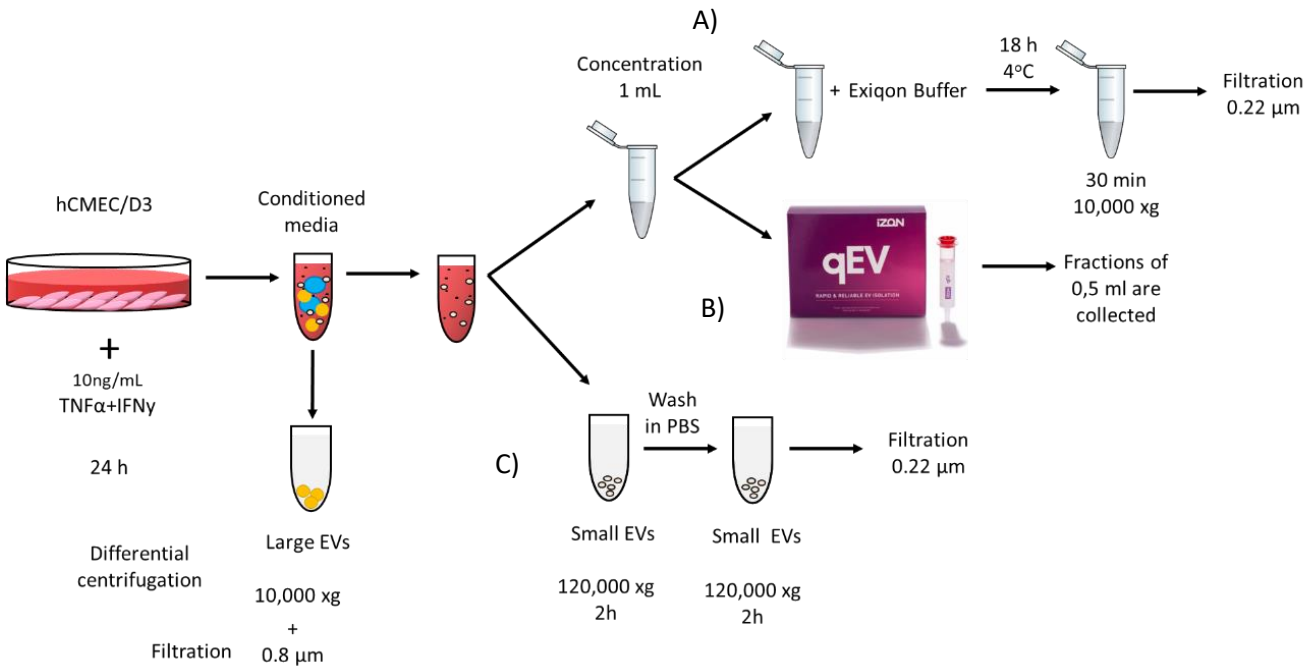

Figure 2.1. Work-flow for the isolation of hCMEC/D3 cell-derived EVs. hCMEC/D3 cells were seeded onto 175 cm^2 tissue culture flask for 48h. Media was replaced for EV medium with or without combination of cytokines (10 ng/ml TNFα and IFNγ) and cell conditioned media (CCM) was collected 24h later. Small and large EV (sEVs and L-EVs) were concentrated by removal of large particles by differential centrifugation (300 x g for 10 min and 2000 x g for 20 min). L-EVs were isolated by centrifugation and filtration.

sEVs were isolated from remaining CCM supernatant following either of the three different method: precipitation-based method (A), size exclusion (B) and ultracentrifugation (C). All EVs were aliquoted and stored at -80 ºC.

2.3.1. Ultracentrifugation

CCM supernatant from the first spin of L-EVs was used to isolate sEVs. CCM was centrifuged at 120,000 x g for 120 min, subsequently washed by resuspending and pooling the pellets together in 30 ml of PBS and centrifuged again at 120,000 x g for 120 min. sEVs were resuspended and filtered through 0.22µm filter (Merk Millipore, Watford, UK). EVs were aliquoted and stored at – 80 ºC for up to two months to minimise vesicle/RNA degradation (Wu, Deng and Klinke, 2015). All ultracentrifugation steps were performed using the Sorvall Discovery (Brea, CA, USA) Superspin 630 Sorvall rotor (k factor 226.3) at 4 °C.

2.3.2. Precipitation-based method

Cold CCM was concentrated using Amicon Ultra-15 filters of 100K (CAR, Merk Milipore, UK) by centrifuging at 4,000 x g for 20 min at 4 ºC. If CCM was greater than 15 ml, the concentration procedure was repeated until 1 ml or less of CCM was obtained. CCM was brought to a final volume of 1 ml with fresh PBS and filtered with a 0.22 µm filter. Then, sEVs were isolated using miRCURY^{TM} Exosome Isolation Kit (Exiqon, Vedbæk, Denmark) according to manufacturer's instructions. Briefly, 1 ml of CCM was transferred to a 2 ml Eppendorf tube, mixed with 400 µl of Precipitation Buffer B and the tube was inverted and vortexed thoroughly. CCM was incubated overnight (~18 h) at 4 ºC. Then, sEVs were isolated by centrifuging the CCM at 10,000 x g for 30 min at 20 ºC. Supernatant was removed and a quick spin was applied to remove excess of supernatant.

EV pellet was resuspended in 100 µl of Exiqon resuspension buffer. Samples were aliquoted and kept at -80 ºC.

2.3.3. Size exclusion

Cold CCM was concentrated using Amicon Ultra-15 filters with 100K (CAR, Merk Milipore, UK) by centrifuging at 4,000 x g for 20 min at 4 ºC. If CCM was greater than 15 ml, the concentration procedure was repeated until 1 ml or less of CCM was obtained. CCM was brought to a final volume of 1 ml with fresh PBS filtered with a 0.22 µm filter. Size exclusion columns, qEV, purchased from IZON (Oxford, Oxfordshire, United Kingdom) were used to separate sEVs from non-vesicular components. CCM was layered on top of the column and was eluted in PBS. After 3 ml of void volume, 0.5 ml fractions were collected to a final volume of 8 to 9 ml. Fractions were aliquoted and stored at -80ºC.

2.4. Nanoparticle tracking analysis

The size and concentration of the EVs were measured using nanoparticle tracking analysis (NTA). The Nanosight LM10 (Malvern, Worcestershire, UK) was used to compare EVs generated by the different methods of isolation. Prior to analysis, Nanosight LM10 was calibrated using synthetic silica microspheres of 100 nm diameter (Polyscience Inc, Warrington, PA, USA). LM10 was set to capture videos during 30 seconds (s) with a camera level of 11; these settings were kept across all samples. Briefly, after calibration of LM10, the chamber was washed three times in PBS and samples were loaded manually using a Luer-lock disposable 1 ml syringe (Fisher Scientific, Paisley,

Renfrewshire, UK). The injected sample was allowed to equilibrate in the chamber for 60 s and followed by 30 s video capture. Five technical replicates were recorded for each sample and the specific temperatures of the LM10 system at each time were annotated. Quantification of both size and concentration of sample was assessed using NTA 1.5 software (Malvern, UK). The NTA software tracks the Brownian motion of each particle and calculates particle size and concentration using the Stokes–Einstein equation (Equation 1). This equation measures the diffusion coefficient of each particle (D_t) and the sphere-equivalent, hydrodynamic radius (rn).

Equation 1 Strokes-Einstein equation

$$D_t = \frac{K\ B\ T}{6\pi\eta\mathrm{rn}}$$

Where the KB is Boltzmann's constant, T is temperature and η is viscosity.

The chamber was washed three times with PBS between samples in order to remove remaining vesicles.

LM10 Nanosight was used to select the method of isolation of EVs. Characterisation of EV size and number was carried out using the NS500 Nanosight, an upgraded version of LM10 after an unexpected equipment failure of the LM10. The mechanism by which EVs are quantified on the NS500 is the same as LM10 although handling of the instrument was less user-dependent. Briefly, the fluidics of the system were primed and flushed with PBS prior loading of EVs. Camera focus was adjusted to ensure that individual particles could be distinguished and camera level was set at 14 for all recordings. Three 30-second videos were recorded for each sample with a delay of 5 s between each recording. The accuracy of size detection was calibrated with 100 nm diameter silica nanoparticles. NS500 operates with NTA 2.3 software, which followed

the same principle of Brownian motion and quantification described above for LM10. The NTA system used in individual experiments is indicated in specific figure legends.

2.5. Transmission electron microscopy

Uranyl-oxalate solution (pH 7): 4 % (w/v) uranyl acetate, pH 4 was mixed with 0.15 M solution of oxalic acid (0.945 g in 50 ml distilled water), at a 1:1 ratio. Then, pH was adjusted to 7 by adding 25 % (w/v) NH_4OH in drops to prevent formation of insoluble precipitates.

Isolated EVs were resuspended in an equal volume of 4% (w/v) of *p*-formaldehyde (PFA) diluted in PBS. EVs in 2% (w/v) PFA were stored up to 1 week at 4 ºC before proceeding further. A drop of 10 µl of EV suspension was placed on a clean parafilm and Formvar-carbon coated EM grids (AgarScientific, Stansted, Essex, UK) were placed on the surface. Three grids were placed per sample and incubated for 20 min at RT. Grids were transferred into 100 µl PBS with clean forceps being careful not to wet the EV-free side of the grid. Then, the grids were transferred to a 50 µl drop of 1 % (v/v) glutaraldehyde for 5 min. To wash grids with EVs, eight drops of 100 µl of PBS were sequentially added to grids for 2 min each wash step. Grids containing the same EV sample were placed in the same drops. Grids were transferred to a 50 µl drop of uranyl-oxalate solution (pH 7) for 5 min. Grids containing EV samples were embedded in a drop of 50 µl of a mixture of 2 % (w/v) methyl cellulose and 4 % uranyl acetate at a ratio of 1:9 and incubated with the embedding solution for 10 min on ice. Grids were removed with stainless steel loops and, excess fluid was blotted and discarded by gently pushing the loop sideways on Whatman no. 1 filter paper so that a thin film was left behind over

the sEV side of the grid. Grids were air-dried for 5 to 10 min in the steel loop. After the grids were ready, EVs were observed under EM (JEM1400) at 80 kV.

2.6. Immunoblotting

For Western blot analysis, different buffers were prepared as described below:

- 10 x Tris-buffered saline (TBS-T): 24.22 g/l of Tris-HCl (pH 8.0), 80 g/l of NaCl and 0.2% (v/v) Tween-20 were mixed.
- 2 x Tris glycine sample buffer (pH 6.8): 0.151 g/l Tris-HCl (pH 8.0), 20 % (v/v) Glicerol, 1 % (w/v) of bromophenol blue with 2 mercaptoethanol in a 1:250 proportion were mixed in 80 ml of distilled water.
- 1 x Tris Glycine running buffer for reducing conditions: 3.038 g/l Tris-HCl (pH 8.0), 14 g/l glycine, 1 g/l SDS were mixed with distilled water.
- 1x Tris-glycine transfer buffer (reducing conditions): 20 % (v/v) 1 X tris-glycine running buffer, 20% (v/v) methanol were mixed with distilled water.
- RIPA buffer: 20 mM Tris base (pH = 8), 20 mM Tris-HCl (pH 8.0), 150 mM NaCl, 1 mM EDTA, 0.1% (w/v) SDS, 1% (v/v) Igepal, 50 mM NaF, and 1 mM NaVO3 were mixed with distilled water.
- Stripping buffer: 3.91 mM Tris buff (pH 6.8), 20 % (v/v) of 10 % (w/v) SDS and 0.8 % (v/v) β-mercaptoethanol.

Isolated EVs or cells were lysed in 1x RIPA Buffer supplemented with protease inhibitor cocktail (Merk Millipore, Watford, Hertfordshire, UK). Samples were sonicated twice at 20% of amplitude for 10 s on ice (Fisherbrand™ Model 120 Sonic Dismembrator, Fisher Scientific, Paisley, Renfrewshire, UK). Protein concentration was measured using a DC™ Protein Assay kit (Bio-Rad, Watford, UK). Samples were mixed with 2x Tris

glycine sample buffer in a 1:1 ratio and protein were denatured by heating the sample at 75 ºC for 5 min. Then, pre-cast gel of 4-20 % (w/v) Tris-Glycine (Invitrogen, Paisley, Renfrewshire, UK) were loaded with 5 µg of EV sample or 20 µg of cell lysates and run at 120 V for 2 h using Superlock western blot system (Thermofisher, Paisley, Renfrewshire, UK). Proteins were transferred onto a nitrocellulose membrane at 300 mA for 2 h at RT using Superlock western blot system (Thermofisher, Paisley, Renfrewshire, UK). Then, the membrane was blocked with 8 % (w/v) of skimmed milk (Marvel, Premier Foods, St. Albans, Hertfordshire, UK) diluted in TBS-T. Each membrane was incubated overnight at 4 ºC with the appropriated antibody diluted in 8 % (w/v) skimmed milk diluted in TBS-T (Table 2.1). Subsequently, membranes were washed 3 times with TSB-T for 10 min and then incubated with their corresponding secondary antibody, goat anti-rabbit or anti-mouse HRP (System Bioscience Palo Alto, CA, USA), at 1:5000 diluted in 8% (w/v) of skimmed milk diluted in TBS-T for 60 min at RT (Table 2.1). Subsequently, the secondary antibody was removed and the membrane was washed 6 times with TBS-T for 10 min per wash. After the final wash, enhanced chemiluminescence (ECL) (GE Healthcare, Amersham, UK) was used to visualize the immunoblot at 2, 10 and 30 min of exposure using G:Box (Syngene, Cambridge, UK).

To ensure equal protein loading, membranes were stripped by incubating them in Stripping buffer at 65 ºC for 20 min with continuous stirring. Stripped membranes were washed 6 times in TBS-T for 10 min per wash at RT. Then, membranes were blocked, stained and imaged for Glyceraldehyde 3-phosphate dehydrogenase (GAPDH) as described in the paragraph above.

Protein quantification was carried out using Image J Software. Images were converted to 8 bit and pixel intensity of a defined section surrounding the band of interest was measured. Protein expression is calculated by normalised protein expression of the

investigated protein over internal control, GAPDH. Relative expression to the control is represented.

Snap-frozen kidneys were used to isolated protein content from cortex using RIPA buffer. Immunoblotting was carried out as described above using specific antibodies for NCC (1:500), NKCC2 (1:500) at (1:1000 diluted in 8% (w/v) of skimmed milk diluted in TBS-T overnight at 4ºC. GADPH (1:50000 diluted in 8% (w/v) of skimmed milk diluted in TBS-T RT for 2h was used an internal loading control.

Table 2.1. List of primary antibodies used for Western Blotting analysis

Primary antibody	Host	Dilution	Company
Anti-human CD63	Rabbit	1:1000	System Bioscience, USA
Anti-human CD9	Rabbit	1:1000	System Bioscience, USA
Anti-human HSP70	Rabbit	1:1000	System Bioscience, USA
Anti-human Ocluddin	Rabbit	1:150	Life technology, UK
Anti-human Claudin-5	Rabbit	1:150	Life technology, UK
Anti-human VCAM1	Mouse	1:300	R&D Systems, UK
Anti-human ICAM1	Mouse	1:300	R&D Systems, UK
Anti-human/mouse GAPDH	Rabbit	1:50,000	Life technology, UK

Anti-mouse NCC	Rabbit	1:500	Sigma-Aldrich, UK
Anti-mouse KNCC2	Rabbit	1:500	Sigma-Aldrich, UK

2.7. TNFα and IFNγ sandwich ELISA

Enzyme-linked immunosorbent assay (ELISA) kit from DuoSet® (R&D Systems, Abingdon, United Kingdom) was used to measure residual levels of TNFα and IFNγ in sEVs following manufacturer's instructions. Capture antibodies for TNFα and IFNγ were diluted to working concentrations (4 or 2 µg/ml respectively) in PBS. Then, 100 µl was pipetted per well, and the plate was sealed and incubated overnight at RT. Capture antibodies were then aspirated, washed three times with 1x wash buffer (0.05% (v/v) Tween® 20 in PBS) and wells were thoroughly dried between washes by tapping the plate on a clean paper. Subsequently, blocking buffer (1 % (w/v) bovine serum albumin (BSA) in PBS) was pipetted in each well and incubated for 1 h at RT in order to block unspecific binding. Then, wells were washed as described above.

On the day of the experiment, fresh standard dilutions from purified TNFα and IFNγ were prepared by diluting stocks to a working concentration in reagent diluent (1% (w/v) bovine serum albumin (BSA) in PBS). Working concentration was further diluted by 2-fold dilution for eight times to prepare the standard curve. 100 µl of standards or sample (sEVs diluted in PBS to 10^8 sEVs/µl) were pipetted in each well. Plates were sealed and incubated at RT for 2 h. Then, samples were washed as described above and streptavidin-horseradish peroxidase solution, which was diluted to the working concentration specified on the vial label using reagent diluent, was added for one h. Subsequently, the plate was washed again, the substrate solution added and the plate was incubated for 20 min before the reaction was stopped. The plate was read using FLUOstar

Optima fluorescence plate reader (BMG Labtech, Aylesbury, UK) at 450 nm and background measures taken at 570 nm were subtracted.

Standard curves were generated for each cytokine by applying the regression to the curve with the best fit (Figure 2.2). TNFα standard curve was calculated with a second order polynomial (quadratic) equation (Figure 2.2A), whereas IFNy standard curve was calculated with a linear regression (Figure 2.2B). Values were inferred using GraphPad Prism version 7.1 to draw the best fit curve (GraphPad Software, San Diego, CA, USA).

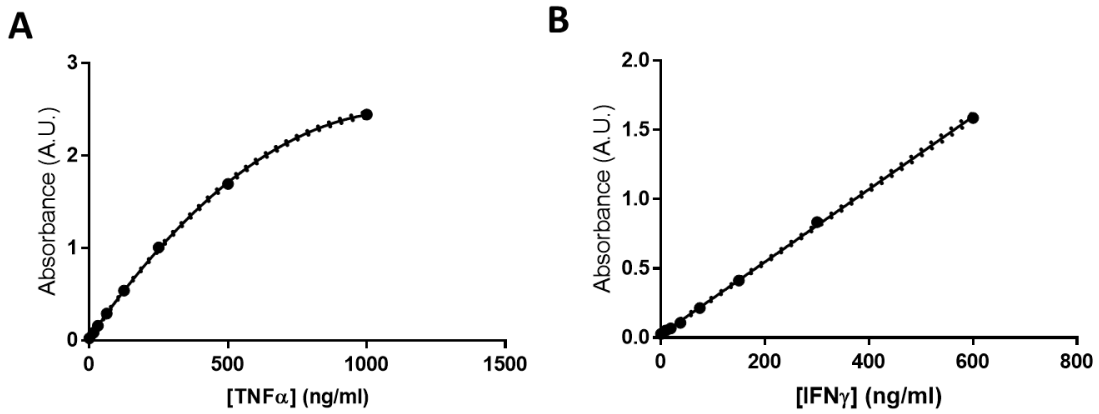

Figure 2.2. Standard curves for measuring TNFα and IFNγ. DuoSet® kit ELISA kit was used to determine residual levels of TNFα and IFNγ in small EVs. Standard curves were generated to infer the values for the concentration of the cytokines. TNFα standard curved was calculated with a second order polynomial (quadratic) equation **(A)**, whereas IFNγ standard curve was calculated with a linear regression **(B)**. Graphs are representative of two technical replicates. Absorbance is shown as arbitrary units (AU).

2.8. Extraction of RNA from EVs and hCMEC/D3 cells.

RNA was isolated from either cultured cells or sEVs using miRCURY RNA isolation kit (Exiqon, Vedbæk, Denmark which is now part of Qiagen, Manchester, UK) following manufacturer's instructions. Briefly, cells or sEVs were incubated with lysis buffer, homogenised using a vortex mixer and precipitated by adding an equal volume of

pure ethanol. Samples were concentrated using miRCURY columns, washed and eluted in 50 µl of elution buffer. RNA concentration and quality (absorbance ratio of 260/280 and 260/230) was measured using Nanodrop ONE (Thermofisher, Paisley, Renfrewshire, UK).

2.9. RT-qPCR analysis for microRNAs and mRNAs.

The reverse transcription for miRNAs was performed using Taqman miRNA transcription kit (ThermoFisher, Paisley, Renfrewshire, UK) with specific pre-design Taqman primers for miRNA-155-5p (000479-4427975), 126-5p (000451-4427975), 126-3p (000419-4427975), 24-3p (000402-4427975), 146a-5p (000468-4427975) and 146b-5p (001097-4427975) following manufacturer's instructions. Small nuclear U6 RNA (U6; 001093-4440887) was used as internal control for cellular miRNAs levels whereas let-7g (002282-4440887) was used as control of miRNAs levels in sEVs. Levels of miRNAs were analysed using Taqman Universal Master mix with 1.7 ng of cDNA per reaction, loaded in Optima thermocycler (Bio-Rad Laboratories Ltd., Watford, Hertfordshire UK) and probes were amplified and analysed.

For mRNA analysis, total cDNA was generated using TaqMan High Capacity cDNA Reverse Transcription kit (Applied Biosystem, Life Technologies, Warrington, UK) using random primers. QuantiTect Syber® Green master mix (Qiagen, Manchester, UK) was used to study the relative levels of mRNAs with 10 ng of cDNA. Pre-designed primers for ICAM1, VCAM1, lysine deficient protein kinase 1 (WNK1), annexin A2 (ANXA2), Carcinoembryonic antigen-related cell adhesion molecule 1 (CEACAM1), occludin (OCLN) and claudin-5 (CLDN5) were tested whereas β-actin primers were used as a housekeeping control of cDNA loading (Merk Millipore, Watford, UK). Gene

expression was detected using an Optima thermocycler (Bio-Rad Laboratories Ltd., Watford, Hertfordshire UK).

The relative levels of miRNA or mRNA was calculated using the $2^{-\Delta\Delta Ct}$ (delta-delta Ct) method and normalised with β-actin for mRNA and U6 or let-7g for miRNAs.

Equation 2. Relative RNA expression.

$$\Delta Ct = C_{tg} - C_{ti}$$

$$\Delta\Delta Ct = \Delta C_{tt} - \Delta C_{tc}$$

$$\text{Relative expression} = 2^{-\Delta\Delta Ct}$$

Where C_t = threshold cycle, C_{tg} = gene of interest Ct, C_{ti} = internal control Ct, C_{tt} = treated samples Ct and C_{tc} = control sample Ct.

The results of microRNA/mRNA relative levels in treated hCMEC/D3 cells, cytokine-treated hCMEC/D3 cell-derived small EVs (cytokine-sEVs) or transfected hCMEC/D3 cells were expressed as microRNA/mRNA relative expression to unstimulated hCMEC/D3 cells, quiescent small EVs (quiescent sEVs) or scramble-transfected hCMEC/D3 cells, respectively (refer to specific figure legends for more detail).

2.10. Uptake of sEVs by cells of the neurovascular unit.

sEVs were isolated using ultracentrifugation as described above with a modification in the final washing step. After the first 120,000 x g centrifugation spin, sEVs were resuspended in 5 ml of PBS and labelled with 10 % (v/v) Vybrant-DiO (Life technology, Paisley, UK) for 30 min at 37 ºC. Same volume of PBS with no sEVs was labelled and treated in the same manner in order to control for any free Vybrant-DiO dye left in the solution. Samples were then diluted further with 25 ml of PBS, isolated as

described above, resuspended in PBS and stored at -80 ºC. sEVs were then quantified using the Nanosight S500 as described above.

hCMEC/D3, HBMP and hA cells were grown in 24-well plates until they reached sub-confluency (~95%). Then, cells were washed twice in HBSS and incubated with DiO-labelled sEVs at concentrations and times specified in figure legends. At the end of the incubation time, cells were washed with HBSS, collected using trypsin/EDTA and washed twice with HBSS prior to flow cytometry analysis. Washed cells were analysed on a Becton-Dickinson FACScalibur (Reading, UK) with a FL1 detector set at 530 V and results are reported as the mean±SEM (n=3/4) of the median fluorescence of the analysed cells unless stated otherwise in the figure legend.

For qualitative analysis of the uptake of sEVs, hCMECD3 cells were grown in collagen- and fibronectin-coated Nunc® Labteck chamber slides (Merk Millipore, Watford, UK). Briefly, Nunc® Labteck chamber slides were first incubated with 1/20 (v/v) calf skin I collagen diluted in HBSS for 1h at RT. Then coating was replaced by 1:100 (v/v) bovine fibronectin solution (Merk Millipore, Watford, UK) diluted in HBSS for 1h at RT. Cells were cultured with DiO-labelled sEVs for 6, 24 and 48h prior they were fixed in 4% PFA for 10 min at RT. PFA was removed and washed three times with PBS and once with double-distilled water (ddH_2O) prior to addition of the mounting media containing DAPI dye (Vector Laboratories, Burlingame, USA) for nuclear staining. Images were analysed using confocal laser scanning microscopy (Leica TCS SP5, Leica Microsystems, Milton Keynes, UK) and showed as the maximum projection of a z-stack of images. images of ten Z stacks of 2.5 μm in depth were acquired using a 100x oil immersion objective and projected onto one image.

2.11. Electric cell-impedance sensing method

Electric cell-impedance sensing method (ECIS) Z-Theta (Applied BioPhysics, Troy, NY, USA) was used to measure the TEER (Ωcm^2) of the hCMEC/D3 cell monolayers in real time as described previously (Keese *et al.*, 2004).

Approximately 20,000 cells were seeded onto each well of an array (model 96W10E+ Applied BioPhysics, Troy, NY, USA) previously coated with calf skin collagen type I (as described in section 2.2). Cells were grown to confluency and TEER monitored prior to treatment via ECIS. When cells formed a complete monolayer, they were treated with sEVs (0.1 to $1x10^8$ sEVs/µl) alone and/or in combination of cytokines (TNFα and IFNγ, 1 ng/ml) at doses and times described in specific figure legends. TEER was monitored for up to 60 h after cells were treated with cytokines and impedance data were collected at different frequencies (250, 500, 1000, 2000, 4000, 8000, 16000, 32000, 64000 Hz) and at intervals of 12 min through the extension of the experiment.

To further investigate the effect of sEVs in cytokine-activated cells, confluent hCMEC/D3 cells were pre-activated with 1 ng/ml TNFα and IFNy for 18 h and sEVs were then added in the presence or absence of cytokines.

The ECIS measurements were further analysed and subjected to a mathematical modelling to calculate the TEER at each time point (Giaever and Keese, 1991). Experimental differences were analysed every 5 h since beginning of the treatment and Rb data are shown as percentage of control at each time point.

2.12. Flow-based leukocyte adhesion assay

T cell adhesion was measured using a flow-based adhesion assay adapted from previously published data (Wu, Cerutti, Miguel A Lopez-Ramirez, *et al.*, 2015; Cerutti *et al.*, 2017). The system is based on a multi-channel plate specifically designed for experiments including shear stress (Ibidi® µ-Slide VI0.4, Ibidi® GmbH, Martinstreid, Germany).

hCMEC/D3 cells were collected, centrifuged and counted in order to dilute 20,000 cells in 30 µl of EBM2 complete medium. Diluted cells were seeded per channel of collagen-coated Ibidi® µ-Slide VI0.4. Twenty minmin after seeding, channels were topped-up with EBM2 complete medium and cells were kept in culture until confluence unless stated otherwise.

After reaching confluence, hCMEC/D3 cells were incubated with sEVs (0.1 to $1x10^8$ sEVs/µl) alone or in combination with cytokines (TNFα and IFNy, 1ng/ml for 24 h) at times (0 to 48h) described in specific figure legends. At the end of the incubation time, cells were washed twice with HBSS and kept in EBM2 complete media. Incubation with 1 ng/ml TNFα and IFNy for 24h was used as positive control for the experiment (Cerutti *et al.*, 2016). 2×10^6 cells/ml Jurkat T cells were labelled with 5 µM 5–chloromethylfluoresceindiacetate (CMFDA, Life Technologies, Eugene, USA) for 30 min in RPMI basal media at 37 ºC. Cells were washed in complete RPMI media for 45 min, centrifuged and resuspended in EBM2 complete media at 2×10^6 cells/ml Jurkat T cells. Then, cells were flowed through the channel containing endothelial monolayers at 0.5 dyn/cm^2 for 5 min. After that, the flow was increased to 1.5 dyn/cm^2 to mimic venular vessel wall shear stress for 1 min to remove non-adhered leukocytes. Interactions between leukocyte and endothelial cells were recorded for 6 min and firm leukocyte adhesion was quantified. Eight to ten different fields of vision (FOV, 640 × 480 µm) along the centre of the channel were imaged and firmed adhered leukocytes were manually counted. Image

acquisition was carried using inverted fluorescence microscope (Olympus IX70, Tokyo, Japan) with an X10 objective. Microscope was controlled by the Image Pro Plus software (Media Cybernetics Inc. Bethesda, USA).

To study the role of VCAM1 and ICAM1 in sEV-induced leukocyte adhesion, hCMEC/D3 cells were washed and incubated with 30 µg/ml neutralising antibodies against ICAM1, VCAM1 or mouse IgG (R&D Systems, Abingdon, United Kingdom) for 1 h at 37 ºC in EBM-2 basal media. After incubation, cells were washed and experiment carried as described above. Firmly adhered Jurkat T cells were counted and expressed as fold change of sEVs treated cells over the corresponding untreated control.

2.13. Transfection of hCMEC/D3 cells

hCMEC/D3 cells were transfected using lipofection techniques with two different reagents: Siport™ (Life Technologies, Paisley, Renfrewshire, UK) for pre-miRNA-155 and Lipofectamine 2000 (Thermofisher, Paisley, Renfrewshire, UK) for siRNAs and anti-miRNAs.

hCMEC/D3 cells were seeded at 25,000 cells/cm^2 and 8 h after, cell culture medium was replaced with complete EBM2 media without GA-1000. Twenty-four hh after seeding, cells were transfected with either Siport™ or Lipofectamine 2000 following manufacturer's instructions. Briefly, lipofection reagent was mixed with OptiMEM I reduced serum medium and incubated for 10 min (Siport™) or 5 min (Lipofectamine 2000). Next, the mix was diluted with the desired oligonucleotides (Table 2.2) and incubated for 10 min (Siport™) and 20 min (Lipofectamine 2000) at RT. Finally, the transfection reaction was diluted in complete EBM2 lacking GA-1000 to obtain a final concentration of the oligonucleotides of 30 nM (Siport™) or 60 nM (Lipofectamine).

Media was replaced 6h (Siport™) or 24 h (Lipofectamine) after transfection. Cells were kept in culture from 0 to 48h post-transfection.

Table 2.2. List of oligonucleotides used for transfection of hCMEC/D3 cells.

Oligonucleotide	Target	Company
miRNA precursor	miRNA-155-5p	Thermofisher, UK
miRNA precursor	Scramble control 1	Thermofisher, UK
siRNA pool	WNK1	Dharmacon, USA
siRNA pool	Scramble control	Dharmacon, USA

In order to assess the efficacy of transfection of hCMEC/D3 cells with Siport™ reagent, hCMEC/D3 cells were transfected as described above but using Cy3-labelled oligonucleotide as a negative control (Thermorefisher, Paisley, UK). Both immunofluorescent microscopy using inverted fluorescence microscope (Olympus IX70, Tokyo, Japan) and flow cytometry analysis, using a Becton-Dickinson FACScalibur (Reading, UK) as described in Section 2.10 showed a high efficiency of transfection.

2.14. Immunocytochemistry

hCMEC/D3 cells were seeded onto collagen- and fibronectin-coated (1:100) Lab-Tek™ multiwell chamber slides (Sigma, UK), transfected as described above or treated

with 1 ng/ml TNFα and IFNy for 24 h. At the end of the experiment, hCMEC/D3 cells were washed twice in HBSS and incubated with 4 % (w/v) PFA in PBS for 20 min at RT. Subsequently, cells were washed with PBS three times and permeabilised with 0.5 % (v/v) Triton-X100 (Merck Millipore, Watford, Hertfordshire, UK) in PBS for 10 min at RT. Cells were blocked with 10% (v/v) FBS for 1 h. Primary antibody rabbit anti-human WNK1 was incubated overnight at 4 ºC (1:50). Cells were washed with PBS three times and twice with PBS containing 0.025 % (v/v) Tween-20 at pH 7.4 (Merk Millipore, Watford, Hertfordshire, UK) and incubated for 1h at RT with a corresponding secondary goat anti-rabbit or anti-mouse antibody conjugated to Alexa Fluor 488 (Zymed, Life Technologies Ltd. Invitrogen division, Paisley, UK). Cell nuclei were stained using Dapi Fluoromount-G obtained from SouthernBiotech (Alabama, USA). Slides were viewed with a fluorescent microscope (Olympus BX61,Olympus, Hertfordshire, UK). Signal was quantified by pixel intensity and normalised by DAPI signal using Image J software.

2.15. Databases for putative mRNA targets of miRNAs

Open-access database for target identification was HumanTargetScan 7.2 (http://www.targetscan.org/vert_72/, last access on September 2020). Tarbase v.8 (http://carolina.imis.athena-innovation.gr/diana_tools/web/index.php?r=tarbasev8%2Findex, last access on September 2020) was used to obtain the list of validated targets for miRNA-155. Comparisons among databases and mRNA/protein expression data was carried out with Microsoft Excel.

2.16. Animal husbandry

C57bl/6 (wild-type (WT)) and B6.Cg-miR-155 (miRNA-155 knock-out (KO)) mice (Charles River, Kent, UK) were used in this study. All genetic modified strains had a C57bl/6 genetic background. All animal work was approved by The Open University Animal Welfare and Ethics Research Board and the UK Home Office (PPL 80/2612). Animals were housed on a 12 h light/dark cycle at temperature range from 19 to 22 °C, relative humidity 55±10% (v/v). Mice were housed in groups of 3 or 4 mice per polypropylene mouse (NPK, Selbitz, Germany) stored in ventilated cabinet (Scanteiners; Scanbur, Karlslune, Denmark). Diet (SDS Rat and Mouse No. 3), bedding (Enviro-Dri® and Sizzle-Pet, Paper Wool and Shavings), nesting (LBS Gold Aspen Midi 8/20), woodblocks (Aspen Blocks) and fun tunnels (GLP Fun Tunnels) were obtained from LBS Biotechnology (UK). Food and water was provided ad libitum.

2.17. Genotyping miRNA-155 KO mice

Ear punches were collected from each mouse and stored at -21 ^{o}C until tissue was processed. Digestion solution was prepared by mixing protenease K (final concentration 0.52 mg/ml; Sigma-Aldrich, Watford, Hertfordshire, UK) and tail buffer (0.05 M Tris pH 7.5, 0.1M EDTA and 2.5 % (v/v) of 20 % (v/v) SDS). Ear punches were resuspended in 100 µl of digestion buffer and incubate at 55 ^{o}C in a heat block overnight. Proteinase K was deactivated by heating the sample at 85 ^{o}C for 1 h. Samples were centrifuged at 13,000 rpm for 1 min. Subsequently, DNA concentration was measured by Nanodrop ONE (Thermofisher, Paisley, Renfrewshire, UK). Samples were diluted to 10 ng/µl and stored at -21 ^{o}C.

Master Mix was prepared according to manufacter´s instructions. Briefly, 1x Taq Red Master Mix Kit (1.5 mM MgCl2, Genesee Scientific, El Cajon, USA), 1 µM primer WT forward (GTGCTGCAAACCAGGAAGG), primer WT Reverse (CTGGTTGAATCATTGAAGATG) and primer mutant (CGGCAAACGACTGTCCTGGCCG). Master mix was mixed with 20 ng of DNA material in a reaction with a total volume of 25 µl. Samples were run in a thermocycle at 94 ºC for 5 min, then 35 cycles of 94 ºC/30 sec, 61.8 ºC/1 min and 72 ºC/1 min, followed by 72 ºC for 2 min. PCR reactions were separated based on size using E-gel pre-cast 2% (w/v) agarose (Thermofisher, Paisley, Renfrewshire, UK) and 100 bp DNA loading control (15628-019, Invitrogen, Paisley, Renfrewshire, UK). Gels were revealed and imaged using the G:Box (Syngene, Cambridge, UK).

2.18. Water and food intake

Both miRNA-155 KO and WT mice were housed in cages with three to four animals each according to both genotype and sex. Water and diet intake was measured for seven days every four weeks from the time of weaning. On day 1, the bottle of water, the food pellets and the mice themselves were weighed in the morning. Every day thereafter and at the same time, the bottle of water was weighed and refilled. On day 7, food pellets remaining in the cage, mice as well as the bottle of water were weighed. Daily water and food intake were calculated as the average over the period of measurement divided by the number of mice housed in a cage. Both water and diet intake are expressed as “parameter” gained from the initial measurement (4 weeks of age).

2.19. Urine and Blood analysis

Urine specific gravity was used to assess the extent of urine concentration. Briefly, a drop of urine was collected from each mouse after finishing the measurement of the water and diet intake by gently grabbing the mice over a Parafilm-coated surface. Urine concentration was measured during three consecutive days at the same time of the day using a refractometer for urine and serum specific gravity (Burtons, Kent, UK).

Blood was collected by intracardiac puncture in 18-month female miRNA-155 KO and WT mice. Blood was transferred to a heparinised tube (serum- or plasma-specific) and inverted once. Tubes were incubated at RT for 30 min followed by centrifugation at 8,000 x g for 10 min at 4 ºC. Supernatants, containing either plasma or serum, were transferred to a clean Eppendorf tube.

Osmolality and electrolytes of serum and urine were analysed by an external laboratory managed by IDEXX BioResearch (Ludwigsburg, Germany).

In addition to this protocol, blood was also collected after fasting 18 month female B6.Cg-miR155 mice for 8 h. Subsequently, glucose levels in blood were measured using a glucometer (Accu check-meter, Roche, Germany).

2.20. Arg8-Vasopressin ELISA assay

Standards for AVP ELISA assay kit (Abcam, Cambridgeshire, UK) were made following manufacturer's instructions. Briefly, a stock solution of AVP was serially diluted to obtain standards ranging from 10.24 pg/ml to 10,000 pg/ml. For analysis, plasma samples were thawed and AVP was concentrated using the manufacturer's extraction protocol. Two volumes of cold acetone were added to each sample, followed

by vortex mixing and centrifugation at 3,000 x g for 20 min at 4 ºC. Then, the supernatant was transferred into a clean Eppendorf tube and 5 volumes of petroleum ether were added. The mix was vortex mix and centrifuged at 3,000 x g for 10 min at 4 ºC. Subsequently, the top layer was discarded and the aqueous phase was transferred into a clean glass tube. Then, the tube was dried down under oxygen. The remaining pellet was reconstituted using Assay buffer, provided by the ELISA assay kit.

Once standards and samples were ready, the ELISA plate was prepared following manufacturer's instructions. Briefly, 100 µl of each standard, sample and blank solution were loaded onto their corresponding wells. Then, 50 µl of vasopressin biotin conjugate was added to each well, except for the blank wells, followed by 50 µl of vasopressin polyclonal rabbit antibody. The plate was then incubated at 4 ºC for 24 h. After incubation, the plate was washed three times with wash solution (provided by the kit) and finally 200 µl of streptavidin-conjugated HRP were added to each well, except for the blank wells. The plate was sealed and incubate at RT on a plate shaker for 30 min at 500 rpm.

After incubation of the plate for 30 min, the plate was washed as described above. Then, 200 µl of the 3,3',5,5'-Tetramethylbenzidine substrate was added to every well. The plate was sealed again with parafilm and incubated at RT for 30 min on a plate shaker. Finally, the reaction was stopped by adding 100 µl of Stop solution and the optical density of each well was read at 450 nm using a FluoStart Optima plate reader (BMG Labtech, Aylesbury, UK)

2.21. Desmopressin challenge

To study kidney response to AVP, 18-month female miRNA-155 mice were injected with 0.04 µg/Kg of desmopressin (DDAVP) (Sigma, Poole, Dorset, UK) diluted in saline solution (0.9 NaCl % (w/v)) subcutaneously. Urine was collected prior to injection and 1 and 2 h after. Urine collection was carried out with a Pasteur pipette and mice were placed over a para-film sheet. Water availability was restricted during the period of the experiment. Experiment was carried twice in each animal with a period of 48 h between injections. Urine was analysed for osmolality as described above.

2.22. RT-qPCR of animal tissue

For hypothalamus, PBS-perfused brain was collected in RNA*later* solution (ThermoFisher, Paisley, Renfrewshire, UK) and incubated for 24 h at 4 ºC. A brain slicer (Zivic Instruments, Pittsburgh, USA) was used to dissect the tissue into slices and the hypothalamus was separated under a microscope. Morphological identification of the hypothalamus was used following the mouse Allen brain atlas (https://mouse.brain-map.org/static/atlas). Briefly, 1 cm from the third ventricle was used to dissect the area of the hypothalamus. The hypothalamus was disrupted in Qiazol® (Qiagen, Manchester, Greater Manchester, UK) solution using a tissue homogenizer pestle (Fisher Scientific, Paisley, Renfrewshire, UK). RNA was isolated with miRNesy kit (Qiagen, Manchester, Greater Manchester, UK) following manufacturer's instructions. For kidney, the cortex was dissected manually and stored in RNA*later* solution overnight at 4ºC. Renal cortex was manually disrupted with a scalpel prior Qiazol® solution was added. Then, tissue homogenizer was used to further disrupt the tissue. One seventh of the kidney solution was further diluted with Qiazol® and RNA isolated following miRNesy isolation kit´s

instructions. RNA was measured by Nanodrop ONE (Thermofisher, Paisley, Renfrewshire, UK).

Reverse transcription was carried out using high capacity reverse transcription kit as described in 2.1.9. (Thermofisher, Paisley, Renfrewshire, UK). Taqman chemistry was used for interrogating hypothalamus mRNAs using specific primers for AVP and oxytocin (OXC) and β-actin as housekeeping internal control. Sybr green chemistry (Sybr Green Master Mix, Qiagen Manchester, Greater Manchester, UK) was used for measuring levels of WNK1 using specific primers (Kickstart pre-designed primers, Merk Sigma, Poole, Dorset, UK) and β-actin as housekeeping internal control.

2.23. Immunohistochemistry

Mice were deeply anesthetised with an overdose of sodium pentobarbitone (20% (w/v) via intraperitoneal injection (IP), Animalcare, York, UK) and perfused intracardially with PBS followed by 4 % (w/v) PFA in PBS at a rate of 5 ml/min. Isolated organs were post-fixed in 4 % (w/v) PFA overnight at 4^{o}C. To prepare brains for slicing, PFA was replaced with 30 % (w/v) sucrose solution in PBS at 4^{o}C until the brain sunk to the bottom of the tube. Brains were mounted on a slicing platform and embedded with optimal cutting temperature (OCT) solution at -21 ^{o}C. Frozen OCT-embedded brains were cut into coronal slices of 20 µm thickness using a cryostat. Brain slides were collected into wells from a 24-well plate containing freezing media (30 % (v/v) glycerol, 30 % (v/v) ethylene glycol, 40 % (v/v) PBS).

Sections were transferred onto a new plate containing PBS and washed 3 times in PBS for 5 min each on a 100 rpm on lab bench shaker (Twist Shaker TW3, FINEPCR, Korea). Slides were cultured in 3 % (v/v) H_2O_2 diluted in PBS for 15 min on a shaker.

Slides were then washed three times in PBS for 5 min each time in a shaker. Slides were blocked using 15 % (v/v) Normal Donkey Serum (NDS) in PBS for 15 min on a shaker at RT. Subsequently, NDS solution was removed and slides were cultured with primary antibody (1:1000 rabbit anti- mouse AVP was diluted in PBS + 0.1 % (v/v) Triton-x100) (AVP antibody, Abcam, Cambridge, UK) overnight at 4 ^{o}C on shaker. Next day, slides were washed three timeswith PBS for 5 min on shaker and then incubated in a biotinylated secondary antibody against rabbit diluted in PBS + 0.1 – 0.5% Triton-x100 at 1:400 for 1 h. Sections were washed in PBS for 5 min during three cycles and subsequently incubated in Vectastain™ ABC kit (Vector Laboratories Ltd, Peterborough, UK) (1:200) diluted in PBS+0.01 % (v/v) Triton-x100 for 1 h. Staining was developed using DAB chromagen (Merk Millipore, Dorset, UK) with glucose oxidase enhancement, which was followed by slide mounting and dehydration through a series of alcohols and xylenes. Coverslips were then placed on slides using DPX (Fisher Scientific, Loughborough, UK). Photomicrographs from DAB-stained tissue were obtained using a Nikon Eclipse 80i light microscope and Picture Frame Software.

2.25. Statistical analysis

All data are presented as mean ± SEM (standard error of the mean) from a number of independent experiments (n) with replicates specified in each figure legend. Normality of data was assessed with Shapiro-Wilk test. *P* values were calculated using one-way ANOVA and Tukey's multiple comparisons test when all groups were compared or Dunnet´s post hoc when groups were compared only to control group. Two-way ANOVA was used to compare experiments where two independent variables were compared followed by Tukey´s post hoc test. Paired two-tailed *t*-test was used when one comparison

between only two groups was designed in the experiment. Statistically significant differences are presented as $P < 0.05$ (*), $P < 0.01$ (**), $P < 0.001$ (***) $P < 0.0001$ (****). Statistical calculations and graphic figures were performed using the statistical and graphical software GraphPad Prism 7 (GraphPad Software, San Diego, CA, USA).

CHAPTER 3: Isolation and characterisation of brain endothelial cell-derived extracellular vesicles in inflammation

3.1. Introduction

In recent years, pioneering research on the biology of EVs has demonstrated that these lipid membrane-enclosed carriers can carry inflammatory mediators such as miRNAs and mRNAs to modulate the inflammatory response in both the vasculature and immune system (Ramirez *et al.*, 2018). However, one of the challenges faced to achieve reproducible results across experiments is the optimisation of the method of isolation for EVs (Théry *et al.*, 2018).

Because there is no definitive isolation method, the ISEV released a collection of guidelines (MISEV2014 and MISEV2018) to help researchers to select an isolation method that is best suited to their experimental design (Lötvall *et al.*, 2014; Théry *et al.*, 2018). Currently, methods are categorised in four groups based on the degree of recovery (proportion of EV isolated in comparison to the source fluid of EVs) and specificity (isolation of EV components from non-EV components or other EV subtypes). These categories are: 1) high recovery and low specificity (e.g. precipitation-based method), 2) intermediate recovery and intermediate specificity (e.g. differential centrifugation), 3) low recovery and high specificity (e.g. size exclusion), and 4) high recovery and high specificity. This latest group is unachievable with the current methodologies (Théry *et al.*, 2018).

A world-wide survey of EV research revealed that the majority of studies opted for ultracentrifugation as their preferred method for isolation of EVs in an attempt to balance recovery and specificity (Gardiner, Di Vizio, *et al.*, 2016). Many researchers also

routinely use a combinatorial approach for EV isolation such as density gradient isolation followed by size exclusion (Gardiner, Vizio, *et al.*, 2016; Onódi *et al.*, 2018). Once selected, it is important that the method is then tested and optimised for the conditions and cellular source used within the experimental design (Théry *et al.*, 2018).

Only few reports have attempted to characterise the different EVs derived from cells comprising the NVU, in particular, BECs. Haqqani *et al.* described an ultracentrifugation-based method for separating sEVs from CCM of cultured human BECs (hCMEC/D3 cells) under naïve conditions (Haqqani *et al.*, 2013). Treatment of hCMEC/D3 cells with TNFα increased the number of EVs as well as the amount of pro-inflammatory proteins carried within such as VCAM1, ICAM1 or pentraxin 3 (PTX3) (Dozio & Sanchez, 2017). This study showed for the first time a proteomic characterisation of human BEC-derived EVs in inflammation. However, characterisation of pro-inflammatory RNAs (miRNAs and mRNAs) carried by human BEC-derived EVs is still poorly understood. Interestingly, Yamamoto *et al.*, investigated the miRNome of EVs derived from murine BECs after treatment with a cocktail of inflammatory modulators (pro-inflammatory cytokines and LPS) and identified mmu-miR-328-3p, mmu-miR-211-5p and mmu-let-7d-3p as the highest up-regulated miRNAs within the EVs (Yamamoto *et al.*, 2015). Indeed, mmu-let-7d-3p was proposed to target Yin and yang 1 mRNA (YY1) to regulate YY1´s downstream gene vascular endothelial growth factor B (VEGFB) in mouse pericytes (Yamamoto *et al.*, 2015). Unfortunately, it is possible that the cargo of BEC-derived sEV differs across species.

Lastly, it is very likely that the effect of secreted EVs and their cargo contents are both treatment- and target cell-dependent. Different pro-inflammatory modulators (e.g. LPS, TNFα or IFNγ) have been previously shown to affect endothelial function and mimic phenotypes observed in neuroinflammatory disorders (Lopez-Ramirez *et al.*, 2013;

Liang *et al.*, 2014; Ni *et al.*, 2017). LPS is a lipopolysaccharide protein from Gram-negative bacteria normally used to study the effect of bacterial infection and general systemic inflammation in cells (Liang *et al.*, 2014). However, the study of systemic inflammation can also be approached by investigating the single or combinatory effect of pro-inflammatory cytokines relevant to neuroinflammatory disorders. Previously, TNFα and IFNγ have been reported to modulate the function of human BECs via the modulation of miRNAs including hsa-miRNA-155, hsa-miRNA-126-3p or hsa-miRNA-146a-5p (MA. Lopez-Ramirez *et al.*, 2016). Whether these intracellular changes are reflected in the secreted EVs by BECs is still poorly understood.

The aim of this chapter was to determine an EV isolation method that yielded the most concentrated EV population with a suitable purity (e.g. enriched EV markers) from human BECs under naïve and inflamed conditions. To achieve this aim, a systematic comparison of the number of isolated sEVs by ultracentrifugation, precipitation-based and size exclusion methods for the separation of sEVs were carried out. Subsequently, determination of the specificity of sEVs isolated via the two methods that generated the greatest yield of sEVs following isolation was analysed by western blot.

The physical properties of EVs isolated from hCMEC/D3 cells were studied. For this purpose, a comparison of the number, diameter size and morphology of sEVs and L-EVs isolated from CCM of hCMEC/D3 cells treated with pro-inflammatory cytokines was carried out. Based on these results, RNA cargo of one subset of EVs (either sEVs or L-EVs) was also analysed. Therefore, measurement of the levels of pro- or anti-inflammatory miRNAs and mRNAs in the cargo of EVs isolated from cytokine-stimulated and untreated hCMEC/D3 cells were studied.

3.2. Results

3.2.1. Dose-dependent effect of cytokines on the yield of sEVs isolated from hCMEC/D3 cells.

Prior to selecting the standard method to isolate sEVs, the impact of the combination of cytokines (TNFα and IFNγ) on the number of isolated sEVs from hCMEC/D3 cells was investigated using the precipitation-based method. Under basal/unstimulated conditions, the hCMEC/D3 cells secreted 1.4±0.2x10^7 sEVs/cm^2 of confluent cells (n=4) (Figure 3.1.A). Low doses of TNFα and IFNγ (1 ng/ml) did not significantly increase the secretion of sEVs (2.7±0.7x10^7 sEVs/ cm^2 of confluent cells, P>0.05 and n=4) (Figure 3.1.A). However, treatment with medium and high doses of TNFα and IFNγ (10 and 100 ng/ml) significantly increased the number of sEVs recovered from the CCM of hCMEC/D3 cells compared to untreated cells (6.7±0.8x10^7, P<0.05, and 8.0±1.4x10^7 sEVs/cm^2 of confluent cells, P<0.05 and n=4, respectively). No differences were observed in the number of isolated sEVs from hCMEC/D3 cells treated with either 10 or 100 ng/ml of pro-inflammatory cytokines (P>0.05).

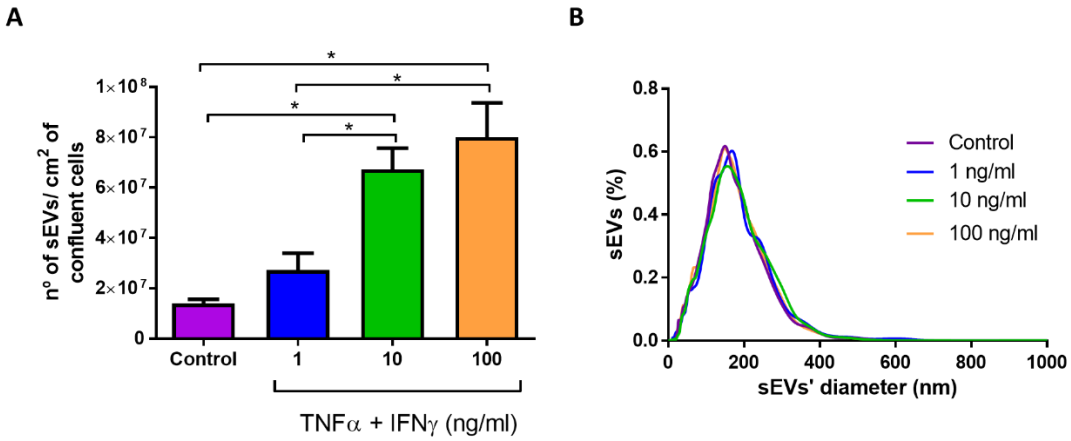

Figure 3.1. Effect of the combination of cytokines in the diameter size and number of sEVs isolated from hCMEC/D3 cells. hCMEC/D3 cells were treated with increasing doses of a combination of TNFα and IFNγ (0, 1, 10 and 100 ng/ml) for 24 h following small EVs (sEVs) isolation by the precipitation method. **(A)** Number of sEVs recovered after treatment with pro-inflammatory cytokines as measured by nanoparticle tracking analysis using an LM10 Nanosight. **(B)** Histogram of the distribution in diameter of sEVs. Data are showed as mean±SEM of n = 4 independent replicates with 5 technical replicates, *P**<0.05. Differences were measured by one-way ANOVA with Tukey's multiple comparisons test.

The histogram distribution for the diameter size of the isolated sEVs secreted by hCMEC/D3 cells remained similar regardless of the treatment with the combination of cytokines (TNFα and IFNγ) (Figure 3.8.B). Indeed, both mean and mode diameter size of sEVs were not significantly altered with treatment of pro-inflammatory cytokines (Table 3.1.).

Table 3.1. Average data on hCMEC/D3 cell-derived sEVs after treatment with TNFα and IFNγ and isolated by precipitation-based method (n=4, mean±SEM)

Samples	Mean (nm)	Mode (nm)
Control	177±6	159±9
1 ng/ml TNFα & IFNγ	187±8	170±9
10 ng/ml TNFα & IFNγ	191±5	165±6
100 ng/ml TNFα & IFNγ	179±4	169±7

3.2.2. Comparison of the methods of isolation of BEC-derived sEVs on vesicle number and size by NTA

To determine which of three well-known methods for the isolation of sEVs – ultracentrifugation, precipitation-based and size exclusion – yielded the purest and most concentrated fraction of sEVs from hCMEC/D3 cells, a systematic comparison was carried out. Based on Figure 3.1., hCMEC/D3 cells were treated with 10 ng/ml TNFα and IFNγ for 24 h to stimulate a high recovery of sEVs. Using cytokine-treated hCMEC/D3 cells was a decision made for practical reasons to reduce the quantity of cultured hCMEC/D3 cells needed to harvest a greater number of sEVs to carry the comparison of these three methods of EV isolation.

Before carrying out a systematic comparison of the isolation methods, the concentration of sEVs and protein content across the fractions collected using size exclusion were screened. Seventeen fractions of 0.5 ml were generated from the CMM. Fractions two and three were observed to contain the highest concentration of sEVs with the lowest amount of protein content (Figure 3.2). Fractions five and higher were enriched in soluble proteins and showed very low concentration of sEVs (Figure 3.2). Based on these findings, fractions 2 and 3 were pooled together for further experiments.

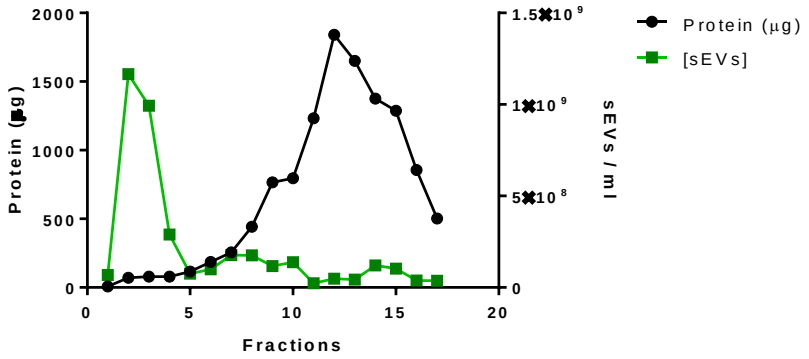

Figure 3.2. qEV histrogram of EV number and protein content. Size exclusion method provided by Izon Science (Oxford, UK) was used to separate small EVs (sEVs) from pre-treated conditioned cell media (CCM) of hCMEC/D3 cells. Fractions were measured for protein content (black line) and sEVs concentration (sEVs/ml, green line). Data are the raw value of one experiment.

Next, the number and size of particles isolated using the three EV isolation methods were compared using NTA with an LM10 Nanosight (Malvern, Worcestershire, UK). As shown in Figure 3.3.A, the calibrated instrument detected nanoparticles in between 7 to 617 nm in diameter size, with a mode of 107±1 nm diameter.

Systematic comparison of sEVs isolated from all three methods revealed that the precipitation-based method and ultracentrifugation isolated $3.7\pm0.8x10^7$ and $3.2\pm0.1x10^7$ sEVs/cm^2, respectively, whereas size exclusion recovered $1.02\pm0.07x10^7$ sEVs/cm^2 from the CCM of confluent hCMEC/D3 cells (Figure 3.4.B). Indeed, precipitation-based and ultracentrifugation techniques isolated significantly higher number of sEVs than size exclusion ($P<0.01$ and $P<0.05$, respectively; n=3).

Then, whether there were any differences in the diameter size distribution of the sEVs isolated from each method was investigated. All three methods isolated vesicles ranging mostly from 0 to 250 nm in size. The mode for the diameter of sEVs isolated by size exclusion was 160±5 nm whereas mode for the diameter of sEVs isolated using

precipitation and ultracentrifugation were 170±16 and 173±14 nm respectively (Figure 3.3.C). However, there was no significant difference in the size distribution of all three methods.

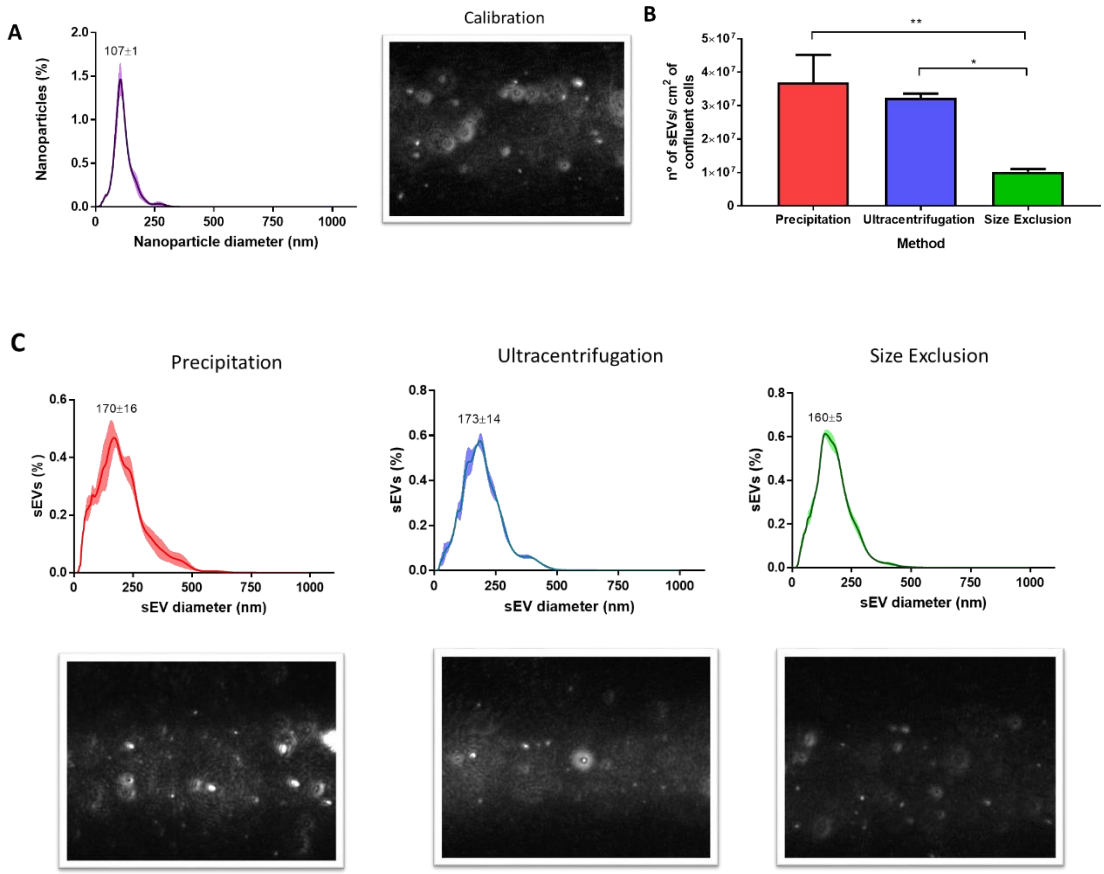

Figure 3.3. Systematic comparison of three methods for the isolation of sEVs. (A) Histogram of particles size distribution with a representative image of the video recorded. LM10 Nanosight was calibrated using 100 nm silica nanoparticles prior measurements and size of the nanoparticles were confirmed (mode=107±1 cm), **(B)** Number of small EVs (sEVs) recovered per cm^2 of confluent hCMEC/D3 cells by each method: precipitation, ultracentrifugation and size exclusion as measured using nanoparticle tracking analysis via an LM10 Nanosight. **(C)** Representative video images of particle recordings and histograms of the size distribution of vesicles recovered by each method. Data are shown as mean±SEM of n=3 of independent replicates with 3 technical replicates, *P**<0.05, *P***<0.01. Results were analysed using one-way ANOVA with post-hoc Tukey's multiple comparisons test.

These results revealed that both the ultracentrifugation and precipitation-based method recovered a significantly higher number of vesicles than size exclusion without

affecting the general size of sEVs. Therefore, the size exclusion method was not pursued further.

3.2.3. Effect of the method of isolation on markers for sEVs.

To compare the purity of sEVs between the precipitation or ultracentrifugation methods, samples isolated from both methods were analysed for protein and RNA content per vesicle as well as expression of specific protein markers for sEVs (Figure 3.4). No significant differences were observed between both isolation methods regarding the ratio of ng of RNA per vesicle ($6.6\pm1.4x10^{-8}$ and $4.7\pm1.5x10^{-8}$ ng RNA/sEVs respectively, $P>0.05$, n=3) (Figure 3.4.A). Conversely, sEVs recovered using the precipitation-based method contained significantly higher amount of protein per vesicle than sEVs isolated by ultracentrifugation ($2.3\pm0.4x10^{-8}$ and $0.8\pm0.2x10^{-8}$ µg/sEVs, respectively and $P<0.05$; n=3) (Figure 3.4.B). This observation suggested an increased extracellular protein contamination in the precipitation-based method-isolated sEVs.

The expression of sEV markers, tetraspanins CD63 and CD9 as well as heat shock protein HSP70, were evaluated by Western blotting. Following standard guidelines for immunoblotting, equal amounts of protein were loaded and semi-quantitative comparison of protein expression was carried out. The immunoblot revealed stronger intensity in the bands for all three markers in the samples isolated by ultracentrifugation when compared to the precipitation-based method (Figure 3.4.C). Equal protein amounts of cell lysates were used as positive controls for the detection of sEV markers by immunoblotting. Indeed, this result was in accordance with Figure 3.4.B suggesting increased extracellular protein contamination.

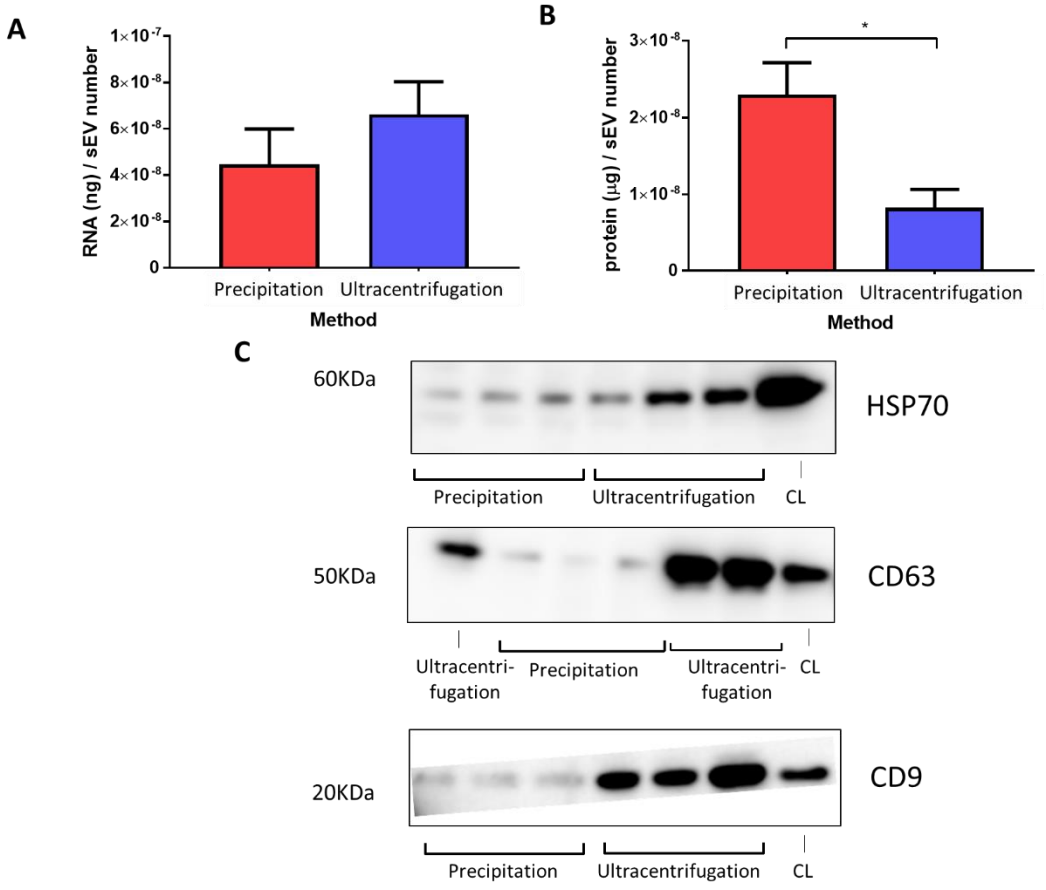

Figure 3.4. Analysis of the purity of the sEVs. (A) Quantification of total RNA per small EVs (sEVs), separated from the same cell culture supernatant and isolated by ultracentrifugation or precipitation method. **(B)** Quantification of total protein per sEVs measured by DC protein assay (Bio-Rad, Watford, UK). Differences were analysed by paired two-tailed *t*-test. Data presented as mean ± SEM (n =3), *P**<0.05. **(C)** Cropped images from western blot analysis of EV markers (CD9, CD63 and HSP70) from sEVs isolated using precipitation method or ultracentrifugation. Equal amount of protein from cell lysates (CL) was used as positive controls.

Taking all these results together, ultracentrifugation appeared to be the optimal method to isolate sEVs from hCMEC/D3 cells as it provided the highest yield combined with low extracellular protein contamination. However, ultracentrifugation may also pull down some of the soluble TNFα and IFNγ remaining in the CCM following treatment thereby impacting on downstream applications. Therefore, the concentration of residual TNFα and IFNγ in the CCM following 24 h of cytokine incubation with BECs was measured by ELISA. TNFα and INFγ residual concentration in the CCM was

117.52±19.82 and 142.25±32.43 ng, respectively. In isolated EVs, concentrations of TNFα and IFNγ were 0.012±0.008 and 0.015±0.005 ng respectively (Figure 3.5), suggesting that less than 1% of residual exogenously added TNFα and IFNγ was contained within the EV mixture.

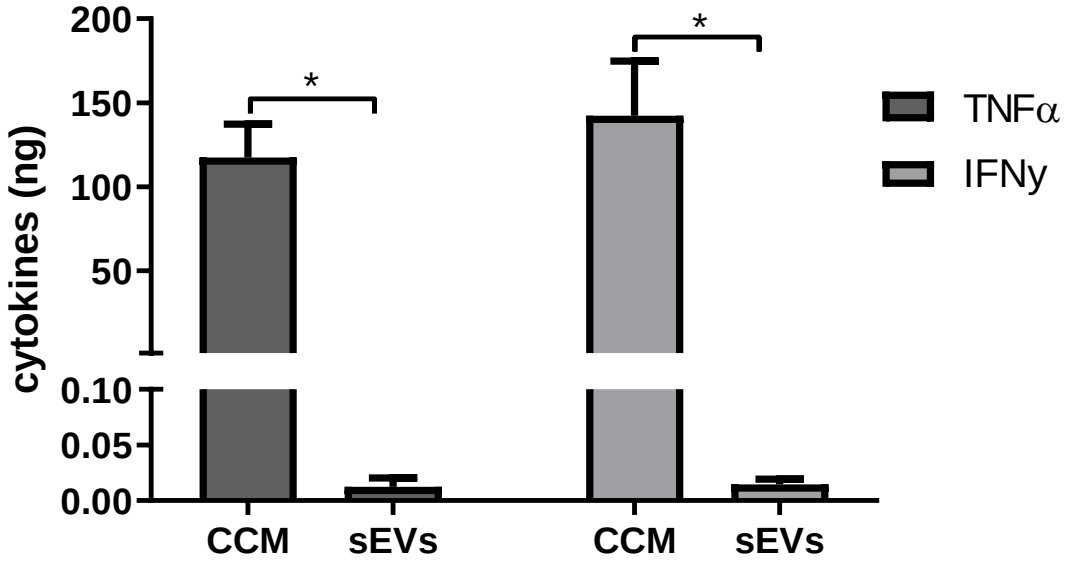

Figure 3.5. Residual quantity of pro-inflammatory cytokines TNFα and IFNγ. Measurement of soluble TNFα and IFNγ in cell conditioned media (60 ml, CCM) and intact small EVs (1 ml, sEVs) with DuoSet ELISA. Data are showed as mean ± SEM of n= 3 *P**<0.05. Differences were measured by paired two-tailed *t*-test.

3.2.4. hCMEC/D3 cells secrete higher number of sEVs than L-EVs

Conventional methods for the isolation of EVs enrich for two fractions of EVs: sEVs (<200nm) or L-EVs (>200nm) (Théry *et al.*, 2018), which have different functional roles (Tkach *et al.*, 2017). To determine the proportion of L-EVs and sEVs isolated following ultracentrifugation, the number, size and morphology of EVs under basal (quiescent sEVs and quiescent L-EVs) and inflammatory conditions (10 ng/ml of TNFα

and IFNγ, therefore, cytokine-sEVs and cytokine-L-EVs) was measured using NTA via a Nanosight S500 and TEM (Figure 3.7).

A high degree of overlap was noted in the size distribution of sEVs and L-EVs (Figure 3.7A). Indeed, mean diameter size was not changed among the four groups (Table 3.2.). These results were consistent with the measurement of the most frequent diameter size of isolated EVs represented by the mode. The mode of isolated EVs was not significantly different in any group and highlight the heterogeneity of the sample (Table 3.2). A percentile analysis of the low population (10%, D10), middle/median population (50%, D50) and high population (90%, D90) based on diameter size was studied. The range in diameters of EVs was similar to both subtypes for smaller particles (D10) and medium size particles among four studies groups (Table 3.2). However, the diameter size for the top percentage of EVs was significantly higher in cytokine-L-EVs (Table 3.2). D90 for quiescent, cytokine-sEVs and quiescent-L-EVs were 223±20, 268±25 and 238±24 nm, respectively, whereas cytokine-L-EVs´ D90 was 330±29 nm.

Table 3.2. Average data on hCMEC/D3 cell-derived EVs measured by NTA.

Samples	Mean (nm)	Mode (nm)	D10 (nm)	D50 (nm)	D90 (nm)
Quiescent sEVs	166 ± 14	129 ± 16	97 ± 8	141 ± 12	223 ± 20 ****
Cytokine-sEVs	177 ± 12	135 ± 12	98 ± 7	148 ± 10	268 ± 25 *
Quiescent L-EVs	164 ± 10	134 ± 5	84 ± 5	149 ± 6	238 ± 24 ***
Cytokine-L-EVs	206 ± 13	144 ± 17	97 ± 8	178 ± 13	330 ± 29

Abbreviations: EVs, extracellular vesicles; sEVs, small EVs; L-EVs, large EVs; NTA, NanoSight particle tracking analysis; *P values <0.05, ***P values <0.001, ****P values <0.0001 cytokine-sEVs vs. cytokine-L-EVs. Data are shown as mean±SEM with n=4 of independent replicates. Repeated measures, two-way ANOVA with Tukey´s post hoc test for multiple comparison.

In accordance with Figure 3.1, number of isolated cytokine-sEVs ($6.21\pm0.77x10^7$ sEVs/cm^2 of confluent cells) was significantly higher than isolated quiescent sEVs ($1.43\pm0.70x10^7$ sEVs/cm^2 of confluent cells, $P<0.001$; n=4). Under basal condition, number of isolated L-EVs was $0.11\pm0.02x10^7$ L-EVs/cm^2 of confluent cells, which showed a trend but no-significant decrease of number of EVs when compared to quiescent sEVs. Similarly, the effect of 10 ng/ml of TNFα and IFNγ did not significantly increase the number of cytokine-L-EVs when compared to quiescent L-EVs. However, analysis of the number of cytokine-EVs isolated from hCMEC/D3 cells showed that the number of sEVs was significantly higher than the number of L-EVs (sEVs = $6.21\pm0.77x10^7$ vs. L-EVs = $0.46\pm0.14x10^7$ EVs per cm^2 of confluent cells, $P<0.0001$; n=4) (Figure 3.7B).

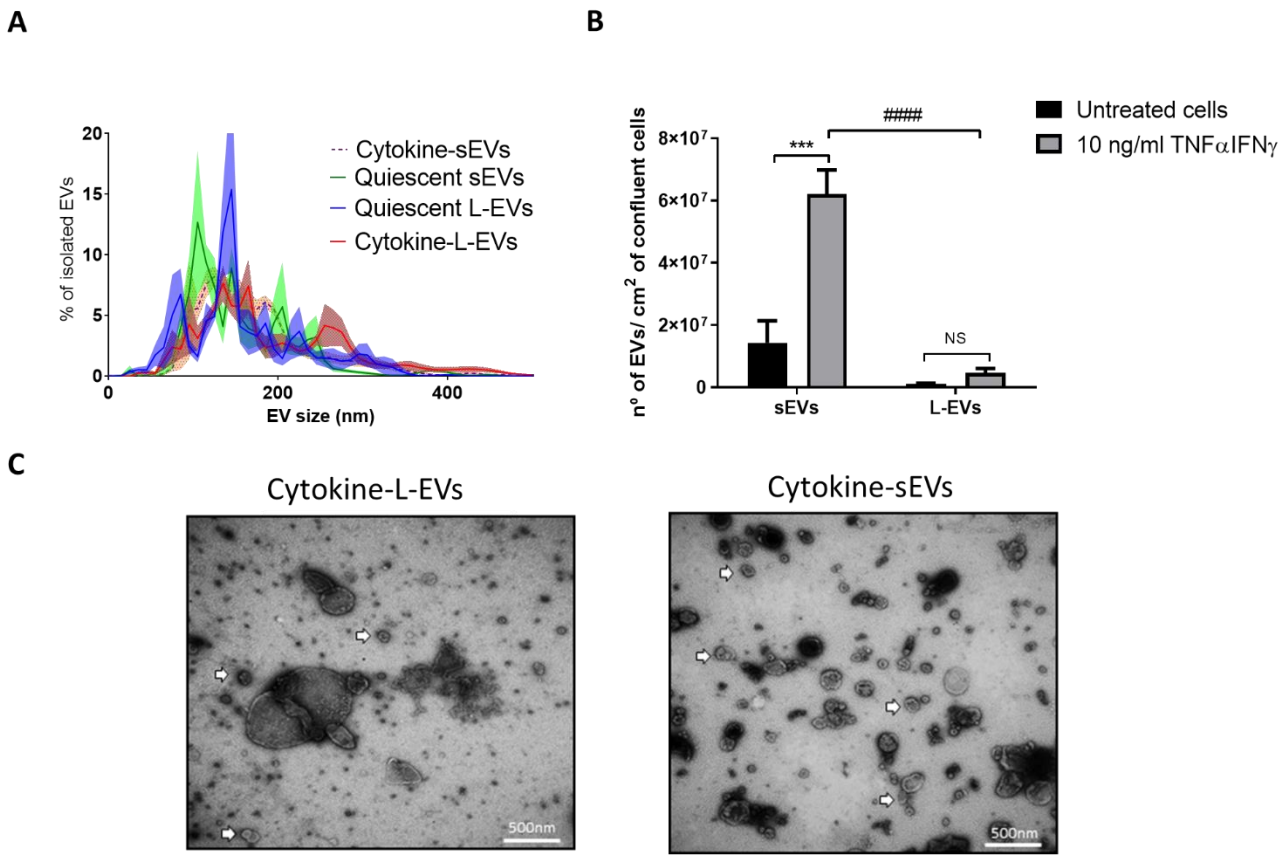

Figure 3.7. Characterisation of both sEVs and L-EVs isolated from hCMEC/D3 cells under inflammatory conditions. hCMEC/D3 cells were treated with 10 ng/ml of TNFα and IFNγ or left untreated for 24h. Cell conditioned media was then collected and small and large EVs (sEVs and L-EVs) were separated by differential centrifugation. **(A)** Histogram of size distribution of EVs isolated under basal conditions (quiescent sEVs and quiescent L-EVs) and after treatment with pro-inflammatory cytokines (cytokine-sEVs and cytokine-L-EVs), which was analysed by nanoparticle tracking analysis (NTA, NS500). **(B)** Measurement of number of sEVs and L-EVs with NS500. Data are showed as mean ± SEM of n=4 (A and B), Two-way ANOVA using Tukey´s post hoc test for multiple comparison with *** $P<0.001$ to quiescent sEVs and #### $P<0.0001$ to cytokine-sEVs. **(C)** Transmission electron microscopy (TEM) images of cytokine-L-EVs (left panel) and cytokine-sEVs (right panel) stained with uranyl acetate. Images are representative of two biological experiments with two technical replicates each. Scale bar = 500 nm

The morphology of both types of EVs (sEVs and L-EVs) was confirmed using TEM (Figure 3.7C). TEM images of cytokine-L-EVs (right panel of figure 3.7.C) showed lipid bilayer round vesicles ranging from 40 to 600 nm whereas TEM images of cytokine-

sEVs (left panel of figure 3.7.C) was enriched for cup-shaped and lipid bilayer vesicles smaller than 250 nm.

These results suggested that the isolation of the number of sEVs from hCMEC/D3 cells under inflammatory conditions was greater than the number of L-EVs. As such, the remainder of the characterisation studies were focused on sEVs.

3.2.5. Profile of miRNAs and mRNAs in sEVs after treatment with pro-inflammatory cytokines

sEVs can carry both proteins and nucleic acids (including DNA, mRNA and miRNAs) (Kalra, Drummen and Mathivanan, 2016). The expression of miRNAs within sEVs is dependent on the stimulus used to activate secreting cells (Geis-Asteggiante *et al.*, 2018). Consequently, the expression of TNFα/IFNγ-related miRNAs in hCMEC/D3-derived sEVs was investigated by RT-qPCR. For this purpose, six miRNAs whose expression under inflammatory conditions had been previously described in hCMEC/D3 cells, were selected (Lopez-Ramirez *et al.*, 2014; Wu, *et al.*, 2015; Cerutti *et al.*, 2017). These miRNAs have been previously observed to be either up-regulated (miRNA-155-5p, miRNA-146b-5p and miRNA-146a-5p), down-regulated (miRNA-126-5p and miRNA-126-3p) or unchanged (miRNA-24-5p) in hCMEC/D3 cells during conditions of inflammation (Reijerkerk *et al.*, 2013).

RT-qPCR revealed that miRNA-155 expression was increased in the cargo of cytokine-sEVs when compared to quiescent sEVs. Interestingly, miRNA-155 levels showed maximal expression after treatment with 10 ng/ml of pro-inflammatory cytokines (8.2±1.2 fold change over unstimulated, $P<0.001$; n=3) (Figure 3.9). No changes were observed in the other miRNAs examined at any cytokine concentration.

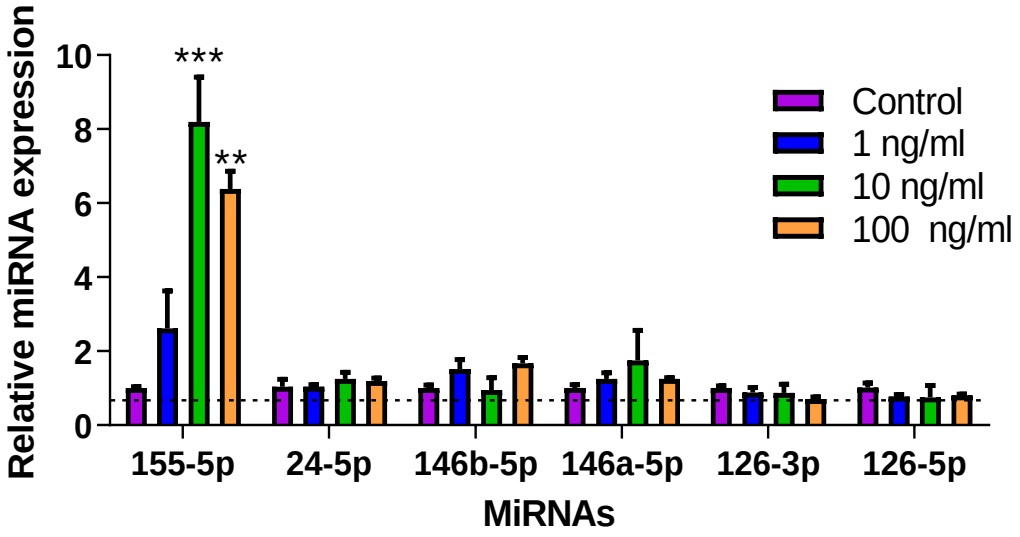

Figure 3.9. Expression of inflammation-related microRNAs in sEVs. MiRNAs expression in the cargo of small EVs (sEVs) isolated from cytokine-treated (TNFα and IFNγ at 1, 10 or 100 ng/ml) hCMEC/D3 cells or untreated cells. Data were normalised to miRNA-let7g as internal control. Data is showed as mean±SEM of n = 3 of independent replicates **(A)**, *P***<0.01 and *P****<0.001 to control/unstimulated sEVs. One-way ANOVA with Dunnet´s post hoc**.**

To determine whether sEVs also contained mRNAs associated with cerebral endothelial inflammation, cargo levels of adhesion molecules CEACAM1, ICAM1 and VCAM1 were measured by RT-qPCR (Figure 3.10). Levels of both ICAM1 and VCAM1 mRNA were significantly increased in the cargo of sEVs derived from inflamed hCMEC/D3 cells compared to those sEVs isolated from naïve hCMEC/D3 cells. VCAM1 levels were significantly greater at 10 and 100 ng/ml of TNFα and IFNγ (10 ng/ml = 3.76±0.93 whereas control levels were 1.09±0.33, $P<0.05$; n=5) (Figure 3.10). On the other hand, ICAM1 levels were increased at all three doses investigated but only significantly at 10 and 100 ng/ml (1.01±0.08, 2.91±0.44, 6.21±1.33 and 10.10±0.355, $P>0.05$, $P<0.01$ and $P<0.001$, respectively; n=3) (Figure 3.10). No differences in CEACAM1 mRNA levels were noted between quiescent sEVs and those from TNFα and IFNγ-stimulated cells at any concentration.

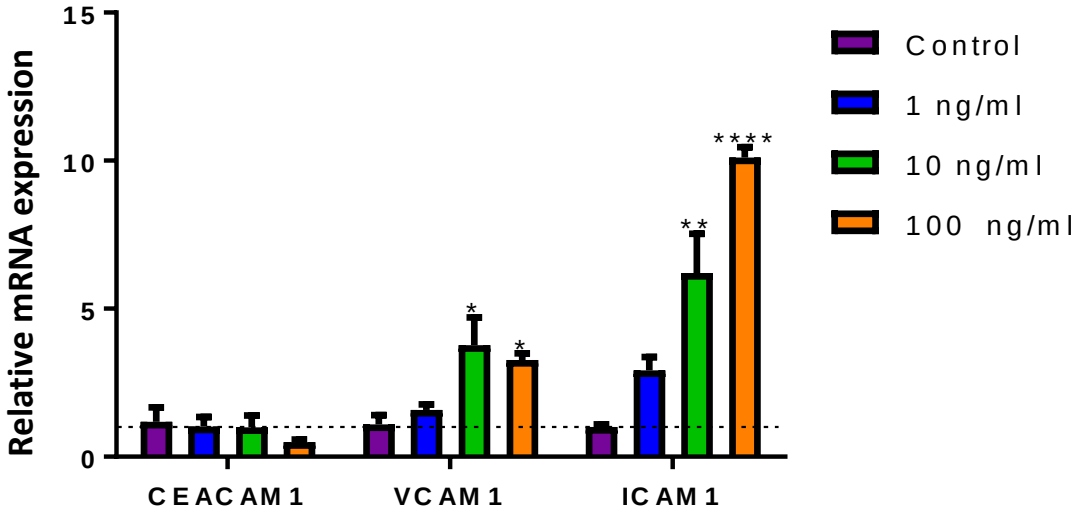

Figure 3.9. Expression of inflammation-related mRNAs in sEVs. Analysis of inflammation-related mRNAs in sEVs (CEACAM, VCAM1 and ICAM1) by RT-qPCR. Data was normalized to β-actin. Data are showed as mean ± SEM of n = 3 or n = 5 (VCAM1 mRNA), *P**<0.05 and *P***<0.01, *P*****<0.0001. One-way ANOVA with post-hoc Dunnet´s post hoc.

To determine whether the sEV miRNA and mRNA contents reflected inflammation-induced changes in levels in hCMEC/D3 cells, levels of miRNA-155 and of VCAM1 and ICAM1 mRNA were measured in cell extracts after treatment with 10 ng/ml of TNFα and IFNγ. As expected, intracellular miRNA-155 levels were 6.40±0.56, *P*<0.0001 (n=3) higher in cells stimulated with 10 ng/ml when compared to untreated cells (Figure 3.11A). As shown in Figure 3.11, cytokine treatment significantly increased levels of VCAM1 and ICAM1 mRNA compared to untreated conditions (Figure 3.11A and 3.11B). Interestingly, the up-regulation of VCAM1 was 8 fold higher in the hCMEC/D3 cells than VCAM1 mRNA levels within the cargo of sEVs (28.9±0.28 intracellularly and 2.87±0.77 within cytokine-sEVs) whereas ICAM1 levels were only 1.5 fold change (7.65±0.43 intracellularly and 6.04±0.75 within cytokine-sEVs). These

results suggested there was an enrichment of pro-inflammatory miRNA and mRNAs in sEVs that partially reflect the intracellular status of the secreting hCMEC/D3 cells.

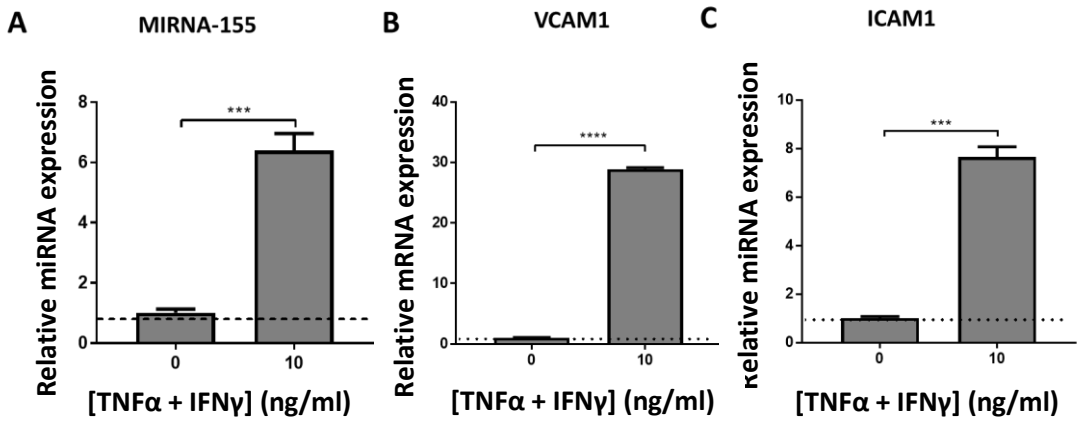

Figure 3.11. Effect of treatment with a combination of cytokines (TNFα and IFNγ) in hCMEC/D3 cells on transcript levels. hCMEC/D3 cells were treated with 10 ng/ml of TNFα and IFNγ and miRNA-155 and mRNA were analysed by RT-qPCR. Treatment with combination of cytokines led to increased levels of microRNA-155-5p **(A)**, VCAM1 **(B)** and ICAM1 mRNAs **(C)**. Data are showed as mean±SEM of n = 3 of independent replicates. *P***<0.01 and *P****<0.001. Differences were analysed by paired two-tailed *t*-test.

3.1. Discussion

In this chapter, a systematic comparison of three well-established methods for the isolation of sEVs demonstrated that ultracentrifugation was the optimal method for isolation of cerebral endothelial sEVs. Characterisation of sEVs and L-EVs from cytokine-stimulated hCMEC/D3 cells identified differences in number of EVs and morphology. Finally, miRNA-155 as well as VCAM1 and ICAM1 mRNAs were shown to be up-regulated in the cargo of cytokine-sEVs in comparison to quiescent sEVs.

3.1.1. Size exclusion and precipitation method were outperformed by ultracentrifugation method for the isolation of sEVs based on sEV number and markers.

Numerous studies have compared the different available methods for the separation of sEVs from CCM and/or biological fluids (Van Deun *et al.*, 2014; Lane *et al.*, 2015; Lobb *et al.*, 2015; Taylor and Shah, 2015; Tang *et al.*, 2017). However, great discrepancies in the selection of the method of isolation are observed across the literature, which makes assessing the reproducibility of a method difficult (Helwa *et al.*, 2017). For these reasons, this study was initiated by comparing three well-established methods to determine an optimal technique that generated the greatest sEV recovery and purity from hCMEC/D3 cells.

A greater number of sEVs were recovered from endothelial CCM using both precipitation-based and ultracentrifugation methods compared to the size exclusion method (qEVs). These results disagree with a published comparative study of qEVs and a precipitation-based method (ExoQuick), which showed that qEV performed better at recovering sEVs from CCM. However, differences among CCM pre-treatment as well as among precipitation-based methods might explain these differences in recovery (Lobb *et al.*, 2015). The method from Exiqon (now part of Qiagen) was selected because this company had a published track record of generating products for the handling and analysis of miRNAs (Brunet-Vega *et al.*, 2015). These commercial available kits rely on a PEG polymer with formulations that vary among the different manufacturers (García-Romero *et al.*, 2019). Interestingly, another study observed a better recovery of sEVs using non-commercial PEG-based precipitation kits when compared to size exclusion (Gámez-Valero *et al.*, 2016). It is possible that the better performance of Exiqon may be

due to its unique PEG formulation that might be optimised for EV isolation. This formulation is not available to the general public.

In the previous section, the two methods that recovered the highest yield of sEVs from the endothelial CCM (precipitation and ultracentrifugation methods) were selected. Next, the purity of the sample isolated by those two methods was studied. Although no significant difference in the amount of RNA recovered from each method was observed, the precipitation-based method carried a higher amount of protein per vesicle. It is well established that the higher the ratio protein content over sEV number is, the more likely that the method is co-isolating non-vesicular particles (Théry *et al.*, 2018). Previous findings comparing different methods for the isolation of serum EVs showed that purity measured via band densitometry of soluble albumin protein of both Exiqon and ultracentrifugation was low in both cases (Buschmann *et al.*, 2018). Given that performance of these methods relies on other factors such as CCM, EV population and user, confirmation of the purity of EVs was carried out by detecting the presence of markers for sEVs by Western blotting (Théry *et al.*, 2018). All three EV markers (CD9, CD63 and HSP70) were present in sEVs isolated by both methods, however, there was a clear enrichment of all three markers in vesicles recovered by ultracentrifugation. This is in agreement with reports from other studies that reported that sEVs isolated using PEG-based methods expressed fewer sEV protein markers (Lobb *et al.*, 2015; Gheinani *et al.*, 2018). It is also possible that as equal loading was calculated by protein concentration, the additional protein may have masked the protein content of sEVs.

Ultracentrifugation was the most common method used for the isolation of sEVs according to a world-wide survey (Gardiner, Di Vizio, *et al.*, 2016). The recovery and purity of this method is very dependent of the parameters for centrifugation (temperature, rotor type, speed…) applied (Cvjetkovic, Lötvall and Lässer, 2014). The set-up carried in

this work was considered good to optimise the recovery of sEVs and the results showed that this method out-performed size exclusion and precipitation-based method. Therefore, size exclusion and precipitation were no longer used in the following experiments.

3.2.6. Removal of pro-inflammatory cytokines after isolation of sEVs with ultracentrifugation

Although ultracentrifugation was determined to provide the highest yield and purity in sEV isolation of the three methods studied, there was still a possibility that the samples were not pure enough for the downstream application. Other studies have reported that this method also isolates non-vesicular components such as albumin protein in serum derived sEVs (Tang *et al.*, 2017). Although some residual TNFα and IFNγ were found in the sEV isolates, these concentrations were 10 times lower than the lowest dose reported to affect endothelial function (Cerutti *et al.*, 2017). Thus, although there is no certainty that any biological effects induced by sEVs isolated from the CCM were not also influenced by residual pro-inflammatory cytokine contaminants, this influence is likely to be minimal.

3.2.7. Endothelial cells secrete higher number of sEVs than L-EVs although both populations are heterogeneous

Current methods for separation of EVs allow only partial purification of specific EV populations (Dozio and Sanchez, 2017). Thus, additional characterisation is needed to determine if the isolated EVs contained sEVs, L-EVs or a combination of both, as sEVs and L-EVs have been reported to have both overlapping and distinct biological effects (Théry *et al.*, 2018). It was observed that hCMEC/D3 cells secreted a higher number of

sEVs than L-EVs. In another study using the same cell line and TNFα as stimulus, the authors reported that EV secretion was higher under inflammatory conditions, however they did not compare differences between sEV and L-EVs in terms of numbers (Dozio and Sanchez, 2017). For the current work, we will focus in investigating the role of sEVs in endothelial function.

3.2.8. Morphology of sEVs by ultracentrifugation

Observation of sEVs preparation using electronic microscopy is a requirement for the efficient characterisation of sEVs according to ISEV (Théry *et al.*, 2018). Similarly to previously published reports, it was observed cup-shaped vesicle structures that are traditionally associated with sEVs (Théry *et al.*, 2006). However, current evidence suggests that this morphology may be an artefact created by the technique for imaging sEVs (Raposo and Stoorvogel, 2013). Cryo-EM has proven that the most likely endogenous conformation of sEVs is spherical (Conde-Vancells *et al.*, 2008). TEM also revealed some sEVs that had lost their membrane integrity. There is a high possibility this was due to the method of isolation because previous studies have shown that ultracentrifugation can damage some EVs during isolation (Helwa *et al.*, 2017). In summary, the morphology of sEVs represented the typical shape observed for sEVs processed for TEM.

3.2.9. Inflammation modulates secretion of sEVs by hCMEC/D3 cells.

Modulators of inflammation such as cytokines have been reported to regulate secretion of sEVs in many different cell types (Sohda, Misumi and Oda, 2015; Podbielska *et al.*, 2016; Wang *et al.*, 2017). Most studies treat the secreting cells with one type of cytokines (Dozio and Sanchez, 2017). However, other studies have previously demonstrated a synergic effect of TNFα and IFNγ on brain endothelial function (Pan *et al.*, 2011; Lopez-Ramirez *et al.*, 2013; Reijerkerk *et al.*, 2013). Therefore, how the treatment with a combination of these two cytokines affected the recovery of sEVs as well as their size distribution was investigated. Indeed, treatment with increasing doses of TNFα and IFNγ promoted a greater recovery of sEVs. Previous studies have suggested that TNFα increases the rate of vesicular formation in hCMEC/D3 cells, which might explain the increased number of sEVs observed. Only two other studies have attempted to characterise the sEVs isolated from hCMEC/D3 cells (Haqqani *et al.*, 2013) and only one of them used an inflammatory stimulus such as TNFα (Dozio and Sanchez, 2017). However, TNFα has previously shown to increase sEV in HUVECs (Li *et al.*, 2019). Indeed, results from this work confirmed that treatment of cytokines increased the number of sEVs recovered from hCMEC/D3 cells, as previously reported in other cell types (Podbielska *et al.*, 2016; Tkach *et al.*, 2017; Wang *et al.*, 2017).

Treatment with cytokines did not alter the size distribution of the sEVs, which is also in keeping with previous studies that demonstrated that treatment of hCMEC/D3 cells with TNFα did not affect the size of the recovered sEVs (Dozio and Sanchez, 2017). However, it was noted that treatment with cytokines enriched for larger vesicles in cytokine-L-EVs when compared to quiescent-L-EVs represented by D90 of diameter size. A similar result was described by Yang and colleagues, who showed that LPS-stimulated microglia released larger vesicles (also represented by D90) than naïve

microglia (Yang *et al.*, 2018). In this article, vesicle number was not compared. However, it is tempting to speculate that although cytokine treatment may not increase the number of L-EVs released by hCMEC/D3 cells, a slight but significant increase into the secretion of larger vesicles might have a biological role in cell-to-cell communication in inflammation. Although for this work, focus was given to sEVs based on total number of isolated sEVs, future experiments to characterise L-EVs cargo and their role on BBB function will help to elucidate the role of L-EVs in inducing BBB dysfunction.

3.2.10. Endothelial sEVs are enriched with pro-inflammatory miRNA-155 and VCAM1 and ICAM1 mRNAs

MiRNAs released from sEVs have been implicated in regulating immunomodulation (Balusu *et al.*, 2016) and vascular function (Taverna *et al.*, 2014) among other functions. Here, it was reported that miRNA-155 levels are enriched in the cargo of sEVs after treatment with pro-inflammatory cytokines. This miRNA was also increased intracellularly in treated hCMEC/D3 cells. However, miRNA fold change between control and cytokine-treated conditions was proportionally different between sEVs and hCMEC/D3 extracts. Some miRNAs are proposed to be actively exported by sEVs and that their physiological effects are dependent on the cellular context (de Jong *et al.*, 2012; Djebali *et al.*, 2012). Therefore, it is not surprising that these results differed from other published studies. For instance, mouse brain endothelial cells stimulated with a combination of inflammatory modulators (LPS and cytokines) released sEVs that were not enriched in miRNA-155 (Yamamoto *et al.*, 2015). The specific up-regulation of miRNA-155 within the cargo of sEVs might suggest sEVs work as a vehicle for the

transmission of this microRNA to other target cells. In fact, cellular stress has been proven to be reflected in the RNA cargo of sEVs (de Jong *et al.*, 2012)

On the other hand, recent in-depth analysis of RNA species carried within sEVs and endothelial cells suggested that sEVs are enriched for long RNAs rather than short RNAs such as miRNAs (Pérez-Boza, Lion and Struman, 2018). Enrichment of miRNAs above other RNA species is likely to be cell-specific (Sork *et al.*, 2018). Nevertheless, specific modulation under cellular stress (e.g. TNFα) indicate that they are likely to play a role in cell function. Furthermore, it is important to acknowledge that other RNA molecules might be contributing to the function of sEVs (Chen *et al.*, 2017; Ragni *et al.*, 2017; Pérez-Boza, Lion and Struman, 2018). Indeed, mRNAs encoding for adhesion molecules VCAM1 and ICAM1 were up-regulated in the cargo of sEVs upon treatment with combination of cytokines (TNFα and IFNγ). This is particularly interesting because both adhesion molecules have been involved in the pathogenesis of neuroinflammatory disorders (Lopes Pinheiro *et al.*, 2016). In the next chapter, the role of sEVs modulating BBB function and how VCAM1, ICAM1 and miRNA-155 are altered by sEVs will be investigated.

CHAPTER 4: Role of small extracellular vesicles on cerebrovascular function in inflammation

4.1. Introduction

In the previous chapter, it was observed that inflammation of BECs induced the release of sEVs containing pro-inflammatory vascular modulators such as miRNA-155 and mRNAs for ICAM1 and VCAM1. Up-regulation of these three molecules has been linked to neuroinflammatory disorders such as MS (Alvarez, Cayrol and Prat, 2011; Lopez-Ramirez *et al.*, 2014; Ortiz *et al.*, 2014; Cerutti *et al.*, 2016). Furthermore, sEVs have been previously described to promote inflammation in recipient peripheral endothelial, immune cells, brain pericytes and distant organs (for a review see Ramirez *et al.*, 2018). Indeed, LPS-induced sEVs from the mouse brain endothelial cell line (b.End5) were shown to promote VEGFB expression in recipient pericytes (Yamamoto *et al.*, 2015). On the other hand, quiescent BEC-derived sEVs were shown to decrease apoptosis by acceptor oligodendrocytes (Kurachi, Mikuni and Ishizaki, 2016). Currently little is known about the role of BEC-derived sEVs in modulating endothelial function in inflammation. Cerebrovascular dysfunction at the level of BECs can be measured by investigating the state of key endothelial properties such as elevated TEER, low paracellular permeability or controlled T cell transmigration (e.g. via leukocyte adhesion).

The aim of the experiments in this chapter was to characterise the effect of sEVs isolated from TNFα- and IFNγ-activated hCMEC/D3 cells (cytokine-sEVs) on cerebrovascular function in comparison with untreated cells and/or cells treated with quiescent sEVs. In order to carry this work, the uptake of sEVs by different cells of the NVU was analysed by flow cytometry and confocal microscopy. The effect that sEVs

have on modulating TEER across BEC monolayers was investigated by ECIS. Then, whether treatment with sEVs induced leukocyte cell adhesion to brain endothelium was measured using an in-house flow-based method to analyse firm cell adhesion (Cerutti *et al.*, 2016). Finally, a preliminary study on the molecular changes promoted by sEVs in acceptors cells was performed using RT-qPCR and western blotting.

4.2. Results

4.2.1. Uptake of endothelial sEVs by cells of the neurovascular unit

To compare the uptake of cytokine- and quiescent endothelial sEVs by the three main cellular types of the NVU - endothelial cells, astrocytes and pericytes (Abbott, Adjanie A K Patabendige, *et al.*, 2010) – the uptake of DiO-labelled sEVs by hCMEC/D3, HBMP and hA cell lines was assessed by flow cytometry. Uptake of quiescent sEVs by naïve hCMEC/D3 cells was 23±12 arbitrary units of median fluorescence (A.U.) compared to 6±1 A.U. for cytokine-sEVs (Figure 4.1.A). A similar pattern of uptake was observed by naïve astrocytes (the uptake of quiescent sEV was 112±54 A.U. and the uptake of cytokine sEVs was 53±21 A.U.) and pericytes (the uptake of quiescent sEVs was 30±6 A.U. and the uptake of cytokine sEVs was 11±2 A.U.). However, no statistically significant differences were observed among these groups (P>0.05, n=3). Given the intrinsic differences among cellular types (e.g. cell surface) which might have biased the comparison of the uptake among all three cell types, uptake of sEVs by NVU cells was normalised to the uptake of quiescent sEVs in each cell line. The uptake fold change for sEVs was 0.45±0.16 for BECs, 0.53±0.08 for astrocytes and 0.39±0.08 for pericytes. These ratios were not significantly different among the three cell lines (P>0.05,

n=3) (Figure 4.1.B) suggesting there is not a preference of uptake of endothelial sEVs by any of the three NVU cell types.

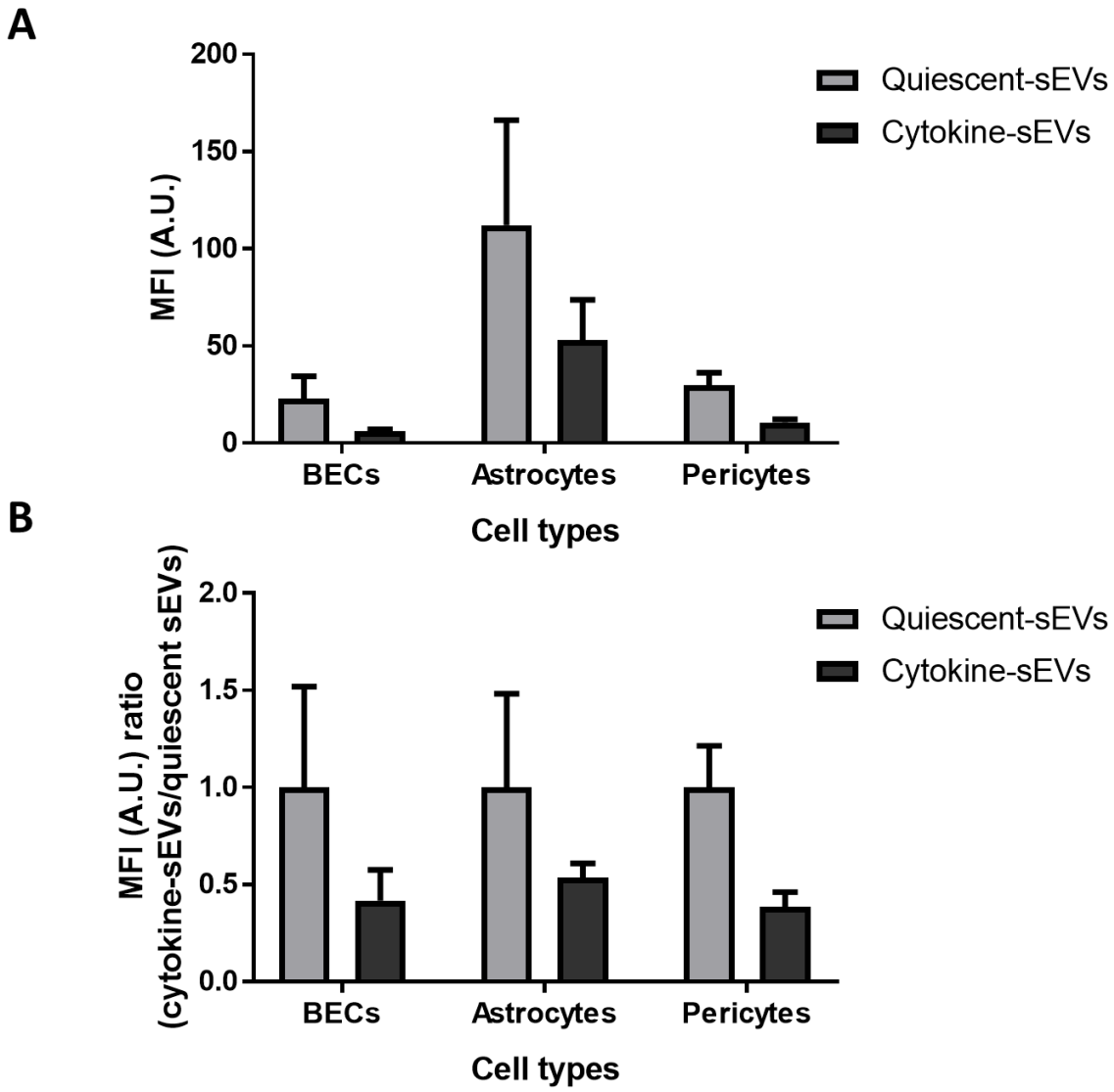

Figure 4.1. Characterisation of the uptake of sEVs by cells of the neurovascular unit. Brain endothelial cells (BECs, hCMEC/D3 cells), pericytes (human brain pericytes) and astrocytes (human foetal cortical astrocytes) were cultured with 0.1 x 10^8 EVs/µl DIO-labelled small EVs isolated from 10 ng/ml TNFα and IFNγ-treated hCMEC/D3 (cytokine-sEVs) or quiescent hCMEC/D3 cells (quiescent sEVs). **A)** Flow cytometry analysis of sEVs uptake. **B)** Normalisation of data by cell type using ratio of median fluorescent intensity (MFI) of cytokine-sEVs MFI quiescent sEVs MFI. Data are shown as mean ± SEM, n = 3 of independent experiments; differences were assessed by two-way ANOVA with Tukey´s post-hoc test.

4.2.2. Dose- and time- dependent uptake of cytokine-sEVs by hCMEC/D3 cells

To study the temporal uptake of sEVs by BECs, naïve hCMEC/D3 cells were incubated with DiO-labelled cytokine-sEVs for 6, 24 and 48 h. Confocal microscopy showed a predominantly perinuclear localization of DiO dye within recipient cells (Figure 4.2.A.). Uptake of cytokine-sEVs by hCMEC/D3 cells was qualitatively similar between 24h and 48h of incubation, suggesting a level of saturation was achieved by 24 h. Based on these observations, a 24 h end-point was selected to carry out a dose response using flow cytometry. Quantification of the median fluorescence of BECs treated with DiO-labelled cytokine-sEVs revealed that cellular uptake was dose-dependent (Figure 4.2.B). The uptake of $0.1x10^8$ cytokine-sEVS/µl (90±13 A.U.) showed a non-significant increase in signal intensity compared to cells treated only with PBS (6±1 A.U.) (P>0.05). The fluorescent intensity was significantly higher in cells incubated with $0.5x10^8$ and $1x10^8$ DiO-labelled cytokine-sEVs/µl compared to the PBS control (427±65 and 749±120 A.U., P<0.05 and P<0.001, respectively and n=3) (Figure 4.2.B). For the remainder of the study, treatment with 10^8 number of sEVs/µl for 24 h was selected to investigate their role in the inflammatory state of BECs.

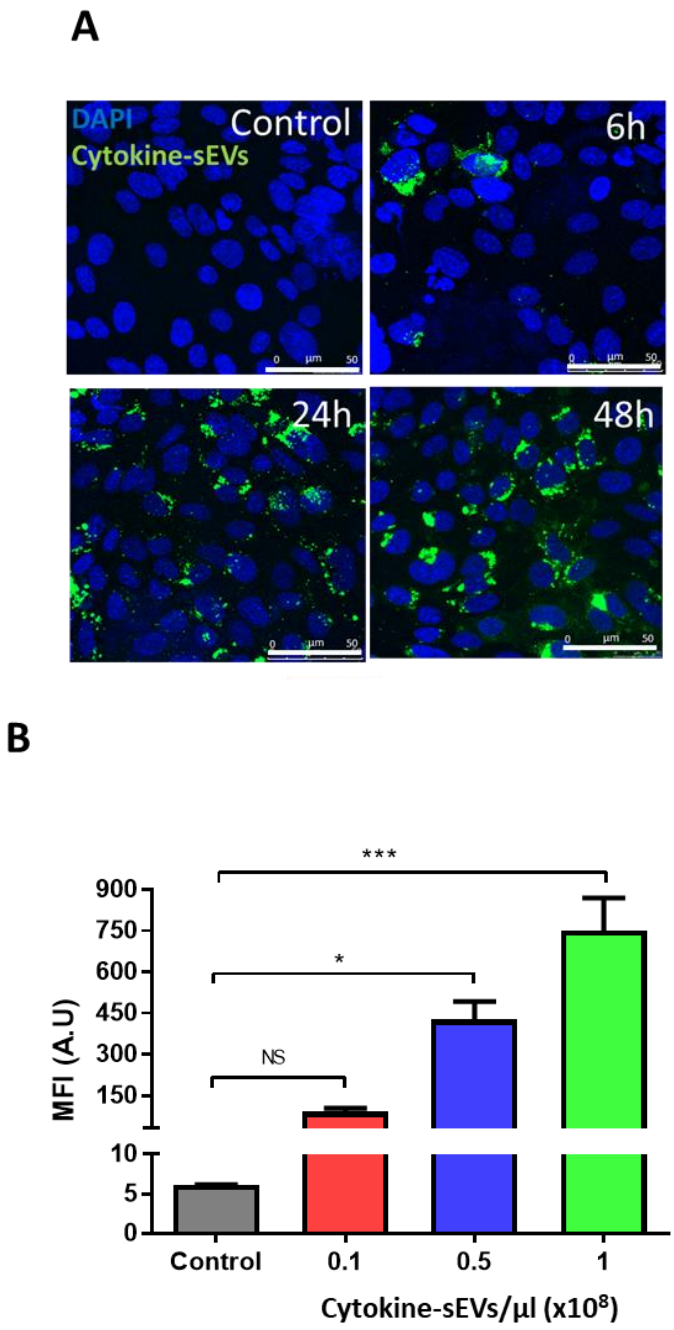

Figure 4.2. Characterisation of the uptake of cytokine-sEVs by naïve brain endothelium. (A) DIO-labelled small EVs (cytokine-sEVs) isolated from 10 ng/ml of TNFα and IFNy-treated hCMEC/D3 cells and incubated with human microvascular brain endothelial cells (hCMEC/D3) were imaged by confocal microscopy to analyse the uptake of $0.5x10^8$ cytokine-sEVs/µl at different times (0, 6, 24 and 48h). **(B)** Quantification of flow cytometry of the median fluorescent intensity (MFI) of DIO-labelled cytokine-sEVs (0.1, 0.5, $1x10^8$ sEVs/µl) by naïve hCMEC/D3 cells for 24h. Data are showed as mean ± SEM (B, n = 3 independent experiments) $*P < 0.05$ and $****P < 0.0001$ or non-significant (N.S.). Differences were measured with one-way ANOVA and Dunnet´s multiple comparison test. Arbitrary Units (AU). Scale bar = 50µm.

4.2.3. Effect of cytokine-sEVs on the TEER

Loss of TEER is a well-known feature of CNS endothelial dysfunction and can be indirectly assessed by measuring the electrical impedance of the endothelial monolayer *in vitro* (Urdapilleta, Bellotti and Bonetto, 2006). First, the TEER of hCMEC/D3 cells under basal conditions or after treatment with a low dose of pro-inflammatory cytokines (1 ng/ml TNFα and IFNy) was investigated. Two days after seeding, naïve hCMEC/D3 cells in culture reached a maximum TEER value of 3.53±0.03 $\Omega \cdot cm^2$. Incubation with 1 ng/ml of TNFα and IFNy significantly reduced the TEER of the endothelial monolayer in a time-dependent manner (Figure 4.3.A). TEER values for hCMEC/D3 monolayers under basal conditions started to decrease 24 hh after reaching confluence (Figure 4.3.A). For this reason, each time point of a treatment condition was normalised to their control time point of untreated cells. TEER values were then expressed as percentage of the treated condition (e.g. 1ng/ml TNFα and IFNγ) over untreated cells (Figure 4.3.B). Differences in TEER between naïve and cytokine-treated cells were analysed in 10 h periods (Figure 4.3.C). As mentioned above, treatment with 1 ng/ml TNFα and IFNγ significantly decreased TEER value over time and a biphasic decrease was observed. TEER rapidly decreased over the first 30 h of treatment, plateaued at 40 and further decreased at later times (Figure 4.3.C). Hence, this method was used to analyse the effect of sEVs in the TEER of hCMEC/D3 cells in future experiments.

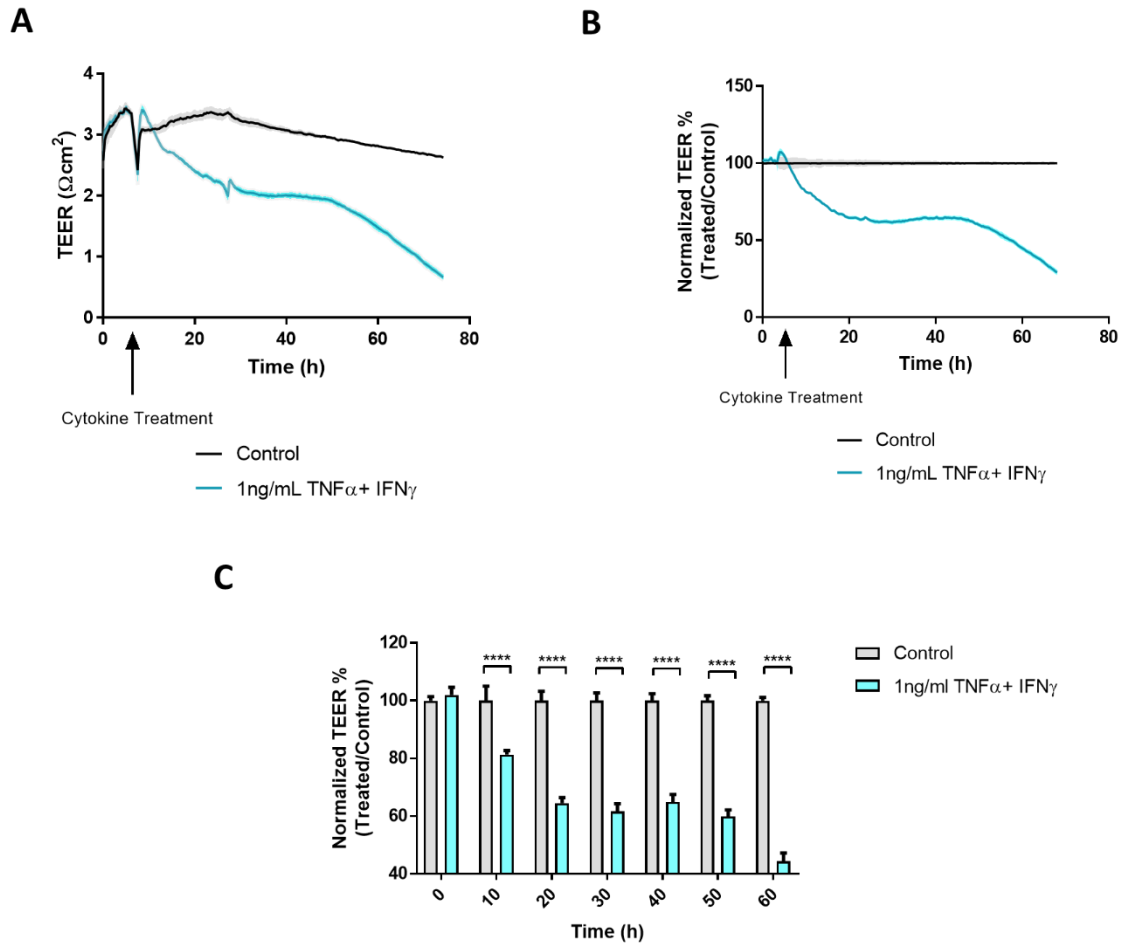

Figure 4.3. Combination of TNFα and IFNγ affect hCMEC/D3 cells' TEER. (A) Impedance values of untreated (control) hCMEC/D3 cells and those treated with 1 ng/ml of TNFα and IFNy were collected every 12 min intervals and transformed into transendothelial resistance (TEER) values. (B) Data wre transformed to percentage of treated vs. untreated cells at each time point. (C) Data were analysed at 10 h intervals using repeated measures two-way ANOVA with Tukey´s post hoc test. Data is shown as mean±SEM, n = 3 independent replicates and **P*<0.0001 to control condition.

Next, the effect of cytokine-sEVs on the TEER of naïve BECs was evaluated. After cells were grown to confluence, the hCMEC/D3 monolayers were cultured with increasing doses of cytokine-sEVs (0.1, 0.5, 1x10^8 sEVs/µl) during 60 h, which resulted in a dose-dependent decrease in TEER (Figure 4.4A). A maximum decrease in TEER to 83±3% of that in control cells was observed over a 20 h incubation time with 10^8 cytokine-sEVs/µl (*P*<0.0001, n=4). Longer incubation times did not further decrease the TEER (Figure 4.4.A).

In order to investigate whether the observed effect was specific to cytokine-sEVs, BECs were incubated with $0.5x10^8$ sEVs/µl derived from either quiescent BECs or cytokine-treated BECs. Cytokine-sEVs decreased TEER similarly as reported above (Figure 4.4.A). Cells treated with quiescent sEVs had a small transient decrease in TEER 10h after incubation (89.7±1.5 %, P<0.05 and n=3) whereas longer incubation times had no significant effect on TEER (Figure 4.4.B).

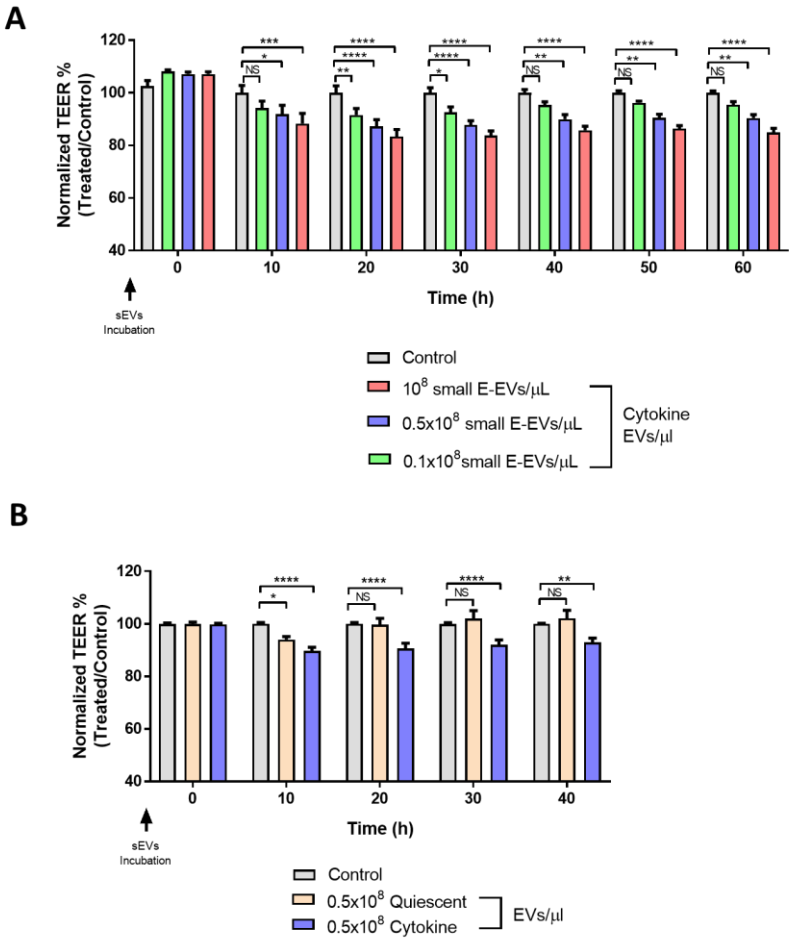

Figure 4.4. Cytokine-sEVs but not quiescent sEVs decrease TEER. Trans-endothelial resistance (TEER) of hCMEC/D3 cells was calculated and data are shown as percentage of treated vs. untreated cells at each time point. (A) TEER values following incubation of hCMEC/D3 cells with increasing concentrations of cytokine-derived small EVs (cytokine-sEVs) (0.1, 0.5 and 1 x 10^8 sEVs/µl). (B) Comparison of the effect of 0.5 sEVs/µl of cytokine-sEVs or quiescent sEVs on BECs TEER. Data are shown as mean ± SEM, n = 3 (B) and 4 (A) independent replicates. **P*<0.05, ***P*<0.01, ****P*<0.001, ****P*<0.0001 compared to untreated hCMEC/D3 cells, using repeated measures two-way ANOVA with Tukey´s multiple comparison test

4.2.4. Synergy between cytokine-sEVs and cytokines (TNFα and IFNγ) on TEER

sEVs are likely to encounter other modulators of inflammation such as cytokines and chemokines when released into the blood stream. Therefore, whether cytokine-sEVs had any effect on already inflamed BECs was investigated. For this reason, hCMEC/D3 cells were pre-activated with a low dose of combination of cytokines (1 ng/ml TNFα and IFNy overnight) and cultured with two different doses of cytokine-sEVs (either 0.1 or $1x10^8$ sEVs/µl) in the presence of TNFα and IFNy for up to 20 h (Figure 4.5.A). Treatment with $0.1x10^8$ cytokine-sEVs/µl did not further decrease the effect of cytokine-induced TEER during the course of the experiment when compared to hCMEC/D3 cells treated only with TNFα and IFNy. Indeed, TEER percentage change was 77.8±0.7% after 20h of $0.1x10^8$ cytokine-sEVs/ µl incubation TEER when compared to hCMEC/D3 cells treated only with pro-inflammatory cytokines (79.9±1.3%, $P>0.05$ and n=4) (Figure 4.5.B). However, incubation with $1x10^8$ cytokine-sEVs/µl together with TNFα and IFNy further decreased the TEER within 5 h after incubation (80.7±1.6 % for cytokine+cytokine-sEVs and 86.3±1.8 % for cells treated only with TNFα and IFNy at 5h, $P<0.01$ and n=4). The observed effect was maintained over the full course of the experiment. Accordingly, TEER values were decreased to 71.9±1.9% of values of untreated cells in the presence of 10^8 cytokine-sEVs/ µl of cytokine-sEV (Figure 4.5.B) in comparison to 79.9±1.3% on hCMEC/D3 cells treated only with TNFα and IFNy ($P<0.0001$, n=4) (Figure 4.5.B). These results suggested that cytokine-sEVs are able to further decrease TEER under inflammatory conditions, which might have implication in cytokine-sEV amplifying the cytokine-induced effect in the BBB.

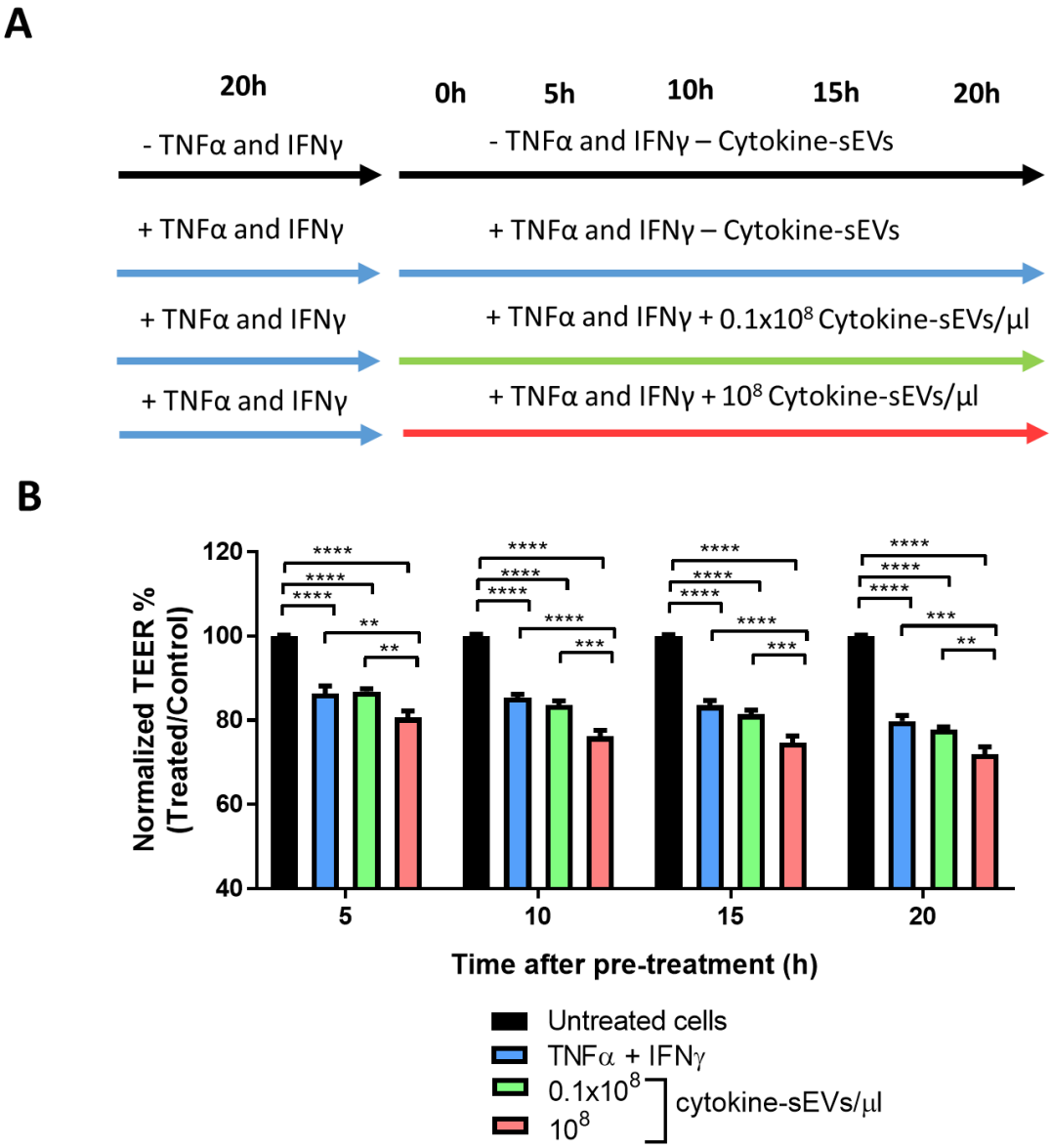

Figure 4.5 Effect of cytokine-sEVs in combination with cytokines on TEER. (A) Diagram of the experimental set-up. hCMEC/D3 cells were pre-treated with 1ng/ml of TNFα and IFNy for 20h or left untreated (untreated cells/control, black line). The media of treated cells was replaced with the same dose of cytokines in the absence (TNFα and IFNy, blue line) or presence of cytokine-sEVs (0.1 or 1x10^8 sEVs/µl, green and red lines) for 20 h. **(B)** TEER values of cells pre-treated with TNFα and IFNy at 0, 5, 10, 15 and 20h post-incubation with cytokine-sEVs. Data are shown as mean± SEM of the normalised TEER percentage of treated group over untreated cells, n=4 of independent replicates. Differences are studied with repeated measures two-way ANOVA and Tukey´s post-hoc for multiple comparisons among all studied groups ***P* <0.01, ****P* <0.001 *****P* <0.0001.

Next, the effect of cytokine-sEVs on modulating the recovery of pre-activated hCMEC/D3 cells from the cytokine treatment was studied (Figure 4.6.A). Following removal of TNFα and IFNγ, it was observed that TEER values started to increase, but values similar to untreated cells were not achieved over the time-course of the experiment (TEER percentage change was 86.8±3.6 % for cells left with no post-treatment after 40 h of the pre-treatment). This suggested that longer times might be needed for hCMEC/D3 cells to recover from cytokine-induced loss of TEER. Incubation with $0.1x10^8$ cytokine-sEVs/µl did not delay the recovery of TEER percentage change. Indeed, TEER percentage change was 78.4±2.5 % after 40h treatment. Similarly, treatment with $1x10^8$ cytokine-sEVs/µl failed to significantly delayed the recovery from the cytokine-induced loss of TEER in BECs. However, a non-significant trend was observed in those cells treated with the higher dose of cytokine-sEVs. For example, after 40h of the pre-treatment, 10^8 sEVs/µl-incubated cells had a TEER percentage of 71.3±2.8 % of control (P=0.07, n=3) (Figure 4.6.B.). It is likely that further incubation time with this concentration of cytokine-sEVs would significantly delayed the recovery of hCMEC/D3 cells, hence, supporting the hypothesis that cytokine-sEVs modulate TEER under inflammatory stimulus.

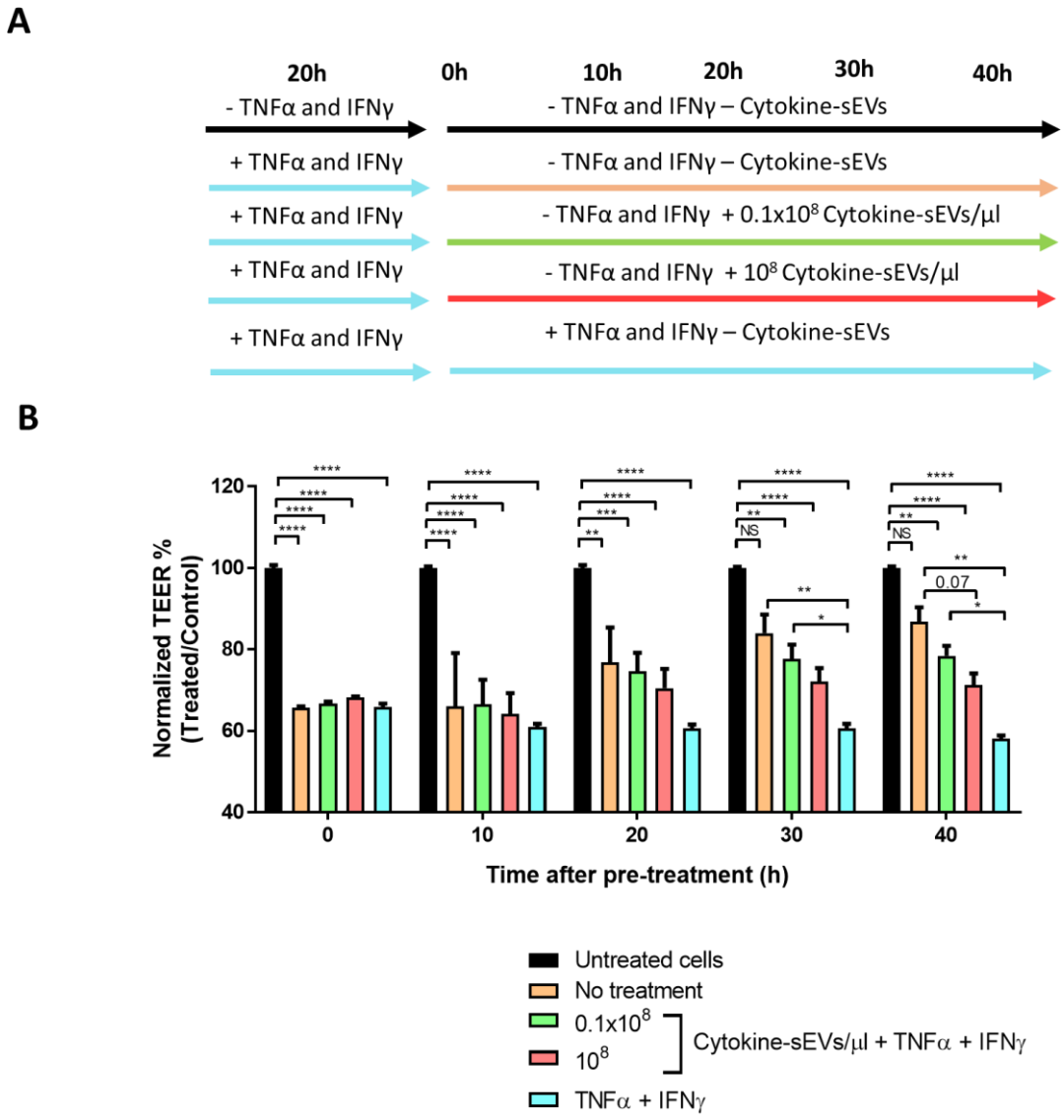

Figure 4.6. Effect of cytokine-sEVs on hCMEC/D3 cells recovery from cytokine treatment. (A) Diagram of the experimental set-up. hCMEC/D3 cells were pre-treated with 1 ng/ml of TNFα and IFNγ for 20h or left untreated (untreated control, black line). The media of treated cells was replaced with fresh media without cytokines (positive control, orange line) or containing cytokine-sEVs (0.1 or $1x10^8$ sEVs/µl, red and green lines). In last group, media was replaced with fresh media supplemented with 1ng/ml of TNFα and IFNγ and used as negative control of cell recovery from cytokine effect (blue line) (B) TEER values of TNFα and IFNγ pre-treated cells at 0 to 40h post-incubation with cytokine-sEVs. Data are shown as mean ± SEM of the normalised TEER percentage of treated group over untreated cells, n=3 of independent replicates. Differences are studied as repeated measures two-way ANOVA with Tukey´s post-hoc for multiple comparisons among all studied groups **P* <0.05, ***P* <0.01, ****P* <0.001 *****P* <0.0001.

4.2.5. Effect of cytokine-sEVs in leukocyte adhesion to brain endothelium

As described above, T cell transmigration is also a main cause of endothelial dysfunction in neuroinflammation (Lopes Pinheiro *et al.*, 2016). Leukocyte adhesion is a crucial step for the successful cell migration across the endothelium (Engelhardt and Ransohoff, 2012). Therefore, the effect of cytokine-sEVs on T cell adhesion to BECs was assessed using a flow-based assay. This system allows for the cells to be exposed to shear-stress, which has been demonstrated to better mimic *in vivo* conditions (Uzarski, Scott and McFetridge, 2013; Cerutti *et al.*, 2017).

First, the effect that cytokine-sEVs had on modulating the adhesion of Jurkat T cells to hCMEC/D3 cells was studied. Fluorescent microscopy revealed bright spherical shapes corresponding to Jurkat T cells that were adhered to the hCMEC/D3 cell monolayer (spindle-shaped cells) (Figure 4.7.A). Under control conditions (no treated hCMEC/D3 cells), 51±8 Jurkat T cells/FOV (FOV, 640 × 480 μm) were adhered to hCMEC/D3 cells. Incubation with increasing doses of cytokine-sEVs amplified T cell adhesion to BECs in a dose-dependent manner (Figure 4.7.A). Indeed, treatment with 10^8 cytokine-sEV/μl resulted in approximately 2 fold increase of Jukat T cell adhesion to BECs. A linear increase in cell adhesion was observed with a peak at 10^8 cytokine-sEV/μl of 96±10 Jurkat T cells/FOV ($P<0.01$, n=4) (Figure 4.7B). Combination of the low dose of cytokines (1 ng/ml TNFα and IFNγ for 24h) was used as a positive control of T cell adhesion. Unsurprisingly, treatment with 1 ng/ml of TNFα and IFNy significantly increased 4 times Jurkat T cell adhesion to brain endothelium (203±14 Jurkat T cells/FOV, $P<0.001$, n=4) (Figure 4.7.B).

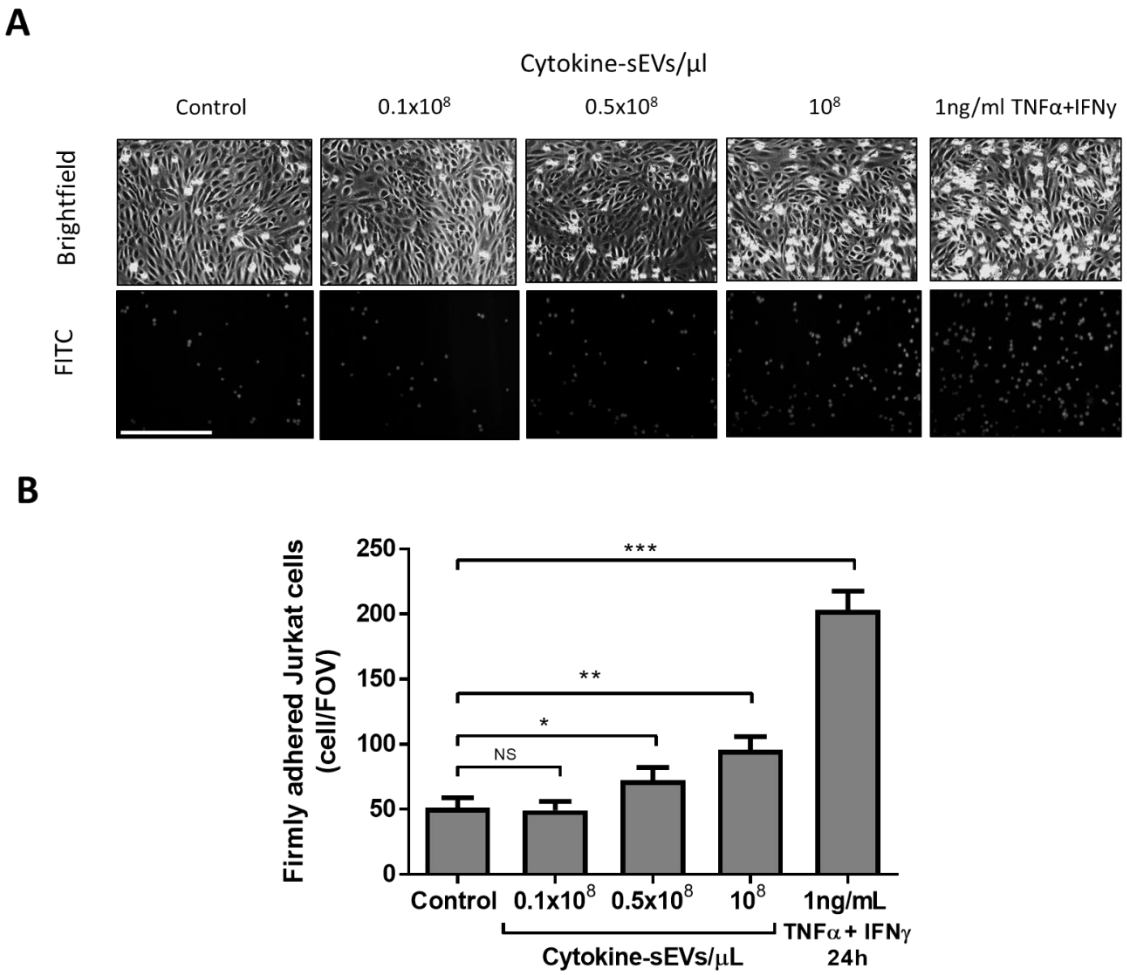

Figure 4.7. Dose-response of cytokine-sEVs on modulating Jurkat T cell adhesion to brain endothelium. (A) Representative brightfield (top) and fluorescent (FITC, bottom) images of Jurkat T cell adhesion under flow conditions (from left to right) in the absence (control), presence of cytokine-sEVs (cytokine-sEVs) at $0.1x10^8$, $0.5x10^8$ or $1x10^8$ cytokine-sEVs/µl or combination of cytokines (1ng/ml of TNFα+IFNγ). (B) Quantification of the number of firmly adhered T cells per field of view (FOV) following incubation with increasing doses of cytokine-sEVs for 24h. Data are shown as mean ± SEM and n = 4 of independent experiments. Differences were studied as repeated measures one-way ANOVA with Dunnet´s post-hoc for multiple comparisons to control with *P<0.05 and **P<0.01 and ***P < 0.001 or non-significant (N.S.) to untreated/control condition. Scale bar = 320 µm.

Next, the kinetics of the cytokine-sEV-induced effect on T cell adhesion to BECs were investigated. Jurkat T cell adhesion to hCMEC/D3 cells after incubation with 10^8 cytokine-sEVs/µl for 6, 24 and 48 h was measured (Figure 4.8.A). In accordance with the time-course of the previous TEER experiments (Figure 4.5), a rapid increase of T cell adhesion to BECs after 6 h of incubation was observed (Fig. 4.8A). Jurkat T cell adhesion to untreated brain endothelium was 27±5 Jurkat T cells/FOV whereas after 6h of incubation with cytokine-sEVs resulted in 96±10 Jurkat T cells/FOV (P<0.05, n=4) (Figure 4.8.B). Additional incubation time with cytokine-sEVs did not further increase the adhesion (Figure 4.8.B). Treatment of BECs with 1 ng/ml of TNFα and IFNy increased T cell adhesion by approximately twice as much as cytokine-sEVs (201±12 Jurkat T cells/FOV, P<0.01, n=4) (Figure 4.8.B). These results demonstrated that cytokine-sEVs can increase the adhesion of Jurkat T cells to hCMEC/D3 cells.

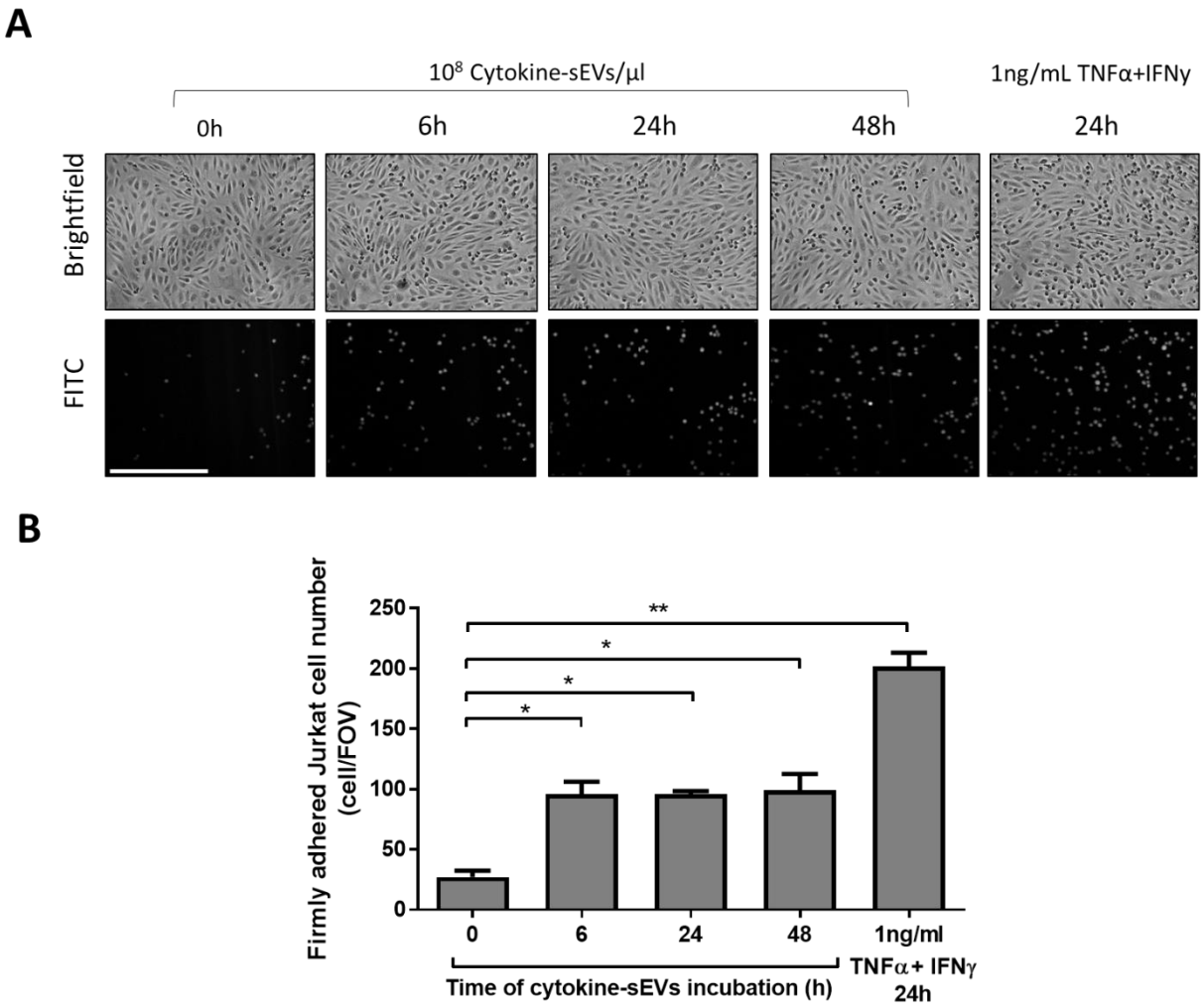

Figure 4.8. Time-course effect of cytokine-sEVs in Jurkat T cell adhesion to brain endothelium. (A) Representative brightfield (top) and fluorescent (FITC, bottom) images of Jurkat T cell adhesion under flow conditions (from left to right) in the absence (0h), presence of $1x10^8$ cytokine-derived small EVs (cytokine-sEVs)/µl after 6, 24 and 48h of incubation or combination of cytokines (1ng/ml of TNFα and IFNγ for 24h). Jurkat T cells appear as dark round-shaped cells whereas hCMEC/D3 cells appear as spindle-shaped cells in brightfield images. Jurkat T cells are depicted as bright round-shaped cells at FITC images **(B)** Quantification of the number of firmly adhered T cells per field of view (FOV) following incubation with cytokine-sEVs at different times. Data are shown as mean ± SEM and n = 4 of independent experiments. Means were analysed using repeated measures one-way ANOVA with Dunnet´s post-hoc for multiple comparisons with **P*<0.05 and ***P*<0.01 and ****P*<0.001 to untreated/control condition. Scale bar = 320µm

4.2.6. Effect of quiescent sEVs on leukocyte adhesion to hCMEC/D3 cells

To determine whether the effect of cytokine-sEV on adhesion of Jurkat T cells to hCMEC/D3 cells was specific to their inflammatory profile, the adhesion experiments were repeated with quiescent sEVs. hCMEC/D3 cells were exposed to the same concentration of sEVs ($0.5x10^8$ sEVs/µl) of either cytokine- or quiescent sEVs for 24 h prior to assessment of leukocyte adhesion (Figure 4.9.A). As observed previously, cytokine-sEVs increased firmly adhered Jurkat T cell number on endothelial monolayer as described in figure 4.8 (42±3 Jurkat T cells/FOV, $P<0.05$ and n=3) (Figure 4.9.B). Furthermore, incubation of hCMEC/D3 cells with quiescent sEVs did not increase leukocyte adhesion to brain endothelium. Quiescent-sEV-treated hCMEC/D3 cells showed 23±4 firmly adhered Jurkat T cells/FOV whereas untreated cells had 25±2 adhered Jurkat T cells/FOV (Figure 4.9.B). These results confirmed that only cytokine-sEVs affected binding of leukocytes to endothelial cells under basal conditions.

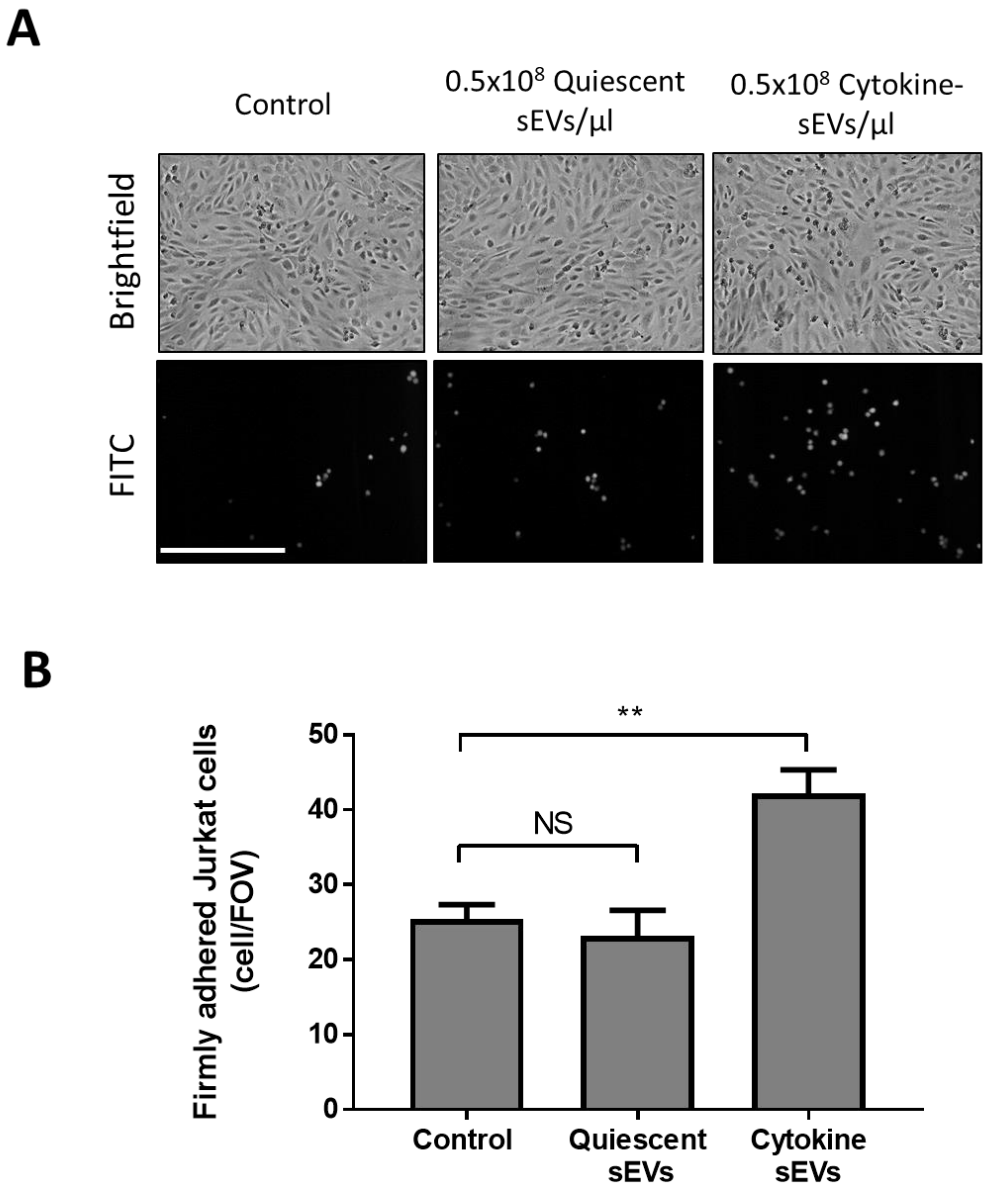

Figure 4.9. Effect of quiescent-derived sEVs on Jurkat T cell adhesion to brain endothelium under basal conditions. (A) Representative brightfield (top) and fluorescent (FITC, bottom) images of Jurkat T cell adhesion under flow conditions (from left to right) in the absence (control), or presence of $0.5x10^8$ quiescent hCMEC/D3 cell-derived small EVs (quiescent sEVs)/µl or $0.5x10^8$ cytokine-derived small EVs (cytokine-sEVs)/µl after 24h of incubation. Jurkat T cells appeared as dark round-shaped cells whereas hCMEC/D3 cells appeared as spindle-shaped cells in brightfield images. Jurkat T cells are depicted as bright round-shaped cells at FITC images (B) Quantification of the number of firmly adhered T cells per field of view (FOV) following incubation with cytokine-sEVs or quiescent-sEVs. Data are shown as mean ± SEM and n=3 of independent experiments. Differences are studied as repeated measures one-way ANOVA with Dunnets´s post-hoc for multiple comparisons with $^{**}P<0.01$ to untreated/control condition. Scale bar = 320µm.

4.2.7. Effect of quiescent sEVs on cytokine-induced leukocyte adhesion to brain endothelium

It has been already reported that endothelial cell-derived quiescent EVs are able to suppress the inflammatory signal by inhibiting monocyte activation (Njock, Boudreau, *et al.*, 2015). However, whether quiescent sEVs released by naïve hCMEC/D3 cells may be able to counteract the effects of cytokine-induced leukocyte adhesion to brain endothelium is still unknown.

To test this hypothesis, hCMEC/D3 cells were cultured with a combination of cytokines (1 ng/ml of TNFα and IFNy) and quiescent-sEVs ($0.5x10^8$ sEVs/µl) for 24 h before Jurkat T cell adhesion was analysed (Figure 4.10 A). In accordance with the previous results, incubation of naïve hCMEC/D3 cells with quiescent-sEVs did not alter endothelial function. Indeed, the number of Jurkat T cells adhered to hCMEC/D3 cells (33±8 Jurkat T cells/FOV) was not significantly different from the number of T cells in untreated conditions (43±6 Jurkat T cells/FOV, $P>0.05$ and n=4) (Figure 4.10.B). However, a reduction of 20% on number of leukocytes were shown to be adhered when hCMEC/D3 cells were cultured with both TNFα/IFNy and quiescent-sEVs when compared to cytokine treatment by itself (cytokines = 164±9 Jurkat T cells/FOV vs. cytokines+quiescent sEVs = 133±8 Jurkat T cells/FOV, $P=<0.01$ and n=4) (Figure 4.10.B). This result suggested that quiescent sEVs might play a role to balance the effect of cytokines in the BBB.

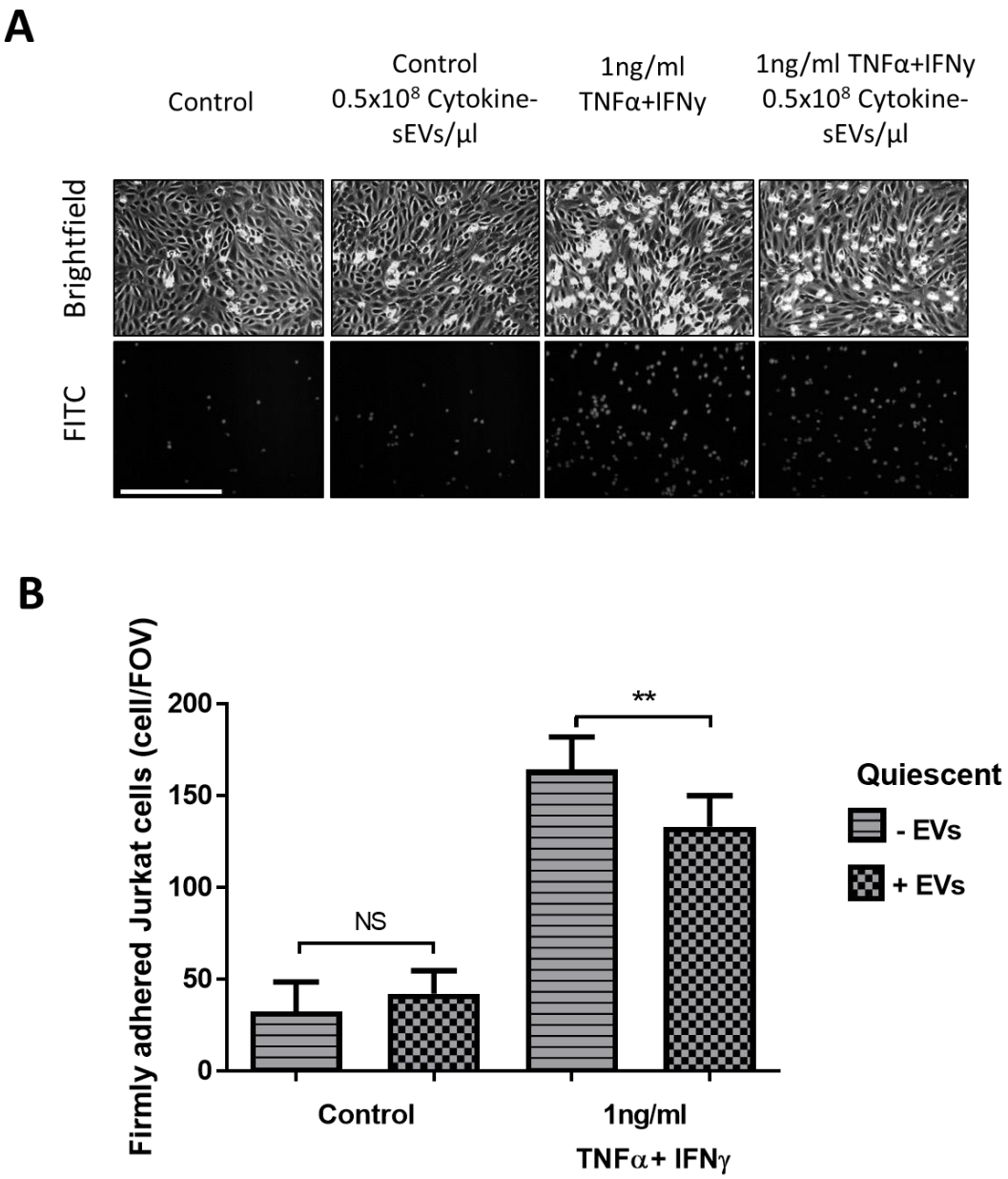

Figure 4.10. Effect of quiescent sEVs on Jurkat T cell adhesion to brain endothelium under inflamed conditions. (A) Representative brightfield (top) and fluorescent (FITC, bottom) images of Jurkat T cell adhesion under flow conditions. From left to right, representative images in the absence of cytokines and quiescent sEVs (control) or presence of $0.5x10^8$ quiescent hCMEC/D3 cell-derived small EVs (quiescent sEVs)/µl. Cells treated with 1 ng/ml of TNFα and IFNγ in the absence or presence of $0.5x10^8$ quiescent sEVs /µl after 24h of incubation. Jurkat T cells appear as round-shaped cells whereas hCMEC/D3 cells appear as spindle-shaped cells in brightfield images. Jurkat T cells are depicted as bright round-shaped cells at FITC images. **(B)** Quantification of the number of firmly adhered T cells per field of view (FOV) following incubation with combination of cytokines and/or quiescent-sEVs and/or left untreated. Data are shown as mean ± SEM and n = 4. Repeated measures two-way ANOVA with Tukey´s post hoc and $^{**}P<0.01$ and NS = no significant to control (cell treated with without quiescent sEVs) condition. Scale bar = 320µm.

4.2.8. Effect of cytokine-sEVs and quiescent sEVs on miRNA and mRNA levels in recipient hCMEC/D3 cells

Previous studies have demonstrated that the molecular cargo carried within EVs can be transferred to the recipient cells, driving phenotypic changes (Valadi *et al.*, 2007). Alternatively, EVs can induce changes in gene expression in the acceptor cells instead. Therefore, the impact of sEVs on the expression profile of selected inflammation regulatory mRNAs and miRNAs of recipient BECs was assessed.

hCMEC/D3 cells were cultured with both cytokine- and quiescent sEVs for 24 h prior to RNA extraction. In the context of miRNAs, levels of miRNA-155 were significantly up-regulated in hCMEC/D3 cells after incubation with cytokine-sEVs (1.45±0.07 fold change, $P<0.05$ and n=3) (Figure 4.11.A). On the other hand, expression of the anti-inflammatory miRNA-126-3p was not altered following sEV treatment (1.01±0.13, $P>0.05$, n=3) (Figure 4.11A). MiRNA-24 was measured as a control of a miRNA, whose expression is not altered by TNFα and IFNγ treatment in hCMEC/D3 cells. As expected, quiescent sEVs did not alter the expression levels of any of the before-mentioned miRNAs (Figure 4.11.A)

Levels of mRNAs related to BEC inflammation were also investigated. Both ICAM1 and VCAM1 mRNA were up-regulated after cytokine-sEVs incubation for 24h. This up-regulation was small but significant (1.55±0.19 ICAM1 fold change, and 1.45±0.08 VCAM1 fold change with $P<0.01$ and $P<0.01$ respectively), n=3 (Figure 4.11.C). Levels of mRNAs for the tight junctional protein CLDN5 and OCLN were not changed following incubation with sEVs. In accordance with the results of the miRNA analysis, incubation of hCMEC/D3 cells with quiescent sEVs did not change endogenous levels of any of the mRNAs studied (Figure 4.11.B).

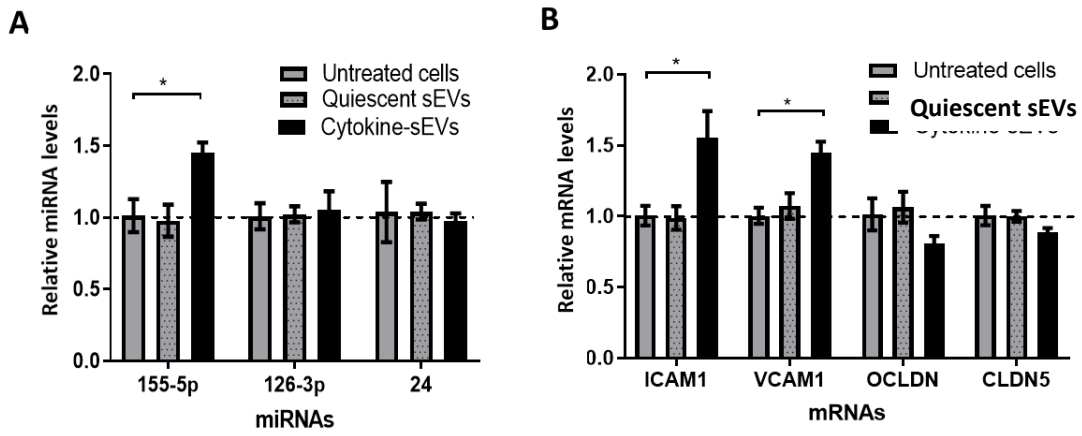

Figure 4.11. Endothelial sEVs induce pro-inflammatory markers in recipient hCMEC/D3 cells. (A) qPCR of levels of microRNAs: miRNA-155-5p, miRNA-126-5p and miRNA-24 after treatment with cytokine-derived small EVs (cytokine-sEVs) or quiescent sEVs. Relative levels were normalised to the reference gene, small nuclear RNA U6. **(B)** Measurement of mRNA levels by qPCR after incubation of hCMEC/D3 cells with cytokine-sEVs or quiescent-sEVs of intracellular adhesion molecules 1 (ICAM1), vascular cell adhesion molecule 1 (VCAM1), occludin (OCLN) and claudin-5 (CLDN5) mRNAs. Data are shown as mean±SEM, n=3 of independent experiments. One-wat ANOVA followed by Dunnet´s post-hoc test **P*<0.05 in comparison to untreated cell levels.

4.2.9. Protein expression is regulated by cytokine-sEVs in hCMEC/D3 cells

To determine whether the changes in mRNA levels observed in hCMEC/D3 cells following incubation with cytokine-sEVs resulted in corresponding changes in protein expression, the levels of key proteins involved in either leukocyte adhesion to BECs or TEER were investigated by Western blotting (Figure 4.12.A).

Immunoblotting using primary antibodies against ICAM1 and VCAM1 revealed detectable levels of ICAM1 and VCAM1 under basal conditions in hCMEC/D3 cells (Figure 4.12.A). Normalisation of protein band intensity to a control confirmed that protein levels of ICAM1 and VCAM1 were significantly up-regulated in recipient BECs after incubation with cytokine-sEVs (1.66±0.19 and 5.06±0.96 relative to untreated hCMEC/D3 cells, *P*<0.05, respectively, n=3) (Figure 4.12 B). Regarding OCLDN and

CLDN5, both tight junctional proteins were detectable in hCMEC/D3 cells (Figure 4.12.A). However, quantification of band densitometry of these proteins revealed that treatment with cytokine-sEVs did not alter the total levels of CLDN5 and OCLDN proteins in recipient hCMEC/D3 cells. (Figure 4.12 B).

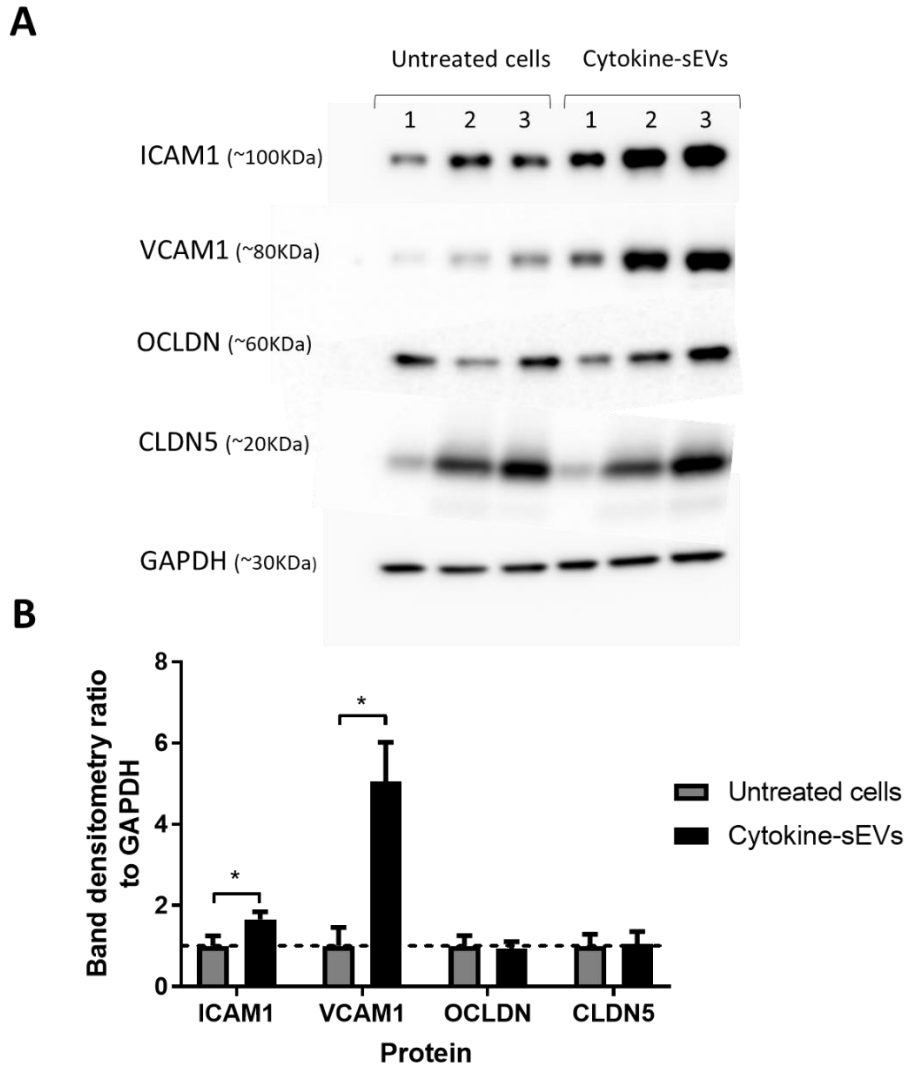

Figure 4.12. Cytokine-sEVs induce expression of pro-inflammatory adhesion molecules in recipient hCMEC/D3 cells. (A) Immunoblot of cytokine-sEV-treated or untreated (control) hCMEC/D3 cells for adhesion molecules, ICAM1 and VCAM1, tight junction related protein, OCLDN and CLDN5 and internal control GADPH. **(D)** Band densitometry was measured, normalised by GAPDH and expressed as ratio of cytokine-sEV treated vs untreated hCMEC/D3 cells. Data are shown as mean ± SEM, n = 3 of independent experiments, paired t test, **P*<0.05, ***P*<0.01, ****P*<0.001 in comparison to control.

4.2.10. Role of VCAM1 and ICAM1 in leukocyte adhesion to BECs induced by cytokine-sEVs.

To confirm the role of VCAM1 and ICAM1 proteins in modulating T cell adhesion to brain endothelium (Lopes Pinheiro *et al.*, 2016), blocking antibodies against ICAM1 and VCAM1 alone or in combination were incubated with recipient hCMEC/D3 cells for 1h prior T cell adhesion assays. Incubation with non-specific mouse IgG antibodies was used as control for blocking antibodies. IgG antibody treatment resulted in no differences in the number of T cells adhered to BECs in comparison to non-antibody treated cells. Then, blocking ICAM1 failed to prevent cytokine-sEV-induced T cell adhesion to brain endothelium compared to IgG-treated hCMEC/D3 cells (93±22% and 103±7 fold change respectively, n=4) (Figure 4.13 A). However, blocking VCAM1 partially blocked T cell adhesion to BECs (32±11%, $P<0.05$ and n=4). Furthermore, blocking VCAM1 and ICAM1 simultaneously completely prevented the effect of cytokine-sEV on hCMEC/D3 cell function (4±17%, $P<0.05$) (Figure 4.13.B)

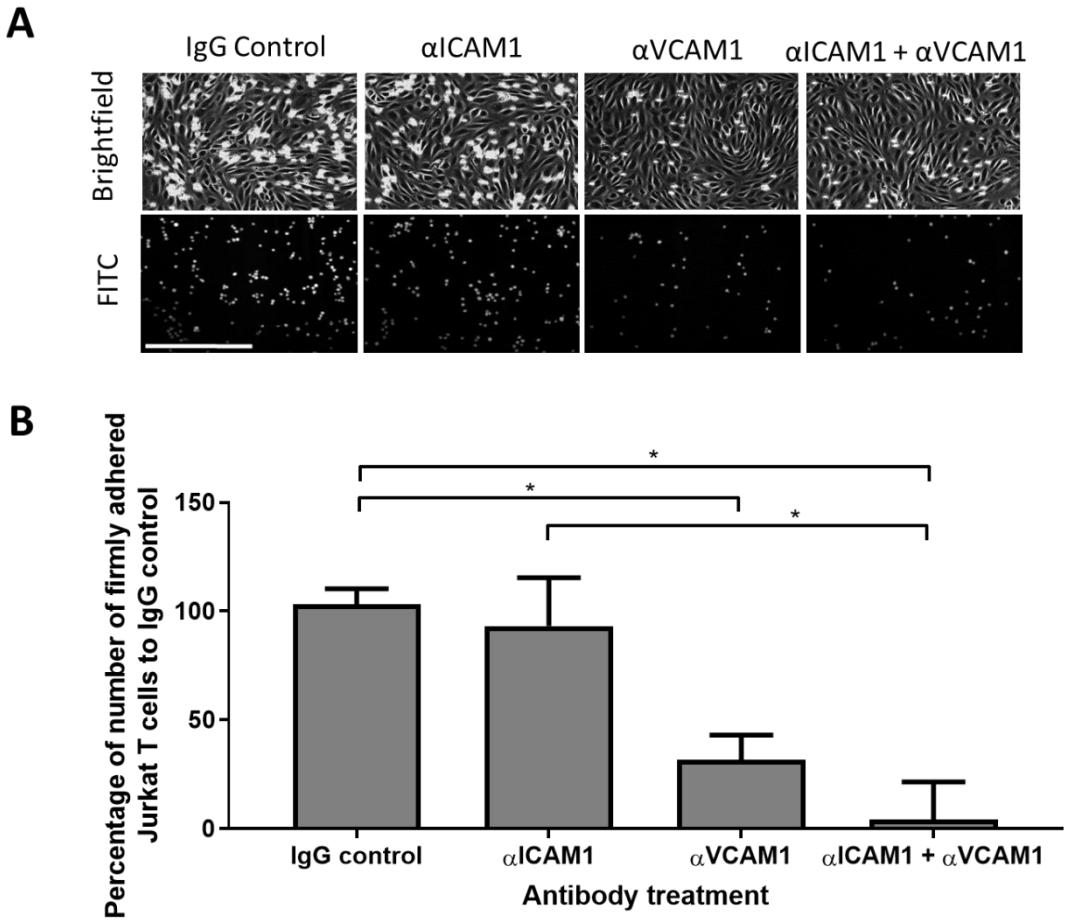

Figure 4.13. Effect of VCAM1 and ICAM1 in cytokine-sEV-induced Jurkat T cell adhesion to BECs (A) Representative images of Jurkat T cell adhesion (round points in FITC images and bright points in brightfiled images) to hCMEC/D3 (spindle-shaped cells in brightfield images). Prior to T cell adhesion assay, cells were treated from left to right images with mouse IgG control, 30 µg/ml ICAM1 antibody, 30 µg/ml VCAM1 antibody or combination of 30 µg/ml ICAM1 and VCAM1 antibodies. **(B)** Cell adhesion was quantified in eight to ten field of view (FOV 640 × 480 µm) and expressed as percentage of number of Jurkat T cell adhered to cytokine-sEV treated hCMEC/D3 cells. Data are shown as mean ± SEM (n=4), one-way ANOVA with Dunnet´s post hoc **P*<0.05 in comparison to IgG control. Scale bar = 320µm

4.3. Discussion

Findings from these experiments indicated that treatment of BECs with sEVs induced cerebrovascular dysfunction by reducing trans-endothelial electrical resistance and by increasing leukocyte adhesion to brain endothelium. These results also suggested that sEVs derived from cytokine-treated BECs act as a novel pro-inflammatory regulator by modulating protein and RNA expression (miRNA-155, VCAM1 and ICAM1) in recipient naïve endothelial cells whereas quiescent sEVs decreased cytokine-induced T cell adhesion to BECs.

4.3.1. Non-specific uptake of sEVs by cells of the neurovascular unit

Few studies have compared the uptake of sEVs by different cells of the NVU. For example, Ramirez and colleagues showed qualitative uptake of sEVs by astrocytes, pericytes and brain endothelial cells (Ramirez *et al.*, 2018). Accordingly, in this project, the uptake of sEVs was detected in the three main cell types of the NVU. Although not significant, uptake of sEVs tended to be higher in astrocytes than pericytes and BECs. Astrocytes have a larger cell surface that might have biased the uptake of sEVs. On the other hand, normalised uptake of cytokine-sEVs was shown be similar for all three cellular types. These results suggested that uptake of sEVs is not enhanced during inflammation. Indeed, uptake of cytokine-sEVs appeared to be decreased in comparison to quiescent-sEV uptake. This result suggested a preference of uptake of quiescent sEVs by the cells of the NVU, which might be explained by differences in the route of vesicular uptake. However, little is known about the specific pathways involved in vesicular uptake and the different common methods for vesicular uptake have been proposed to modulate sEVs uptake by different cells types (Théry *et al.*, 2018). Indeed, a recent study attempted to study the uptake of endothelial sEVS by endothelial cells using pharmaceutical

inhibitors of vesicular uptake (Banizs *et al.*, 2018). The authors showed that sEV uptake was preferentially mediated by clathrin-dependent internalisation and to a lesser degree to micropinocytosis and caveolin-dependent internalisation (Banizs *et al.*, 2018). Unfortunately, the receptors involved are not well understood.

The ISEV recommends to include both time- and dose- dependent experiments when evaluating both the function and uptake of sEVs by the acceptor cells (Théry *et al.*, 2018). In these experiments, the uptake of cytokine-sEVs by BECs was observed to be dependent on both time of incubation and concentration of EVs. These results were not surprising and the trend of uptake was in accordance with the general view of sEVs´ uptake. The staining pattern of DiO in cytokine-sEV-treated BECs was predominantly perinuclear. This is in accordance with a previous study where uptake of sEVs by HUVECs was evaluated (Gao *et al.*, 2016; Durak-Kozica *et al.*, 2018). However, little is known about the fate of sEVs once inside the acceptor cells (Mathieu, Thery 2019). Future experiments using double labelling for markers for different subcellular location such as the reticulum endoplasmatic (e.g. calnexin) will help to determine the fate of these sEVs after they have entered the BECs.

4.3.2. Cytokine-derived sEVs reduce TEER

sEVs derived from pro-inflammatory cytokine-activated cells have been previously shown to be capable of inducing cytokine-like effects in recipient cells (Buzas *et al.*, 2014). However, most studies have investigated the role of sEV-mediated communication and their impact in vascular function using plasma- or serum-derived EVs (Marcos-Ramiro *et al.*, 2014). As a result, these studies cannot differentiate EVs that originate from both vascular as well as non-vascular cells (e.g. immune cells) (Horstman *et al.*, 2007). In contrast, this study focused on the specific role of BEC-derived sEVs and

supports the hypothesis that secretion of EVs by BECs modulates the susceptibility of naïve brain endothelial cells to inflammation-induced damage.

Findings from experiments in this chapter suggested that pro-inflammatory cytokines (TNFα and IFNγ) rapidly decreased TEER in BECs, as previously reported in different studies (M Alejandro Lopez-Ramirez *et al.*, 2016; Ni *et al.*, 2017). Each time point was normalised to match an untreated control to account for a natural loss of TEER of hCMEC/D3 during culture (Raymond *et al.*, 2016). Cytokine-sEVs were also observed to decrease BEC resistance under basal conditions in a subtle manner. Whether this "fine-tuning" leads to significant alteration in the transport of components across BECs is still unknown. However, it was noted that treatment with cytokine-sEVs caused a further decrease in the TEER of BECs under inflammatory conditions. This is especially relevant because during neuroinflammation, cells shed many pro-inflammatory mediators (e.g. cytokines, chemokines, EVs) into the blood that contribute to the activation of the endothelium (Tang *et al.*, 2016). Therefore, it is likely that sEVs will interact and compete with many of these molecules *in vivo*. Szabó G et al showed that the combination of human monocyte-derived sEVs and TNFα have additive effects on the monocyte transcriptome (Szabó *et al.*, 2014). The results from this study suggest that cytokine-sEVs may amplify cytokine-signalling in BECs, thereby contributing to the inflammatory response at the BBB.

It is likely that the synergistic effect between sEVs and pro-inflammatory cytokines observed in the TEER experiments is due to the cytokines adhered to the surface of the sEVs (Kolowos *et al.*, 2005) or both mediators enhancing signalling pathways such as NF-Kappa B (Szabó *et al.*, 2014). sEVs can modulate cellular function by different mechanisms that involve EV protein- cell membrane´s protein interaction and/or release of EV cargo within the acceptor cell (van der Pol *et al.*, 2012). Several

studies have shown that endothelial-derived sEVs can influence recipient cell function towards activation or suppression of inflammatory genes via transmission of RNA cargo (e.g. mRNA and microRNAs) (Njock, Cheng, *et al.*, 2015). It was observed that the molecular cargo contained within sEVs partially reflected the intracellular RNA profile of the donor cells, which is consistent with the current understanding that there is variability between levels of vesicular RNA and the secreting cells/tissue (Ragusa *et al.*, 2017).

Only a trend for decreased levels were found in the mRNA of occludin, but no changes were observed at the protein level. It is very likely that changes in endothelial resistance might occur due to alterations in the expression or location of other proteins such as ZO-1 or VE-cadherin. A study using plasma-derived EVs from MS patients showed that the decreased TEER was caused by re-organization of the junctional complexes (Marcos-Ramiro *et al.*, 2014). In this study, the effect on claudin-5 and occludin were evaluated given their importance in maintaining endothelial structure. However, future evaluations of other proteins might clarify the mechanism by which sEVs decreased the TEER of brain endothelium.

4.3.3. Cytokine-sEVs increase leukocyte adhesion to BECs via VCAM1 and ICAM1

In particular, leukocyte adhesion to brain endothelium is a key step in the process for T cells to migrate into the brain (Lopes Pinheiro *et al.*, 2016). Data strongly suggested that cytokine-sEV participate in this event by almost doubling the number of adherent leukocytes. Other studies have already shown that EVs can increase leukocyte adhesion to endothelium of other vascular beds (Tang *et al.*, 2016; Wadey *et al.*, 2019). Indeed, a recent study showed that EVs derived from HUVECs treated with TNFα, increased the

pro-inflammatory status of naïve HUVECS and human monocytic cells (THP-1), leading to an increase of monocyte adhesion and transmigration *in vitro* (Hosseinkhani *et al.*, 2018a). However, no study had evaluated this effect on BBB function. Interestingly, the degree to which cytokine-sEVs induced changes in BEC function was higher for leukocyte adhesion than trans-endothelial electrical resistance. Therefore, it can be speculated that cytokine-sEV might play a major role in modulating leukocyte adhesion to BECs under basal conditions than modulating BBB leakiness.

ICAM1 and VCAM1 protein and mRNA levels were up-regulated in recipient hCMEC/D3 cells after incubation with cytokine-sEVs. Similarly, another study evaluating the effect of primary aortic endothelial cell-derived sEVs shown this type of sEVs increased VCAM1 expression when cultured with VSMC, hence increasing leukocyte cell adhesion (Boyer *et al.*, 2020). Furthermore, blocking VCAM1 but not ICAM1 with neutralizing antibodies (Lam *et al.*, 2018) decreased T cell adhesion to BECs. This result was not unexpected since VCAM1 has been shown to play a crucial role in modulating leukocyte adhesion to endothelium (Lopes Pinheiro *et al.*, 2016). It can be speculated that the contribution of ICAM1 to sEV-induced T cell adhesion is minor in comparison to VCAM1 given that ICAM1 protein levels in recipient cells were lower than VCAM1 after cytokine-sEV treatment.

4.3.4. Cytokine-sEV-induced miRNA-155 expression in BECs

Previous studies have reported that sEVs can transfer miRNA-155 and modulate the function of the recipient cells (Alexander *et al.*, 2015). Furthermore, miRNA-155 is a widely accepted modulator of cellular inflammation and previous reports have demonstrated its relationship with brain endothelial function in inflammation (Lopez-

Ramirez *et al.*, 2014; Cerutti *et al.*, 2016). Therefore, it is proposed that in neuroinflammation BECs increase miRNA-155 expression, which is packaged in associated with sEVs. MiRNA-155-enriched sEVs can spread a pro-inflammatory signal to other quiescent endothelial cells. However, the precise mechanism by which this miRNA-155-enriched sEVs mediates T cell adhesion and how blocking of miRNA-155 may affect the observed phenotype remains to be elucidated. In addition, EVs are composed of many different molecules (protein, mRNA, microRNAs) that likely signal as whole to promote specific functions. The observed effects of cytokine induced-sEVs through miRNA-155-5p and VCAM1 and ICAM1 protein are most likely part of a larger combination of molecules, both vesicular and non-vesicular, orchestrating the activation of brain endothelium.

4.3.5. Quiescent sEVs reduced T cell adhesion to inflamed BECs

In this chapter, it has been consistently shown that quiescent EV had no effect on cerebrovascular function under basal conditions (regarding their effect on modulating the TEER and T cell adhesion to BECs). However, quiescent sEV decreased T cell adhesion in the presence of pro-inflammatory cytokines. These results are in agreement with a study from 2015, which observed that sEVs released from endothelial cells inhibited monocyte activation and decreased their transmigration in the presence of the systemic inflammatory stimulus LPS (Njock, Cheng, *et al.*, 2015). Indeed, other reports have shown the beneficial effect of quiescent sEVs (Isola and Chen, 2016), especially those sEVs that help promoting tissue regeneration (Dorronsoro and Robbins, 2013) or angiogenesis (Salomon *et al.*, 2013). The mechanism of action by which sEVs may exert their effects on endothelia is unknown. One could speculate that since sEVs are packed with miRNAs, the release of anti-inflammatory miRNAs such as miR-126 and miR-146a,

whose anti-inflammatory role in brain endothelial cells has been previously described, could drive a protective phenotype (Wu, Cerutti, Miguel A Lopez-Ramirez, *et al.*, 2015; Cerutti *et al.*, 2017). However, alternative pathways might be involved such as protein-protein interactions or induction of intracellular signalling pathways. Further experiments in evaluating the mechanism by which quiescent sEVs decrease cytokine-induced T cell adhesion to brain endothelium are needed, however, the present data support the concept that quiescent sEVs may play a protective role in neuroinflammation.

Findings from the current study support a novel role for brain cytokine-sEVs in promoting and perpetuating endothelial dysfunction during inflammation. Our data suggested that this mechanism may be driven in part by the transmission of pro-inflammatory modulators such as miRNA-155 as well as adhesion molecules, ICAM1 and VCAM1 from the EVs to the recipient cells. In the next chapter, the mechanism of miRNA-155-induced T cell adhesion will be investigated.

CHAPTER 5: Mechanism of miRNA-155-mediated T cell adhesion to brain endothelium

5.1. Introduction

In the previous Chapters, the mechanism by which cytokine-sEVs modulated the function of naïve BECs was investigated. Interestingly, the levels of miRNA-155 were up-regulated both in the cytokine-sEV cargo and intracellularly in the recipient BECs. In addition, cytokine-sEVs were able to up-regulate leukocyte adhesion to BECs. MiRNA-155 has been previously shown to be a potent modulator of cerebrovascular function in inflammation (Lopez-Ramirez *et al.*, 2014; Cerutti *et al.*, 2016). Cerutti and colleagues described that miRNA-155 overexpression led to increased shear-resistant T cell adhesion to hCMEC/D3 cells. Leukocyte adhesion is a crucial step in the multi-step process of leukocytes migration into the brain (Lopes Pinheiro *et al.*, 2016). This mechanism is tightly regulated by the temporal expression of surface molecules that modulate the adhesion of leukocytes to brain endothelium (Greenwood *et al.*, 2011). MiRNA-155 overexpression increases the expression of VCAM1 and ICAM1 in hCMEC/D3 cells (Cerutti *et al.*, 2016). However, the mechanism(s) by which miRNA-155 increases the expression of these two adhesion molecules and affect leukocyte adhesion to BECs are still poorly understood.

The aim of this chapter was to identify targets for miRNA-155 with the purpose of characterising the mechanism of action of miRNA-155-induced T cell adhesion to brain endothelium. In particular, whether overexpression of miRNA-155 led to leukocyte T cell adhesion to BECs was further investigated. Subsequently, identification of targets for miRNA-155 using preliminary proteomic data from a previous project was carried out

(Table 1, Annex 1). Top candidate proteins were further investigated and confirmation of their role in modulating leukocyte adhesion to BECs was studied. Finally, the relationship between the mRNA-miRNA-155 paired candidate was analysed by measuring mRNA and protein expression upon miRNA-155 overexpression.

5.2. Results

5.2.1. Effect of overexpression of endothelial miRNA-155 on T cell adhesion to BECs.

To investigate the mechanism by which miRNA-155 mediates leukocyte adhesion to BECs, the consequences of miRNA-155 overexpression in hCMEC/D3 cells were characterised. To do so, the efficacy of Siport^{TM} transfection with Cy3-labelled scrambled control was evaluated (Figure 5.1). Fluorescent microscopy revealed a strong Cy3 signal across the FOVs whereas a fluorescent signal was absent in the negative control cells (hCMEC/D3 cells culture with Cy3-labelled scrambled control without Siport^{TM} treatment) (Figure 5.1.A). Flow cytometry confirmed that the fluorescent signalling was significantly higher in cells transfected with Cy3-oligonucleotides compared to controls (control hCMEC/D3 cells=5±1 %, Cy3+ hCMEC/D3 cells =96±2 %, $P<0.001$; n=3) (Figure 5.1.B).

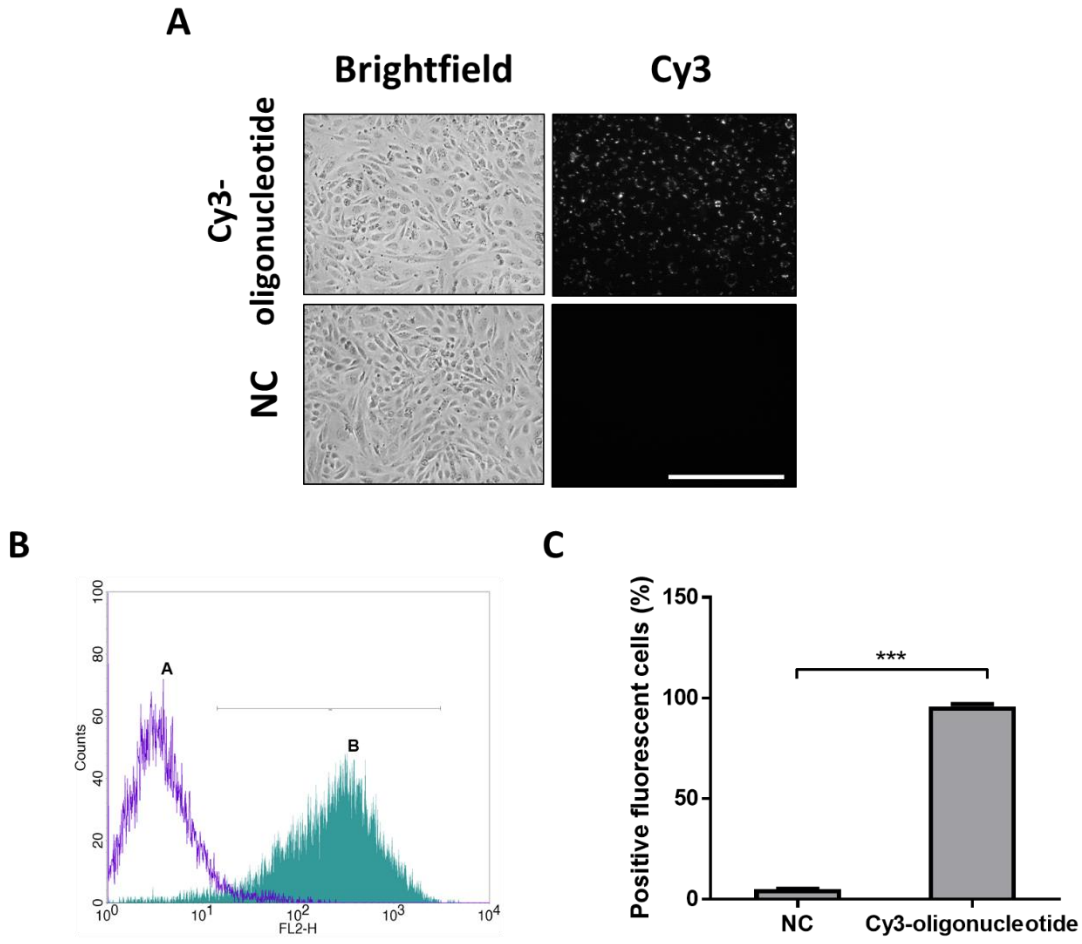

Figure 5.1. Efficiency of transfection of hCMEC/D3 cells with Siport™ reagent. (A) Immunofluorescent images of hCMEC/D3 cells transfected with Siport™ containing Cy3-labelled oligonucleotides (Cy3-oligonucleotide) or Cy3-labelled oligonucleotide alone (negative control, NC). **(B)** Representative histogram of flow cytometry analysis of 10,000 hCMEC/D3 cells transfected with Cy3-oligonucleotide (B in the graph) or NC (A in the graph). **(C)** Percentage of positive cells to NC was calculated and differences were compared by two-tails paired *t*-test, n=3 independent experiments, ***P<0.001. Scale bar=340µm.

The kinetics of miRNA-155 overexpression using transient transfection of miRNA-155 mimic were then analysed at 0, 24 and 48 h post-transfection. RT-qPCR demonstrated that miRNA-155 was highly up-regulated at every time point when compared to scramble-transfected hCMEC/D3 cells (872±573, 1724±569 and 2308±1056 relative miRNA-155 expression to scramble-transfected cells, P<0.0001, n=3,

respectively) (Figure 5.2). For subsequent experiments, 48 h end-point was used for remaining transfection experiments using miRNA-155 mimics.

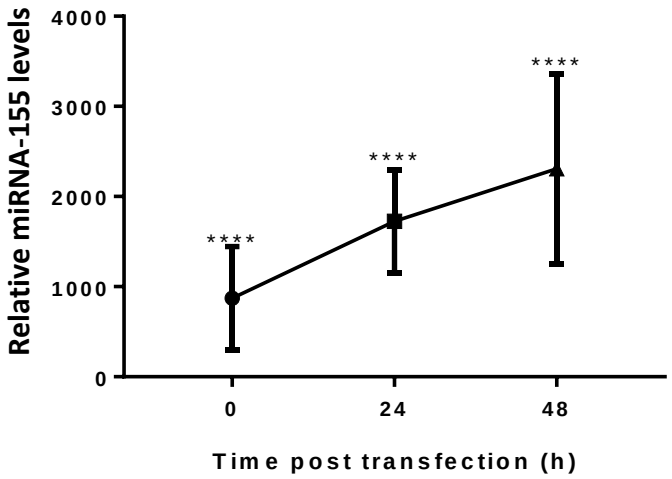

Figure 5.2. Levels of miRNA-155 after transfection of hCMEC/D3 cells. RT-qPCR analysis of miRNA-155 at 0, 24 and 48 h post-transfection with 30 nM of miRNA-155 precursor. Small nuclear RNA U6 was used as housekeeping gene to normalised miRNA-155 expression values. Data are shown as mean±SEM, n=3 of independent experiments and ****P<0.0001. One-way ANOVA followed by post hoc test Dunnet´s multiple comparison test.

Next, confirmation of the overexpression of miRNA-155 in hCMEC/D3 cells leading to increased leukocyte adhesion to brain endothelium was validated. As described in Chapters 2 and 4, CFMDA-labelled Jurkat T cells appeared as bright cells on top of spindle-shaped hCMEC/D3 cells (Figure 5.3.A). Under basal conditions (scramble-transfected hCMEC/D3 cells), 47±6 Jurkat T cells/FOV were adhered to brain endothelium whereas overexpression of miRNA-155 led to 68±4 adhered cells/FOV (P<0.05 and n=5), which confirmed that miRNA-155 overexpression increased T cell adhesion to hCMEC/D3 cells (Figure 5.3.B).

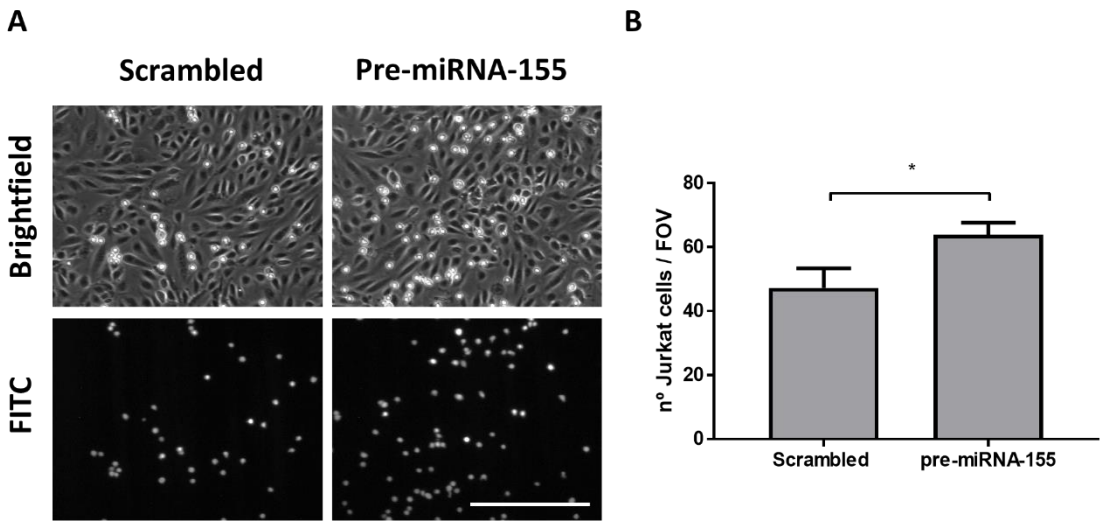

Figure 5.3. Firmly Jurkat T cell adhesion to hCMEC/D3 cells after miRNA-155 overexpression. **(A)** Representative brightfield (top) and fluorescent (FITC, bottom) images of Jurkat T cell adhesion (round-shaped cells) to hCMEC/D3 cells (spindle-shaped cells) under flow conditions after transfection with scramble--oligonucleotide control (Scrambled, left panels) or pre-miRNA-155 oligonucleotide (pre-miRNA-155, right panels) with a 10x objective. **(B)** Quantification of the number of firmly adhered T cells per field of view (FOV 640 × 480 μm) following transfection with scramble-oligonucleotide control or pre-miRNA-155 oligonucleotide for 48 h. Data are shown as mean ± SEM and n = 5 of independent experiments. Differences were evaluated with paired *t*-test with **P<0.05* to scramble-transfected control. Scale bar=340μm.

Subsequently, impact of miRNA-155 overexpression on the expression of cell adhesion molecule, VCAM1, was investigated in hCMEC/D3 cells. RT-qPCR analysis revealed that VCAM1 mRNA levels were increased after miRNA-155 overexpression in hCMEC/D3 cells (2.77±0.43 relative VCAM1 expressione to scrambled-transfected cells 1.04±0.18, $P<0.05$ and n=3) (Figure 5.4.A). In addition to the mRNA analysis, VCAM1 protein expression showed clear increased levels in miRNA-155-overexpressing hCMEC/D3 cells (n=2) (Figure 5.4.B and 5.4.C). These results validated previous published data and confirmed the usefulness of this model in order to characterise the mechanism of action underlying Jurkat T cell adhesion to hCMEC/D3 cells.

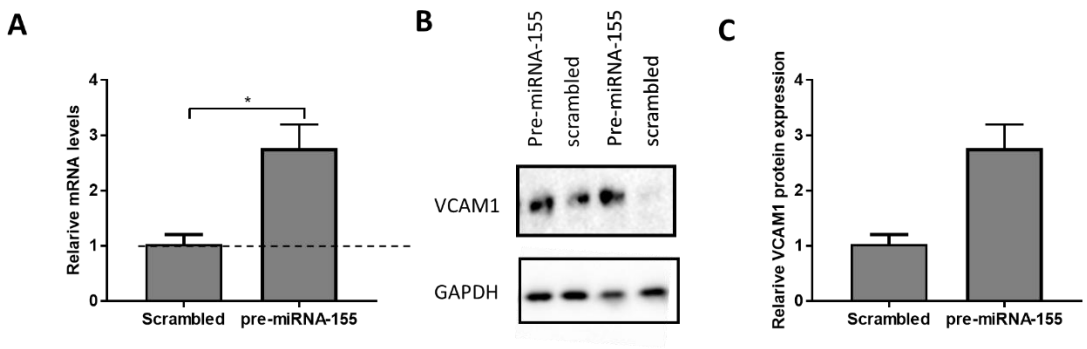

Figure 5.4. Overexpression of miRNA-155 increased VCAM1. (A) RT-qPCR analysis of vascular cell adhesion molecule 1 (VCAM1) mRNA after overexpression of miRNA-155 in hCMEC/D3 cells for 48 h. mRNA levels were normalised to internal control, β-actin mRNA. **(B)** Cropped image of two experiments of western blotting analysis of VCAM1 expression after transfection of hCMEC/D3 cells with miRNA-155 precursor (pre-miRNA-155) or scrambled control (scrambled). GAPDH was used a loading control. **(C)** Quatification of band densitometry of VCAM1 western blot with normalisation to loading control GAPDH and values showed as expression relative to values for the scrambled control transfected hCMEC/D3 cells. Data are shown as mean±SEM (A), n=3 independent experiments and two technical replicates, **P*<0.05 and n=2 independent experiments (B). Differences were measured with two-tailed paired *t*-test.

5.2.2. Identification of mRNA targets for miRNA-155

To identify the downstream gene targets of miRNA-155 that may participate in leukocyte adhesion, online microarray datasets generated by miRNA-155 overexpression in hCMEC/D3 cells were referenced (Geo accession GSE44694, platform GPL6883). In the original publication, the authors studied the effect of miRNA-155 modulating BBB permeability, therefore, no annotation was observed related to pathways involving leukocyte adhesion (Lopez-Ramirez *et al.*, 2014).

Given that the analysis of the microarray data did not result in the discovery of feasible candidates, identification of miRNA-155 targets was approached from a different angle. Preliminary analysis was conducted on proteomic data of miRNA-155-overexpressing hCMEC/D3 cells generated by Dr. Arsalan Haqani (National Research Council of Canada, Human Health Therapeutics Portfolio, Canada) (n=1) (Annexe 1).

Proteins that were observed to be down-regulated by > 1 log_2 fold change (97 proteins) were selected and compared to the list of predicted targets for miRNA-155 obtained from TargetScan (Figure 5.5.A). Indeed, six proteins showed at least one predicted site for binding of miRNA-155 according to TargetScan. The list of down-regulated proteins were also compared to the list of validated targets according to Tarbase and two mRNA targets were identified. Therefore, these two proteins have been previously shown to be targets of miRNA-155. Subsequently, a literature search was carried out on these 8 proteins to identify links to endothelial function and/or regulation of immune response by using keywords of "endothelial", "inflammation" or "leukocytes" in the National Center for Biotechnology Information (https://www.ncbi.nlm.nih.gov/). Only nuclear factor of activated T cells 5 (NFAT5), tight junction protein 1 (TJP1), REL proto-oncogene, NF-kB subunit (REL) and WNK1 were cited in publications related to any of the before mentioned keywords.

A

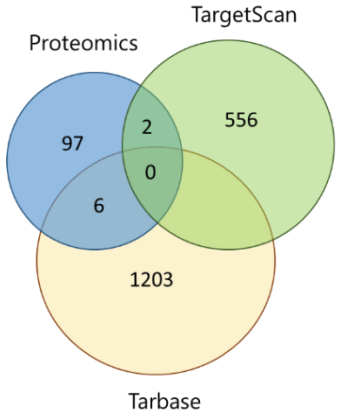

B

Gene	FC	TargetSCan	Tarbase	Relevant literature
TNKS	-2.94	0	0	N/A
FAM177A1	-2.47	0	1	N/A
NFAT5	-2.19	1	0	Inflammation Ma P. et al., 2019
TJP1	-1.73	0	1	EC structure Zhang L., et al 2015
DDX10	-1.25	0	1	N/A
CCDC137	-1.15	0	1	N/A
REL	-1.03	0	1	Inflammation Guo M. et al., 2004
WNK1	-1.02	1	0	Leukocyte adhesion to EC Köchl R. et al., 2016

Figure 5.5. Analysis of proteins in miRNA-155 overexpressing hCMEC/D3 cells. (A) Venn diagram of down-regulated proteins upon miRNA-155 overexpression in hCMEC/D3 cells (proteomics), predicted targets of miRNA-155 by TargetScanHuman 7.8 (TargetScan), validated list of miRNA-155 targets by Tarbase (Tarbase) and corresponding number of matched target with the proteomic analysis. **(B)** Table summarising matched targets, log_2 fold change (FC) to scrambled-transfected hCMEC/D3 cells, number of online database matches (targetScan or Tarbase) and relevant representative literature to endothelial, inflammation and or leukocyte function keywords.

Next, the expression of these four proteins was investigated at the mRNA level in murine brain cells using open-access data on single cell RNA-seq of murine brain cells (He *et al.*, 2018). This database contained transcriptomic data on different groups of brain cells including pericytes (PC); smooth muscle cells (SMCs) either venular (veSMC), arteriolar (arSMC) or arterial (aSMC), microglia (MG), fibroblast-like type 1 or 2 (FPB1 and FPB2, respectively), oligodendrocytes (OG) and endothelial cells (EC). ECs were grouped in 6 groups, three groups were identified as venous EC (vEC), capillary EC (capEC) or arterial EC (arEC), whereas there were three novel groups of ECs (EC1, EC2 and EC3). Nfat5, tjp1 and wnk1 were abundantly expressed in the different clusters of ECs whereas rel expression was very low. Comparative analyses were not carried out, however, tjp1 seemed to show the highest level of expression among EC when compared to nfat5 and wnk1 (Figure 5.6). Differential expression was observed in the other brain murine cell types.

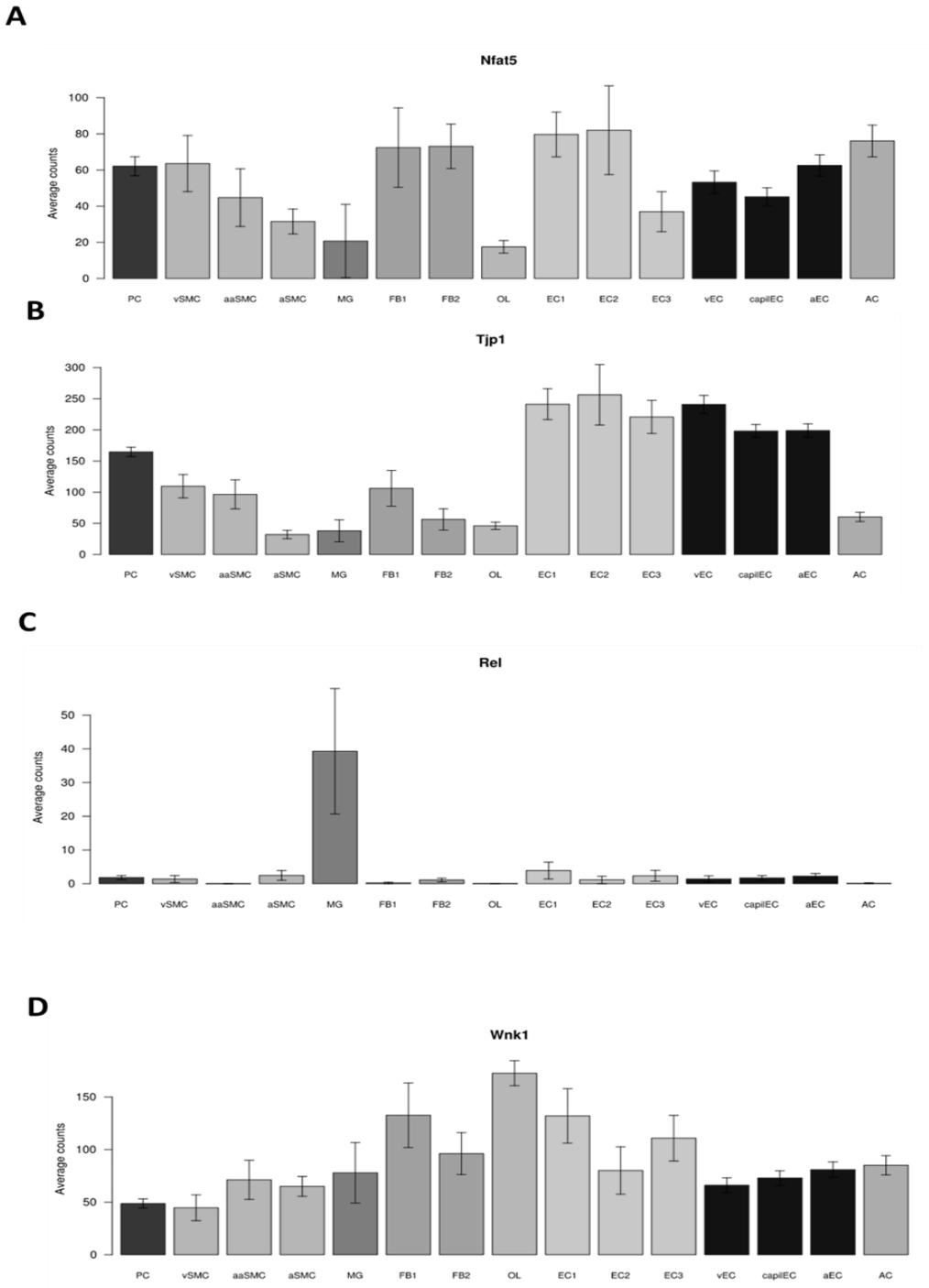

Figure 5.6. Expression of miRNA-155 target mRNAs in the mouse brain cells. Average expression of single cell RNA-seq provided by the open-access web dataset (http://betsholtzlab.org/VascularSingleCells/database.html, last accessed September 2020) for different mouse brain cells to screen for the expression of nfat5 **(A)**, tjp1 **(B)**, rel **(C)** and wnk1 **(D)**. Abbrevations: PC, pericytes; veSMC, arSMC and aSMC, venous, arteriolar and arterial smooth muscle cells, respectively; MG, microglia; FPB1, FPB2, fibroblast-like type 1 or 2; OG, oligodendrocytes; EC, endothelial cell; vEC, venous EC; capEC, capillary EC; aEC; arterial EC.

Subsequently, whether these proteins were expressed in human brain endothelial cells *in vivo* was investigated. For this purpose, open-access online database Human Protein Atlas (https://www.proteinatlas.org/; last accessed May 2020) and immunohistochemistry analysis of human cortex section were used (Figure 5.7.). The human protein atlas offered an estimation of the signal of the interrogated protein in endothelial, glial and neural cells. This information was collected and compared (Table 5.1.). Only TJP1 and WNK1 had positive staining co-localising with endothelial cells (Figure 5.7).

A

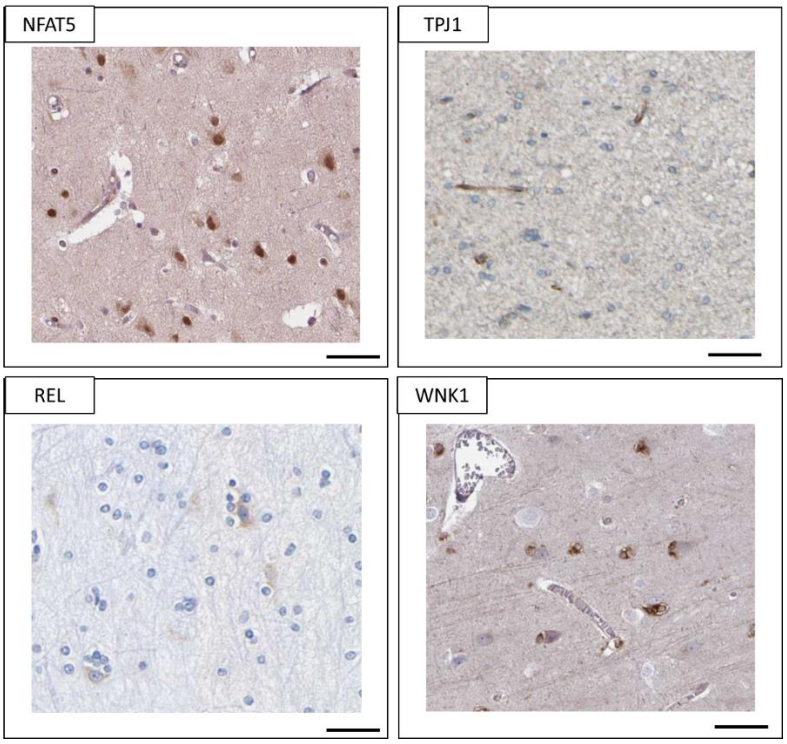

B

Gene	BECs	Glial Cells	Neuronal Cells
NFAT5	N/A	Medium	Medium
TJP1	High	N/A	N/A
REL	N/A	N/A	Medium
WNK1	Medium	High	N/A

Figure 5.7. Expression of miRNA-155 target proteins in the human cerebral cortex. **(A)** Immunohistochemestry analysis from The Human Protein Atlas (https://www.proteinatlas.org/) for NFAT5, TJP1, REL and WNK1. Staining is represented by brown signal. Scale bar is 50 µm. **(B)** Summary of expression of miRNA-155 predicted target proteins in neural, glial and endothelial cells of the human cerebral cortex and proteomic analysis in hCMEC/D3 cells. Abbreviations: FC, fold change; BEC, brain endothelial cells; N/A, not applicable

TJP1 plays a role in BBB structure and permeability but there is currently no strong evidence to suggest it is involved in leukocyte transmigration into the brain (Reinhold and Rittner, 2017). Köchl R *et al.*, (2016) proposed that deficiency of WNK1 in leukocytes plays an important role modulating the adhesion of leukocytes to endothelial cells (Köchl *et al.*, 2016). Furthermore, WNK1 is also a predicted target of the murine version of miRNA-155 (TargetScanMouse, http://www.targetscan.org/mmu_72/), which suggested that WNK1-miRNA-155 interaction is conserved in the two species. Therefore, WNK1/miRNA-155 pair was selected for further investigation.

5.2.3. Effect of WNK1 silencing on T cell adhesion to BECs

To explore whether WNK1 played a role in modulating leukocyte adhesion to BECs, hCMEC/D3 cells were transiently transfected with siRNAs against WNK1 mRNA to decrease the levels of WNK1. Efficiency of WNK1 silencing was analysed from the expression of WNK1 protein and mRNA in transfected hCMEC/D3 cells (Figure 8). Firstly, testing of several antibodies for WNK1 by western blotting resulted in several unspecific bands. Furthermore, immunostaining revealed majority nuclear staining of WNK1, which is a cytoplasmic protein (data not shown). These different antibodies were discarded, finally, a new antibody against WNK1 yielded specific staining of WNK1 confirmed by cytoplasmic signal intensity (Figure 5.A.). Immunostaining of WNK1 demonstrated the loss of WNK1 staining on WNK1-siRNA transfected hCMEC/D3 cells (Figure 5.8.A). Upon transfection, WNK1 signal dropped to 49±8% of pixel intensity when compared to scrambled-transfected hCMEC/D3 cells ($P<0.05$, n=3) (Figure 5.8.B). RT-qPCR confirmed a significant decrease in the levels of WNK1 mRNA to 0.31±0.04 ($P<0.01$, n=3) in WNK1-siRNA transfected hCMEC/D3 cells relative to levels of WNK1 in the scrambled transfected control (Figure 5.8.C).

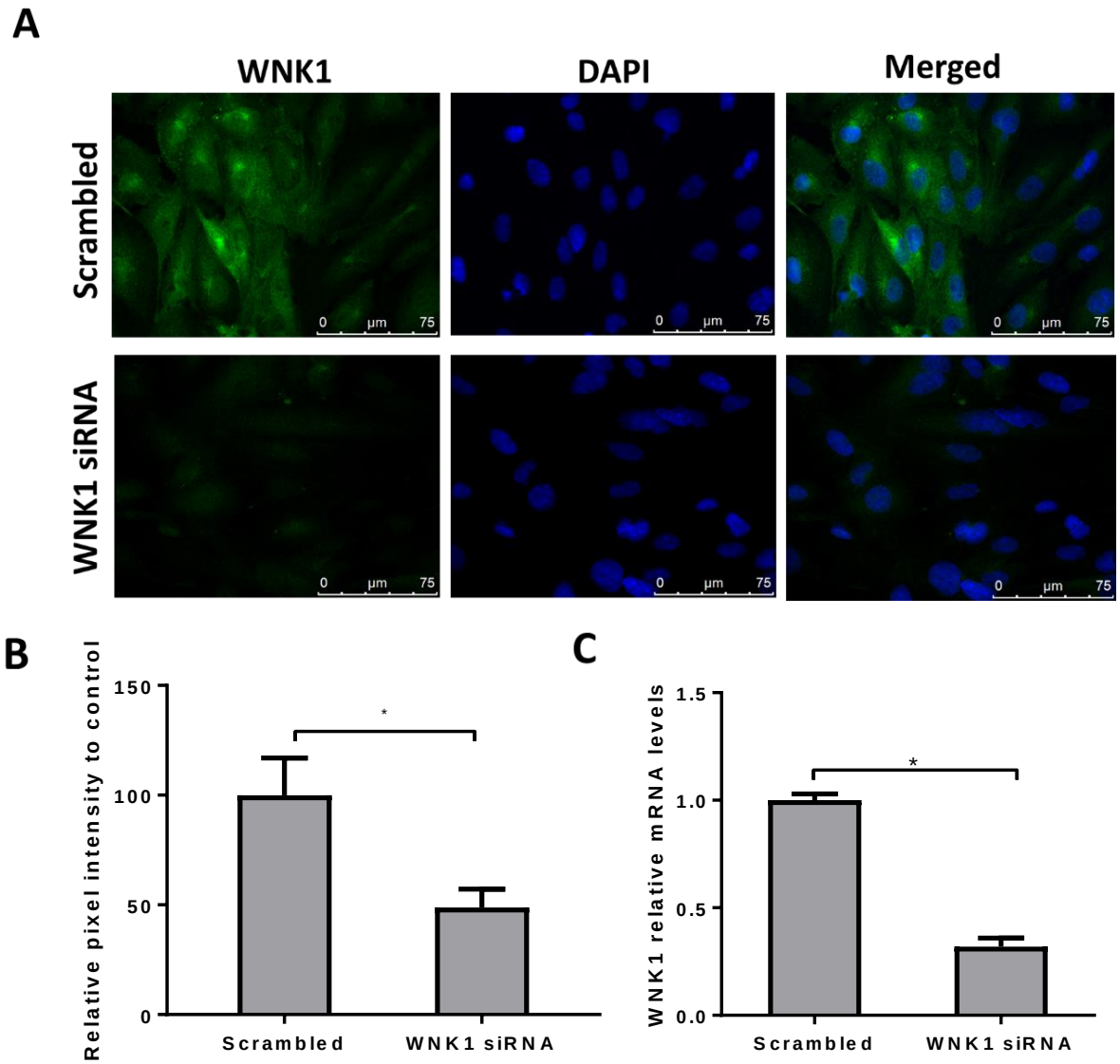

Figure 5.8. WNK1 silencing in hCMEC/D3 cells was demonstrated at the RNA and protein level. (A) Immunocytochemistry of hCMEC/D3 cells transfected with WNK1 siRNA or scrambled control. The green channel represents WNK1 signal whereas the blue channel represents nuclear staining (DAPI). Scale bar = 75 µm **(B)** Quantification of the fluorescent staining of transfected hCMEC/D3 cells on 10 random images and normalized WNK1 signal by number of cells per image. **(C)** RT-qPCR analysis of WNK1 expression after WNK1 siRNA transfection of hCMEC/D3 cells. Levels of WNK1 were normalized to internal control β-actin mRNA. Data are shown as mean±SEM, n=3 independent experiments, differences were quantified by paired-t test with P*<0.05 to scrambled control.

Subsequently, whether silencing WNK1 in hCMEC/D3 cells affected leukocyte adhesion to BECs was investigated (Figure 5.9.A). Under basal conditions (hCMEC/D3 cells transfected with scrambled siRNA), 58±7 Jurkat T cells/FOV adhered to scrambled transfected hCMEC/D3 cells. Knockdown of WNK1 significantly increased the number of firmly Jurkat T cells adhered to hCMEC/D3 cells (74±7 Jurkat T cells/FOV, $P<0.0001$ and n=7) (Figure 5.9.B). Under inflammatory conditions (1 ng/ml TNFα and IFNy for 24 h) (Figure 5.9.C), 271±8 Jurkat T cells/FOV adhered to scramble-transfected hCMEC/D3 cells (Figure 5.9.C). Deficiency of WNK1 in hCMEC/D3 cells did not alter the overall number of firmly adhered Jurkat T cells to cytokine-treated hCMEC/D3 cells compared to scramble-transfected hCMEC/D3 cells (290±17 number of firmly adhered Jurkat T cells/FOV for WNK1 siRNA-transfected cells, $P>0.05$ and n=3) (Figure 5.9.D). These results suggested that WNK1 played a role in modulating leukocyte adhesion to BECs only under basal conditions whereas stimulation with pro-inflammatory cytokines might mask WNK1-effect on T cell adhesion.

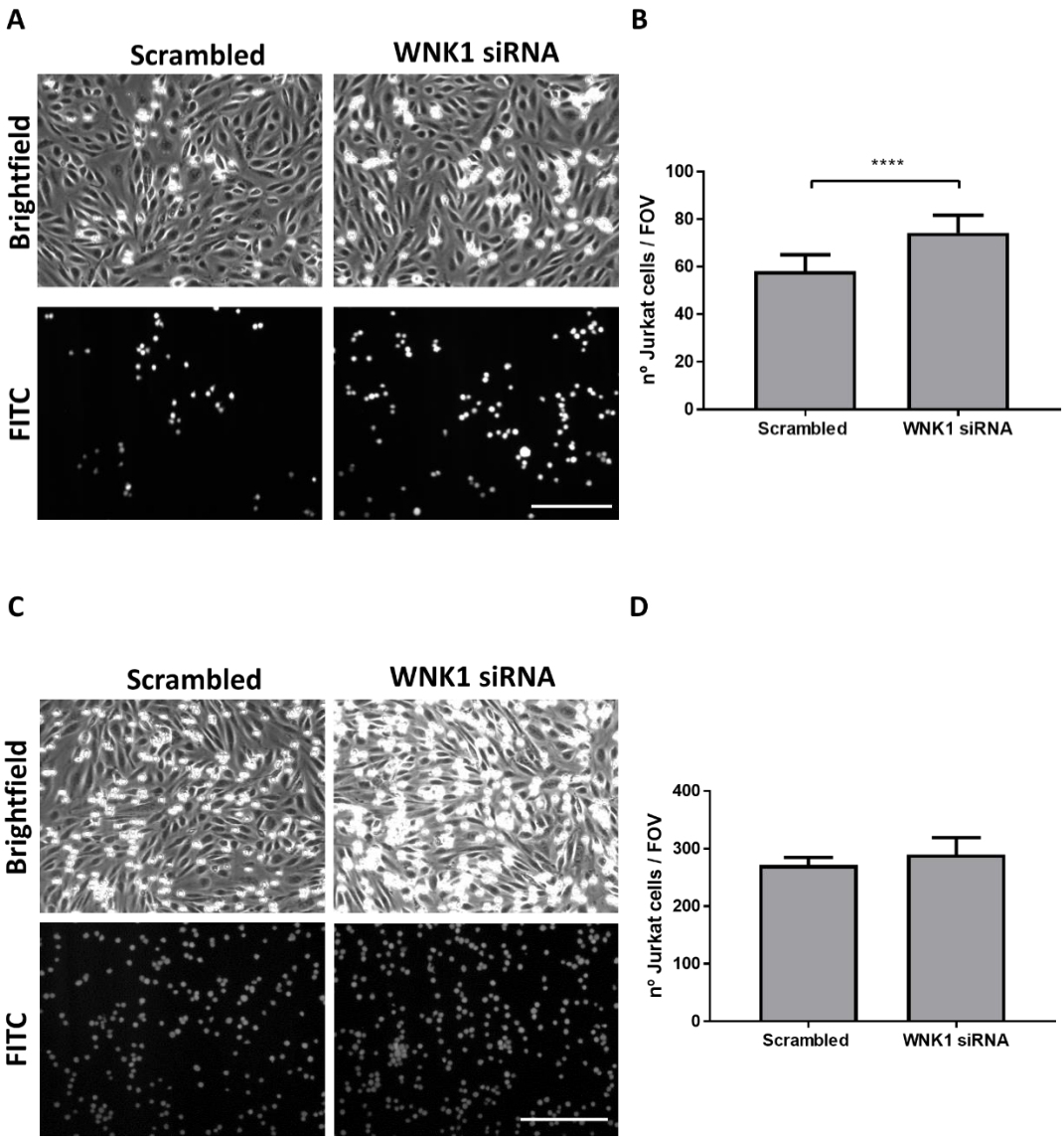

Figure 5.9. WNK1 deficiency increased firmly leukocyte adhesion to hCMEC/D3 cells after under basal conditions. **(A)** Representative brightfield (top) and fluorescent (FITC, bottom) images of Jurkat T cell adhesion (round-shaped cells) to hCMEC/D3 cells (spindle-shaped cells) under flow conditions after transfection with scrambled control (Scrambled, left panels) or WNK1 siRNA (WNK1 siRNA, right panels) under basal conditions. **(B)** Quantification of the number of firmly adhered T cells per field of view (FOV) following transfection with scrambled control or WNK1 siRNA oligonucleotide for 48h under basal conditions. (**C)** Representative brightfield (top) and fluorescent (FITC, bottom) images of Jurkat T cell adhesion (round-shaped cells) to hCMEC/D3 cells (spindle-shaped cells) under flow conditions after transfection with scrambled control (Scrambled, left panels) or WNK1 siRNA (WNK1 siRNA, right panels) under inflammatory conditions (1ng/ml TNFα and IFNγ for 24h prior leukocyte adhesion was measured). **(D)** Quantification of the number of firmly adhered T cells per field of view following transfection with scrambled control or WNK1 siRNA for 48h under inflammatory conditions. Data are shown as mean±SEM and n=7 (A) and n=3 (B) independent experiments. ****$P<0.0001$ to scrambled control. Differences were assessed using a paired, two-tailed *t*-test.

5.2.4. WNK1 expression is not modulated by overexpression of miRNA-155 in hCMEC/D3 cells

In order to study whether WNK1 expression is modulated by miRNA-155, hCMEC/D3 cells were transfected with miRNA-155 mimic and levels of WNK1 were measured by qPCR and immunohistochemistry (Figure 5.10). Overexpression of miRNA-155 in hCMEC/D3 cells did not alter WNK1 mRNA expression (0.92±0.24 expression levels of WNK1 relative to scrambled oligonucleotide-transfected cells) (Figure 5.10.A). Furthermore, analysis of WNK1 protein expression by immunohistochemistry revealed levels of the WNK1 protein were unchanged following miRNA-155 siRNA transfection in hCMEC/D3 cells when compared to scrambled-transfected cells (Figure 5.10.C). Indeed, quantification of pixel intensity confirmed that WNK1 was unaltered upon silencing WNK1 in hCMEC/D3 cells (n=3). These results suggested that overexpression of miRNA-155 with miRNA-155 mimic did not modulate the expression of WNK1. Hence, this questioned whether WNK1 is an actual target of miRNA-155 in human BECs.

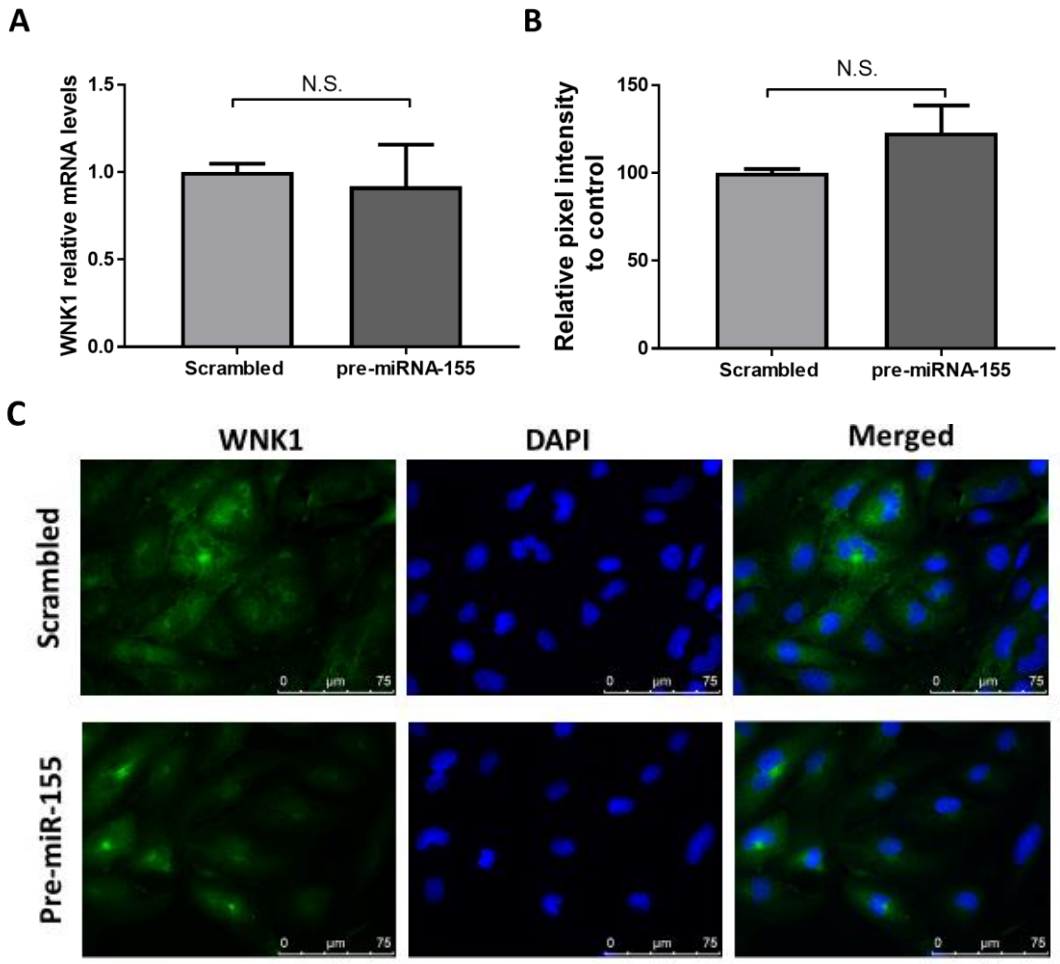

Figure 5.10. Overexpression of miRNA-155 did not alter WNK1 levels in hCMEC/D3 cells. **(A)** RT-qPCR analysis of WNK1 expression after WNK1 siRNA transfection of hCMEC/D3 cells. Levels of WNK1 were normalised to internal control β-actin mRNA. **(B)** Immuno-cytochemistry of hCMEC/D3 cells transfected with WNK1 siRNA or scrambled control. Green channel represents WNK1 signal whereas blue channel represents nuclear staining (DAPI). Scale bar = 75 µm **(C)** Quantification of the fluorescent staining of transfected hCMEC/D3 cells on 5-10 random images and normalized WNK1 signal by number of cells per image. Data are shown as mean±SEM, n=3 independent experiments, differences were quantified by paired-t test with P*<0.05 to scrambled control. Scale bar = 75µm.

5.3. Discussion

In this chapter, the mechanism by which miRNA-155 mediated leukocyte adhesion to brain endothelium was investigated. WNK1 was identified as a possible target of miRNA-155 and it was confirmed that silencing of WNK1 led to increased leukocyte adhesion to BECs. However, the stable expression of WNK1 following overexpression of miRNA-155 suggested that WNK1 is not likely to be regulated by miRNA-155 overexpression in human BECs.

5.3.3. Efficient transfection of hCMEC/D3 cells with miRNA-155 precursor

Transfection of hCMEC/D3 cells with miRNA modulators has been previously characterised (Lopez-Ramirez *et al.*, 2014; Cerutti *et al.*, 2016). Similar to previous reports, transfection with pre-miRNA-155 resulted in high expression of miRNA-155 in the hCMEC/D3 cells (Lopez-Ramirez *et al.*, 2014). Overexpression of miRNA-155 subsequently led to increased adhesion of T cells to brain endothelia. These results were in accordance with Cerutti *et al.*, (2016), who demonstrated a role for miRNA-155 in stimulating leukocyte adhesion to brain endothelium. However, results from the current experiments differed from this earlier report on absolute numbers as they were higher number of firmly adhered T cells to BECs. It is possible that these differences might be due to user variability as well as cell lot. Furthermore, it was confirmed that miRNA-155 increased levels of VCAM1, one of the two proteins suggested to be involved in miRNA-155-induced T cell adhesion to brain endothelium (Cerutti *et al.*, 2016). Cerutti et al (2016) previously showed the linked between levels of miRNA-155 and VCAM1 expression, which was confirmed in the current experiments. Therefore, this model and transfection method were robust and consistent with the previous literature.

5.3.4. Identification of miRNA-155 targets from existing microarray dataset

Previous analysis of published microarray data on miRNA-155 overexpressing BECs identified a list of possible candidates that can be modulated by miRNA-155 (Lopez-Ramirez *et al.*, 2014). However, none of the predicted genes were known to be involved in leukocyte adhesion to the endothelium. Interestingly, Cerutti *et al.*, showed that silencing miRNA-155 under inflammatory conditions had a stronger effect in modulating leukocyte adhesion than silencing under basal conditions (Cerutti *et al.*, 2016). It is likely that a complex network of miRNA-155 targets might be modulated upon inflammation. Therefore, it is possible that target identification for key players at the mRNA level modulating leukocyte adhesion might be more evident if they were to be studied under a pro-inflammatory scenario. Alternatively, miRNAs can also modulate protein levels without altering total mRNA levels (Cottrell, Szczesny and Djuranovic, 2017). For this reason, it is also feasible that miRNA-155-induced leukocyte adhesion had no direct effect at the mRNA level.

5.3.5. WNK1 is a possible modulator of leukocyte adhesion to BECs

Proteomic analysis of miRNA-155-overexpressing hCMEC/D3 cells identified 8 candidate proteins that were either predicted or validated targets of miRNA-155. Only four of these candidates were related to inflammation, endothelial cells and/or leukocytes mechanisms by different research papers. Single-cell RNA-seq data showed that nfat5, wnk1 and tjp1 were expressed in murine brain endothelial cells. However, both NFAT5 and REL were observed not to be expressed in the human tissue section of cerebral cortex according to the Human Protein Atlas (www.proteinatlas.org). These differences might be due to species-specific expression (murine and human) or simply than NFAT5 protein expression is not high enough to be detected in brain endothelium. This latest approach

would be in disagreement with a recent study. Indeed, authors identified the inflammatory role of NFAT5 in BECs (Wu, Cerutti, Miguel A Lopez-Ramirez, *et al.*, 2015) and showed that inhibition of NFAT5 decreased leukocyte adhesion to BECs. Furthermore, NFAT5 is a transcription factor that has been shown to have a protective role in oxygen-glucose-serum deprived astrocytes (Xia *et al.*, 2017). Accordingly, NFAT5 expression was detectable in glial cells. REL is a crucial protein for NFKappaBeta activation, a major transcription factor that regulates many inflammatory pathways (Wulczyn, Krappmann and Scheidereit, 1996). Under pro-inflammatory conditions REL has been shown to be up-regulated (Tian, Nowak and Brasier, 2005). For this reason, it was hypothesised that under miRNA-155-induced status REL should have been up-regulated as well, however, proteomic analysis suggested otherwise. It is possible that down-regulation of REL in hCMEC/D3 cells might be a compensatory mechanism to cope with miRNA-155-induced inflammatory status. These two proteins were not further investigated because 1) no detection in cortical brain endothelial cells and 2) weak link on promoting T cell adhesion upon down-regulation. Then, it was confirmed that TJP1 was expressed in endothelial cells of human tissue sections of the cerebral cortex. TJP1 has been extensively characterised as a key protein for brain endothelium structure and function (Reinhold and Rittner, 2017). However, little is known about its possible link to leukocyte adhesion to brain endothelium.

WNK1 was identified as a possible candidate for miRNA-155. WNK1 is a kinase protein that is mainly responsible for mediating the signalling of ion co-transporter whose main function has been linked to water balance in the kidney (Shekarabi *et al.*, 2017). Interestingly, a recent report has showed that WNK1 is relevant in immune function (Köchl *et al.*, 2016). In this research, the authors demonstrated that upon silencing in T cells, WNK1 increased T cell adhesion to endothelial cells but decreased their migration,

suggesting a fine-tune expression of WNK1 in order to respond to the cellular requirements. MiRNAs have been previously described as fine-tune regulators of gene expression (Zhang *et al.,* 2012), thus, likely modulators of WNK1 expression. Results from the current study demonstrated that silencing WNK1 in hCMEC/D3 cells increased number of T cells adhered to brain endothelial cells under basal conditions. However, this phenotype was not replicated under inflammatory conditions. It is feasible that the mechanism by which WNK1-mediated T cell adhesion to BECs is saturated by the stimulation of BECs with TNFα and IFNγ, hence no further effect can be observed upon inhibition of WNK1 under inflammatory conditions. To understand these differences of T cell adhesion regulation by WNK1, the molecular players involved in WNK1-induced endothelial dysfunction are required. WNK1 has been proposed to control endothelial cell proliferation and angiogenesis mediated by OSR1 and SPAK1, two well-known targets of WNK1 (Dbouk *et al.*, 2014). However, it is difficult to speculate the mechanism by which WNK1 might be mediating leukocyte adhesion, hence, future proteomic analysis of WNK1-deficient cells would be important to understand this phenotype.

MiRNA-155 has been extensively studied for playing major roles in T cell function (Faraoni *et al.*, 2009). MiRNA-155 showed a highly conserved binding site in the 3' UTR of WNK1. For this reason, modulation of WNK1 expression might be partly controlled by miRNA-155. However, these results showed that overexpression of miRNA had no effect on mRNA or protein WNK levels. As mentioned previously, there is still a possibility where under basal conditions, the effect of miRNA-155 in WNK1 expression is undetectable. Furthermore, the proteomic analysis was based on only one sample for the screening. Hence, future experiment will include analysis of WNK1 expression under inflammatory conditions where miRNA-155 has been depleted.

CHAPTER 6: Investigating the unexpected polydipsia in aged miRNA-155 deficient mice

6.1. Introduction

In the previous chapters, the mechanism by which sEVs and miRNA-155 affected cerebrovascular function in the context of inflammation was investigated. Initially, i*n vivo* experiments were planned to evaluate the *in vitro* findings described in Chapter 4 and 5. Hence, a mouse model where miRNA-155 was knocked out (KO) (Lopez-Ramirez *et al.*, 2014) was maintained in the lab facilities. This model was used by other lab members to evaluate BBB function during healthy ageing. It was observed that there were no significant differences in BBB permeability and tight junction expression (unpublished data). However, over the course of the colony maintenance and ageing, it was noted that aged female miRNA-155 KO mice developed an unexpected increase in water intake compared to the WT mice. This phenotype has not been previously described in the literature of miRNA-155 KO mice, for this reason, a systematic analysis of this phenotype and a molecular characterisation was designed to be a side project of this thesis.

An increase in the rate of water intake is commonly known as polydipsia (Ball, 2007). The physiology of polydipsia is related to changes in the water balance and/or thirst (Knepper, Kwon and Nielsen, 2015). Polydipsia is often associated with diabetes *mellitus*, diabetes *insipidus*, psychogenic thirst as well as rare syndromes affecting the kidney function (Makaryus and McFarlane, 2006; Ball, 2007; Aznar Rodríguez *et al.*, 2012).

Diabetes *mellitus* is characterised by a deregulation of the glucose levels and is often associated with polydipsia, polyuria (increase urine secretion) and weight loss among other symptoms (Aznar Rodríguez *et al.*, 2012). Therefore, diagnosis of diabetes *mellitus*

that may be associated with an increased water intake can be achieved by measuring fasting blood glucose levels (Aznar Rodríguez *et al.*, 2012).

Diabetes *insipidus* is the most common cause of polydipsia (Makaryus and McFarlane, 2006). Whereas diabetes *mellitus* is the consequence of a deregulation of the glucose-insulin system, diabetes *insipidus* is caused by a deregulation of the arginine vasopressin hormone (AVP), also known as antidiuretic hormone (Robertson, 1995; Valtin, 1995). Diabetes *insipidus* is considered "central" when the AVP production in the hypothalamus is impaired or if the pituitary gland fails to secrete it into the blood stream. Therefore, reduced levels of AVP in the blood will lead to compensatory mechanisms involving blood pressure, osmo-receptors and eventually increased thirst (Ball, 2007; Knepper, Kwon and Nielsen, 2015). "Nephrogenic" diabetes *insipidus* is caused when the production and secretion of AVP is normal but this hormone fails to activate its receptor in the kidney, likely due to renal dysfunction (Bichet, 2006). Diagnosis of both diabetes *insipidus* and its subtypes is achieved by measuring AVP levels in blood as well as performing a water deprivation test in combination with injection of desmopressin, an analogue of the AVP (Robinson, 1976).

AVP is synthesised in the large magnocellular neurons situated in the hypothalamus. This region overlaps with the synthesis area for oxytocin. This molecule is a neuropeptide closely related to AVP. Oxytocin and AVP differ by only two amino acids located at position 3 and 8. Both oxytocin and AVP have functions closely related to social behaviour (Baribeau and Anagnostou, 2015). Water homeostasis can also be regulated by AVP-independent mechanism involving oxytocin (Cheng, Chu and Chow, 2009).

Psychogenic thirst is a rare condition resulted in the deregulation of pathways involved in water intake independently from AVP. Pathological conditions such as brain

cancer or vascular dysfunction can lead to polydipsia (Ball, 2007). Diagnosis is normally achieved after eliminating the most common causes of polydipsia (Makaryus and McFarlane, 2006).

Another reason for increased water intake may be associated with kidney malfunction, independently of AVP signalling (Ball, 2007). There are well-known mutations in the ion co-transporters that have been reported to lead to increased polydipsia. Bartter´s syndrome is the most common condition associated with co-transporter dysfunction and can be sub-classified according to the mutations in different genes e.g. Na-K-2Cl symporter (SLC12A1 or NKCC2 gene) or thick ascending limb K+ channel (ROMK or KCNJ1 gene) (Fulchiero and Seo-Mayer, 2019).

A putative role for miRNA-155 in regulating water balance has not been demonstrated previously. There is evidence that deficiency of this miRNA can lead to higher levels of angiotensin II type 1 receptor resulting in vascular constriction and higher blood pressure (DuPont *et al.*, 2016). However, this mechanism would not explain increased water intake. Therefore, these preliminary observations suggest that there might be novel pathways by which miRNA-155 regulates water intake.

In this chapter, a systematic study investigating the physiological attributes (water and diet intake, weight and urine specific gravity) of both male and female miRNA-155 KO mice and WT at different months of age (3, 6, 12 and 18) was carried out. Furthermore, aged female mice (18 month-old) were used to further investigate the aetiology of the observed physiological attributes. Finally, a systematic comparison between traditional miRNA-155 KO mice and newly generated miRNA-155 KO mouse obtained by cross-breeding the in-house WT mouse strain with miRNA-155 KO mice

was carried out to determine whether or not spontaneous genetic mutations may have arisen that might have explained the observations made.

6.2.Results

6.2.1. Genotype of miRNA-155 KO and WT mice

To ensure the model has not lost the deletion of miRNA-155, both miRNA-155 KO and WT mice were genotype by PCR. Imaging of resolved gels showed two distinct bands (Figure 6.1). WT mice showed a single band around 450 bp (predicted size was 465 bp) whereas miRNA-155 KO mice presented a higher amplicon sized band. Indeed, the identified band was approximately 550 bp (predicted size for the amplicon of miRNA-155 primers was 600 bp) (Figure 6.1). Therefore, this results confirmed that miRNA-155 KO mice carried the mutated miRNA-155 gene. A systematic study was carried out to determine weight, water and diet intake as well as urine concentration

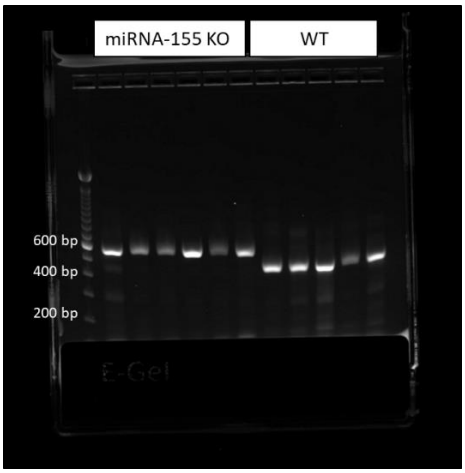

Figure 6.1. Genotype of miRNA-155 KO mice. Representative image of genotyping miRNA-155 KO deletion by PCR. 2 to 7 wells are samples from miRNA-155 KO mouse whereas 8 to 12 are samples from wild-type (WT) mice.

6.2.2. Systematic study of weight, water and diet intake and urine specific gravity

A systematic study was carried out to determine weight, water and diet intake as well as urine concentration in male and female WT and miRNA-155 KO mice over an 18-month period. As expected, both WT and miRNA-155 KO male mice showed higher weight gain compared to female mice of both strains (Figure 6.2.A). Genotype did not affect body weight within the same sex (Fig. 6.2.A). Food intake over time did not differ among any groups at any time point studied. In fact, no differences were found in food intake percentage calculated from month 3 of the study (Figure 6.2.B).

Mean daily water intake ranged between 2 to 4 ml per 25g of body weight for WT mice. These mice maintained constant fluid consumption across the study (Figure 6.1.C). Consistent water intake was also observed in male miRNA-155 KO mice. Although there was a trend for an increased gained water consumption at the later age of 15 and 18 months (145% and 135%, respectively), this was no significant when compared to their aged-matched WT control (Figure 6.1.C). Female miRNA-155 KO mice showed the strongest increased of water intake amongst all groups studied. In fact, fluid consumption in this group was significantly higher than their age-matched control WT mice from 15 month-old of age ($P<0.001$). This increase in water intake was also significantly higher in KO female mice compared to aged and genotype-matched male KO mice (Figure 6.2.C).

Urine concentration was analysed by measuring urine specific gravity every three months. Neither female nor male WT mice showed any changes in urine specific gravity at any point of the study. However, both female and male miRNA-155 KO mice showed a decreased in their urine specific gravity with age (Figure 6.1.D). Male miRNA-155 KO mice showed significant differences in urine specific gravity at late age of 18 months old ($P<0.0001$), whereas this effect was observed from 12 months of age for female miRNA-155 KO mice ($P<0.0001$).

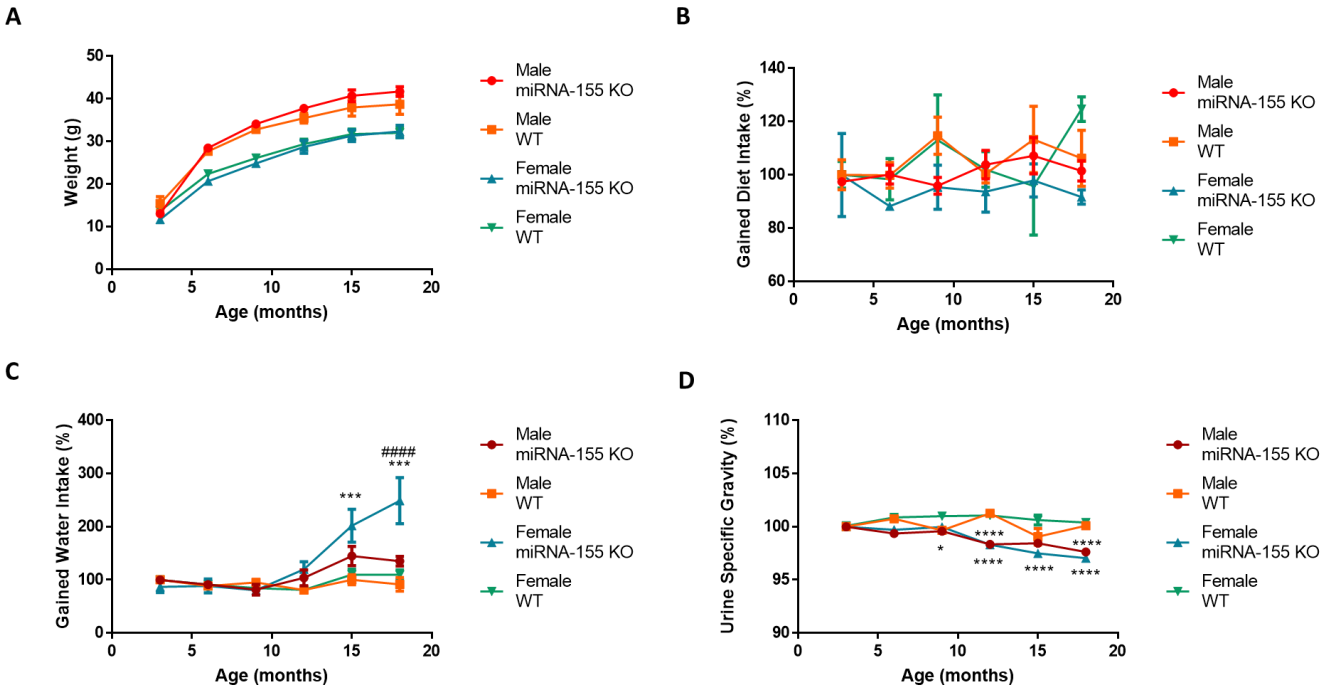

Figure 6.1. Systematic study of physiological parameters of miRNA-155 KO and WT mice. (A) Weight of miRNA-155 knock-out (KO) and wild type (WT) mice (female and male) from 3 to 18 months old (n= 8 (mate WT), 10 (male and female miRNA-155 KO) and 13 (female WT) different mice). **(B)** Gained diet intake percentage of miRNA-155 KO and WT mice (female and male) from 3 to 18 months old (n = 3 (male WT and miRNA-155 KO) and 4 (female WT and miRNA-155 KO) cages). **(C)** Gained water intake percentage of miRNA-155 KO and WT mice (female and male) from 3 to 18 months old (n = 3 (male WT and miRNA-155 KO) and 4 (female WT and miRNA-155 KO) cages). **(D)** Urine specific gravity percentage of microRNA-155 KO and (WT) mice (female and male) from 3 to 18 months old (n= 4 (male WT), 6 (male miRNA-155 KO), 9 (female WT) and 11 (female miRNA-155 KO) different mice). Data are shown as mean ± SEM. Differences were measured with two-way anova and Tukey´s post-hoc test for multiple comparisons. **P*<0.05, ****P*<0.001, *****P*<0.0001 to aged- and sex- matched WT mice. ####*P*<0.0001 to age- and genotype-matched male mice.

6.2.3. Urine and serum analysis

Based on the results described in section 6.2.1, remaining analysis were centred in female 18-month old mice in order to investigate the pathology underlying the observed phenotype.

To further characterise the effect of polydipsia in both urine and blood, serum and urine was analysed by an external company (IDDTEX, Germany). Total concentrations of sodium, magnesium and chloride were found to be significantly decreased in urine isolated from female miRNA-155 KO mice (Table 6.1), whereas calcium and magnesium urine levels were not changed. Urine osmolality was also decreased in the samples from miRNA-155 KO mice when compared to WT mice. These results are in accordance with the previous measurements of urine specific gravity (Figure 6.2.D).

Table 6.1. Electrolyte and osmolality of urine samples from miRNA-155 KO and WT mice (n=5).

Urine	WT	miRNA-155 KO	*p-value*
Electrolytes (mmol/l)	**mean ± SEM**	**mean ± SEM**	
Sodium	68.8 ± 14.66	31 ± 3.58	0.04
Potassium	155.4 ± 34.14	62.6 ± 11.63	0.03
Calcium	1.64 ± 0.42	2.72 ± 0.64	0.2
Magnesium	15.34 ± 4.84	10.98 ± 1.84	0.42
Inorganic Phosphate	16.7 ± 6.28	1.42 ± 0.73	0.04
Chloride	94.8 ± 21.77	44.2 ± 5.26	0.05
Osmolality (mosmol/Kg)	2236 ± 180.9	716.2 ± 71.6	<0.001

Abbreviations: wild type (WT), microRNA (miRNA, knock-out (KO)

Serum analysis resulted in no significant differences in any of the electrolytes analysed neither the osmolality of samples taken from female miRNA-155 KO mice were altered compared to control mice (Table 6.2).

Table 6.2. Electrolyte and osmolality of serum samples taken from miRNA-155 KO and WT mice (n=5).

Serum	WT			miRNA-155 KO			*p-value*
Electrolytes (mmol/l)	**mean ± SEM**			**mean ± SEM**			
Sodium	155.6	±	0.68	156	±	1.1	0.76
Potassium	6.86	±	0.33	5.9	±	0.39	0.1
Calcium	2.24	±	0.02	2.22	±	0.04	0.67
Magnesium	1.64	±	0.04	1.76	±	0.04	0.07
Inorganic Phosphate	2.96	±	0.15	2.96	±	0.14	1
Chloride	114.2	±	0.2	111.2	±	1.46	0.08
Osmolality (mosmol/Kg)	348	±	9.3	340.8	±	6	0.5

Abbreviations: wild type (WT), microRNA (miRNA, knock-out (KO)

6.2.4. Investigating mechanisms underlying the polydipsia and diluted urine observed in female miRNA-155 KO mice with age

In the previous section, female miRNA-155 KO mice were observed to develop a strong phenotype characterised by an increased water intake and diluted urine (Figure 6.2). This phenotype is associated with different pathologies that affect water balance (Valtin, 1995; Ball, 2007). Figure 6.3 shows the flowchart outlining the steps taken to make a differential diagnosis of the phenotype of female miRNA-155 KO mice.

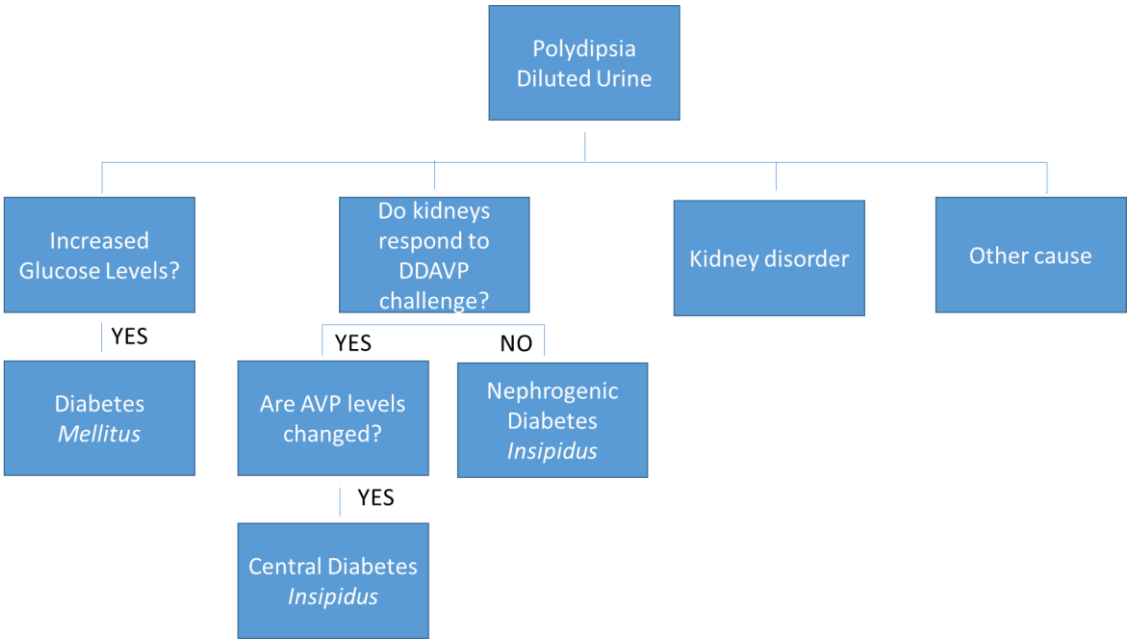

Figure 6.3. Schematic diagram for diagnosing the pathology underlying mouse polydipsia and diluted urine.

6.2.5. Levels of glucose in the plasma of fasting miRNA-155 KO and WT mice

Diabetes *mellitus* is characterised by a loss of function or decreased levels of the insulin hormone, which results in an increased concentration of the glucose in plasma (Aznar Rodríguez *et al.*, 2012). Mice were fasted for 8 h prior the collection of blood samples to ensure glucose differences were not affected by their food intake. Measurement of glucose levels in the plasma revealed that there were no significant differences between miRNA-155 KO and WT mice (Figure 6.4). Therefore, it was unlikely that these mice were suffering from diabetes *mellitus*.

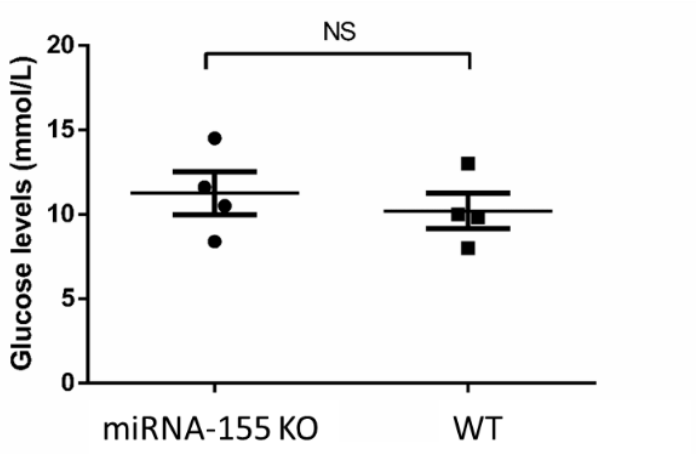

Figure 6.4. Glucose levels on miRNA-155 KO and WT mice after fasting. Quantification of glucose levels in blood of miRNA-155 KO and wild type (WT) mice after 8h of fasting. Data are shown as mean ± SEM, n = 4 of different mice. Differences were measured with unpaired two-tailed t-test. NS: no significant.

6.2.6. Effect of desmopressin challenge in miRNA-155 KO mice´s urine osmolality

Diabetes *insipidus* is the most frequent cause of water balance disorders. There are two different type of diabetes *insipidus,* which are classified either as central due to dysfunction of the hypothalamus and/or the pituitary gland, or as nephrogenic because of an ineffective response in the kidney to AVP (Robinson, 1976). To investigate whether either of these mechanisms may be contributing to the observed polydipsia, mice were first administrated with DAVP and the osmolality of urine collected 2 and 4h post-injection was compared to baseline values. In order to reduce the number of animals tested, this test was only carried on miRNA-155 KO mice. Measurement of urine osmolality of aged female miRNA-155 KO mice revealed a significant increase in osmolality after treatment with DDAVP (Figure 6.5). These results suggested that the kidneys were able to respond to DDAVP, hence, it is unlikely these mice were suffering from nephrogenic diabetes *insipidus*. Furthermore, urine osmolality of miRNA-155 KO

mice after DDAVP challenge was similar to previously reported urine osmolality of WT mice (between 1000 to 2000 (mosmol/kg)) (Roncal-Jimenez *et al.*, 2017).

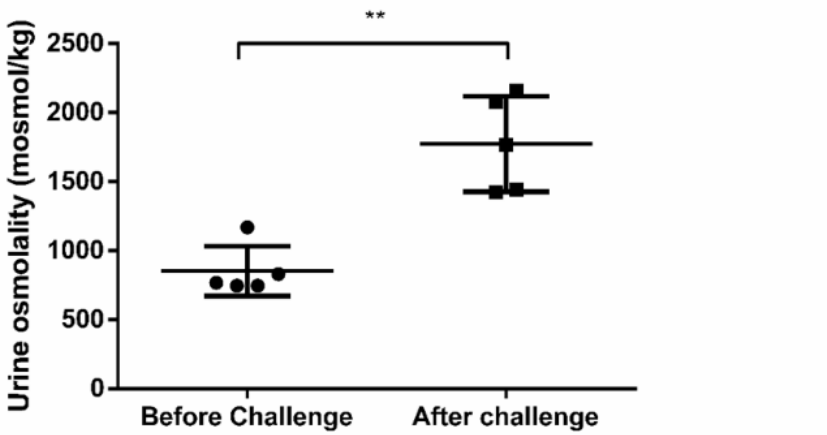

Figure 6.5. Urine osmolality of miRNA-155 KO mice after injection with desmopressin Quantification of the urine osmolality of miRNA-155 KO before and after they were challenged with a desmopressin compound (0.04 µg/Kg). Samples were collected 2 and 4h after injection and pulled together for analysis of urine osmolality. Data are shown as mean ± SEM, n = 5 of independent replicates and un-paired two-tailed t-test.

6.2.7. Levels of vasopressin in the hypothalamus and plasma between female miRNA-155 KO and WT mice

AVP is produced in response to thirst stimulus in the hypothalamus and then transported to the pituitary gland and AVP is stored at the posterior lobe of the pituitary gland (Ooi, Tawadros and Escalona, 2004). When levels of circulating AVP drop, this hormone is release into the bloodstream and AVP concentration is restored (Knepper, Kwon and Nielsen, 2015). Therefore, concentrations of AVP in the hypothalamus and/or plasma of female miRNA-155 KO and WT mice were measured.

RT-qPCR analysis of hypothalamic samples showed that relative expression of mRNA AVP was 1.1±0.2 in WT mice and 0.9±0.3 in miRNA-155 KO mice (P>0.05)

(Figure 6.5.A). Given that OXC and AVP are produced by similar neurons, OXC mRNA levels were also analysed. OXC mRNA levels were not changed between WT and miRNA-155 KO mice (WT = 1.1±0.2 vs. KO = 0.9±0.3 relative mRNA levels, *P*>0.05; n=5) (Figure 6.6.A). To determine whether the expression and localization of AVP protein was different between WT and KO mice, immunohistochemistry for AVP was carried out in the hypothalamus of fixed brain sections. Qualitative analysis of the staining showed no obvious differences in the number of positive neurons for AVP (Figure 6.6.B).

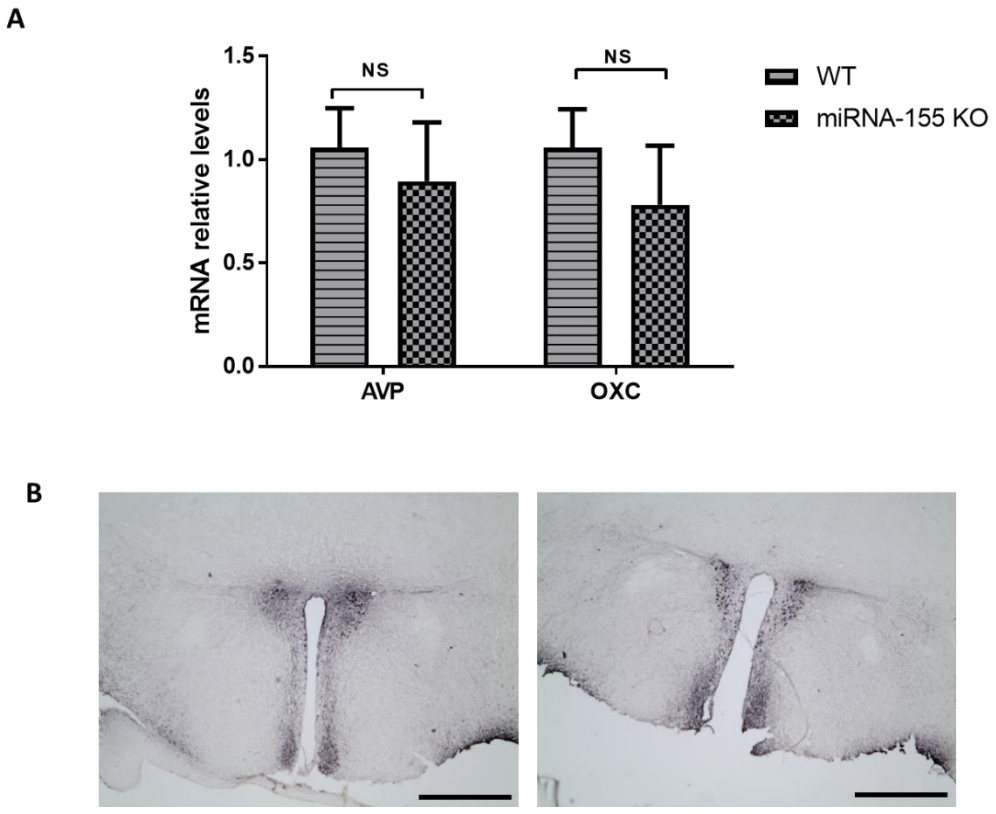

Figure 6.6. Vasopressin levels are not altered in the hypothalamus of miRNA-155 KO mice. (A) RT-qPCR analysis of vasopressin (AVP) and oxytocin (OXC) in hypothalamus samples isolated from miRNA-155 KO mice and wild type (WT) mice. Data are shown as mean±SEM, n=5 independent replicates, unpaired two-tailed t-test. **(B)** Immunohistochemistry images of DAB-staining for AVP in the hypothalamus of miRNA-155 KO (left) and WT (right) mice. N = 5 of different animals with different brain slice per animal.

Production of AVP can occur normally and still have reduced levels of AVP in the circulation. This might occur if the pituitary gland fails to secrete the AVP that is stored ready to be delivered into the circulation (Baribeau and Anagnostou, 2015). Therefore, plasma concentrations of AVP were measured by ELISA. In WT mice, AVP concentrations were 79.21±26.85 pg/ml whereas miRNA-155 KO mice showed 55.18±19.87 pg/ml of AVP in plasma (P>0.05; n=5) (Figure 6.7).

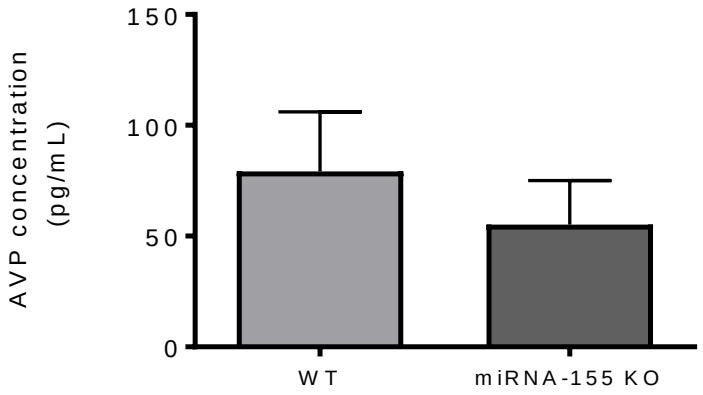

Figure 6.7. Levels of vasopressin in plasma are not changed between miRNA-155 KO and WT mice. ELISA measurement of soluble vasopressin (AVP) in plasma isolated from miRNA-155 KO and wild type (WT) mice. Data are shown as mean ± SEM, n=5 of independent replicates, unpaired two-tailed t-test.

Taken together, these results suggested that aged female miRNA-155 KO mice are unlikely to be suffering from central diabetes *insipidus*.

6.2.8. Levels of ion co-transporter NKCC2, NCC and WNK1 mRNA in renal tissue of miRNA-155 KO and WT mice.

Next, the expression of proteins involved in water transport in the kidney were analysed in female WT and miRNA-155 KO mice (Figure 6.8). Kidneys were extracted

and protein homogenates were produced from the renal cortex. Immunoblotting revealed (Figure 6.8.A) that levels of the Na-K-2Cl cotransporter (NKCC2) ion channel were significantly reduced in female miRNA-155 KO mice (WT= 1.00±0.14 and miRNA-155 KO = 0.44±0.08 protein band densitometry ratio, $P<0.01$; n=4), whereas, Na-2Cl cotransporter (NCC) ion channel appeared unaltered (WT=1±0.15 and miRNA-155 KO=1.44±0.31, P>0.05; n=4) (Figure 6.8.B).

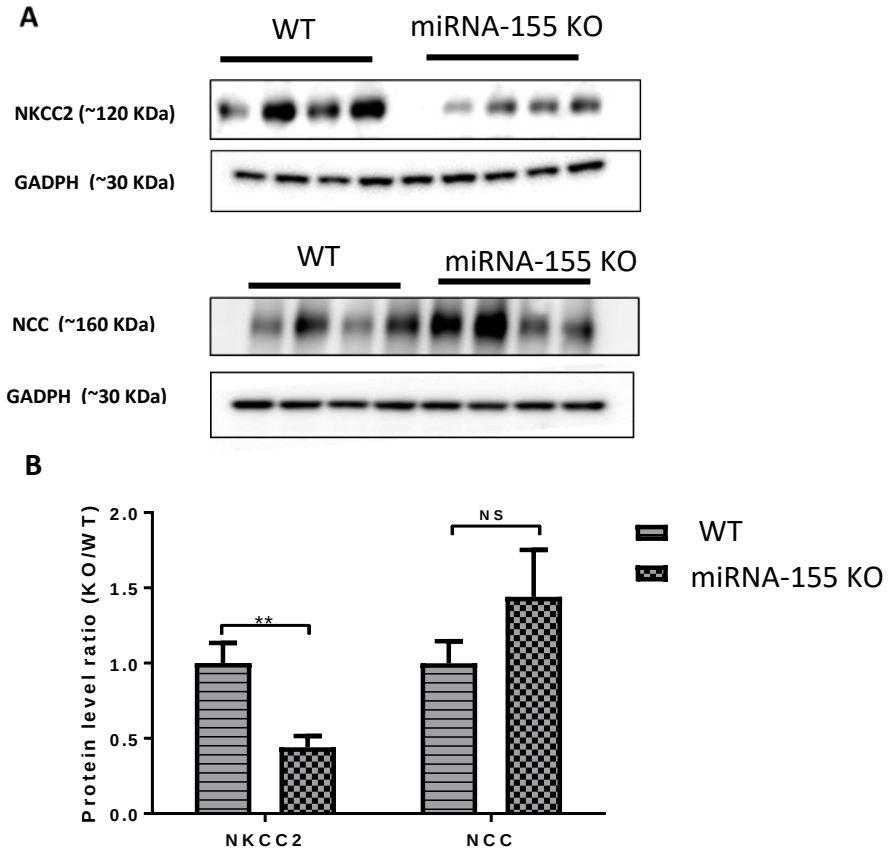

Figure 6.8. Levels of NKCC2 and NCC on cortical kidney. Cropped image of an immunoblot from samples isolated from the cortex of the kidney of female miRNA-155 KO (KO) or Wild Type (WT) mice. Antibodies used were against NKCC2, NCC and GADPH as internal control. (B) Quantification of protein expression on the immunoblot by band densitometry and normalized to expression of wildtype mice (WT). Data are shown as mean ± SEM, n = 4 of independent replicates, unpaired two-tailed t-test.

NKCC2 protein activity is regulated up-stream by a network of kinases and proteins that include WNK1 (Shekarabi *et al.*, 2017). As described in Chapter 5, WNK1 is a predicted target of murine-miRNA-155, hence, expression of kidney-specific WKN1 (which shares the same 3'UTR as the long-isoform WNK1) was studied. RT-qPCR analysis revealed that miRNA-155 KO mice expressed higher levels of WNK1 mRNA in the renal cortex than WT mice (1.96±0.07 relative levels to WT, $P<0.01$; n=4). Due to the inefficiency of tested antibodies to detect WNK1 (as described in Chapter 5), protein expression was not measured.

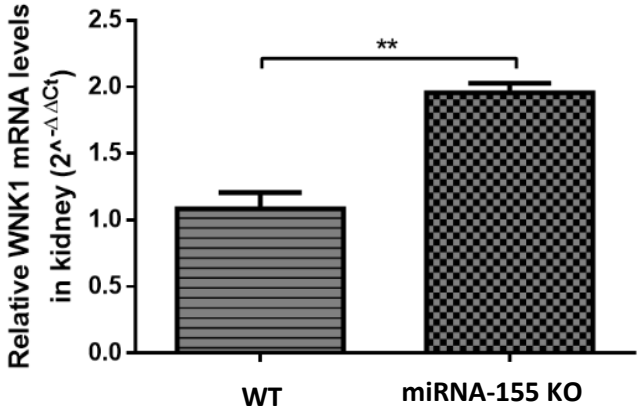

Figure 6.9. Levels of WNK1 mRNA in the cortex of the kidney of female mice. RT-qPCR analysis of WNK1 mRNA (kidney-specific variant) in the cortex from kidneys isolated from female miRNA-155 KO (KO) or wild type (WT) mice. B-actin mRNA was used a housekeeping gene. Data are shown as mean ± SEM, n = 4 independent replicates, unpaired two-tailed t-test.

6.2.9. Effect of cross-breeding miRNA-155 KO mice on water intake

The miRNA-155 KO mouse colony had been maintained in the facility for over 20 breeding cycles. Half way through the study, the colony presented difficulties in breeding, hence, miRNA-155 KO mice were backcrossed with the in-house WT strain C57Bl/6J mice. After three breeding cycles, an Open University (OU) line of

homozygous miRNA-155 KO mice was generated as confirmed by PCR (data not shown). The miRNA-155 OU KO mice were aged for 18 months and water intake was measured. Female miRNA-155 OU KO mice showed water intake of 3.5±0.6 ml of water per 25g body weight and WT mice drank 2.4±0.1 ml (P>0.05) (Figure 6.9). The new mouse line failed to replicate the phenotype observed in the original miRNA-155 KO mouse line (10.7±2.6 ml of water per body weight) (Figure 6.9). In light of the termination of the original breeding line and the discrepancy between the polydipsia in the original and OU KO strains, it was decided to conclude these phenotyping studies.

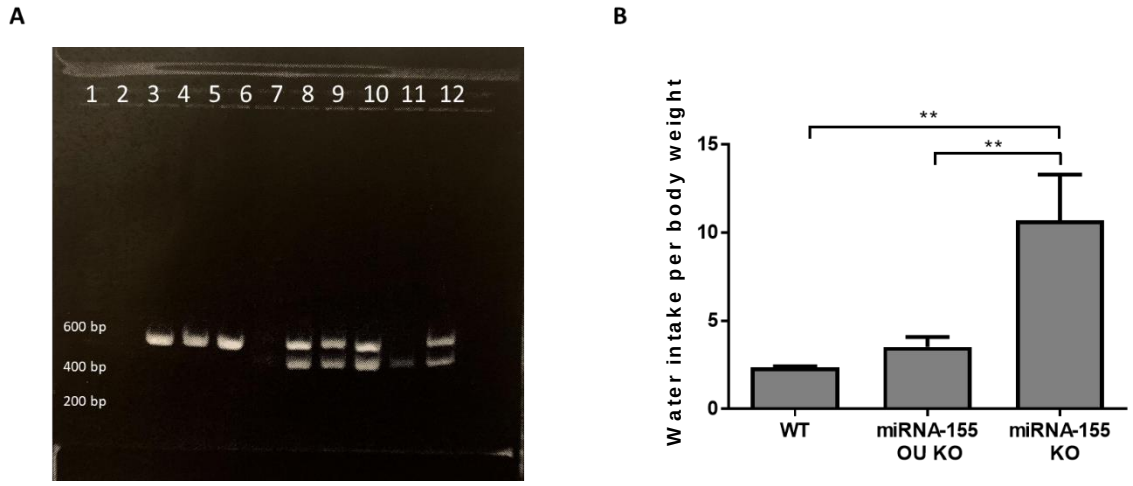

Figure 6.10. Water intake of miRNA-155 KO, WT and new-bred miRNA-155 KO mice. Wild type (WT) and miRNA-155 KO mice were crossed to generate a new miRNA-155 KO mouse line (miRNA-155 OU KO mice). **(A)** Example of genotyping gel for miRNA-155 OU KO homozygous (well 3,4, and 5), wild type (WT) (wells 7 and 11) and miRNA-155 OU KO heterozygous (wells 8, 9, 10 and 12). **(B)**. Mice (WT, miRNA-155 KO and miRNA-155 OU homozygous) were aged to 18 months and water intake was measured. Data are shown as mean±SEM and differences were asset by one-way anova with Tukey´s post-hoc for multiple comparison **P<0.01, n= 3 (WT), 4 (miRNA-155 OU KO) and 2 (miRNA-155 KO).

6.3. Discussion

In this chapter, a systematic longitudinal study of miRNA-155 KO mice identified and characterised the effect and the molecular mechanism underlying the polydipsia

observed on these mice. Phenotypically, female miRNA-155 KO mice suffered from polydipsia, diluted urine as well as low levels of sodium, potassium and osmolality in urine. Mechanistically, levels of NKCC2 were decreased whereas WNK1 mRNA was increased in these mice. However, the phenotype observed might be due to a cause unrelated to the deficiency of miRNA-155 because the resulting mouse line from miRNA-155 KO mice backcrossed with WT mice failed to manifest polydipsia.

6.3.1. Diagnosing female miRNA-155 KO mice underlying condition

As mentioned before, aged female miRNA-155 KO mice showed an increased water intake and lower urine specific gravity than their aged- and sex-matched WT mice. However, no differences in food intake and neither in body weight were found among all four studied groups.

A literature search was carried to identify the most likely pathologies underlying the observed phenotype. Based on the results obtained in this chapter, diabetes *mellitus* and both types of diabetes *insipidus* were unlikely to be the cause of the underlying female miRNA-155 KO mice´s polydipsia. Instead, these mice showed decreased levels of renal ion exchanger NKCC2 protein, which has been previously implicated in the kidney disorder, Bartter syndrome (Fulchiero and Seo-Mayer, 2019). Indeed, inactivating mutations in *NKCC2* are of clinical relevance in Bartter Syndrome type 1 (Jeck *et al.*, 2005). In mice, a recent study demonstrated that loss of NKCC2 activity led to Bartter-like phenotype, which included decreased levels of plasma K^+ and higher plasma pH (Rieg *et al.*, 2013). Interestingly, the serum analysis in this chapter showed a trend for down-regulated levels of serum K+ in the aged female miRNA-155 KO mice. It is fair to mention that this study was performed in only four different mice, whereas the differences

reported by Rieg and colleagues were observed in a cohort of 9-10 mice per group (Rieg *et al.*, 2013). Therefore, the analysis of an increased number of mice might help elucidate whether the levels of serum K^+ were changed in the aged female miRNA-155 KO mouse model. Furthermore, active reabsorption of NaCl by NKCC2 is a necessary step for the process of urine secretion mediated by nephrons (for a review see (Castrop and Schießl, 2014)). Therefore, defective NKCC2 is a crucial step in the polyuria observed in Bartter´s syndrome type 1. Indeed, deficiency of NKCC2 leads to severe polydipsia and short survival rate of mice (Takahashi *et al.*, 2000). These results suggested that the low expression of NKCC2 in the aged female miRNA-155 KO mice was likely to be responsible for the low concentrated urine, hence, the polydipsia too.

Many proteins are involved in the regulation of the expression and activity of NKCC2. Among these, WNK1 has been previously shown to control reabsorption of sodium in the kidney (Liu *et al.*, 2011). WNK1 has several isoforms, being a short one specifically expressed in the kidney together with the long (full) isoforms (Shekarabi *et al.*, 2017). Overexpression of kidney-specific WNK1 (KS-WNK1) was shown to decrease the expression and phosphorylation of NKCC2 (Liu *et al.*, 2011). In the current experiments, WNK1 mRNA was observed to be increased upon deletion of miRNA-155 in the kidney. However, confirmation of changes in WNK1 at the protein levels will still be needed to confirm the up-regulation of WNK1 by miRNA-155 deletion. As mentioned in Chapter 5, WNK1 is a predicted target of murine miRNA-155, therefore study of the miRNA-155/WNK1 mRNA binding would be necessary to validate this relationship. Interestingly, there are other proteins involved in NKCC2 activity (WNK3 and OSR) that were also predicted targets for mmu-miR-155-5p (as shown in TargetScan database, http://www.targetscan.org/mmu_72/ ; last accessed September 2020). So it could be

speculated that miRNA-155 might affect different key points in the signalling pathway to control ion cotransporters such as NKCC2 that will affect water balance.

The effect of either sex or age was not further characterised in this piece of work, however, it is possible to speculate the contribution of these factors to the observed phenotype. Regarding age, no study has previously investigated the aging of miRNA-155 KO mice in physiology. Only one study carried a systematic comparison of both young WT and miRNA-155 KO mice after 42 days post-weaning in normal healthy aging (Zhang *et al.*, 2017). According to the results in this piece of work, authors observed no significant differences across groups (body weight, serum chemistry, liver function etc) (Zhang *et al.*, 2017). The study of age-dependent polydipsia in STR/N mouse model suggested a possible degeneration of kidneys including enlarged kidneys, renal lesions or loss of renal medulla function (Kutscher and Miller, 1974). STR/N mice do not show alterations on the AVP gene and the genetic cause of polydipsia is still poorly understood (Chu *et al.*, 2015). Another report proposed that murine age-dependent polydipsia in STR/N mice might be caused due to reduced expression of renal AVP receptor, hence, affecting AQP2 levels (Tsumura *et al.*, 2006). It was suggested that humoral factors might be involved in the upstream regulation of these genes. Given that deletion of *nkcc2* is lethal (Takahashi *et al.*, 2000), it is possible to speculate that physiological changes in aging might contribute to the development of the effect of polydipsia.

Physiological data in this study showed that female miRNA-155 KO mice were affected to a greater extent by polydipsia than age-matched male miRNA-155 KO mice. It is possible to speculate that sex differences played a major role in the observed phenotype. These differences can include sex hormones such as testosterone and oestrogen. Indeed, oestrogen has previously shown to modulate body fluid in rodents (Somponpun, 2007). Oestrogen levels decrease with age in rodent (Gee, Flurkey and

Finch, 1983), hence, it might enhance the appearance of polydipsia in female aged miRNA-155 KO mice. Future analysis of sex hormones between miRNA-155 KO and WT mice would help to elucidate differences between these two models.

6.3.2. Loss of polydipsia phenotype in new miRNA-155 KO mouse line

MiRNA-155 KO mice was originally obtained from collaborators at Queen´s Mary in London. This strain was maintained in the facilities without any previous backcrossing with the in house WT mice. Following Jackson Lab guidelines (https://www.jax.org/) mice were kept inbred. As described above, lack of breeding in the miRNA-155 KO mice led to the generation of new miRNA-155 KO OU mice. Unfortunately, polydipsia was not observed in this new mouse line. Therefore, it is likely that the studied phenotype might have been caused by a miRNA-155-independent pathway and/or a combination of the loss of miR-155 with further genetic alterations There are previous reports of genetic drifts in inbred mouse lines that have been bred for a high number of breeding cycles (Brekke, Steele and Mulley, 2018). For instance, Cariappa and colleagues attributed a defect in B-cell development to the deficiency of Sialic acid acetyl esterase (Siae) gene in their genetic engineer mouse model (Cariappa *et al.*, 2009). However, authors realised that this phenotype was caused by an inherited mutation in the *dock2* gene. Indeed, *siae*-KO mice bred for 13 generations did not exhibit the attributed phenotype on defective B-cell development (Zeldovich, 2017). Regarding miRNA-155 KO mice, it is likely that an inherited mutation from the vendor mouse line was indeed the cause of the observed phenotype. It is also possible that accumulation of sporadic mutations has affected some of the key processes involved in water balance. The relationship between WNK1 and miRNA-155 in this chapter might be serendipity and

unrelated to the observed phenotype. However, a future comparative study might help to identify which genes differed among different mouse lines that were responsible for the underlying polydipsia and diluted urine. This future data might help to unravel and discover novel genes involved in water balance

Regardless the implications in water balance, this miRNA-155 KO mouse model has been previously used to study BBB function and miRNA biology. For this reason, both the miRNA-155 KO WT mouse models will be useful tool to translate some of the findings described in the previous chapters. Here there´s a list of experiments using these models.

For Chapter 3 and 4

Induce systemic inflammation (either with pro-inflammatory cytokines or LPS) on miRNA-155 KO and WT mice, then collect plasma and/or serum and isolate mouse-derived cytokine-sEVs. Subsequently, the following experiments are carried out:

a) Isolate RNA and measure miRNA-155, VCAM1 and ICAM1 mRNA expression by RT-qPCR to study whether plasma/serum-derived sEVs showed a pro-inflammatory profile similar to the one described in Chapter 6.
b) Treat mouse brain endothelial cells with plasma/serum-derived sEVs (either quiescent or cytokine-sEVs) and analyse both the induced effect on these cells by cell-based assay (e.g. T cell adhesion assays) and measuring molecular changes (expression of cytokine-sEV-induced miRNA and ICAM1/VCAM1 protein).
c) Similar experiment to b using miRNA-155 KO-derived sEVs will help to study the role of miRNA-155 in cytokine-sEV-induced BEC dysfunction.
d) After a, b and c experiments have been successfully carried out, WT mouse can be treated with plasma/serum-derived cytokine-sEVs and quiescent sEVs to analyse their impact on BBB function. Firstly, fluorescently-stained sEVs should

be injected (intracarotid injection preferably) to evaluate they reach BECs *in vivo*. BECs can be isolated from microvessels and fluorescent analysed by flow cytometry. Once this process is being optimised, expression of miRNA-155, VCAM1 and ICAM1 can be measured by RT-qPCR. Other markers of induced systemic inflammation will include immunocytochemistry for VCAM1/ICAM1 protein expression and microglia activation (e.g. Allograft inflammatory factor 1, iba1).

For Chapter 5:

Whether loss of miRNA-155 alters levels of WNK1 mRNA and/or protein in BECs *in vivo* can be studied with both miRNA-155 KO and WT mouse models. This analysis can be done both under naïve and inflamed conditions (treatment with LPS or pro-inflammatory cytokines). Then, analysis of WNK1 expression can be achieved by

a) RT-qPCR and western blot on BECs isolated from microvessels
b) Immunocytochemistry of WNK1 on brain slides with co-localisation with endothelial marker (e.g. PECAM).

CHAPTER 7: GENERAL DISCUSSION

Neuroinflammatory disorders are characterised by an activated BBB that facilitates the extravasation of immune cells into the brain thereby contributing to disease progression (Blanchette and Daneman, 2015). Recently, EVs have gained growing attention for their role in modulating the cellular status of the recipient cells in inflammation (Ciardiello *et al.*, 2016). However, little is known about the contribution of endothelial EVs to BBB function (Ramirez *et al.*, 2018). Therefore, the main aim of this thesis was to characterise EVs derived from BECs and investigate their impact on naïve BEC´s function in inflammation. Secondly, to identify whether miRNA-155 was relevant for EV function and study the mechanism by which miRNA-155 mediates leukocyte adhesion to brain endothelium as it has been previously described to modulate BBB function in inflammation (Cerutti *et al.*, 2016). In parallel, given the unexpected polydipsia developed by female miRNA-155 KO mice, a systematic study of the physiology and the molecular mechanism(s) underlying this phenotype was carried out.

The results described in this thesis have shown that:

1) Upon TNFα and IFNγ treatment, hCMEC/D3 cells secreted higher number of sEVs than L-EVs. These sEVs carried pro-inflammatory modulators such as VCAM1 and ICAM1 mRNA and miRNA-155.
2) Cytokine-sEVs led to decreased TEER and increased leukocyte adhesion to BECs. VCAM1, ICAM1 and miRNA-155 were also up-regulated in hCMEC/D3 cells upon stimulation with cytokine-sEVs
3) Quiescent sEVs had no effect on naïve BEC function. However, stimulation of inflamed BECs with quiescent sEVs decreased leukocyte adhesion to BECs.

4) WNK1 was identified as modulator of leukocyte adhesion to BECs. However, although it was a predicted target of miRNA-155, overexpression of miRNA-155 via pre-miRNA-155 transient transfection did not alter WNK1 mRNA nor protein levels in brain endothelium.
5) MiRNA-155 KO mice showed polydipsia and diluted urine as well as reduced NKCC2 levels and increased WNK1 mRNA level. However, the observed polydipsia was likely to be independent of the loss of miRNA-155.

7.1. sEVs modulate neurovascular function in inflammation

In recent years, there have been several reports suggesting that EVs play a role in modulating the immune response in physiology (Kalani, Tyagi and Tyagi, 2014) and pathology (Howitt and Hill, 2016; Kalluri, 2016). In particular, special attention has been given to the mechanisms by which EVs modulate inflammation in the CNS (Li *et al.*, 2018) and specifically, how they might affect cells of the NVU As described above, this work has advanced the understanding in the field of the BBB and how ECs communicate with each other by identifying a novel pathway of BEC dysfunction mediated by endothelial sEVs released from inflamed BECs (Figure 7.1). Specifically, this model contributes to the field of EV research in 1) investigating the specific effect of BEC-derived EVs on cerebrovascular function, 2) supporting the vision that endothelial EVs promote endothelial dysfunction in inflammation regardless of their vascular bed of origin and 3) improving the understanding of the molecular players involved in endothelial EV-induced cerebrovascular dysfunction. Ultimately, this working model sets the basis and rationale for future investigations of sEVs in models of neuroinflammation *in vivo* such as EAE.

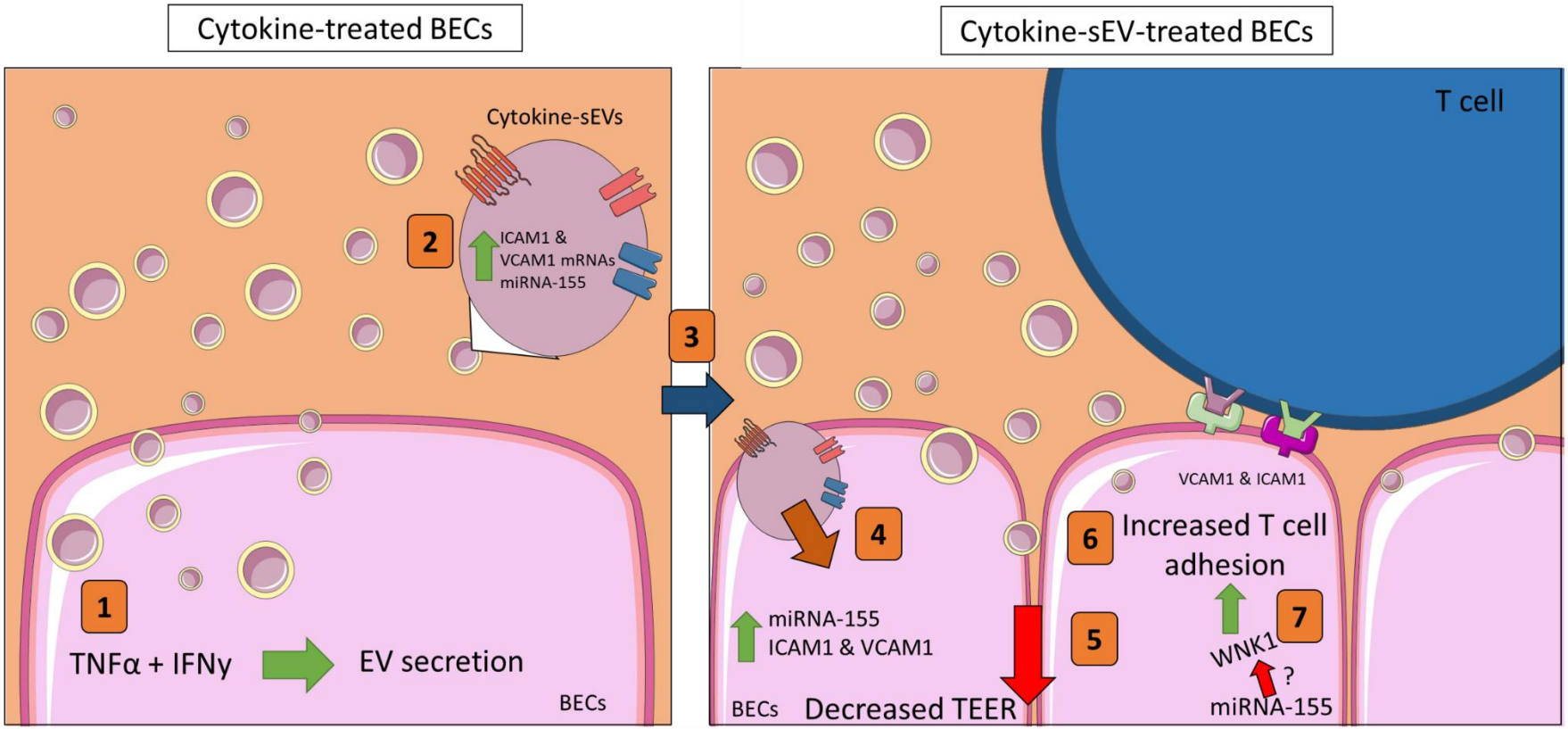

Figure 7.1. Summary of effect and mechanism of intercellular communication of brain endothelial cells via extracellular vesicles.1) hCMEC/D3 cells increase the secretion of sEVs (cytokine-sEVs) upon treatment with TNFα and IFNγ; 2) Cytokine-sEVs carry higher levels of ICAM1, VCAM1 mRNAs and miRNA-155 than quiescent sEVs; 3) Cytokine-sEVs can be taken up by naïve brain endothelial cells (BECs) and 4) increase the levels of miRNA-155, ICAM1, VCAM1 in the repicient cells; 4) Cytokine-sEVs reduce the value of TEER and 6) increased T cell adhesion to BECs; 7) deficiency of WNK1 increased T cell adhesion to BECs, however whether WNK1 is modulated by miRNA-155 and relevant to cytokine-sEV-induced vascular dysfunction is still unknown.

In the context of neuroinflammation, endothelial EVs have been previously shown to contribute to BBB dysfunction (for a review see (Ramirez *et al.*, 2018)). However, most of these studies focused on 1) the effect of endothelial EVs on immune cells and other cells of the CNS (Yamamoto *et al.*, 2015; Hosseinkhani *et al.*, 2018, 2020; Ramirez *et al.*, 2018) or 2) endothelial EVs from a heterogeneous mix of circulating endothelial EVs from the serum/plasma of patients with neuroinflammatory disorders (Marcos-Ramiro *et al.*, 2014; Ramirez *et al.*, 2018). Indeed, circulating endothelial EVs have been reported to promote vascular dysfunction in different neuroinflamamtory disorders and models including MS¡(Jy *et al.*, 2004; Marcos-Ramiro *et al.*, 2014). The results described in this piece of work highlighted how brain endothelial EVs also affected the function of naïve BECs. Hence, proposing EVs as a route to disseminate cytokine-like effects to not only immune cells but other naïve BECs as well. Indeed, cytokine-sEVs consistently induce BEC dysfunction as studied in Chapter 4. It is important to note that experiments in this study were carried out in an *in vitro* model of the BBB, hence, validation *in vivo* is necessary to confirm these findings. One possible experiment to demonstrate whether cytokine-sEVs promote endothelium activation would be the intracarotid delivery of cytokine-sEVs in mice and the analysis of their downstream impact in BEC function.

Cell-to-cell communication between BECs might be particular relevant in the context of neuroinflammatory disorders, where pro-inflammatory cytokines are increased in the circulation (Martins *et al.*, 2011) and known to modulate cerebrovascular function (Lopes Pinheiro *et al.*, 2016). Hence, release of cytokine-sEVs is enhanced but whether they are biologically functional or only a consequence of cell activation *in vivo* is still unknown. Data from Chapter 4 demonstrated that cytokine-sEVs were able to increase the effect of cytokine-loss of TEER, hence suggesting they might still be biologically functional even in the presence of pro-inflammatory cytokines in the blood. This working model is still

dependent on future *in vitro* (validation of the combined cytokine+cytokine-sEV effect on T cell adhesion and endothelial CAMs) and *in vivo* characterisation.

As mentioned above, endothelial EVs can promote endothelial dysfunction during inflammation. This has been previously reported to be the case in other endothelial beds (Table 7.1) (Letsiou and Bauer, 2018). Indeed, TNFα-treated HUVECs-derived EVs increased the expression of pro-inflammatory cell adhesion ICAM1, hence, increasing monocyte transmigration (Hosseinkhani *et al.*, 2018). Induction of a pro-inflammatory state by endothelial EVs has also been reported in pulmonary and aortic ECs (Curtis *et al.*, 2009; Liu *et al.*, 2017). Therefore, results from this piece of work contribute to the hypothesis that after an inflammatory stimulus, endothelial cells release EVs that can affect endothelial function in a similar way regardless of their vascular bed. This was already proposed by Ramirez *et al.* in an overview article on the field of EVs in the CNS (Ramirez *et al.*, 2018). Most studies analysing the impact of endothelial EVs on EC function have been performed with L-EVs. Therefore, the work described in Chapters 3 and 4 improves the field of research on sEVs modulating vascular function. Interestingly, it was noted that pro-inflammatory cytokines did not increase the number of L-EVs in Chapter 3. Given the broad literature on L-EVs (Table 7.1), it can be speculated that cytokine-L-EVs might still biologically functional despite their numbers not changing in inflammation. As described in Chapter 3, an increase in the larger percentile of cytokine-L-EVs was observed in comparison to quiescent L-EVs. It is possible that the pro-inflammatory stimulus induces the production of larger EVs without changing their total number but modulating their cargo as well. Hence, future analysis of the downstream impact of cytokine-L-EVs on endothelial function will help to elucidate their function in brain vasculature during inflammation.

Table 7.1. Summary of the impact of TNFα-induced endothelial EVs on EC function

Secreting cell type	Stimulus	Type of EVs	Receptor cells	Effect	Reference
HBMEC	TNFα + IFNγ	sEVs	HBMEC	Increased T cell adhesion, miRNA-155, ICAM1 and VCAM1 expression and decreased TEER	Chapter 4
HUVECS	TNFα	sEVs	HUVECs	Reduced tube formation, migration and increased apoptosis	(Li *et al.*, 2019)
HUVECS	TNFα	L-EVs	HUVECs	Induced expression of pro-apoptotic molecules, ICAM1 and monocyte adhesion	(Lee *et al.*, 2014)
HAEC	TNFα	L-EVs	HAEC	Pro-inflammatory activation towards release of sICAM1	(Curtis *et al.*, 2009)
HPMECs	TNFα	L-EVs	HPMECs	Pro-inflammatory activation of ECs via NF-KB pathway	(Liu *et al.*, 2017)

Abbreviations, HBMEC, human brain microvascular endothelial cells; HUVECs, human umbilical vein endothelial cells; HAEC, human aortic endothelial cells; HPMECs, human pulmonary microvascular endothelial cells; TNFα, tumour necrosis factor-α; IFNγ, interferon gamma; EV, extracellular vesicles; sEVs, small EVS; L-EVs, large EVs; ICAM1, intracellular cell adhesion molecule-1; VCAM1, vascular cell adhesion molecule 1; EC, endothelial cell.

Mechanistically, blocking of VCAM1 with neutralising antibodies significantly decreased cytokine-sEV-induced T cell adhesion whereas treatment with ICAM1 neutralising antibodies did not prevent this phenotype (Chapter 4). Ligands for both VCAM1 and ICAM1 (VLA-4 and LFA-1, respectively) have been shown to mediate arrest of T cell in CNS vessels in inflammation in EAE models using intravital microscopy (Rossi *et al.*, 2011). T cell migration into the CNS is a critical event in EAE and MS (Lopes Pinheiro *et al.*, 2016). Interestingly the effect of blocking VLA-4 with antibodies led to a reduction of the onset of EAE whereas blocking LFA-1 had a minor impact on the development of EAE (Rossi *et al.*, 2011). It is suggested that VLA-4/VCAM1 play a key role in the pathogenesis of EAE (Rossi *et al.*, 2011; Lopes Pinheiro *et al.*, 2016). Therefore, it is possible to speculate whether cytokine-sEVs might play an important role in VCAM-1-driven diseases such as EAE in mice or MS in humans.

The data produced in this work showed no changes into claudin-5 and occludin after stimulation with cytokine-sEVs. Therefore, it still remains unknown the mechanisms by which cytokine-sEVs affected TEER in BECs. Future transcriptomic and/or proteomic analysis of cytokine-sEV-treated BECs will be useful to dissect the mechanism of action involved. In parallel, staining of the main molecular players in endothelial cytoskeletal and TJ structure (such as ZO-1) would be beneficial to investigate the mechanism of action of sEVs on TEER.

Among the different miRNAs studied, miRNA-155 was the only miRNA up-regulated in the cargo of sEVs upon TNFα and IFNγ treatment (Chapter 3) and also after BECs were cultured with cytokine-sEVs (Chapter 4). MiRNA-155 levels have been widely described to be increased upon inflammation (O'Connell *et al.*, 2007), in neuroinflammatory disorders (Devier, Lovera and Lukiw, 2015; Pogue and Lukiw, 2018) as well as linked to the modulation of the immune response (Wu and Chen, 2016) and

BBB function in inflammation (Lopez-Ramirez *et al.*, 2014). Regarding the impact of sEVs-induced miRNA-155 on endothelial function, a small increase of expression of miRNA-155 was observed in the recipient BECs. However, the contribution of miRNA-155 on sEV-induced BEC dysfunction still remains unknown. Future experiments involving modulation of miRNA-155 both in secreting and acceptor cells will help to elucidate the contribution of miRNA-155 to the total outcome of sEVs-induced phenotype in BECs. Given the highly heterogenous composition of sEVs and the low abundance of miRNAs per vesicle (Sork *et al.*, 2018), it is very likely that miRNA-155 might only partially contribute to the total outcome of the sEV-activated phenotype and that other molecular players (such as the already identified VCAM1) might have an input in modulating the observed phenotypes on target cells. sEVs are a whole package of information rather than a single signalling molecule, hence, future transcriptomic analysis of sEVs will reveal the different players involved in the pathogenesis of sEV-induced endothelial dysfunction. This experiment would be especially useful to identify novel signature of miRNAs/mRNAs involved in sEV-induced BEC dysfunction.

On another note, how quiescent sEVs decreased the inflammatory effect of TNFα and IFNy in inducing leukocyte adhesion was described in this thesis (Chapter 4). This data are in accordance with the growing view that quiescent sEVs have a functional role in physiology (Isola and Chen, 2016). In the last years, researchers have reported that quiescent sEVs help to damp the inflammatory response (Njock, Cheng, *et al.*, 2015), promote cell regeneration (Dorronsoro and Robbins, 2013) and angiogenesis (Salomon *et al.*, 2013) or decrease ischemic injury (Lai *et al.*, 2010). Furthermore, there has been an increasing trend on studies evaluating the transfusion of blood from young donors to elderly individuals (Hofmann, 2018). This work has specially been characterised in mice where authors performed parabiosis procedure in a pair of young and old mice and

observed an improvement in restoring capability of muscle cells upon injury (Conboy *et al.*, 2005). However, this approach is being questioned and there is no evidence than transfusion of blood from young to old patients improves patient survival (Edgren *et al.*, 2017). Nevertheless, these data stress the physiological role of sEVs, which might contribute to balance inflammation in brain endothelium. Future experiments analysing the role of quiescent sEVs modulating cerebrovascular function in inflammation in depth as well as the molecular mechanism involved will help elucidate the likelihood of this type of quiescent sEVS as a therapeutic tool.

7.2. The interaction between miRNA-155 and WNK1 to modulate leukocyte adhesion to brain endothelium

MiRNA-155 negatively regulates BBB function (paracellular permeability and T cell adhesion) and is associated with neurological pathologies (Lopez-Ramirez *et al.*, 2014; Cerutti *et al.*, 2016). The mechanism by which miRNA-155 increased T cell adhesion to BECs is largely unknown. In this work, miRNA-155 was shown to modulate leukocyte adhesion to BECs and WNK1 was identified as a possible target for miRNA-155. However, overexpression of miRNA-155 by pre-miRNA-155 transient transfection did not affect the levels of WNK1. The most likely conclusion is that WNK1 expression is not modulated by miRNA-155. However, analysis of binding sites between miRNA-155 and WNK1 by luciferase assay and expression upon miRNA-155 inhibition might be useful to confirm this conclusion. There is still the unknown of the mechanism by which miRNA-155 modulates T cell adhesion to BECs. Future approaches could include a systematic analysis of the protein profile of hCMEC/D3 cells upon miRNA-155 modulation to identified novel candidates for modulators of leukocyte adhesion to BECs.

Although the results of this study suggested that miRNA-155 did not regulate WNK1 expression, WNK1 silencing led to increased T cell adhesion in brain endothelium. This is interesting because WNK1 function in endothelial cells is still largely unknown. Main focus of research has been given to the role of WNK1 in regulating angiogenesis and development. Conditioned deletion of endothelial *wnk1* in mice led to smaller and collapsed vessels in the heart embryo (Xie *et al.*, 2009). Endothelial WNK1 has also been linked to tumour cell proliferation and angiogenesis in hepatocarcinoma (Sie *et al.*, 2020). Here, it was shown a novel function where loss of WNK1 in BECs led to increased leukocyte adhesion. This in accordance to an earlier report where WNK1 was proposed to be a negative regulator of adhesion in leukocytes. In this report, the authors suggested that the WNK1-repression of leukocyte adhesion is mediated via RAP1-induced LFA-1 clustering (Köchl *et al.*, 2016). However, activation of endothelial RAP1 is known to inhibit the NFκB pathway, hence, leading to decreased levels of VCAM1 and ICAM1 (Ohmura *et al.*, 2017). Therefore, it is likely that the mechanism by which endothelial WNK1 modulates the leukocyte adhesion to BECs is RAP1-independent. Proteomic analysis of WNK1 partners and affected molecules will help to elucidate how WNK1 affect T cell adhesion. Identification of the molecular signalling by which WNK1 affects T cell adhesion on BECs will help to identify novel therapeutic targets to treat brain inflammation.

Here, WNK1 is proposed as a potential modulator of leukocyte adhesion to BECs. Whether WNK1 expression might be modulated by sEVs remains unknown. Preliminary screening showed that WNK1 mRNA levels were down-regulated upon stimulation of hCMEC/D3 cells with cytokine-sEVs (data not shown). For this reason, it is likely that WNK1 might contribute to the sEV-induced leukocyte adhesion (Figure 7.1). Future analysis of WNK1 expression as well as artificial overexpression of WNK1 upon sEV

treatment might help elucidate this pathway. However, future characterisation will also help to elucidate whether vesicular miRNA-155 affects sEV-induced T cell adhesion via down-regulation of WNK1 or other signalling proteins (Figure 7.1).

7.3. MiRNA-155 KO mouse model showing polydipsia as novel tool for the identification of new molecular players in the modulation of water balance

A systematic study on miRNA-155 KO mice revealed that female aged miRNA-155 KO mice developed polydipsia and presented more diluted urine (Chapter 6). Data suggested that these mice were not suffering from diabetes *insipidus* or diabetes *mellitus*. In fact, it was likely that phenotype was caused by a defect in kidney function. In this chapter, it was shown alterations at the levels of ion co-transporter, NKCC2, and its upstream regulator WNK1u. However, generation of new inbred miRNA-155 KO mouse line failed to replicate the observed phenotype. For this reason, it is likely that possibly both polydipsia and diluted urine observed in female aged miRNA-155 KO mice was caused by a miRNA-155 independent mechanism.

Although these mice showed Bartter-like phenotype, the onset of the pathology was observed at a latter age. Batter syndrome is characterised by the loss of function of NKCC2 which leads to early development of water balance problems such as polyuria (Fulchiero and Seo-Mayer, 2019). Hence, it is likely that the mechanism by which NKCC2 is affected in this mouse model differs from classical Bartter Syndrome. This is especially relevant since the phenotype was strongly observed in female mice rather male mice. Future analysis of RNA and/or DNA sequencing will help to reveal differences of expression and/or intrinsic mutation developed in this polydipsia animal line that might

explained the phenotype. Therefore, the tissue collected from this model might be useful for the identification of novel genes, mutation and/or allele variations that are involved in water balance. Changes in the composition and volume of body fluids are critical factors in physiology and especially in the aging population. Discovery of novel molecules or mutations that might enhance the development of these disorders with age is of utmost importance to improve the quality of life of the elderly.

REFRENCES

Abbott, N. J. (2002) ‘Astrocyte-endothelial interactions and blood-brain barrier permeability’, *Journal of Anatomy*, pp. 629–638. doi: 10.1046/j.1469-7580.2002.00064.x.

Abbott, N. J., Patabendige, Adjanie A K, *et al.* (2010) ‘Structure and function of the blood-brain barrier’, *Neurobiology of Disease*, pp. 13–25. doi: 10.1016/j.nbd.2009.07.030.

Abbott, N. J., Patabendige, Adjanie A.K., *et al.* (2010) ‘Structure and function of the blood–brain barrier’, *Neurobiology of Disease*, 37(1), pp. 13–25. doi: 10.1016/j.nbd.2009.07.030.

Abbott, N. J. *et al.* (2018) ‘The role of brain barriers in fluid movement in the CNS: is there a “glymphatic” system?’, *Acta Neuropathologica*, 135(3), pp. 387–407. doi: 10.1007/s00401-018-1812-4.

Abbott, N. J., Rönnbäck, L. and Hansson, E. (2006) ‘Astrocyte–endothelial interactions at the blood–brain barrier’, *Nature Reviews Neuroscience*, 7(1), pp. 41–53. doi: 10.1038/nrn1824.

Abdollahi-Roodsaz, S. *et al.* (2007) ‘Inhibition of toll-like receptor 4 breaks the inflammatory loop in autoimmune destructive arthritis’, *Arthritis and Rheumatism*. doi: 10.1002/art.22848.

Agrawal, S. *et al.* (2006) ‘Dystroglycan is selectively cleaved at the parenchymal basement membrane at sites of leukocyte extravasation in experimental autoimmune encephalomyelitis’, *The Journal of experimental medicine*. The Rockefeller University Press, 203(4), pp. 1007–1019. doi: 10.1084/jem.20051342.

Aird, W. C. (2007) ‘Phenotypic heterogeneity of the endothelium: II. Representative vascular beds’, *Circulation Research*, pp. 174–190. doi: 10.1161/01.RES.0000255690.03436.ae.

Alam, Q. *et al.* (2016) ‘Inflammatory Process in Alzheimer’s and Parkinson’s Diseases: Central Role of Cytokines’, *Current Pharmaceutical Design*. doi: 10.2174/1381612822666151125000300.

Alexander, M. *et al.* (2015) ‘Exosome-delivered microRNAs modulate the inflammatory response to endotoxin.’, *Nature communications*, 6, p. 7321. doi: 10.1038/ncomms8321.

Alexandrov, P. N. *et al.* (2012) ‘MicroRNA (miRNA) speciation in Alzheimer’s disease (AD) cerebrospinal fluid (CSF) and extracellular fluid (ECF)’, *International Journal of Biochemistry and Molecular Biology*.

Alexandrov, P. N. *et al.* (2019) ‘Lipopolysaccharide-stimulated, NF-kB-, miRNA-146a-And miRNA-155-mediated molecular-genetic communication between the human gastrointestinal tract microbiome and the brain’, *Folia Neuropathologica*. doi: 10.5114/fn.2019.88449.

Alexy, T. *et al.* (2014) ‘TNF-α alters the release and transfer of microparticle-encapsulated miRNAs from endothelial cells’, *Physiological Genomics*. Bethesda, MD: American Physiological Society, 46(22), pp. 833–840. doi: 10.1152/physiolgenomics.00079.2014.

Alt, C., Laschinger, M. and Engelhardt, B. (2002) ‘Functional expression of the lymphoid chemokines CCL19 (ECL) and CCL 21 (SLC) at the blood-brain barrier suggests their involvement in G-protein-dependent lymphocyte recruitment into the central nervous system during experimental autoimmune encephalomyeli’, *European*

Journal of Immunology. doi: 10.1002/1521-4141(200208)32:8<2133::AID-IMMU2133>3.0.CO;2-W.

Alvarez, J. I., Cayrol, R. and Prat, A. (2011) 'Disruption of central nervous system barriers in multiple sclerosis', *Biochimica et Biophysica Acta - Molecular Basis of Disease*. doi: 10.1016/j.bbadis.2010.06.017.

Anderson, H. C. (1969) 'Vesicles associated with calcification in the matrix of epiphyseal cartilage.', *Journal of Cell Biology*, 41(1), pp. 59–72. doi: 10.1083/jcb.41.1.59.

András, I. E. and Toborek, M. (2015) 'Extracellular vesicles of the blood-brain barrier.', *Tissue barriers*, 4(1), p. e1131804. doi: 10.1080/21688370.2015.1131804.

Anrather, J. and Iadecola, C. (2016) 'Inflammation and Stroke: An Overview', *Neurotherapeutics*. doi: 10.1007/s13311-016-0483-x.

Ardoin, S. P., Shanahan, J. C. and Pisetsky, D. S. (2007) 'The role of microparticles in inflammation and thrombosis', *Scandinavian Journal of Immunology*. doi: 10.1111/j.1365-3083.2007.01984.x.

Aznar Rodríguez, S. *et al.* (2012) 'Diabetes mellitus', *Medicine: Programa de Formación Médica Continuada Acreditado*, pp. 995–1002. Available at: https://dialnet.unirioja.es/servlet/articulo?codigo=4034166&info=resumen&idioma=SPA.

Bahbouhi, B. *et al.* (2009) 'Peripheral blood CD4+ T lymphocytes from multiple sclerosis patients are characterized by higher PSGL-1 expression and transmigration capacity across a human blood-brain barrier-derived endothelial cell line', *Journal of Leukocyte Biology*. doi: 10.1189/jlb.1008666.

Baj-Krzyworzeka, M. *et al.* (2002) ‘Platelet-derived microparticles stimulate proliferation, survival, adhesion, and chemotaxis of hematopoietic cells’, *Experimental Hematology*, 30(5), pp. 450–459. doi: 10.1016/S0301-472X(02)00791-9.

Baj-Krzyworzeka, M. *et al.* (2006) ‘Tumour-derived microvesicles carry several surface determinants and mRNA of tumour cells and transfer some of these determinants to monocytes’, *Cancer Immunol. Immunother*, 55, pp. 808–18.

van Balkom, B. W. M. *et al.* (2013) ‘Endothelial cells require miR-214 to secrete exosomes that suppress senescence and induce angiogenesis in human and mouse endothelial cells’, *Blood*, 121(19), pp. 3997 LP – 4006. doi: 10.1182/blood-2013-02-478925.

Ball, S. G. (2007) ‘Vasopressin and disorders of water balance: the physiology and pathophysiology of vasopressin.’, *Annals of clinical biochemistry*, 44(Pt 5), pp. 417–31. doi: 10.1258/000456307781646030.

Balusu, S. *et al.* (2016) ‘Identification of a novel mechanism of blood–brain communication during peripheral inflammation via choroid plexus-derived extracellular vesicles’, *EMBO Molecular Medicine*, 8(10), p. e201606271. doi: 10.15252/emmm.201606271.

Bamforth, S. D. *et al.* (1999) ‘A dominant mutant of occludin disrupts tight junction structure and function’, *Journal of Cell Science*.

Banizs, A. B. *et al.* (2018) ‘Endocytosis Pathways of Endothelial Cell Derived Exosomes’, *Molecular Pharmaceutics*. doi: 10.1021/acs.molpharmaceut.8b00765.

Baribeau, D. A. and Anagnostou, E. (2015) ‘Oxytocin and vasopressin: Linking pituitary neuropeptides and their receptors to social neurocircuits’, *Frontiers in*

Neuroscience. doi: 10.3389/fnins.2015.00335.

Barry, O. P. *et al.* (1998) 'Modulation of Monocyte – Endothelial Cell Interactions by Platelet Microparticles', *Journal of Clinical Investigation*, 102(1), pp. 136–144. doi: 10.1172/JCI2592.

Bartel, D. P. (2009) 'MicroRNAs: target recognition and regulatory functions', *Cell*. 2009/01/27, 136(2), pp. 215–233. doi: 10.1016/j.cell.2009.01.002.

Bartel, D. P. (2018) 'Metazoan MicroRNAs', *Cell*. doi: 10.1016/j.cell.2018.03.006.

Bartholomäus, I. *et al.* (2009) 'Effector T cell interactions with meningeal vascular structures in nascent autoimmune CNS lesions', *Nature*. doi: 10.1038/nature08478.

Battistini, L. (2003) 'CD8+ T cells from patients with acute multiple sclerosis display selective increase of adhesiveness in brain venules: a critical role for P-selectin glycoprotein ligand-1', *Blood*. doi: 10.1182/blood-2002-10-3309.

Bayraktar, R., Van Roosbroeck, K. and Calin, G. A. (2017) 'Cell-to-cell communication: microRNAs as hormones', *Molecular oncology*. 2017/10/26. John Wiley and Sons Inc., 11(12), pp. 1673–1686. doi: 10.1002/1878-0261.12144.

Bazzoni, G. *et al.* (2000) 'Homophilic interaction of junctional adhesion molecule', *Journal of Biological Chemistry*. doi: 10.1074/jbc.M003946200.

Begley, D. J. and Brightman, M. W. (2003) 'Structural and functional aspects of the blood-brain barrier', *Progress in Drug Research*. doi: 10.1007/978-3-0348-8049-7_2.

Bell, R. D. *et al.* (2010) 'Pericytes Control Key Neurovascular Functions and Neuronal Phenotype in the Adult Brain and during Brain Aging', *Neuron*. doi: 10.1016/j.neuron.2010.09.043.

Ben-Zvi, A. *et al.* (2014) 'Mfsd2a is critical for the formation and function of the blood-brain barrier', *Nature*. doi: 10.1038/nature13324.

Beninson, L. A. and Fleshner, M. (2015) 'Exosomes in fetal bovine serum dampen primary macrophage IL-1β response to lipopolysaccharide (LPS) challenge', *Immunology Letters*, 163(2), pp. 187–192. doi: https://doi.org/10.1016/j.imlet.2014.10.019.

Benz, E. and Moses, H. (1974) 'Small, virus-like particles detected in bovine sera by electron microscopy', *J Natl Cancer Inst*, 52, pp. 1931–4.

Berezikov, E. (2011) 'Evolution of microRNA diversity and regulation in animals.', *Nature reviews. Genetics*, 12(12), pp. 846–60. doi: 10.1038/nrg3079.

Bernstein, E. *et al.* (2001) 'Role for a bidentate ribonuclease in the initiation step of RNA interference', *Nature*. 2001/02/24, 409(6818), pp. 363–366. doi: 10.1038/35053110.

Beschorner, R. *et al.* (2009) 'Expression of EAAT-1 distinguishes choroid plexus tumors from normal and reactive choroid plexus epithelium', *Acta Neuropathologica*. doi: 10.1007/s00401-009-0519-y.

Bichet, D. G. (2006) '[Nephrogenic diabetes insipidus].', *Néphrologie & thérapeutique*, 2(6), pp. 387–404. doi: 10.1016/j.nephro.2006.07.010.

Blanchette, M. and Daneman, R. (2015) 'Formation and maintenance of the BBB', *Mechanisms of Development*, 138, pp. 8–16. doi: 10.1016/j.mod.2015.07.007.

Bobbie, M. W. *et al.* (2010) 'Reduced connexin 43 expression and its effect on the development of vascular lesions in retinas of diabetic mice', *Investigative Ophthalmology and Visual Science*. doi: 10.1167/iovs.09-4489.

Bohnsack, M. T., Czaplinski, K. and Gorlich, D. (2004) 'Exportin 5 is a RanGTP-dependent dsRNA-binding protein that mediates nuclear export of pre-miRNAs', *RNA*, 10(2), pp. 185–191. Available at: http://www.ncbi.nlm.nih.gov/pubmed/14730017.

Boyer, M. J. *et al.* (2020) 'Endothelial cell-derived extracellular vesicles alter vascular smooth muscle cell phenotype through high-mobility group box proteins', *Journal of Extracellular Vesicles*. doi: 10.1080/20013078.2020.1781427.

Brekke, T. D., Steele, K. A. and Mulley, J. F. (2018) 'Inbred or outbred? Genetic diversity in laboratory rodent colonies', *G3: Genes, Genomes, Genetics*. doi: 10.1534/g3.117.300495.

Broekaart, D. W. M. *et al.* (2020) 'Increased matrix metalloproteinases expression in tuberous sclerosis complex: modulation by microRNA 146a and 147b in vitro', *Neuropathology and Applied Neurobiology*. doi: 10.1111/nan.12572.

Brunet-Vega, A. *et al.* (2015) 'Variability in microRNA recovery from plasma: Comparison of five commercial kits', *Analytical Biochemistry*, 488, pp. 28–35. doi: https://doi.org/10.1016/j.ab.2015.07.018.

Buschmann, D. *et al.* (2018) 'Evaluation of serum extracellular vesicle isolation methods for profiling miRNAs by next-generation sequencing', *Journal of Extracellular Vesicles*. Taylor & Francis, 7(1), p. 1481321. doi: 10.1080/20013078.2018.1481321.

Cabezas, R. *et al.* (2014) 'Astrocytic modulation of blood brain barrier: perspectives on Parkinson's disease.', *Frontiers in cellular neuroscience*, 8(AUG), p. 211. doi: 10.3389/fncel.2014.00211.

Cao, R. *et al.* (2010) 'VEGFR1-mediated pericyte ablation links VEGF and PlGF to

cancer-associated retinopathy', *Proceedings of the National Academy of Sciences of the United States of America*, 107(2), pp. 856–861. doi: 10.1073/pnas.0911661107.

Cariappa, A. *et al.* (2009) 'B cell antigen receptor signal strength and peripheral B cell development are regulated by a 9-O-acetyl sialic acid esterase', *Journal of Experimental Medicine*. doi: 10.1084/jem.20081399.

Carthew, R W and Sontheimer, E. J. (2009) 'Origins and Mechanisms of miRNAs and siRNAs', *Cell*. 2009/02/26, 136(4), pp. 642–655. doi: 10.1016/j.cell.2009.01.035.

Carthew, Richard W. and Sontheimer, E. J. (2009) 'Origins and Mechanisms of miRNAs and siRNAs', *Cell*, pp. 642–655. doi: 10.1016/j.cell.2009.01.035.

Castrop, H. and Schießl, I. M. (2014) 'Physiology and pathophysiology of the renal Na-K-2Cl cotransporter (NKCC2)', *American Journal of Physiology - Renal Physiology*. doi: 10.1152/ajprenal.00432.2014.

Cayrol, R. *et al.* (2008) 'Activated leukocyte cell adhesion molecule promotes leukocyte trafficking into the central nervous system', *Nature Immunology*. doi: 10.1038/ni1551.

Cerutti, C. *et al.* (2016) 'MicroRNA-155 contributes to shear-resistant leukocyte adhesion to human brain endothelium in vitro', *Fluids Barriers CNS*. BioMed Central, 13(1), p. 8. doi: 10.1186/s12987-016-0032-3.

Cerutti, C. *et al.* (2017) 'MiR-126 and miR-126* regulate shear-resistant firm leukocyte adhesion to human brain endothelium', *Scientific Reports*. The Author(s), 7, p. 45284. Available at: http://dx.doi.org/10.1038/srep45284.

Chalovich, J. M. and Eisenberg, E. (2005) 'Th1 and Th17 Cells Regulate Innate Immune Responses and Bacterial Clearance during Central Nervous System Infection',

Biophysical Chemistry, 257(5), pp. 2432–2437. doi: 10.1016/j.immuni.2010.12.017.Two-stage.

Chargaff, E. and West, R. (1946) 'The biological significance of the thromboplastic protein of blood.', *J Biol Chem*, 166, pp. 189–97.

Chen, L. *et al.* (2017) 'Exosomal lncRNA GAS5 regulates the apoptosis of macrophages and vascular endothelial cells in atherosclerosis', *PLoS ONE*. doi: 10.1371/journal.pone.0185406.

Chen, Z. L. *et al.* (2013) 'Ablation of astrocytic laminin impairs vascular smooth muscle cell function and leads to hemorrhagic stroke', *Journal of Cell Biology*. doi: 10.1083/jcb.201212032.

Chen, Z. L. and Strickland, S. (1997) 'Neuronal death in the hippocampus is promoted by plasmin-catalyzed degradation of laminin', *Cell*. doi: 10.1016/S0092-8674(00)80483-3.

Cheng, C. Y. Y., Chu, J. Y. S. and Chow, B. K. C. (2009) 'Vasopressin-independent mechanisms in controlling water homeostasis', *Journal of Molecular Endocrinology*. doi: 10.1677/JME-08-0123.

Choo, K. B. *et al.* (2014) 'MicroRNA-5p and -3p co-expression and cross-targeting in colon cancer cells', *Journal of biomedical science*. BioMed Central, 21(1), p. 95. doi: 10.1186/s12929-014-0095-x.

Chu, C. P. *et al.* (2015) 'Alterations in the baroreceptor-heart rate reflex in conscious inbred polydipsic (STR/N) mice', *Physiological Research*. doi: 10.33549/physiolres.932820.

Ciardiello, C. *et al.* (2016) 'Focus on extracellular vesicles: New frontiers of cell-to-cell

communication in cancer', *International Journal of Molecular Sciences*, 17(2), pp. 1–17. doi: 10.3390/ijms17020175.

Cocucci, E., Racchetti, G. and Meldolesi, J. (2009) 'Shedding microvesicles: artefacts no more', *Trends in Cell Biology*, pp. 43–51. doi: 10.1016/j.tcb.2008.11.003.

Colombo, M., Raposo, G. and Théry, C. (2014) 'Biogenesis, Secretion, and Intercellular Interactions of Exosomes and Other Extracellular Vesicles', *Annu. Rev. Cell Dev. Biol*, 30(August), pp. 255–89. doi: 10.1146/annurev-cellbio-101512-122326.

Conboy, I. M. *et al.* (2005) 'Rejuvenation of aged progenitor cells by exposure to a young systemic environment', *Nature*. doi: 10.1038/nature03260.

Conde-Vancells, J. *et al.* (2008) 'Characterization and comprehensive proteome profiling of exosomes secreted by hepatocytes', *Journal of proteome research*, 7(12), pp. 5157–5166. Available at: https://www.ncbi.nlm.nih.gov/pubmed/19367702.

Cortes-Canteli, M. *et al.* (2010) 'Fibrinogen and β-Amyloid Association Alters Thrombosis and Fibrinolysis: A Possible Contributing Factor to Alzheimer's Disease', *Neuron*. doi: 10.1016/j.neuron.2010.05.014.

Cottrell, K. A., Szczesny, P. and Djuranovic, S. (2017) 'Translation efficiency is a determinant of the magnitude of miRNA-mediated repression', *Scientific reports*. Nature Publishing Group UK, 7(1), p. 14884. doi: 10.1038/s41598-017-13851-w.

Cramer, S. P. *et al.* (2015) 'Permeability of the blood-brain barrier predicts conversion from optic neuritis to multiple sclerosis', *Brain*. doi: 10.1093/brain/awv203.

Crawford, N. (1971) 'The Presence of Contractile Proteins in Platelet Microparticles Isolated from Human and Animal Platelet-free Plasma', *British Journal of Haematology*, 21(1), pp. 53–69. doi: 10.1111/j.1365-2141.1971.tb03416.x.

Crone, C. and Christensen, O. (1981) ‘Electrical resistance of a capillary endothelium’, *Journal of General Physiology*. doi: 10.1085/jgp.77.4.349.

Cui, N., Hu, M. and Khalil, R. A. (2017) ‘Biochemical and Biological Attributes of Matrix Metalloproteinases’, in *Progress in Molecular Biology and Translational Science*. doi: 10.1016/bs.pmbts.2017.02.005.

Cullen, K. M., Kócsi, Z. and Stone, J. (2005) ‘Pericapillary haem-rich deposits: Evidence for microhaemorrhages in aging human cerebral cortex’, *Journal of Cerebral Blood Flow and Metabolism*. doi: 10.1038/sj.jcbfm.9600155.

Curtis, A. M. *et al.* (2009) ‘p38 mitogen-activated protein kinase targets the production of proinflammatory endothelial microparticles’, *Journal of Thrombosis and Haemostasis*. doi: 10.1111/j.1538-7836.2009.03304.x.

Cvjetkovic, A., Lötvall, J. and Lässer, C. (2014) ‘The influence of rotor type and centrifugation time on the yield and purity of extracellular vesicles’, *Journal of Extracellular Vesicles*. Taylor & Francis, 3(1), p. 23111. doi: 10.3402/jev.v3.23111.

Daneman, R. (2012) ‘The blood-brain barrier in health and disease’, *Annals of Neurology*, 72(5), pp. 648–672. doi: 10.1002/ana.23648.

Dbouk, H. A. *et al.* (2014) ‘Actions of the protein kinase WNK1 on endothelial cells are differentially mediated by its substrate kinases OSR1 and SPAK’, *Proceedings of the National Academy of Sciences of the United States of America*. 2014/10/31. National Academy of Sciences, 111(45), pp. 15999–16004. doi: 10.1073/pnas.1419057111.

Deane, R. *et al.* (2004) ‘LRP/amyloid β-peptide interaction mediates differential brain efflux of Aβ isoforms’, *Neuron*. doi: 10.1016/j.neuron.2004.07.017.

Van Deun, J. *et al.* (2014) ‘The impact of disparate isolation methods for extracellular

vesicles on downstream RNA profiling.', *Journal of extracellular vesicles*, 3, pp. 1–14. doi: 10.3402/jev.v3.24858.

Devaux, P. F. *et al.* (2008) 'How lipid flippases can modulate membrane structure', *Biochimica et Biophysica Acta - Biomembranes*, pp. 1591–1600. doi: 10.1016/j.bbamem.2008.03.007.

Devier, D. J., Lovera, J. F. and Lukiw, W. J. (2015) 'Increase in NF-κB-sensitive miRNA-146a and miRNA-155 in multiple sclerosis (MS) and pro-inflammatory neurodegeneration', *Frontiers in Molecular Neuroscience*. doi: 10.3389/fnmol.2015.00005.

Djebali, S. *et al.* (2012) 'Landscape of transcription in human cells', *Nature*. doi: 10.1038/nature11233.

Dorronsoro, A. and Robbins, P. D. (2013) 'Regenerating the injured kidney with human umbilical cord mesenchymal stem cell-derived exosomes', *Stem Cell Research and Therapy*. doi: 10.1186/scrt187.

Dozio, V. and Sanchez, J.-C. (2017) 'Characterisation of extracellular vesicle-subsets derived from brain endothelial cells and analysis of their protein cargo modulation after TNF exposure', *Journal of Extracellular Vesicles*. Taylor & Francis, 6(1), p. 1302705. doi: 10.1080/20013078.2017.1302705.

DuPont, J. J. *et al.* (2016) 'Vascular mineralocorticoid receptor regulates microRNA-155 to promote vasoconstriction and rising blood pressure with aging', *JCI Insight*, 1(14), pp. 1–17. doi: 10.1172/jci.insight.88942.

Durak-Kozica, M. *et al.* (2018) '3D visualization of extracellular vesicle uptake by endothelial cells', *Cellular and Molecular Biology Letters*. doi: 10.1186/s11658-018-

0123-z.

Edgren, G. *et al.* (2017) 'Association of donor age and sex with survival of patients receiving transfusions', *JAMA Internal Medicine*. doi: 10.1001/jamainternmed.2017.0890.

Ehrlich, P. (1885) *Das Sauerstoff-Bedürfniss des Organismus: eine farbenanalytische Studie, Hirschwald, Berlin*. doi: 10.1038/nbt0797-647.

Elton, T. S. *et al.* (2013) 'Regulation of the MIR155 host gene in physiological and pathological processes', *Gene*. doi: 10.1016/j.gene.2012.12.009.

Elton, T. S., Sansom, S. E. and Martin, M. M. (2010) 'Trisomy-21 gene dosage overexpression of miRNAs results in the haploinsufficiency of specific target proteins', *RNA Biology*. doi: 10.4161/rna.7.5.12685.

Enerson, B. E. and Drewes, L. R. (2006) 'The rat blood-brain barrier transcriptome', *Journal of Cerebral Blood Flow and Metabolism*. doi: 10.1038/sj.jcbfm.9600249.

Engelhardt, B. and Ransohoff, R. M. (2012) 'Capture, crawl, cross: The T cell code to breach the blood-brain barriers', *Trends in Immunology*. doi: 10.1016/j.it.2012.07.004.

Faraoni, I. *et al.* (2009) 'miR-155 gene: A typical multifunctional microRNA', *Biochimica et Biophysica Acta - Molecular Basis of Disease*. Elsevier B.V., 1792(6), pp. 497–505. doi: 10.1016/j.bbadis.2009.02.013.

Fernández-Klett, F. *et al.* (2010) 'Pericytes in capillaries are contractile in vivo, but arterioles mediate functional hyperemia in the mouse brain', *Proceedings of the National Academy of Sciences of the United States of America*. doi: 10.1073/pnas.1011321108.

Ferrer, I. and Vidal, N. (2018) 'Neuropathology of cerebrovascular diseases', in

Handbook of Clinical Neurology. doi: 10.1016/B978-0-12-802395-2.00007-9.

Filipowicz, W., Bhattacharyya, S. N. and Sonenberg, N. (2008) 'Mechanisms of post-transcriptional regulation by microRNAs: are the answers in sight?', *Nat Rev Genet*. 2008/01/17, 9(2), pp. 102–114. doi: 10.1038/nrg2290.

Friedman, J. M. and Jones, P. A. (2009) 'MicroRNAs: critical mediators of differentiation, development and disease', *Swiss Med Wkly*. 2009/08/26, 139(33–34), pp. 466–472. doi: smw-12794.

Friedman, R. C. *et al.* (2009) 'Most mammalian mRNAs are conserved targets of microRNAs', *Genome Res*. 2008/10/29, 19(1), pp. 92–105. doi: 10.1101/gr.082701.108.

Fulchiero, R. and Seo-Mayer, P. (2019) 'Bartter Syndrome and Gitelman Syndrome', *Pediatric Clinics of North America*, 66(1), pp. 121–134. doi: https://doi.org/10.1016/j.pcl.2018.08.010.

Gaengel, K. *et al.* (2009) 'Endothelial-mural cell signaling in vascular development and angiogenesis', *Arteriosclerosis, Thrombosis, and Vascular Biology*. doi: 10.1161/ATVBAHA.107.161521.

Gámez-Valero, A. *et al.* (2016) 'Size-Exclusion Chromatography-based isolation minimally alters Extracellular Vesicles' characteristics compared to precipitating agents', *Scientific reports*. Nature Publishing Group, 6, p. 33641. doi: 10.1038/srep33641.

Gao, W. *et al.* (2016) 'Exosomes derived from mature dendritic cells increase endothelial inflammation and atherosclerosis via membrane TNF-α mediated NF-κB pathway', *Journal of Cellular and Molecular Medicine*. doi: 10.1111/jcmm.12923.

Garavelli, S., De Rosa, V. and de Candia, P. (2018) 'The Multifaceted Interface

Between Cytokines and microRNAs: An Ancient Mechanism to Regulate the Good and the Bad of Inflammation', *Frontiers in Immunology*. Frontiers Media S.A., 9, p. 3012. doi: 10.3389/fimmu.2018.03012.

García-Romero, N. *et al.* (2019) 'Polyethylene glycol improves current methods for circulating extracellular vesicle-derived DNA isolation', *Journal of Translational Medicine*, 17(1), p. 75. doi: 10.1186/s12967-019-1825-3.

Gardiner, C., Di Vizio, D., *et al.* (2016) 'Techniques used for the isolation and characterization of extracellular vesicles: results of a worldwide survey', *Journal of extracellular vesicles*. Co-Action Publishing, 5, p. 32945. doi: 10.3402/jev.v5.32945.

Gardiner, C., Vizio, D. Di, *et al.* (2016) 'Techniques used for the isolation and characterization of extracellular vesicles: results of a worldwide survey ′', 1, pp. 1–6. doi: 10.3402/jev.v5.32945.

Gasser, O. and Schifferli, J. A. (2004) 'Activated polymorphonuclear neutrophils disseminate anti-inflammatory microparticles by ectocytosis', *Blood*, 104(8), pp. 2543–2548. doi: 10.1182/blood-2004-01-0361.

Gatto, G. *et al.* (2008) 'Epstein-Barr virus latent membrane protein 1 trans-activates miR-155 transcription through the NF-κB pathway', *Nucleic Acids Research*, 36(20), pp. 6608–6619. doi: 10.1093/nar/gkn666.

Gazzin, S. *et al.* (2008) 'Differential expression of the multidrug resistance-related proteins ABCb1 and ABCc1 between blood-brain interfaces', *Journal of Comparative Neurology*. doi: 10.1002/cne.21808.

Gee, D. M., Flurkey, K. and Finch, C. E. (1983) 'Aging and the regulation of luteinizing hormone in C57BL/6J mice: Impaired elevations after ovariectomy and spontaneous

elevations at advanced ages', *Biology of Reproduction*. doi: 10.1095/biolreprod28.3.598.

Geis-Asteggiante, L. *et al.* (2018) 'Differential Content of Proteins, mRNAs, and miRNAs Suggests that MDSC and Their Exosomes May Mediate Distinct Immune Suppressive Functions', *Journal of proteome research*. 2017/11/27, 17(1), pp. 486–498. doi: 10.1021/acs.jproteome.7b00646.

Gheinani, A. H. *et al.* (2018) 'Improved isolation strategies to increase the yield and purity of human urinary exosomes for biomarker discovery', *Scientific Reports*, 8(1), p. 3945. doi: 10.1038/s41598-018-22142-x.

Giaever, I. and Keese, C. R. (1991) 'Micromotion of mammalian cells measured electrically', *Proceedings of the National Academy of Sciences of the United States of America*. doi: 10.1073/pnas.88.17.7896.

Goldmann, E. (1913) 'Vitalfaerbung am Zentralnervensystem', *Abh Preuss Akd Wiss Phys Math*.

Goldmann, E. E. (1909) 'Die a¨ ussere und innere Sekretion des gesunden und kranken Organismus im Lichte der "vitalen Farbung".', *Beitr. klin. Chir.* doi: 10.1016/S0167-7012(03)00030-7.

Graves, P. and Zeng, Y. (2012) 'Biogenesis of mammalian microRNAs: a global view', *Genomics Proteomics Bioinformatics*. 2012/12/04, 10(5), pp. 239–245. doi: 10.1016/j.gpb.2012.06.004.

Gray, M. T. and Woulfe, J. M. (2015) 'Striatal blood-brain barrier permeability in Parkinson's disease', *Journal of Cerebral Blood Flow and Metabolism*. doi: 10.1038/jcbfm.2015.32.

Greenwood, J. *et al.* (2011) ‘Review: leucocyte-endothelial cell crosstalk at the blood-brain barrier: a prerequisite for successful immune cell entry to the brain’, *Neuropathol Appl Neurobiol*. 2010/10/16, 37(1), pp. 24–39. doi: 10.1111/j.1365-2990.2010.01140.x.

Gregory, R. I. *et al.* (2004) ‘The Microprocessor complex mediates the genesis of microRNAs’, *Nature*. 2004/11/09, 432(7014), pp. 235–240. doi: 10.1038/nature03120.

Griffiths-Jones, S. *et al.* (2006) ‘miRBase: microRNA sequences, targets and gene nomenclature’, *Nucleic Acids Research* , 34(suppl 1), pp. D140–D144. doi: 10.1093/nar/gkj112.

Han, J. *et al.* (2004) ‘The Drosha-DGCR8 complex in primary microRNA processing’, *Genes Dev*. 2004/12/03, 18(24), pp. 3016–3027. doi: 10.1101/gad.1262504.

Haqqani, A. S. *et al.* (2013) ‘Method for isolation and molecular characterization of extracellular microvesicles released from brain endothelial cells.’, *Fluids and barriers of the CNS*, 10(1), p. 4. doi: 10.1186/2045-8118-10-4.

Harding, C., Heuser, J. and Stahl, P. (1983) ‘Receptor-mediated endocytosis of transferrin and recycling of the transferrin receptor in rat reticulocytes.’, *Journal of Cell Biology*, 97(2), pp. 329–339. doi: 10.1083/jcb.97.2.329.

Harris, T. A. *et al.* (2008) ‘MicroRNA-126 regulates endothelial expression of vascular cell adhesion molecule 1’, *Proc Natl Acad Sci U S A*. 2008/01/30, 105(5), pp. 1516–1521. doi: 10.1073/pnas.0707493105.

Hayashi, Y. *et al.* (1997) ‘Induction of various blood-brain barrier properties in non-neural endothelial cells by close apposition to co-cultured astrocytes’, *GLIA*. doi: 10.1002/(SICI)1098-1136(199701)19:1<13::AID-GLIA2>3.0.CO;2-B.

He, L. *et al.* (2018) ‘Data descriptor: Single-cell RNA sequencing of mouse brain and

lung vascular and vessel-associated cell types', *Scientific Data*. doi: 10.1038/sdata.2018.160.

Helwa, I. *et al.* (2017) 'A Comparative Study of Serum Exosome Isolation Using Differential Ultracentrifugation and Three Commercial Reagents', *PloS one*. Public Library of Science, 12(1), pp. e0170628–e0170628. doi: 10.1371/journal.pone.0170628.

Hofmann, B. (2018) 'Young Blood Rejuvenates Old Bodies: A Call for Reflection when Moving from Mice to Men', *Transfusion Medicine and Hemotherapy*. doi: 10.1159/000481828.

Horwood, N. and Davies, D. C. (1994) 'Immunolabelling of hippocampal microvessel glucose transporter protein is reduced in Alzheimer's disease', *Virchows Archiv*. doi: 10.1007/BF00193951.

Hosseinkhani, B. *et al.* (2018) 'Extracellular Vesicles Work as a Functional Inflammatory Mediator Between Vascular Endothelial Cells and Immune Cells', *Frontiers in Immunology*. Frontiers Media S.A., 9, p. 1789. doi: 10.3389/fimmu.2018.01789.

Hosseinkhani, B. *et al.* (2020) '(Sub)populations of extracellular vesicles released by TNF-α –triggered human endothelial cells promote vascular inflammation and monocyte migration', *Journal of Extracellular Vesicles*. doi: 10.1080/20013078.2020.1801153.

Howitt, J. and Hill, A. F. (2016) 'Exosomes in the pathology of neurodegenerative diseases', *Journal of Biological Chemistry*. doi: 10.1074/jbc.R116.757955.

Iadecola, C. (2017) 'The Neurovascular Unit Coming of Age: A Journey through Neurovascular Coupling in Health and Disease', *Neuron*. doi:

10.1016/j.neuron.2017.07.030.

Igarashi, Y. *et al.* (1999) 'Glial cell line-derived neurotrophic factor induces barrier function of endothelial cells forming the blood-brain barrier', *Biochemical and Biophysical Research Communications*. doi: 10.1006/bbrc.1999.0992.

Isola, A. and Chen, S. (2016) 'Exosomes: The Messengers of Health and Disease', *Current Neuropharmacology*. doi: 10.2174/1570159x14666160825160421.

Jabri, E. (2005) 'P-bodies take a RISC', *Nature Structural & Molecular Biology*, 12(7), p. 564. doi: 10.1038/nsmb0705-564.

Janas, A. M. *et al.* (2016) 'Exosomes and other extracellular vesicles in neural cells and neurodegenerative diseases', *Biochimica et Biophysica Acta - Biomembranes*. Elsevier B.V., 1858(6), pp. 1139–1151. doi: 10.1016/j.bbamem.2016.02.011.

Janzer, R. C. and Raff, M. C. (1987) 'Astrocytes induce blood-brain barrier properties in endothelial cells', *Nature*. doi: 10.1038/325253a0.

Jeck, N. *et al.* (2005) 'Salt handling in the distal nephron: Lessons learned from inherited human disorders', *American Journal of Physiology - Regulatory Integrative and Comparative Physiology*. doi: 10.1152/ajpregu.00600.2004.

Jiang, X. *et al.* (2018) 'Blood-brain barrier dysfunction and recovery after ischemic stroke', *Progress in Neurobiology*. doi: 10.1016/j.pneurobio.2017.10.001.

Johnstone, R. M. *et al.* (1987) 'Vesicle formation during reticulocyte maturation. Association of plasma membrane activities with released vesicles (exosomes).', *Journal of Biological Chemistry*, 262(19), pp. 9412–9420. doi: 10.1016/j.biocel.2011.10.005.

de Jong, O. G. *et al.* (2012) 'Cellular stress conditions are reflected in the protein and RNA content of endothelial cell-derived exosomes', *Journal of Extracellular Vesicles*.

Taylor & Francis, 1(1), p. 18396. doi: 10.3402/jev.v1i0.18396.

Junker, A. *et al.* (2009) 'MicroRNA profiling of multiple sclerosis lesions identifies modulators of the regulatory protein CD47', *Brain*, 132(12), pp. 3342–3352. doi: 10.1093/brain/awp300.

Jy, W. *et al.* (2004) 'Endothelial microparticles (EMP) bind and activate monocytes: elevated EMP-monocyte conjugates in multiple sclerosis.', *Frontiers in bioscience : a journal and virtual library*. doi: 10.2741/1466.

Kalani, A., Tyagi, A. and Tyagi, N. (2014) 'Exosomes: Mediators of neurodegeneration, neuroprotection and therapeutics', *Molecular Neurobiology*, 49(1), pp. 590–600. doi: 10.1007/s12035-013-8544-1.

Kalaria, R. N. (2018) 'The pathology and pathophysiology of vascular dementia', *Neuropharmacology*. doi: 10.1016/j.neuropharm.2017.12.030.

Kalluri, R. (2016) 'The biology and function of exosomes in cancer', *Journal of Clinical Investigation*. doi: 10.1172/JCI81135.

Kalra, H., Drummen, G. P. C. and Mathivanan, S. (2016) 'Focus on extracellular vesicles: Introducing the next small big thing', *International Journal of Molecular Sciences*, 17(2). doi: 10.3390/ijms17020170.

Kasashima, K., Nakamura, Y. and Kozu, T. (2004) 'Altered expression profiles of microRNAs during TPA-induced differentiation of HL-60 cells', *Biochemical and Biophysical Research Communications*. doi: 10.1016/j.bbrc.2004.07.130.

Keaney, J. and Campbell, M. (2015) 'The dynamic blood-brain barrier', *FEBS Journal*, 282(21), pp. 4067–4079. doi: 10.1111/febs.13412.

Keshtkar, S., Azarpira, N. and Ghahremani, M. H. (2018) 'Mesenchymal stem cell-

derived extracellular vesicles: Novel frontiers in regenerative medicine', *Stem Cell Research and Therapy*. doi: 10.1186/s13287-018-0791-7.

Kim, V. N. (2004) 'MicroRNA precursors in motion: Exportin-5 mediates their nuclear export', *Trends in Cell Biology*, pp. 156–159. doi: 10.1016/j.tcb.2004.02.006.

Kirk, J. *et al.* (2003) 'Tight junctional abnormality in multiple sclerosis white matter affects all calibres of vessel and is associated with blood-brain barrier leakage and active demyelination', *Journal of Pathology*. doi: 10.1002/path.1434.

Knepper, M. a, Kwon, T.-H. and Nielsen, S. (2015) 'Molecular Physiology of Water Balance.', *The New England journal of medicine*, 372(14), pp. 1349–1358. doi: 10.1056/NEJMra1404726.

Knowland, D. *et al.* (2014) 'Stepwise Recruitment of Transcellular and Paracellular Pathways Underlies Blood-Brain Barrier Breakdown in Stroke', *Neuron*. doi: 10.1016/j.neuron.2014.03.003.

Köchl, R. *et al.* (2016) 'WNK1 kinase balances T cell adhesion versus migration in vivo', *Nature immunology*. 2016/07/11, 17(9), pp. 1075–1083. doi: 10.1038/ni.3495.

Kolowos, W. *et al.* (2005) 'Microparticles Shed from Different Antigen-Presenting Cells Display an Individual Pattern of Surface Molecules and a Distinct Potential of Allogeneic T-Cell Activation', *Scandinavian Journal of Immunology*. John Wiley & Sons, Ltd (10.1111), 61(3), pp. 226–233. doi: 10.1111/j.1365-3083.2005.01551.x.

Korotkov, A. *et al.* (2018) 'Increased expression of matrix metalloproteinase 3 can be attenuated by inhibition of microRNA-155 in cultured human astrocytes', *Journal of Neuroinflammation*. doi: 10.1186/s12974-018-1245-y.

Kozomara, A., Birgaoanu, M. and Griffiths-Jones, S. (2019) 'MiRBase: From

microRNA sequences to function', *Nucleic Acids Research*. doi: 10.1093/nar/gky1141.

Kurachi, M., Mikuni, M. and Ishizaki, Y. (2016) 'Extracellular vesicles from vascular endothelial cells promote survival, proliferation and motility of oligodendrocyte precursor cells', *PLoS ONE*. doi: 10.1371/journal.pone.0159158.

Kutscher, C. L. and Miller, D. G. (1974) 'Age-dependent polydipsia in the SWR/J mouse', *Physiology and Behavior*. doi: 10.1016/0031-9384(74)90308-4.

Lagos-Quintana, M. *et al.* (2001) 'Identification of novel genes coding for small expressed RNAs', *Science*. 2001/10/27, 294(5543), pp. 853–858. doi: 10.1126/science.1064921.

Lai, R. C. *et al.* (2010) 'Exosome secreted by MSC reduces myocardial ischemia/reperfusion injury', *Stem Cell Research*. doi: 10.1016/j.scr.2009.12.003.

Lam, F. W. *et al.* (2018) 'Recombinant Human Vimentin Binds to P-Selectin and Blocks Neutrophil Capture and Rolling on Platelets and Endothelium', *Journal of immunology (Baltimore, Md. : 1950)*. 2018/01/15, 200(5), pp. 1718–1726. doi: 10.4049/jimmunol.1700784.

Lane, R. E. *et al.* (2015) 'Analysis of exosome purification methods using a model liposome system and tunable-resistive pulse sensing.', *Scientific reports*, 5, p. 7639. doi: 10.1038/srep07639.

Lau, N. C. *et al.* (2001) 'An abundant class of tiny RNAs with probable regulatory roles in Caenorhabditis elegans', *Science*. 2001/10/27, 294(5543), pp. 858–862. doi: 10.1126/science.1065062.

Lecrux, C. and Hamel, E. (2011) 'The neurovascular unit in brain function and disease', *Acta Physiologica*, pp. 47–59. doi: 10.1111/j.1748-1716.2011.02256.x.

Lee, R. C. and Ambros, V. (2001) ‘An extensive class of small RNAs in Caenorhabditis elegans’, *Science*. 2001/10/27, 294(5543), pp. 862–864. doi: 10.1126/science.1065329.

Lee, R. C., Feinbaum, R. L. and Ambros, V. (1993) ‘The C. elegans heterochronic gene lin-4 encodes small RNAs with antisense complementarity to lin-14’, *Cell*. 1993/12/03, 75(5), pp. 843–854.

Lee, S. K. *et al.* (2014) ‘Role of tumour necrosis factor receptor-1 and nuclear factor-κb in production of tnf-α-induced pro-inflammatory microparticles in endothelial cells’, *Thrombosis and Haemostasis*. doi: 10.1160/TH13-11-0975.

Lee, Y. *et al.* (2019) ‘Significant roles of neuroinflammation in Parkinson’s disease: therapeutic targets for PD prevention’, *Archives of Pharmacal Research*. doi: 10.1007/s12272-019-01133-0.

Leino, R. L., Gerhart, D. Z. and Drewes, L. R. (1999) ‘Monocarboxylate transporter (MCT1) abundance in brains of suckling and adult rats: A quantitative electron microscopic immunogold study’, *Developmental Brain Research*. doi: 10.1016/S0165-3806(98)00188-6.

Letsiou, E. and Bauer, N. (2018) ‘Endothelial Extracellular Vesicles in Pulmonary Function and Disease’, in *Current Topics in Membranes*. doi: 10.1016/bs.ctm.2018.09.002.

Levéen, P. *et al.* (1994) ‘Mice deficient for PDGF B show renal, cardiovascular, and hematological abnormalities’, *Genes and Development*. doi: 10.1101/gad.8.16.1875.

Lewandwsky, M. (1909) ‘Zur Lehre der Cerebrospinalflussigkeit’, *Z. Klin. Med.*, 40, pp. 480–494. Available at: http://ci.nii.ac.jp/naid/10012242921/en/ (Accessed: 2 April 2019).

Li, B. *et al.* (2019) ‘Effects of tumor necrosis factor-α-induced exosomes on the endothelial cellular behavior, metabolism and bioenergetics’, *Microcirculation*. doi: 10.1111/micc.12515.

Li, J. J. *et al.* (2018) ‘In vivo evidence for the contribution of peripheral circulating inflammatory exosomes to neuroinflammation’, *Journal of neuroinflammation*. BioMed Central, 15(1), p. 8. doi: 10.1186/s12974-017-1038-8.

Li, Y. *et al.* (2005) ‘Structure of the conserved cytoplasmic C-terminal domain of occludin: Identification of the ZO-1 binding surface’, *Journal of Molecular Biology*. doi: 10.1016/j.jmb.2005.07.017.

Liang, Y. *et al.* (2014) ‘Elevated Levels of Plasma TNF-α Are Associated With Microvascular Endothelial Dysfunction in Patients With Sepsis Through Activating the NF-κB and p38 Mitogen-Activated Protein Kinase in Endothelial Cells’, *Shock*, 41(4). Available at: https://journals.lww.com/shockjournal/Fulltext/2014/04000/Elevated_Levels_of_Plasma_TNF___Are_Associated.3.aspx.

Lippoldt, A. *et al.* (2000) ‘Phorbol ester induced changes in tight and adherens junctions in the choroid plexus epithelium and in the ependyma’, *Brain Research*. doi: 10.1016/S0006-8993(99)02355-0.

Liu, Y. *et al.* (2017) ‘Endothelial microparticles activate endothelial cells to facilitate the inflammatory response’, *Molecular Medicine Reports*. doi: 10.3892/mmr.2017.6113.

Liu, Z. *et al.* (2011) ‘Downregulation of NCC and NKCC2 cotransporters by kidney-specific WNK1 revealed by gene disruption and transgenic mouse models’, *Human Molecular Genetics*. doi: 10.1093/hmg/ddq525.

Lobb, R. J. *et al.* (2015) 'Optimized exosome isolation protocol for cell culture supernatant and human plasma', *Journal of Extracellular Vesicles*, 1(27031), pp. 1–11. doi: 10.3402/jev.v4.27031.

Lopes Pinheiro, M. A. *et al.* (2016) 'Immune cell trafficking across the barriers of the central nervous system in multiple sclerosis and stroke', *Biochimica et Biophysica Acta - Molecular Basis of Disease*. Elsevier B.V., 1862(3), pp. 461–471. doi: 10.1016/j.bbadis.2015.10.018.

Lopez-Ramirez, M. A. *et al.* (2013) 'Cytokine-induced changes in the gene expression profile of a human cerebral microvascular endothelial cell-line, hCMEC/D3', *Fluids Barriers CNS*, 10(1), p. 27. doi: 10.1186/2045-8118-10-27.

Lopez-Ramirez, M. A. *et al.* (2014) 'MicroRNA-155 negatively affects blood-brain barrier function during neuroinflammation', *FASEB Journal*, 28(6), pp. 2551–2565. doi: 10.1096/fj.13-248880.

Lopez-Ramirez, Miguel Alejandro *et al.* (2016) 'Regulation of brain endothelial barrier function by microRNAs in health and neuroinflammation', *The FASEB Journal*. Federation of American Societies for Experimental Biology, 30(8), pp. 2662–2672. doi: 10.1096/fj.201600435RR.

Lopez-Ramirez, M Alejandro *et al.* (2016) 'Role of Caspases in Cytokine-Induced Barrier Breakdown in Human Brain Endothelial Cells', *Journal of Immunology*, 189(19), pp. 3130–3139. doi: 10.4049/jimmunol.1103460.

Lötvall, J. *et al.* (2014) 'Minimal experimental requirements for definition of extracellular vesicles and their functions: a position statement from the International Society for Extracellular Vesicles', *Journal of extracellular vesicles*. Co-Action Publishing, 3, p. 26913. doi: 10.3402/jev.v3.26913.

Lund, E. *et al.* (2004) ‘Nuclear export of microRNA precursors’, *Science*. 2003/11/25, 303(5654), pp. 95–98. doi: 10.1126/science.1090599.

Lyck, R. *et al.* (2017) ‘ALCAM (CD166) is involved in extravasation of monocytes rather than T cells across the blood–brain barrier’, *Journal of Cerebral Blood Flow and Metabolism*. doi: 10.1177/0271678X16678639.

Mahringer, A. and Fricker, G. (2016) ‘ABC transporters at the blood-brain barrier’, *Expert Opinion on Drug Metabolism and Toxicology*. doi: 10.1517/17425255.2016.1168804.

Makaryus, A. N. and McFarlane, S. I. (2006) ‘Diabetes insipidus: Diagnosis and treatment of a complex disease’, *Cleveland Clinic Journal of Medicine*, pp. 65–71. doi: 10.3949/ccjm.73.1.65.

Marchetti, L. and Engelhardt, B. (2020) ‘Immune cell trafficking across the blood-brain barrier in the absence and presence of neuroinflammation’, *Vascular Biology*. doi: 10.1530/vb-19-0033.

Marcos-Ramiro, B. *et al.* (2014) ‘Microparticles in multiple sclerosis and clinically isolated syndrome: effect on endothelial barrier function.’, *BMC neuroscience*, 15, p. 110. doi: 10.1186/1471-2202-15-110.

Martin, M. M. *et al.* (2006) ‘MicroRNA-155 regulates human angiotensin II type 1 receptor expression in fibroblast’, *Journal of Biological Chemistry*. doi: 10.1074/jbc.M601496200.

Martins, T. B. *et al.* (2011) ‘Analysis of proinflammatory and anti-inflammatory cytokine serum concentrations in patients with multiple sclerosis by using a multiplexed immunoassay’, *American Journal of Clinical Pathology*. doi:

10.1309/AJCP7UBK8IBVMVNR.

Matera, A. G., Terns, R. M. and Terns, M. P. (2007) ‘Non-coding RNAs: Lessons from the small nuclear and small nucleolar RNAs’, *Nature Reviews Molecular Cell Biology*. doi: 10.1038/nrm2124.

McCandless, E. E. *et al.* (2006) ‘CXCL12 Limits Inflammation by Localizing Mononuclear Infiltrates to the Perivascular Space during Experimental Autoimmune Encephalomyelitis’, *The Journal of Immunology*. doi: 10.4049/jimmunol.177.11.8053.

Meng, W. and Takeichi, M. (2009) ‘Adherens junction: molecular architecture and regulation.’, *Cold Spring Harbor perspectives in biology*. doi: 10.1101/cshperspect.a002899.

Mesri, M. and Altieri, D. C. (1998) ‘Endothelial cell activation by leukocyte microparticles.’, *Journal of immunology (Baltimore, Md. : 1950)*, 161(8), pp. 4382–4387.

Minagar, A. and Alexander, J. S. (2003) ‘Blood-brain barrier disruption in multiple sclerosis.’, *Multiple sclerosis (Houndmills, Basingstoke, England)*, 9(35), pp. 540–549. doi: 10.1191/1352458503ms965oa.

Momma, S. (2015) ‘Neuroimmune signaling by extracellular vesicles.’, *Oncotarget*, 6(30), pp. 28521–2. doi: 10.18632/oncotarget.5249.

Muller, W. A. (2011) ‘Mechanisms of Leukocyte Transendothelial Migration’, *Annual Review of Pathology: Mechanisms of Disease*. doi: 10.1146/annurev-pathol-011110-130224.

Nava, E. and Llorens, S. (2016) ‘The paracrine control of vascular motion. A historical perspective’, *Pharmacological Research*. doi: 10.1016/j.phrs.2016.08.003.

Neilson, J. R. *et al.* (2007) 'Dynamic regulation of miRNA expression in ordered stages of cellular development', *Genes & development*. Cold Spring Harbor Laboratory Press, 21(5), pp. 578–589. doi: 10.1101/gad.1522907.

Ni, Y. *et al.* (2017) 'TNFα alters occludin and cerebral endothelial permeability: Role of p38MAPK', *PloS one*. Public Library of Science, 12(2), pp. e0170346–e0170346. doi: 10.1371/journal.pone.0170346.

Nirwane, A. and Yao, Y. (2019) 'Laminins and their receptors in the CNS', *Biological Reviews*. doi: 10.1111/brv.12454.

Nitta, T. *et al.* (2003) 'Size-selective loosening of the blood-brain barrier in claudin-5-deficient mice', *Journal of Cell Biology*. doi: 10.1083/jcb.200302070.

Njock, M.-S., Boudreau, E., *et al.* (2015) 'Endothelial cells suppress monocyte activation through secretion of extracellular vesicles containing antiin fl ammatory microRNAs', *Blood*, 125(20), pp. 3202–3213. doi: 10.1182/blood-2014-11-611046.The.

Njock, M.-S., Cheng, H. S., *et al.* (2015) 'Endothelial cells suppress monocyte activation through secretion of extracellular vesicles containing antiinflammatory microRNAs', *Blood*. Washington, DC: American Society of Hematology, 125(20), pp. 3202–3212. doi: 10.1182/blood-2014-11-611046.

O'Brien, J. *et al.* (2018) 'Overview of MicroRNA Biogenesis, Mechanisms of Actions, and Circulation ', *Frontiers in Endocrinology* , p. 402. Available at: https://www.frontiersin.org/article/10.3389/fendo.2018.00402.

O'Connell, R. M. *et al.* (2007) 'MicroRNA-155 is induced during the macrophage inflammatory response.', *Proceedings of the National Academy of Sciences of the United States of America*, 104(5), pp. 1604–9. doi: 10.1073/pnas.0610731104.

Obermeier, B., Verma, A. and Ransohoff, R. M. (2016) 'The blood – brain barrier', *Autoimmune Neurology*, 133, pp. 39–59. doi: 10.1016/B978-0-444-63432-0.00003-7.

Ohmura, T. *et al.* (2017) 'Regulation of lung endothelial permeability and inflammatory responses by prostaglandin A2: Role of EP4 receptor', *Molecular Biology of the Cell*. doi: 10.1091/mbc.E16-09-0639.

Olleros, M. L. *et al.* (2012) 'Membrane-bound TNF induces protective immune responses to M. bovis BCG infection: Regulation of memtnf and TNF receptors comparing two memTNF molecules', *PLoS ONE*. doi: 10.1371/journal.pone.0031469.

Onódi, Z. *et al.* (2018) 'Isolation of high-purity extracellular vesicles by the combination of iodixanol density gradient ultracentrifugation and bind-elute chromatography from blood plasma', *Frontiers in Physiology*. doi: 10.3389/fphys.2018.01479.

Ooi, G. T., Tawadros, N. and Escalona, R. M. (2004) 'Pituitary cell lines and their endocrine applications', *Molecular and Cellular Endocrinology*. doi: 10.1016/j.mce.2004.07.018.

Ortiz, G. G. *et al.* (2014) 'Role of the Blood-Brain Barrier in Multiple Sclerosis', *Archives of Medical Research*. Elsevier, 45(8), pp. 687–697. doi: 10.1016/j.arcmed.2014.11.013.

Osteikoetxea, X. *et al.* (2016) 'Extracellular vesicles in cardiovascular diseases, are they Jedi or Sith?', *The Journal of physiology*, 0(July 2015), pp. 1–14. doi: 10.1113/JP271336.

Ostrowski, M. *et al.* (2010) 'Rab27a and Rab27b control different steps of the exosome secretion pathway.', *Nature cell biology*, 12(1), pp. 19–30; sup pp 1-13. doi:

10.1038/ncb2000.

Pan, W. *et al.* (2011) 'Cytokine Signaling Modulates Blood-Brain Barrier Function', *Current Pharmaceutical Design*. doi: 10.2174/138161211798220918.

Pardridge, W. M. (1999) 'Blood-brain barrier biology and methodology', *Journal of NeuroVirology*. doi: 10.3109/13550289909021285.

Parker, R. and Sheth, U. (2007) 'P Bodies and the Control of mRNA Translation and Degradation', *Molecular Cell*, pp. 635–646. doi: 10.1016/j.molcel.2007.02.011.

Pasquinelli, A. E. *et al.* (2000) 'Conservation of the sequence and temporal expression of let-7 heterochronic regulatory RNA', *Nature*. 2000/11/18, 408(6808), pp. 86–89. doi: 10.1038/35040556.

Paul, D. *et al.* (2016) 'Appearance of claudin-5+ leukocytes in the central nervous system during neuroinflammation: a novel role for endothelial-derived extracellular vesicles', *Journal of Neuroinflammation*. Journal of Neuroinflammation, 13(1), p. 292. doi: 10.1186/s12974-016-0755-8.

Paul, J., Strickland, S. and Melchor, J. P. (2007) 'Fibrin deposition accelerates neurovascular damage and neuroinflammation in mouse models of Alzheimer's disease', *Journal of Experimental Medicine*. doi: 10.1084/jem.20070304.

Pena-Philippides, J. C. *et al.* (2016) 'In vivo inhibition of miR-155 significantly alters post-stroke inflammatory response', *Journal of Neuroinflammation*. Journal of Neuroinflammation, 13(1), p. 287. doi: 10.1186/s12974-016-0753-x.

Peppiatt, C. M. *et al.* (2006) 'Bidirectional control of CNS capillary diameter by pericytes', *Nature*. doi: 10.1038/nature05193.

Pérez-Boza, J., Lion, M. and Struman, I. (2018) 'Exploring the RNA landscape of

endothelial exosomes', *RNA*. doi: 10.1261/rna.064352.117.

Peterson, J. W. *et al.* (2002) 'VCAM-1-positive microglia target oligodendrocytes at the border of multiple sclerosis lesions', *Journal of Neuropathology and Experimental Neurology*. doi: 10.1093/jnen/61.6.539.

Pienaar, I. S. *et al.* (2015) 'Deep-brain stimulation associates with improved microvascular integrity in the subthalamic nucleus in Parkinson's disease', *Neurobiology of Disease*. doi: 10.1016/j.nbd.2014.12.006.

Podbielska, M. *et al.* (2016) 'Cytokine-induced release of ceramide-enriched exosomes as a mediator of cell death signaling in an oligodendroglioma cell line', *Journal of lipid research*. 2016/10/27. The American Society for Biochemistry and Molecular Biology, 57(11), pp. 2028–2039. doi: 10.1194/jlr.M070664.

Pogue, A. I. and Lukiw, W. J. (2018) 'Up-regulated Pro-inflammatory MicroRNAs (miRNAs) in Alzheimer's disease (AD) and Age-Related Macular Degeneration (AMD)', *Cellular and Molecular Neurobiology*. doi: 10.1007/s10571-017-0572-3.

van der Pol, E. *et al.* (2012) 'Classification, functions, and clinical relevance of extracellular vesicles.', *Pharmacological reviews*, 64(3), pp. 676–705. doi: 10.1124/pr.112.005983.

Pols, M. S. and Klumperman, J. (2009) 'Trafficking and function of the tetraspanin CD63', *Experimental Cell Research*, pp. 1584–1592. doi: 10.1016/j.yexcr.2008.09.020.

Potente, M. and Mäkinen, T. (2017) 'Vascular heterogeneity and specialization in development and disease', *Nature Reviews Molecular Cell Biology*. doi: 10.1038/nrm.2017.36.

Power, D. M. *et al.* (2000) 'Evolution of the thyroid hormone-binding protein,

transthyretin', *General and Comparative Endocrinology*. doi: 10.1006/gcen.2000.7520.

Proia, P. *et al.* (2008) 'Astrocytes shed extracellular vesicles that contain fibroblast growth factor-2 and vascular endothelial growth factor', *International Journal of Molecular Medicine*, 21(1), pp. 63–67.

Ragni, E. *et al.* (2017) 'Extracellular Vesicle-Shuttled mRNA in Mesenchymal Stem Cell Communication', *STEM CELLS*. John Wiley & Sons, Ltd, 35(4), pp. 1093–1105. doi: 10.1002/stem.2557.

Ragusa, M. *et al.* (2017) 'Asymmetric RNA Distribution among Cells and Their Secreted Exosomes: Biomedical Meaning and Considerations on Diagnostic Applications', *Frontiers in Molecular Biosciences*. doi: 10.3389/fmolb.2017.00066.

Raine CS1, Cannella B, Duijvestijn AM, C. A. (1990) 'Homing to central nervous system vasculature by antigen-specific lymphocytes. II. Lymphocyte/endothelial cell adhesion during the initial stages of autoimmune demyelination.', *Lab Invest.*

Ramirez, S. H. *et al.* (2018) 'Extracellular vesicles: mediators and biomarkers of pathology along CNS barriers', *Fluids and Barriers of the CNS*, 15(1), p. 19. doi: 10.1186/s12987-018-0104-7.

Raposo, G. *et al.* (1996) 'B lymphocytes secrete antigen-presenting vesicles.', *The Journal of experimental medicine*, 183(3), pp. 1161–72. doi: 10.1084/jem.183.3.1161.

Raposo, G. and Stoorvogel, W. (2013) 'Extracellular vesicles: Exosomes, microvesicles, and friends', *The Journal of Cell Biology*, 200(4), pp. 373 LP – 383. doi: 10.1083/jcb.201211138.

Ratajczak, J. *et al.* (2006) 'Embryonic stem cell-derived microvesicles reprogram hematopoietic progenitors: evidence for horizontal transfer of mRNA and protein

delivery', *Leukemia*, 20(5), pp. 847–856. doi: 10.1038/sj.leu.2404132.

Raymond, A. D. *et al.* (2016) 'Microglia-derived HIV Nef+ exosome impairment of the blood–brain barrier is treatable by nanomedicine-based delivery of Nef peptides', *Journal of NeuroVirology*. doi: 10.1007/s13365-015-0397-0.

Reboldi, A. *et al.* (2009a) 'C-C chemokine receptor 6-regulated entry of TH-17 cells into the CNS through the choroid plexus is required for the initiation of EAE.', *Nature immunology*, 10(5), pp. 514–523. doi: 10.1038/ni.1716.

Reboldi, A. *et al.* (2009b) 'C-C chemokine receptor 6–regulated entry of TH-17 cells into the CNS through the choroid plexus is required for the initiation of EAE', *Nature Immunology*. Nature Publishing Group, 10, p. 514. Available at: https://doi.org/10.1038/ni.1716.

Redzic, Z. (2011) 'Molecular biology of the blood-brain and the blood-cerebrospinal fluid barriers: Similarities and differences', *Fluids and Barriers of the CNS*. doi: 10.1186/2045-8118-8-3.

Reese, T. S. and Karnovsky, M. J. (1967) 'Fine structural localization of a blood-brain barrier to exogenous peroxidase.', *Journal of Cell Biology*, 34(1), pp. 207–217. doi: 10.1083/jcb.34.1.207.

Reichenbach, A. and Wolburg, H. (2013) 'Astrocytes and Ependymal Glia', in *Neuroglia*. doi: 10.1093/acprof:oso/9780195152227.003.0002.

Reijerkerk, A. *et al.* (2013) 'MicroRNAs regulate human brain endothelial cell-barrier function in inflammation: implications for multiple sclerosis', *J Neurosci*, 33(16), pp. 6857–6863. doi: 10.1523/JNEUROSCI.3965-12.2013.

Reinhart, B. J. *et al.* (2000) 'The 21-nucleotide let-7 RNA regulates developmental

timing in Caenorhabditis elegans', *Nature*. 2000/03/08, 403(6772), pp. 901–906. doi: 10.1038/35002607.

Reinhold, A. and Rittner, H. (2017) 'Barrier function in the peripheral and central nervous system—a review', *Pflugers Archiv European Journal of Physiology*. doi: 10.1007/s00424-016-1920-8.

Ribatti, D. *et al.* (2006) 'Development of the blood-brain barrier: A historical point of view', *Anatomical Record - Part B New Anatomist*, 289(1), pp. 3–8. doi: 10.1002/ar.b.20087.

Rider, M. A., Hurwitz, S. N. and Meckes, D. G. (2016) 'ExtraPEG: A Polyethylene Glycol-Based Method for Enrichment of Extracellular Vesicles', *Scientific Reports*, 6(October 2015), p. 23978. doi: 10.1038/srep23978.

Rieg, T. *et al.* (2013) 'Adenylyl cyclase 6 enhances NKCC2 expression and mediates vasopressin-induced phosphorylation of NKCC2 and NCC', *American Journal of Pathology*. doi: 10.1016/j.ajpath.2012.09.014.

Rivera, F. J., Hinrichsen, B. and Silva, M. E. (2019) 'Pericytes in Multiple Sclerosis', in *Advances in Experimental Medicine and Biology*. doi: 10.1007/978-3-030-16908-4_8.

De Rivero Vaccari, J. P. *et al.* (2016) 'Exosome-mediated inflammasome signaling after central nervous system injury', *Journal of Neurochemistry*, 136, pp. 39–48. doi: 10.1111/jnc.13036.

Roberts, L. M. *et al.* (2008) 'Expression of the thyroid hormone transporters monocarboxylate transporter-8 (SLC16A2) and organic ion transporter-14 (SLCO1C1) at the blood-brain barrier', *Endocrinology*. doi: 10.1210/en.2008-0378.

Robertson, G. L. (1995) 'Diabetes insipidus.', *Endocrinology and metabolism clinics of*

North America, 24(3), pp. 549–572. doi: 10.1542/pir.21-4-122.

Robinson, A. G. (1976) 'DDAVP in the treatment of central diabetes insipidus.', *The New England journal of medicine*, 294(10), pp. 507–11. doi: 10.1056/NEJM197603042941001.

Roig-Carles, D. *et al.* (2017) 'microRNAs in Brain Endothelium and Inflammation BT - The Blood Brain Barrier and Inflammation', in Lyck, R. and Enzmann, G. (eds). Cham: Springer International Publishing, pp. 153–173. doi: 10.1007/978-3-319-45514-3_7.

Roncal-Jimenez, C. A. *et al.* (2017) 'Effects of exogenous desmopressin on a model of heat stress nephropathy in mice', *American Journal of Physiology - Renal Physiology*. doi: 10.1152/ajprenal.00495.2016.

Rossi, B. *et al.* (2011) 'Vascular inflammation in central nervous system diseases: adhesion receptors controlling leukocyte-endothelial interactions', *Journal of Leukocyte Biology*. doi: 10.1189/jlb.0710432.

Ruirui, J. *et al.* (2007) 'MicroRNA Expression Signature and Antisense-Mediated Depletion Reveal an Essential Role of MicroRNA in Vascular Neointimal Lesion Formation', *Circulation Research*. American Heart Association, 100(11), pp. 1579–1588. doi: 10.1161/CIRCRESAHA.106.141986.

Sáenz-Cuesta, M., Osorio-Querejeta, I. and Otaegui, D. (2014) 'Extracellular Vesicles in Multiple Sclerosis: What are They Telling Us?', *Frontiers in cellular neuroscience*, 8(March), p. 100. doi: 10.3389/fncel.2014.00100.

Saito, Y. and Wright, E. M. (1984) 'Regulation of bicarbonate transport across the brush border membrane of the bull-frog choroid plexus.', *The Journal of Physiology*.

doi: 10.1113/jphysiol.1984.sp015204.

Salomon, C. *et al.* (2013) 'Exosomal Signaling during Hypoxia Mediates Microvascular Endothelial Cell Migration and Vasculogenesis', *PLoS ONE*. doi: 10.1371/journal.pone.0068451.

Satta, N. *et al.* (1994) 'Monocyte vesiculation is a possible mechanism for dissemination of membrane-associated procoagulant activities and adhesion molecules after stimulation by lipopolysaccharide.', *J. Immuno*, 153, pp. 3245–55.

Saugstad, J. A. (2010) 'MicroRNAs as effectors of brain function with roles in ischemia and injury, neuroprotection, and neurodegeneration.', *Journal of cerebral blood flow and metabolism : official journal of the International Society of Cerebral Blood Flow and Metabolism*. Nature Publishing Group, 30(9), pp. 1564–76. doi: 10.1038/jcbfm.2010.101.

Savina, A., Vidal, M. and Colombo, M. I. (2002) 'The exosome pathway in K562 cells is regulated by Rab11.', *Journal of cell science*, 115(Pt 12), pp. 2505–15. doi: 10.1083/jcb.149.1.1/a.

Schorey, J. S. *et al.* (2015) 'Exosomes and other extracellular vesicles in host–pathogen interactions', *EMBO reports*. doi: 10.15252/embr.201439363.

Shekarabi, M. *et al.* (2017) 'WNK Kinase Signaling in Ion Homeostasis and Human Disease', *Cell Metabolism*. doi: 10.1016/j.cmet.2017.01.007.

Shepro, D. and Morel, N. M. (1993) 'Pericyte physiology.', *FASEB journal : official publication of the Federation of American Societies for Experimental Biology*, 7(11), pp. 1031–8. Available at: http://www.ncbi.nlm.nih.gov/pubmed/8370472.

Shulman, Z. *et al.* (2012) 'Transendothelial migration of lymphocytes mediated by

intraendothelial vesicle stores rather than by extracellular chemokine depots', *Nature Immunology*. doi: 10.1038/ni.2173.

Sie, Z.-L. *et al.* (2020) 'WNK1 Kinase Stimulates Angiogenesis to Promote Tumor Growth and Metastasis', *Cancers*. MDPI, 12(3), p. 575. doi: 10.3390/cancers12030575.

Simons, M. and Raposo, G. (2009) 'Exosomes--vesicular carriers for intercellular communication.', *Current opinion in cell biology*, 21, pp. 575–581. doi: 10.1016/j.ceb.2009.03.007.

Sims, P. J. *et al.* (1989) 'Assembly of the platelet prothrombinase complex is linked to vesiculation of the platelet plasma membrane. Studies in Scott syndrome: An isolated defect in platelet procoagulant activity', *Journal of Biological Chemistry*, 264(29), pp. 17049–17057. doi: 10.1007/978-1-61737-950-5.

Sobel, R. A., Mitchell, M. E. and Fondren, G. (1990) 'Intercellular adhesion molecule-1 (ICAM-1) in cellular immune reactions in the human central nervous system', *American Journal of Pathology*.

Sohda, M., Misumi, Y. and Oda, K. (2015) 'TNFα triggers release of extracellular vesicles containing TNFR1 and TRADD, which can modulate TNFα responses of the parental cells', *Archives of Biochemistry and Biophysics*, 587, pp. 31–37. doi: https://doi.org/10.1016/j.abb.2015.10.009.

Somponpun, S. J. (2007) 'Neuroendocrine regulation of fluid and electrolyte balance by ovarian steroids: Contributions from central oestrogen receptors', *Journal of Neuroendocrinology*. doi: 10.1111/j.1365-2826.2007.01587.x.

Sork, H. *et al.* (2018) 'Heterogeneity and interplay of the extracellular vesicle small RNA transcriptome and proteome', *Scientific reports*. Nature Publishing Group UK,

8(1), p. 10813. doi: 10.1038/s41598-018-28485-9.

Stegmayr, B. and Ronquist, G. (1982) ‘Promotive effect on human sperm progressive motility by prostasomes’, *Urological Research*, 10(5), pp. 253–257. doi: 10.1007/BF00255932.

Steiner, O. *et al.* (2010) ‘Differential Roles for Endothelial ICAM-1, ICAM-2, and VCAM-1 in Shear-Resistant T Cell Arrest, Polarization, and Directed Crawling on Blood–Brain Barrier Endothelium’, *The Journal of Immunology*. doi: 10.4049/jimmunol.0903732.

Stern, L. and Gautier, R. (1921) ‘Recherches sur le liquide céphalo-rachidien: I.-les rapports entre le liquide céphalo-rachidien et la circulation sanguine’, *Archives of Physiology and Biochemistry*. doi: 10.3109/13813452109146211.

Su, F., Bai, F. and Zhang, Z. (2016) ‘Inflammatory Cytokines and Alzheimer’s Disease: A Review from the Perspective of Genetic Polymorphisms’, *Neuroscience Bulletin*. doi: 10.1007/s12264-016-0055-4.

Sui, Y. T. *et al.* (2014) ‘Alpha synuclein is transported into and out of the brain by the blood-brain barrier’, *Peptides*. doi: 10.1016/j.peptides.2014.09.018.

Sun, H. X. *et al.* (2012) ‘Essential role of microRNA-155 in regulating endothelium-dependent vasorelaxation by targeting endothelial nitric oxide synthase’, *Hypertension*, 60(6), pp. 1407–1414. doi: 10.1161/HYPERTENSIONAHA.112.197301.

Sweeney, M. D. *et al.* (2019) ‘Blood-brain barrier: From physiology to disease and back’, *Physiological Reviews*. doi: 10.1152/physrev.00050.2017.

Szabó, G. T. *et al.* (2014) ‘Critical role of extracellular vesicles in modulating the cellular effects of cytokines.’, *Cellular and molecular life sciences : CMLS*, 71(20), pp.

4055–4067. doi: 10.1007/s00018-014-1618-z.

Tait, M. J. *et al.* (2008) ‘Water movements in the brain: role of aquaporins’, *Trends in Neurosciences*. doi: 10.1016/j.tins.2007.11.003.

Takahashi, N. *et al.* (2000) ‘Uncompensated polyuria in a mouse model of Bartter’s syndrome’, *Proceedings of the National Academy of Sciences of the United States of America*. doi: 10.1073/pnas.090091297.

Tam, W. (2001) ‘Identification and characterization of human BIC, a gene on chromosome 21 that encodes a noncoding RNA’, *Gene*. doi: 10.1016/S0378-1119(01)00612-6.

Tang, N. *et al.* (2016) ‘Monocyte exosomes induce adhesion molecules and cytokines via activation of NF-κB in endothelial cells’, *FASEB Journal*. doi: 10.1096/fj.201600368RR.

Tang, Y.-T. *et al.* (2017) ‘Comparison of isolation methods of exosomes and exosomal RNA from cell culture medium and serum’, *International journal of molecular medicine*. 2017/07/24. D.A. Spandidos, 40(3), pp. 834–844. doi: 10.3892/ijmm.2017.3080.

Tauro, B. J. *et al.* (2012) ‘Comparison of ultracentrifugation, density gradient separation, and immunoaffinity capture methods for isolating human colon cancer cell line LIM1863-derived exosomes’, *Methods*, 56(2), pp. 293–304. doi: 10.1016/j.ymeth.2012.01.002.

Taverna, S. *et al.* (2014) ‘Exosomal shuttling of miR-126 in endothelial cells modulates adhesive and migratory abilities of chronic myelogenous leukemia cells’, *Molecular Cancer*, 13(1), p. 169. doi: 10.1186/1476-4598-13-169.

Taylor, D. D., Homesley, H. D. and Doellgast, G. J. (1980) 'Binding of Specific Peroxidase-labeled Antibody to Placental-type Phosphatase on Tumor-derived Membrane Fragments', *Cancer Research*, 40(11), pp. 4064 LP – 4069. Available at: http://cancerres.aacrjournals.org/content/40/11/4064.abstract.

Taylor, D. D. and Shah, S. (2015) 'Methods of isolating extracellular vesicles impact down-stream analyses of their cargoes', *Methods*. Elsevier Inc., 87, pp. 3–10. doi: 10.1016/j.ymeth.2015.02.019.

Théry, C. *et al.* (2006) 'Isolation and characterization of exosomes from cell culture supernatants and biological fluids.', *Current protocols in cell biology / editorial board, Juan S. Bonifacino ... [et al.]*, Chapter 3, p. Unit 3.22. doi: 10.1002/0471143030.cb0322s30.

Théry, C. *et al.* (2018) 'Minimal information for studies of extracellular vesicles 2018 (MISEV2018): a position statement of the International Society for Extracellular Vesicles and update of the MISEV2014 guidelines', *Journal of Extracellular Vesicles*. Taylor & Francis, 7(1), p. 1535750. doi: 10.1080/20013078.2018.1535750.

Thompson, R. C., Vardinogiannis, I. and Gilmore, T. D. (2013) 'Identification of an NF-κB p50/p65-responsive site in the human MIR155HG promoter.', *BMC molecular biology*. BMC Molecular Biology, 14(1), p. 24. doi: 10.1186/1471-2199-14-24.

Thounaojam, M. C. *et al.* (2014) 'MicroRNA 155 Regulates Japanese Encephalitis Virus-Induced Inflammatory Response by Targeting Src Homology 2-Containing Inositol Phosphatase 1', *Journal of Virology*. doi: 10.1128/jvi.02979-13.

Tian, B., Nowak, D. E. and Brasier, A. R. (2005) 'A TNF-induced gene expression program under oscillatory NF-κB control', *BMC Genomics*. doi: 10.1186/1471-2164-6-137.

Tkach, M. *et al.* (2017) 'Qualitative differences in T-cell activation by dendritic cell-derived extracellular vesicle subtypes', *The EMBO journal*. 2017/09/21. John Wiley and Sons Inc., 36(20), pp. 3012–3028. doi: 10.15252/embj.201696003.

Toft-Hansen, H. *et al.* (2006) 'Metalloproteinases Control Brain Inflammation Induced by Pertussis Toxin in Mice Overexpressing the Chemokine CCL2 in the Central Nervous System', *The Journal of Immunology*, 177(10), pp. 7242 LP – 7249. doi: 10.4049/jimmunol.177.10.7242.

Tsumura, K. *et al.* (2006) 'Downregulation of AQP2 expression in the kidney of polydipsic STR/N mice', *American Journal of Physiology - Renal Physiology*. doi: 10.1152/ajprenal.00029.2005.

Umezu, T. *et al.* (2012) 'Leukemia cell to endothelial cell communication via exosomal miRNAs', *Oncogene*. Nature Publishing Group, 32(May), pp. 2747–2755. doi: 10.1038/onc.2012.295.

Uzarski, J. S., Scott, E. W. and McFetridge, P. S. (2013) 'Adaptation of endothelial cells to physiologically-modeled, variable shear stress', *PloS one*. Public Library of Science, 8(2), pp. e57004–e57004. doi: 10.1371/journal.pone.0057004.

Valadi, H. *et al.* (2007) 'Exosome-mediated transfer of mRNAs and microRNAs is a novel mechanism of genetic exchange between cells', *Nature Cell Biology*, 9(6), pp. 654–659. doi: 10.1038/ncb1596.

Valtin, H. (1995) 'Differential diagnosis and pathophysiology of diabetes insipidus', *The Japanese Journal of Nephrology*, 37(11), pp. 601–609. doi: 10.14842/jpnjnephrol1959.37.601.

Varatharaj, A. and Galea, I. (2017) 'The blood-brain barrier in systemic inflammation',

Brain, Behavior, and Immunity. doi: 10.1016/j.bbi.2016.03.010.

Ventura, A. *et al.* (2008) 'Targeted Deletion Reveals Essential and Overlapping Functions of the miR-17???92 Family of miRNA Clusters', *Cell*, 132(5), pp. 875–886. doi: 10.1016/j.cell.2008.02.019.

Vigorito, E. *et al.* (2013) 'miR-155: An ancient regulator of the immune system', *Immunological Reviews*, 253(1), pp. 146–157. doi: 10.1111/imr.12057.

Virgintino, D. *et al.* (2012) 'Plasma membrane-derived microvesicles released from tip endothelial cells during vascular sprouting', *Angiogenesis*, 15(4), pp. 761–769. doi: 10.1007/s10456-012-9292-y.

Vogel, R. *et al.* (2016) 'A standardized method to determine the concentration of extracellular vesicles using tunable resistive pulse sensing', 1, pp. 1–13.

Wadey, R. M. *et al.* (2019) 'Inflammatory adipocyte-derived extracellular vesicles promote leukocyte attachment to vascular endothelial cells', *Atherosclerosis*. doi: 10.1016/j.atherosclerosis.2019.01.013.

Wang, K. *et al.* (2017) 'TNF-α promotes extracellular vesicle release in mouse astrocytes through glutaminase', *Journal of neuroinflammation*. BioMed Central, 14(1), p. 87. doi: 10.1186/s12974-017-0853-2.

Wang, K. *et al.* (2018) 'The Properties of Cytokines in Multiple Sclerosis: Pros and Cons', *American Journal of the Medical Sciences*. doi: 10.1016/j.amjms.2018.08.018.

Wang, K. C. and Chang, H. Y. (2011) 'Molecular mechanisms of long noncoding RNAs', *Molecular cell*, 43(6), pp. 904–914. doi: 10.1016/j.molcel.2011.08.018.

Wei, J. W. *et al.* (2017) 'Non-coding RNAs as regulators in epigenetics (Review)', *Oncology Reports*. doi: 10.3892/or.2016.5236.

Weksler, B. B. *et al.* (2005) ‘Blood-brain barrier-specific properties of a human adult brain endothelial cell line’, *FASEB Journal*. doi: 10.1096/fj.04-3458fje.

Weller, R. O. *et al.* (2018) ‘The meninges as barriers and facilitators for the movement of fluid, cells and pathogens related to the rodent and human CNS’, *Acta Neuropathologica*. doi: 10.1007/s00401-018-1809-z.

Wightman, B., Ha, I. and Ruvkun, G. (1993) ‘Posttranscriptional regulation of the heterochronic gene lin-14 by lin-4 mediates temporal pattern formation in C. elegans’, *Cell*. 1993/12/03, 75(5), pp. 855–862.

Williams, M. J. *et al.* (2005) ‘Cadherin-10 is a novel blood-brain barrier adhesion molecule in human and mouse’, *Brain Research*. doi: 10.1016/j.brainres.2005.07.078.

Winkler, E. A. *et al.* (2012) ‘Blood-spinal cord barrier pericyte reductions contribute to increased capillary permeability’, *Journal of Cerebral Blood Flow and Metabolism*. doi: 10.1038/jcbfm.2012.113.

Winkler, E. A., Bell, R. D. and Zlokovic, B. V. (2011) ‘Central nervous system pericytes in health and disease’, *Nature Neuroscience*. doi: 10.1038/nn.2946.

Winter, J. *et al.* (2009) ‘Many roads to maturity: microRNA biogenesis pathways and their regulation.’, *Nature cell biology*, 11(3), pp. 228–234. doi: 10.1038/ncb0309-228.

Withrow, J. *et al.* (2016) ‘Extracellular vesicles in the pathogenesis of rheumatoid arthritis and osteoarthritis’, *Arthritis Research and Therapy*. doi: 10.1186/s13075-016-1178-8.

Witwer, K. W. *et al.* (2013) ‘Standardization of sample collection, isolation and analysis methods in extracellular vesicle research.’, *Journal of extracellular vesicles*, 2, pp. 1–25. doi: 10.3402/jev.v2i0.20360.

Wolburg, H. *et al.* (2001) ‘Claudin-1, claudin-2 and claudin-11 are present in tight junctions of choroid plexus epithelium of the mouse’, *Neuroscience Letters*. doi: 10.1016/S0304-3940(01)01927-9.

Wolf, P. (1967) ‘The Nature and Significance of Platelet Products in Human Plasma’, *British Journal of Haematology*, 13(3), pp. 269–288. doi: 10.1111/j.1365-2141.1967.tb08741.x.

Wu, C. *et al.* (2009) ‘Endothelial basement membrane laminin α5 selectively inhibits T lymphocyte extravasation into the brain’, *Nature Medicine*. doi: 10.1038/nm.1957.

Wu, D., Cerutti, C., Lopez-Ramirez, Miguel A, *et al.* (2015) ‘Brain endothelial miR-146a negatively modulates T-cell adhesion through repressing multiple targets to inhibit NF-κB activation.’, *Journal of cerebral blood flow and metabolism : official journal of the International Society of Cerebral Blood Flow and Metabolism*, 35(3), pp. 412–23. doi: 10.1038/jcbfm.2014.207.

Wu, D., Cerutti, C., Lopez-Ramirez, Miguel A., *et al.* (2015) ‘Brain endothelial miR-146a negatively modulates T-cell adhesion through repressing multiple targets to inhibit NF-κB activation’, *Journal of Cerebral Blood Flow and Metabolism*. doi: 10.1038/jcbfm.2014.207.

Wu, T. and Chen, G. (2016) ‘MiRNAs Participate in MS Pathological Processes and Its Therapeutic Response’, *Mediators of Inflammation*. Hindawi Publishing Corporation, 2016. doi: 10.1155/2016/4578230.

Wu, X.-Y. *et al.* (2014) ‘Regulation of microRNA-155 in Endothelial Inflammation by Targeting Nuclear Factor (NF)-κB P65’, *Journal of Cellular Biochemistry*. John Wiley & Sons, Ltd, 115(11), pp. 1928–1936. doi: 10.1002/jcb.24864.

Wu, Y., Deng, W. and Klinke, D. J. (2015) ‘Exosomes: Improved methods to characterize their morphology, RNA content, and surface protein biomarkers’, *Analyst*. doi: 10.1039/c5an00688k.

Wulczyn, F. G., Krappmann, D. and Scheidereit, C. (1996) ‘The NF-κB/Rel and IκB gene families: mediators of immune response and inflammation’, *Journal of Molecular Medicine*, 74(12), pp. 749–769. doi: 10.1007/s001090050078.

Xia, X. *et al.* (2017) ‘NFAT5 protects astrocytes against oxygen–glucose–serum deprivation/restoration damage via the SIRT1/Nrf2 pathway’, *Journal of Molecular Neuroscience*. doi: 10.1007/s12031-016-0849-x.

Xie, J. *et al.* (2009) ‘Endothelial-specific expression of WNK1 kinase is essential for angiogenesis and heart development in mice’, *American Journal of Pathology*. doi: 10.2353/ajpath.2009.090094.

Xu, L., Nirwane, A. and Yao, Y. (2019) ‘Basement membrane and blood-brain barrier’, *Stroke and Vascular Neurology*. doi: 10.1136/svn-2018-000198.

Yamamoto, S. *et al.* (2015) ‘Inflammation-induced endothelial cell-derived extracellular vesicles modulate the cellular status of pericytes’, *Scientific Reports*, 5, p. 8505. doi: 10.1038/srep08505.

Yáñez-Mó, M. *et al.* (2015) ‘Biological properties of extracellular vesicles and their physiological functions.’, *Journal of extracellular vesicles*, 4, p. 27066. doi: 10.3402/jev.v4.27066.

Yang, Y. *et al.* (2018) ‘Inflammation leads to distinct populations of extracellular vesicles from microglia’, *Journal of Neuroinflammation*. doi: 10.1186/s12974-018-1204-7.

Yao, Y. (2019) ‘Basement membrane and stroke’, *Journal of Cerebral Blood Flow and Metabolism*. doi: 10.1177/0271678X18801467.

Yi, R. *et al.* (2003) ‘Exportin-5 mediates the nuclear export of pre-microRNAs and short hairpin RNAs’, *Genes and Development*, 17(24), pp. 3011–3016. doi: 10.1101/gad.1158803.

Yin, Q. *et al.* (2008) ‘MicroRNA-155 Is an Epstein-Barr Virus-Induced Gene That Modulates Epstein-Barr Virus-Regulated Gene Expression Pathways’, *Journal of Virology*, 82(11), pp. 5295–5306. doi: 10.1128/JVI.02380-07.

Zachariah, M. A. and Cyster, J. G. (2010) ‘Neural crest-derived pericytes promote egress of mature thymocytes at the corticomedullary junction’, *Science*. doi: 10.1126/science.1188222.

Zealy, R. W. *et al.* (2017) ‘microRNA-binding proteins: specificity and function’, *Wiley Interdisciplinary Reviews: RNA*. John Wiley & Sons, Ltd, 8(5), p. e1414. doi: 10.1002/wrna.1414.

Zeldovich, L. (2017) ‘Genetic drift: The ghost in the genome’, *Lab Animal*. doi: 10.1038/laban.1275.

Zhang, B. *et al.* (2016) ‘Focus on extracellular vesicles: Therapeutic potential of stem cell-derived extracellular vesicles’, *International Journal of Molecular Sciences*, 17(2). doi: 10.3390/ijms17020174.

Zhang, D. *et al.* (2017) ‘A comparative study of the characterization of miR-155 in knockout mice’, *PLoS ONE*. doi: 10.1371/journal.pone.0173487.

Zhang, Z. *et al.* (2012) ‘MicroRNA degradation and turnover: regulating the regulators’, *Wiley interdisciplinary reviews. RNA*. 2012/03/28, 3(4), pp. 593–600. doi:

10.1002/wrna.1114.

Zhang, Z. Sen *et al.* (2020) ‘Research advances in pericyte function and their roles in diseases’, *Chinese Journal of Traumatology - English Edition*. doi: 10.1016/j.cjtee.2020.02.006.

Zhou, H. *et al.* (2010) ‘MiR-155 and its star-form partner miR-155* cooperatively regulate type I interferon production by human plasmacytoid dendritic cells’, *Blood*. doi: 10.1182/blood-2010-04-280156.

Zipser, B. D. *et al.* (2007) ‘Microvascular injury and blood-brain barrier leakage in Alzheimer’s disease’, *Neurobiology of Aging*. doi: 10.1016/j.neurobiolaging.2006.05.016.

Zitvogel, L. *et al.* (1998) ‘Eradication of established murine tumors using a novel cell-free vaccine: dendritic cell-derived exosomes.’, *Nature Medicine*, 4(5), pp. 594–600. doi: 10.1038/nm0598-594.

Zlokovic, B. V. (2005) ‘Neurovascular mechanisms of Alzheimer’s neurodegeneration’, *Trends in Neurosciences*, pp. 202–208. doi: 10.1016/j.tins.2005.02.001.

Zonta, M. *et al.* (2003) ‘Neuron-to-astrocyte signaling is central to the dynamic control of brain microcirculation’, *Nature Neuroscience*. doi: 10.1038/nn980.

ANNEXE 1

Table Annexe 1. List of down-regulated proteins upon miRNA-155 overexpression in hCMEC/D3 cells (n=1).

Symbol	Protein_Name	Log2 FC (miRNA-155 / Scamble)
GPR172B	Porcine endogenous retrovirus A receptor 2	-6.573499609
GPC2	Glypican-2	-5.097038479
IRAK1BP1	Interleukin-1 receptor-associated kinase 1-binding protein 1	-4.98602902
SHISA6	Protein shisa-6 homolog	-4.579812381
COL5A3	Collagen alpha-3(V) chain	-3.680521316
SNAP47	Synaptosomal-associated protein 47	-3.559763293
NF1	Neurofibromin	-3.554077579
ECSCR	Endothelial cell-specific chemotaxis regulator	-3.411596802
TNKS	Tankyrase-1	-2.940077139
C7orf51	Uncharacterized protein C7orf51	-2.930906657
C10orf113	Putative uncharacterized protein C10orf113	-2.610237205
DSTYK	Dual serine/threonine and tyrosine protein kinase	-2.600620234
KIAA1210	Uncharacterized protein KIAA1210	-2.550454558
EPCAM	Epithelial cell adhesion molecule	-2.543137532
SYNPO2	Synaptopodin-2	-2.528653089
PDILT	Protein disulfide-isomerase-like protein of the testis	-2.483061619
FAM177A1	Protein FAM177A1	-2.467761733
SHMT1	Serine hydroxymethyltransferase, cytosolic	-2.448859795
SLC8A2	Sodium/calcium exchanger 2	-2.438917161
ATP12A	Potassium-transporting ATPase alpha chain 2	-2.287141484
RAB32	Ras-related protein Rab-32	-2.246461
BTBD11	Ankyrin repeat and BTB/POZ domain-containing protein BTBD11	-2.200011173
NFAT5	Nuclear factor of activated T-cells 5	-2.185314653
C20orf12	Ankyrin repeat-containing protein C20orf12	-2.082872757
FAM149B1	Protein FAM149B1	-2.068396498
ADAM19	Disintegrin and metalloproteinase domain-containing protein 19	-2.041798274
VTCN1	V-set domain-containing T-cell activation inhibitor 1	-2.009195762
PRR18	Proline-rich protein 18	-1.957308087
PKD1L1	Polycystic kidney disease protein 1-like 1	-1.899347811
CLMN	Calmin	-1.753753757
XKR8	XK-related protein 8	-1.732026112
TJP1	Tight junction protein ZO-1	-1.72866411
KLK11	Kallikrein-11	-1.72742747
ZNHIT6	Box C/D snoRNA protein 1	-1.718414934
SCMH1	Polycomb protein SCMH1	-1.709655346
SCARB1	Scavenger receptor class B member 1	-1.646674008
RIMBP3	RIMS-binding protein 3A	-1.611776888

NPTXR	Neuronal pentraxin receptor	-1.608556553
KCNK17	Potassium channel subfamily K member 17	-1.598210699
C12orf48	UPF0419 protein C12orf48	-1.596980353
HSP90AA4P	Putative heat shock protein HSP 90-alpha A4	-1.56543253
MXRA5	Matrix-remodeling-associated protein 5	-1.538278321
BBOX1	Gamma-butyrobetaine dioxygenase	-1.526938002
PCSK7	Proprotein convertase subtilisin/kexin type 7	-1.524728463
SKT	Sickle tail protein homolog	-1.441177713
C3orf49	Putative uncharacterized protein C3orf49	-1.435667216
SNX27	Sorting nexin-27	-1.420500264
PPP1R12C	Protein phosphatase 1 regulatory subunit 12C	-1.388785292
SBF2	Myotubularin-related protein 13	-1.383145647
ZNF516	Zinc finger protein 516	-1.35275685
C12orf23	UPF0444 transmembrane protein C12orf23	-1.337560802
FREM2	FRAS1-related extracellular matrix protein 2	-1.324441655
PRSS48	Serine protease 48	-1.317423428
EDRF1	Erythroid differentiation-related factor 1	-1.270618158
GATA5	Transcription factor GATA-5	-1.259009753
MKLN1	Muskelin	-1.255582648
DDX10	Probable ATP-dependent RNA helicase DDX10	-1.248722335
SYT13	Synaptotagmin-13	-1.239740292
CNTN1	Contactin-1	-1.237682211
PCDHGC5	Protocadherin gamma-C5	-1.230589056
RPS15A	40S ribosomal protein S15a	-1.177520681
CD38	ADP-ribosyl cyclase 1	-1.161149583
RAET1E	NKG2D ligand 4	-1.160918575
WIZ	Protein Wiz	-1.157660849
SMAP2	Stromal membrane-associated protein 2	-1.153242992
NOTUM	Protein notum homolog	-1.152227137
CCDC137	Coiled-coil domain-containing protein 137	-1.150178062
GARNL3	GTPase-activating Rap/Ran-GAP domain-like protein 3	-1.137866833
ACTN3	Alpha-actinin-3	-1.131040638
BTNL8	Butyrophilin-like protein 8	-1.125649598
INVS	Inversin	-1.124046593
RBM15	Putative RNA-binding protein 15	-1.123632957
NME2P1	Putative nucleoside diphosphate kinase	-1.118370773
HAGH	Hydroxyacylglutathione hydrolase, mitochondrial	-1.105376122
SLC25A22	Mitochondrial glutamate carrier 1	-1.101444379
ART5	Ecto-ADP-ribosyltransferase 5	-1.093989365
MMP12	Macrophage metalloelastase	-1.081724855
SPACA3	Sperm acrosome membrane-associated protein 3	-1.079358343
ACCN4	Amiloride-sensitive cation channel 4	-1.079260354
LRRFIP2	Leucine-rich repeat flightless-interacting protein 2	-1.064664611
PRDM16	PR domain zinc finger protein 16	-1.059781517
TCF9	GC-rich sequence DNA-binding factor	-1.04793267

OR52N5	Olfactory receptor 52N5	-1.046461165
CRTC3	CREB-regulated transcription coactivator 3	-1.04338933
AMT	Aminomethyltransferase, mitochondrial	-1.034334695
REL	Proto-oncogene c-Rel	-1.031438749
HMGN2	Non-histone chromosomal protein HMG-17	-1.025997705
CHST2	Carbohydrate sulfotransferase 2	-1.025690969
CCDC69	Coiled-coil domain-containing protein 69	-1.025340905
EIF3I	Eukaryotic translation initiation factor 3 subunit I	-1.02233408
AACS	Acetoacetyl-CoA synthetase	-1.021726301
WNK1	Serine/threonine-protein kinase WNK1	-1.018683046
REEP6	Receptor expression-enhancing protein 6	-1.016549682
MOV10L1	Putative helicase Mov10l1	-1.002250891
ARHGEF18	Rho guanine nucleotide exchange factor 18	-1.000863722